# Anionic self-assembling supramolecular enhancers of antimicrobial efficacy against Gram-negative bacteria

Jessica E. Boles, George T. Williams,* Nyasha Allen, Lisa J. White, Kira L. F. Hilton, Precious I. A. Popoola, Daniel P. Mulvihill* and Jennifer R. Hiscock*

## Contents

## Chemical structures

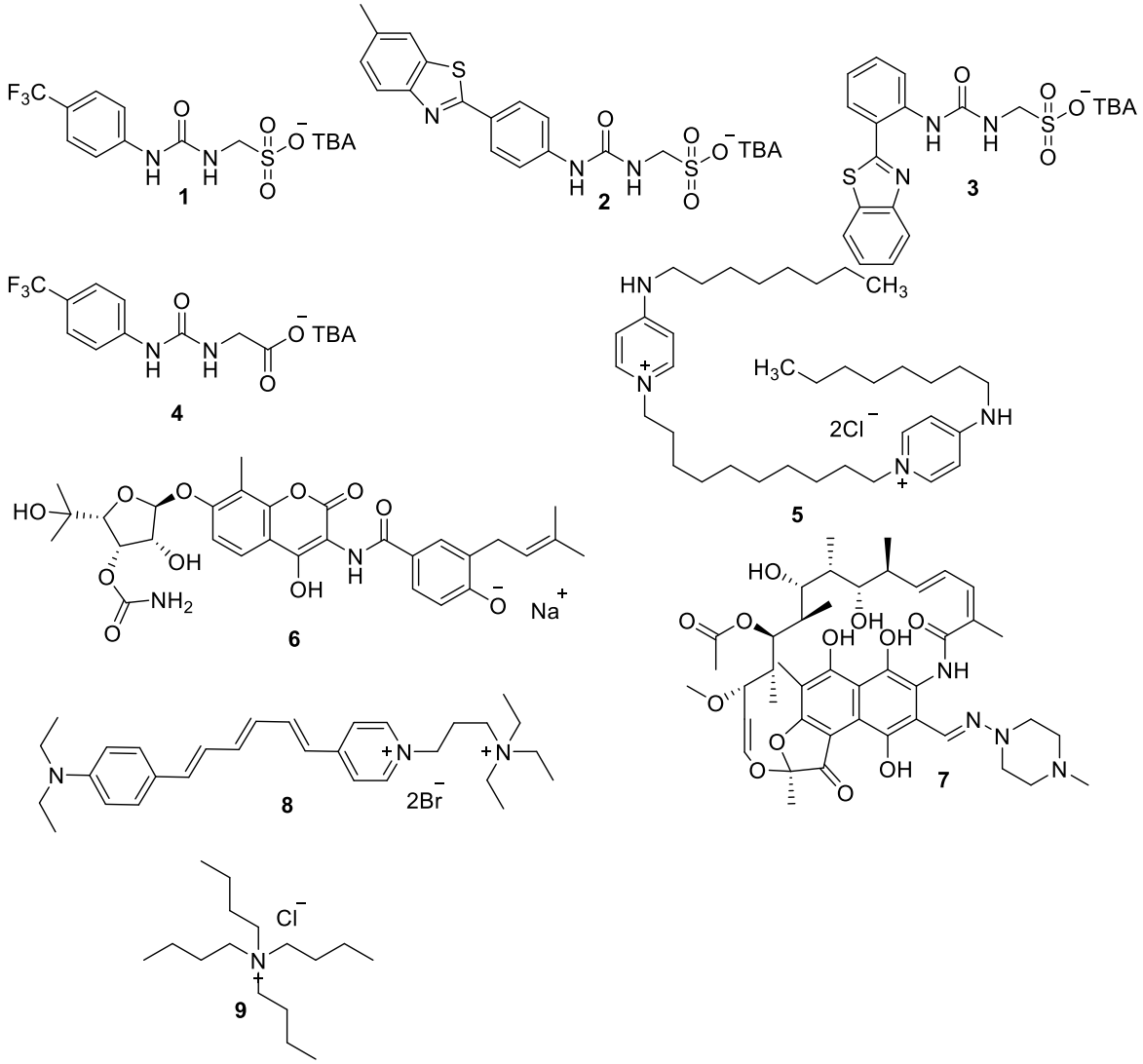


Figure S1 - Chemical structures of SSAs **1**-**4,** co-formulant agents **5**-**7,** cell-impermeable fluorescent styryl-dye, FM4-64, **8**, and TBACl **9**. TBA = tetrabutylammonium.

Table S1 - Molecular components **1**-**7**, supplied in a 1:1 ratio, for co-formulations ***a***-***l***.

| Co-formulation | Molecular components | Co-formulation | Molecular components |
|---|---|---|---|
| ***a*** | **1** + **5** | ***g*** | **3** + **5** |
| ***b*** | **1** + **6** | ***h*** | **3** + **6** |
| ***c*** | **1** + **7** | ***i*** | **3** + **7** |
| ***d*** | **2** + **5** | ***j*** | **4** + **5** |
| ***e*** | **2** + **6** | ***k*** | **4** + **6** |
| ***f*** | **2** + **7** | ***l*** | **4** + **7** |

# Chemical Experimental

**General remarks**: A positive pressure of nitrogen and oven dried glassware were used for all reactions. All solvents and starting materials were purchased from known chemical suppliers or available stores and used without any further purification unless specifically stipulated. The NMR spectra were obtained using a Burker AV2 400 MHz or AVNEO 400 MHz spectrometer. The data was processed using ACD Labs. NMR Chemical shift values are reported in parts per million (ppm) and calibrated to the centre of the residual solvent peak set (s = singlet, br = broad, d = doublet, t = triplet, q = quartet, m = multiplet). Tensiometry measurements were undertaken using the Biolin Scientific Theta Attension optical tensiometer. The data was processed using Biolin OneAttension software. A Hamilton (309) syringe was used for the measurements. DLS and Zeta Potential studies were carried out using Anton Paar Litesizer™ 500 and processed using KalliopeTM Professional. Cellular growth curve measurements obtained using Thermo Scientific Multiscan Go 1510-0318C plate reader and recorded using the SkanIt Software 4.0 and a Clariostar plater reader using MARS data analysis software.

**Self-association constant calculation**: Self-association constants were determined using Bindfit v0.5 (http://app.supramolecular.org/bindfit/). All the data can be accessed online using the hyperlinks provided.

**Tensiometry Studies**: All the samples were prepared in an EtOH:$H_2O$ (1:19) solution. All samples underwent an annealing process in which the various solutions were heated to approximately 40 °C before being allowed to cool to room temperature, allowing each sample to reach a thermodynamic minimum. All samples were prepared through serial dilution of the most concentrated sample. Three surface tension measurements were obtained for each sample at a given concentration, using the pendant drop method. The average values were then used to calculate the critical micelle concentration (CMC).

**DLS Studies**: All solvents used were filtered to remove any particulates that may interfere with the results obtained. All samples underwent an annealing process, in which they were heated to 40 °C before being allowed to cool to 25 °C. A series of 9 runs were recorded at 25 °C.

**Zeta Potential Studies**: All solvents used were filtered to remove any particulates that may interfere with the results obtained. All samples underwent an annealing process in which the various solutions were heated to approximately 40 °C before cooling to room temperature, allowing each sample to reach a thermodynamic minimum. The final zeta potential value given is an average of the number of experiments conducted at 25 °C.

**Crystal X-ray Studies**: Single crystals of **4** were produced through the slow evaporation of an EtOH/H2O 1:19 solution, containing the appropriate compound at room temperature (≈ 25 °C). A suitable crystal was selected and mounted on a Rigaku Oxford Diffraction Supernova diffractometer. Data were collected using Cu Kα radiation at 100 K. Structures were solved with the ShelXT[1] or ShelXS structure solution programs via Direct Methods and refined with ShelXL[1] by least Squares minimisation. Olex2[2] was used as an interface to all ShelX programs (CCDC 2122929).

# Biological experimental

# Biological experiments

**Preparation of Luria Broth media (LB):** Yeast extract (5 g), tryptone (10 g) and sodium chloride (10 g) were dissolved in $dH_2O$ (1 L) then divided into bottles and autoclaved.

**Preparation of Luria Broth (LB) agar plates:** Agar (6 g) was added to LB (400 mL) and autoclaved. Once cool, the LB agar was poured into sterile petri dishes under sterile conditions and allowed to set. LB plates were stored at 4 °C until use.

**Preparation of bacterial plates:** Sterile LB agar plates were streaked using *Escherichia coli* DH10

*β* or *Pseudomonas aeruginosa* PA01 then incubated at 37 °C overnight.

**Preparation of Inoculum:** An initial culture was made up by inoculating LB media (5 mL) with a single colony of bacteria under sterile conditions and incubated at 37 °C with shaking overnight. The following day, overnight bacterial cultures were subcultured into fresh LB medium to a starting $OD_{600}$ of 0.01.

**Preparation of well microplate co-formulation study:** Each drug was serially diluted across the plate with a starting concentration of the minimum inhibitory concentration (MIC). Inoculum was added to SSA, 100 µL of SSA-culture was aliquoted to each well giving a total well volume of 200 µL. Plates were incubated with shaking (180 rpm) at 37 °C for 18 h and the $OD_{600}$ was determined using a Clariostar plate reader (BMG Labtech).

# Chemical synthesis

**Compound 1:** This compound was synthesised in line with our previously published methods. Proton NMR was found to match our previously published values.[3] $^1$H NMR (400 MHz, 298K, DMSO-$d_6$): δ: 9.20 (s, 1H), 7.55 (dd, *J* = 8.72 Hz, 4H), 6.67 (s, 1H), 3.88 (d, *J* = 5.84 Hz, 2H), 3.18 - 3.14 (m, 8H), 1.60-1.56 (m, 8H), 1.33 - 1.26 (m, 8H), 0.93 (t, *J* = 7.28 Hz, 12H).

**Compound 2:** This compound was synthesised in line with our previously published methods. Proton NMR were found to match our previously published values.[4] $^1$H NMR (400 MHz, 298.15 K, DMSO-$d_6$): δ: 9.15 (s, 1H), 7.93 – 7.85 (m, 4H), 7.57 (d, *J* = 8.64 Hz, 2H), 7.31 (m, 1H), 6.84 (s, 1H), 3.90 (d, *J* = 5.60 Hz, 2H), 3.17 – 3.13 (m, 9H), 2.44 (s, 3H), 1.62 – 1.55 (m, 9H), 1.33 – 1.26 (m, 9H), 0.92 (t, *J* = 7.32 Hz, 12H).

**Compound 3:** This compound was synthesised in line with our previously published methods. Proton NMR were found to match our previously published values.[4] $^1$H NMR (400 MHz, 298.15 K, DMSO-$d_6$): δ: 10.64 (s, 1H), 8.36 (d, *J* = 7.77 Hz, 1H), 8.31 (d, *J* = 7.80 Hz, 1H), 8.14 (d, *J* = 7.8 Hz, 1H), 7.83 (m, 2H), 7.58 (t, *J* = 7.80 Hz, 1H), 7.47 (m, 2H), 7.10 (t, *J* = 7.24 Hz, 1H), 3.95 (d, *J* = 5.20 Hz, 2H), 3.17 – 3.13 (m, 8H), 1.59 – 1.52 (m, 8H), 1.35 – 1.26 (m, 8H), 0.93 (t, *J* = 7.28 Hz, 12H).

**Compound 4:** This compound was synthesised in line with our previously published methods. Proton NMR were found to match our previously published.[5] $^1$H NMR (400 MHz, 298.15 K, DMSO-$d_6$): δ: 10.48 (s, 1H), 7.71 (d, *J* = 8.08 Hz, 2H), 7.48 (d, *J* = 8.60 Hz, 2H), 6.85 (s, 1H), 3.17 - 3.13 (m, 8H), 1.60 - 1.54 (m, 8H), 1.31 - 1.25 (m, 8H), 0.93 (t, *J* = 7.36 Hz, 12H).

# NMR

## Characterisation NMR

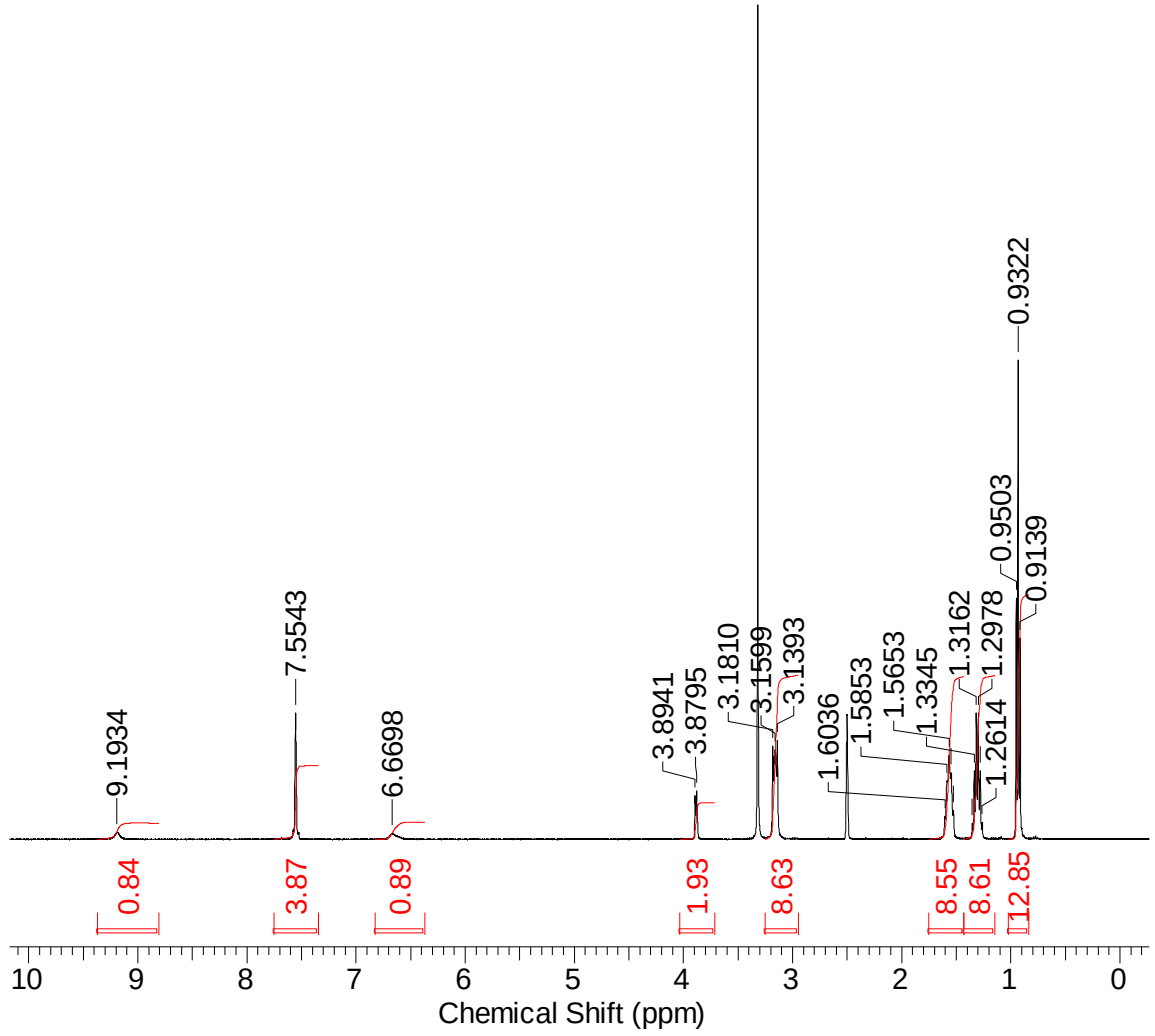


Figure S2 - $^{1}$H NMR of compound **1** in DMSO-$d_6$ conducted at 298 K.

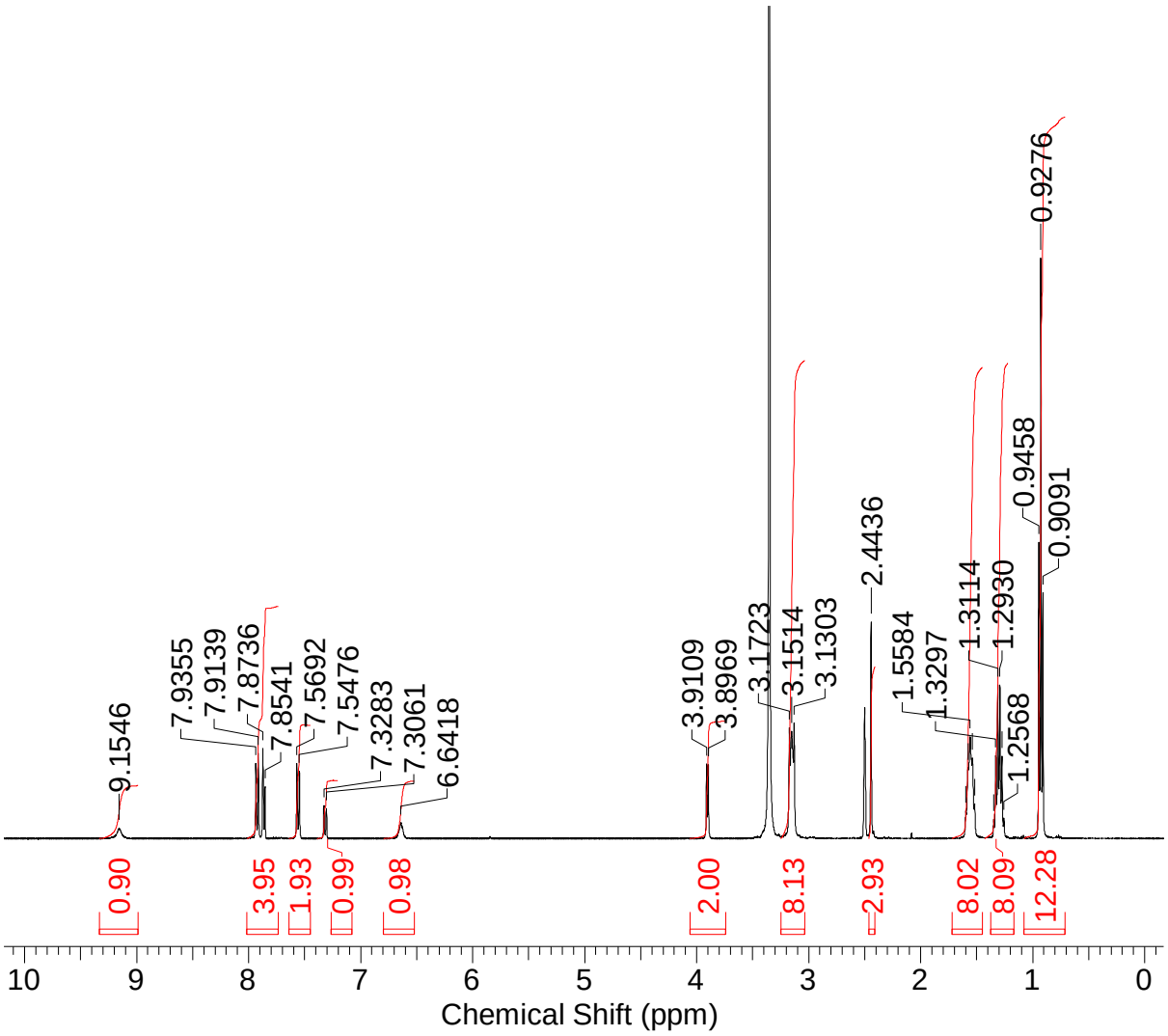


Figure S3 - $^{1}$H NMR of compound **2** in DMSO-$d_6$ conducted at 298 K.

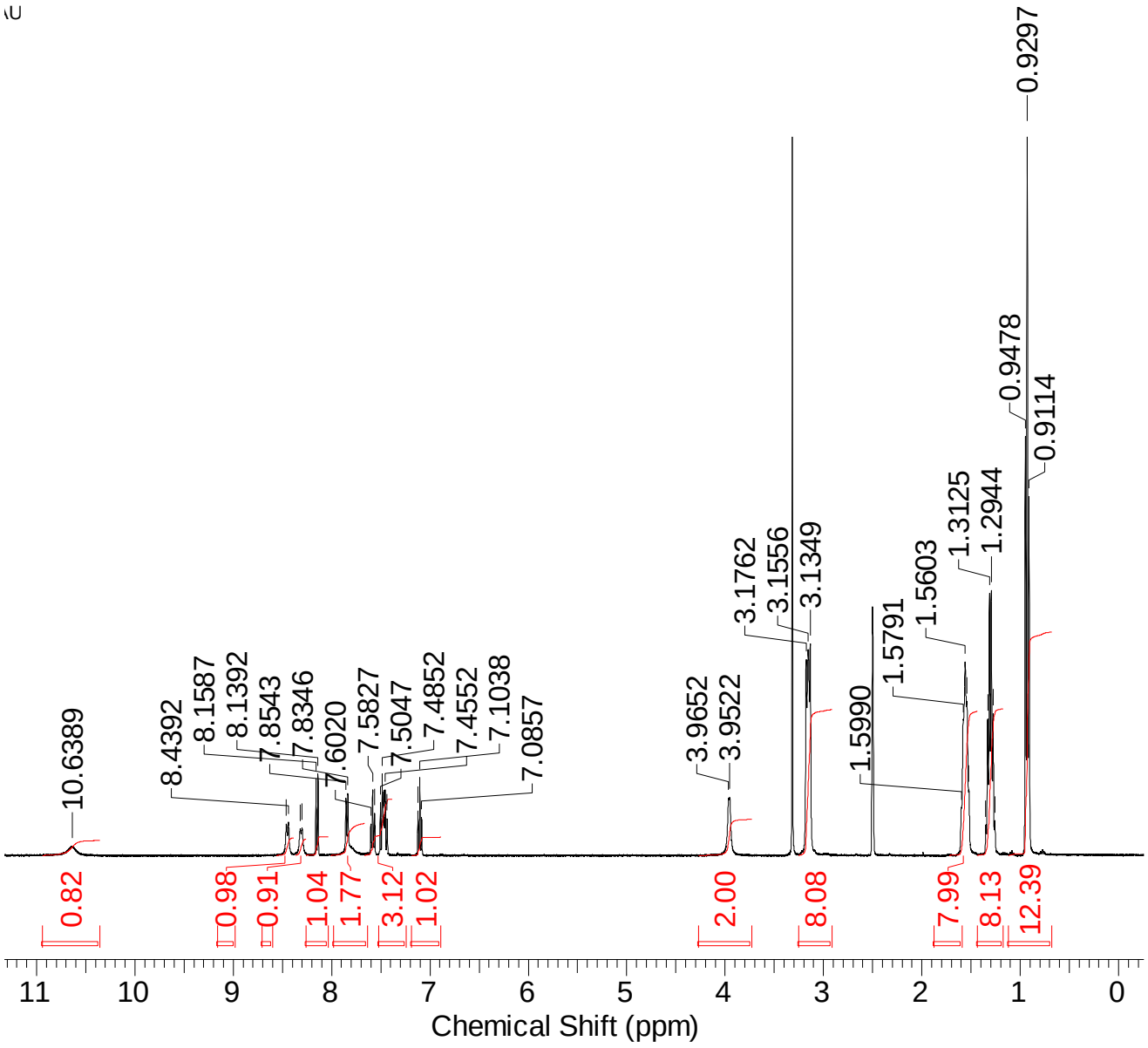


Figure S4 - $^{1}$H NMR of compound **3** in DMSO-$d_6$ conducted at 298 K.

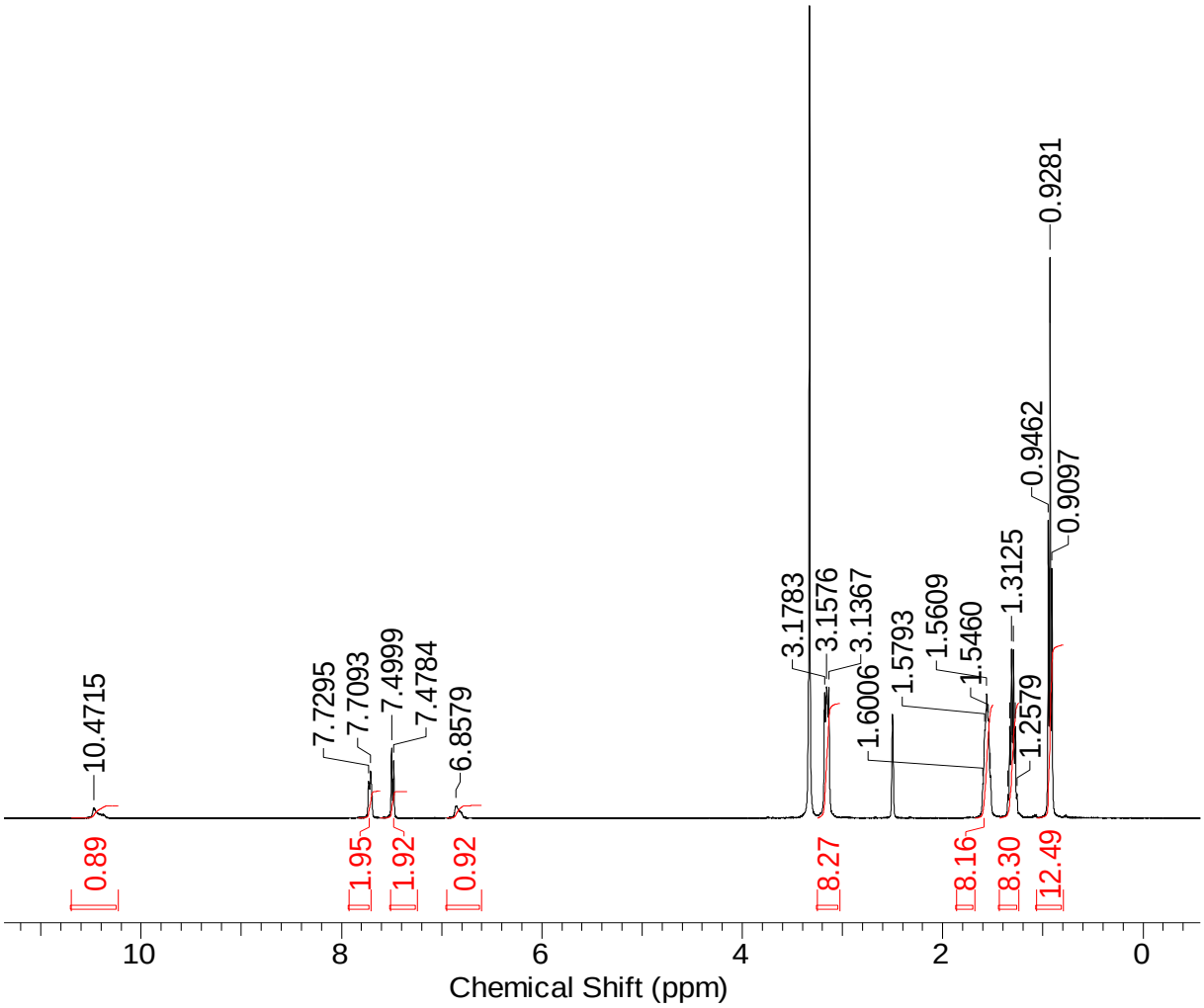


Figure S5 - $^{1}$H NMR of compound **4** in DMSO-$d_6$ conducted at 298 K.

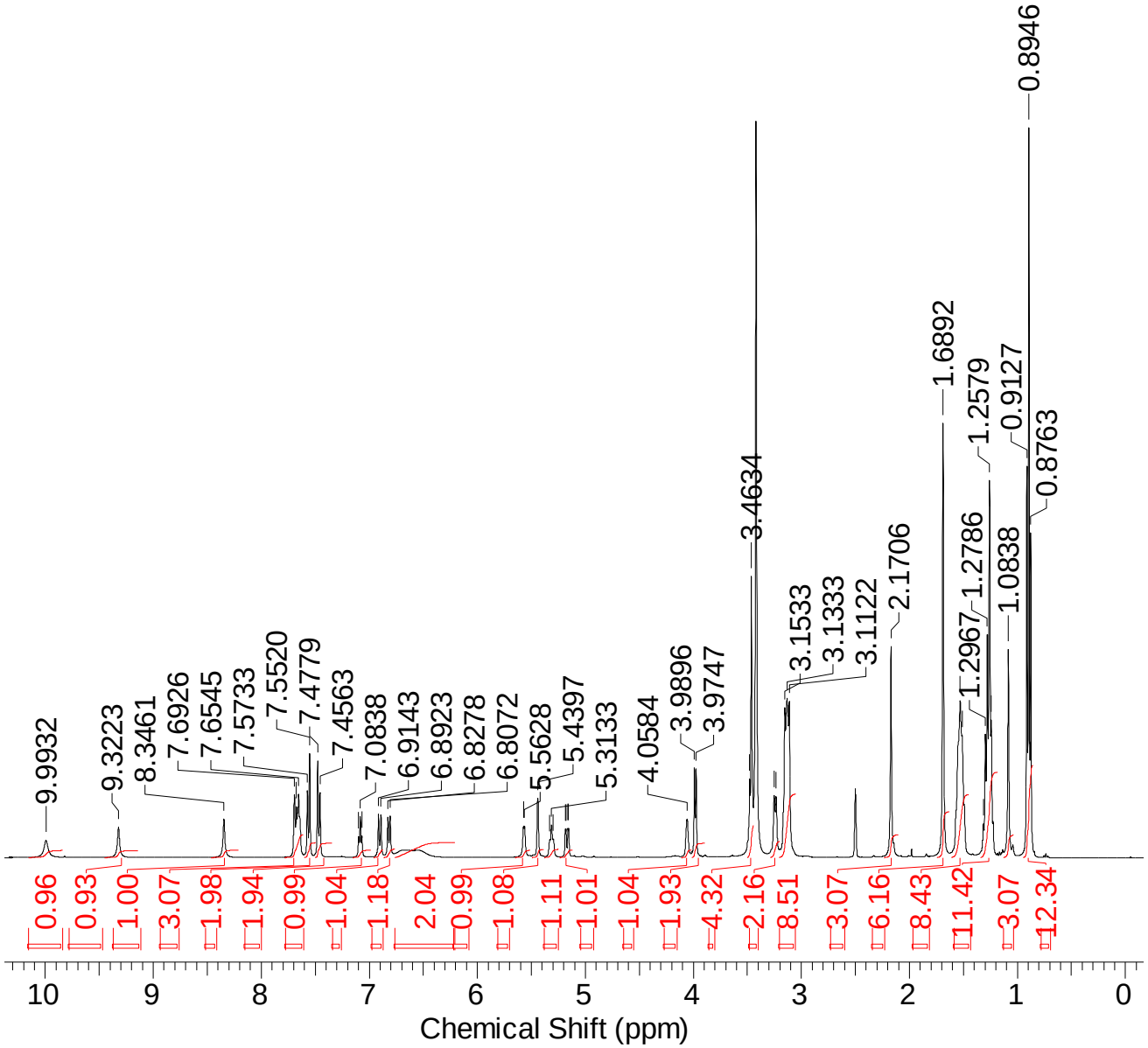


Figure S6 - $^{1}$H NMR of co-formulation ***b*** in DMSO-$d_6$ conducted at 298 K.

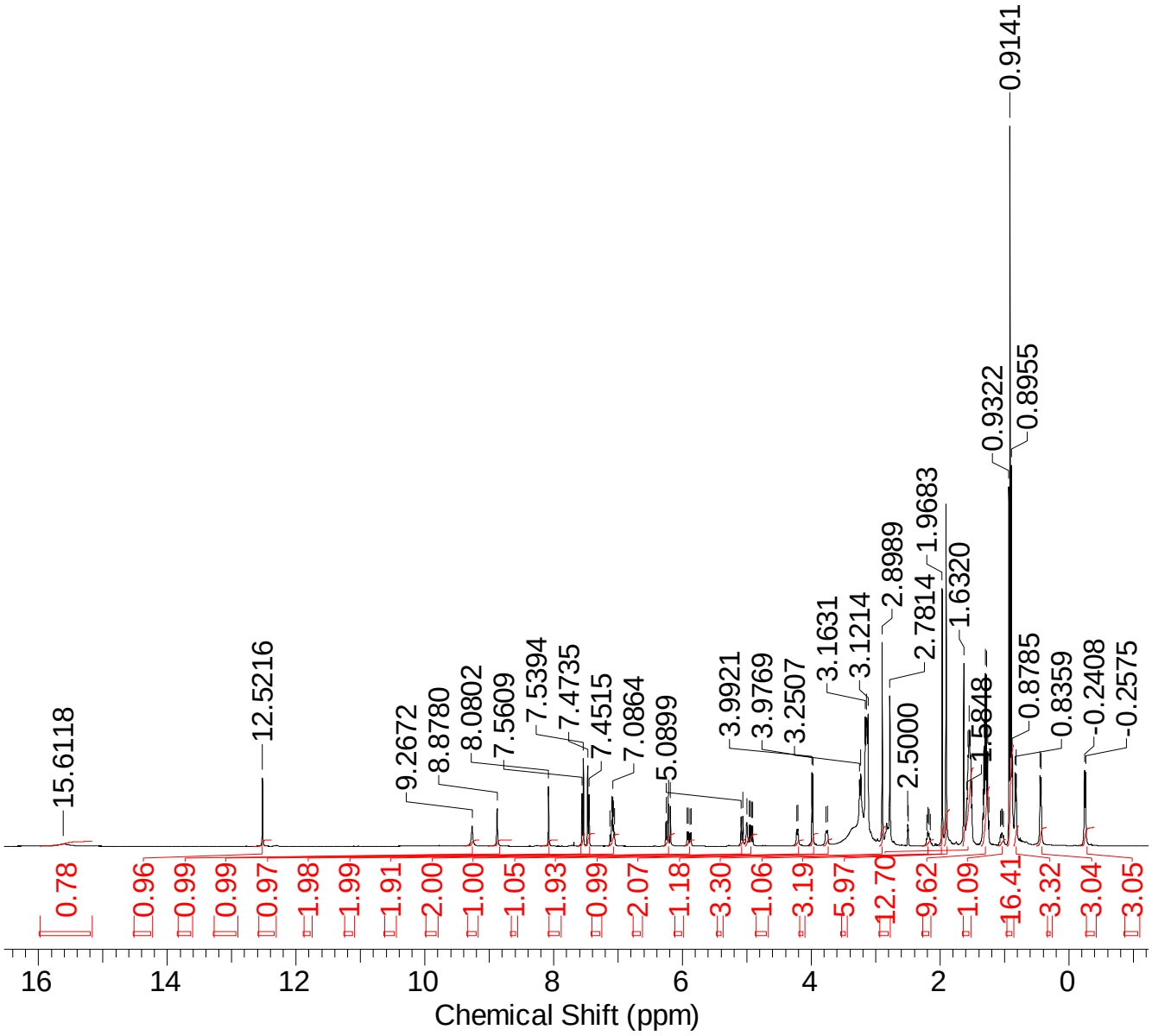


Figure S7 - $^{1}$H NMR of co-formulation ***c*** in DMSO-$d_6$ conducted at 298 K.

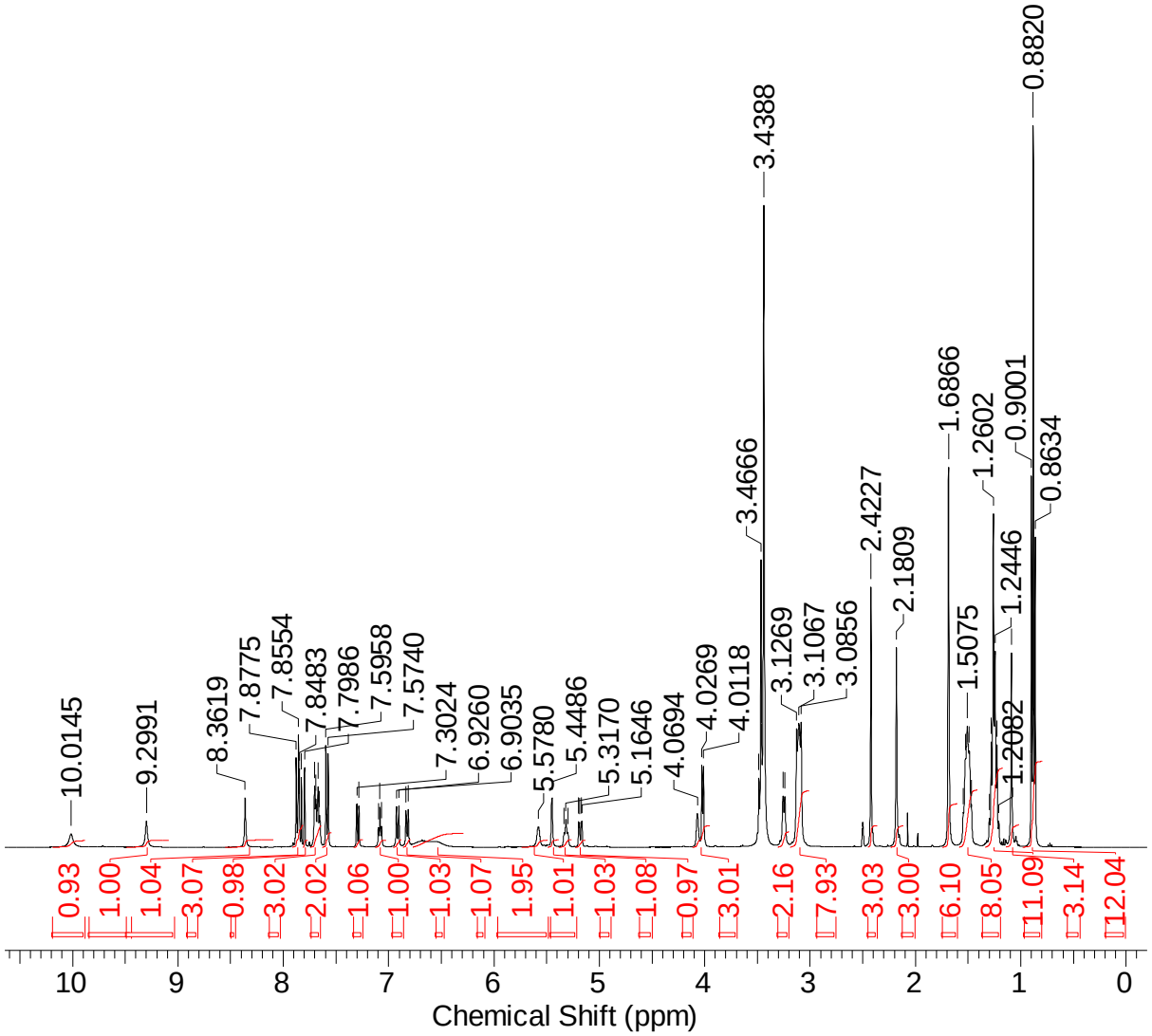


Figure S8 - $^{1}$H NMR of co-formulation ***e*** in DMSO-$d_6$ conducted at 298 K.

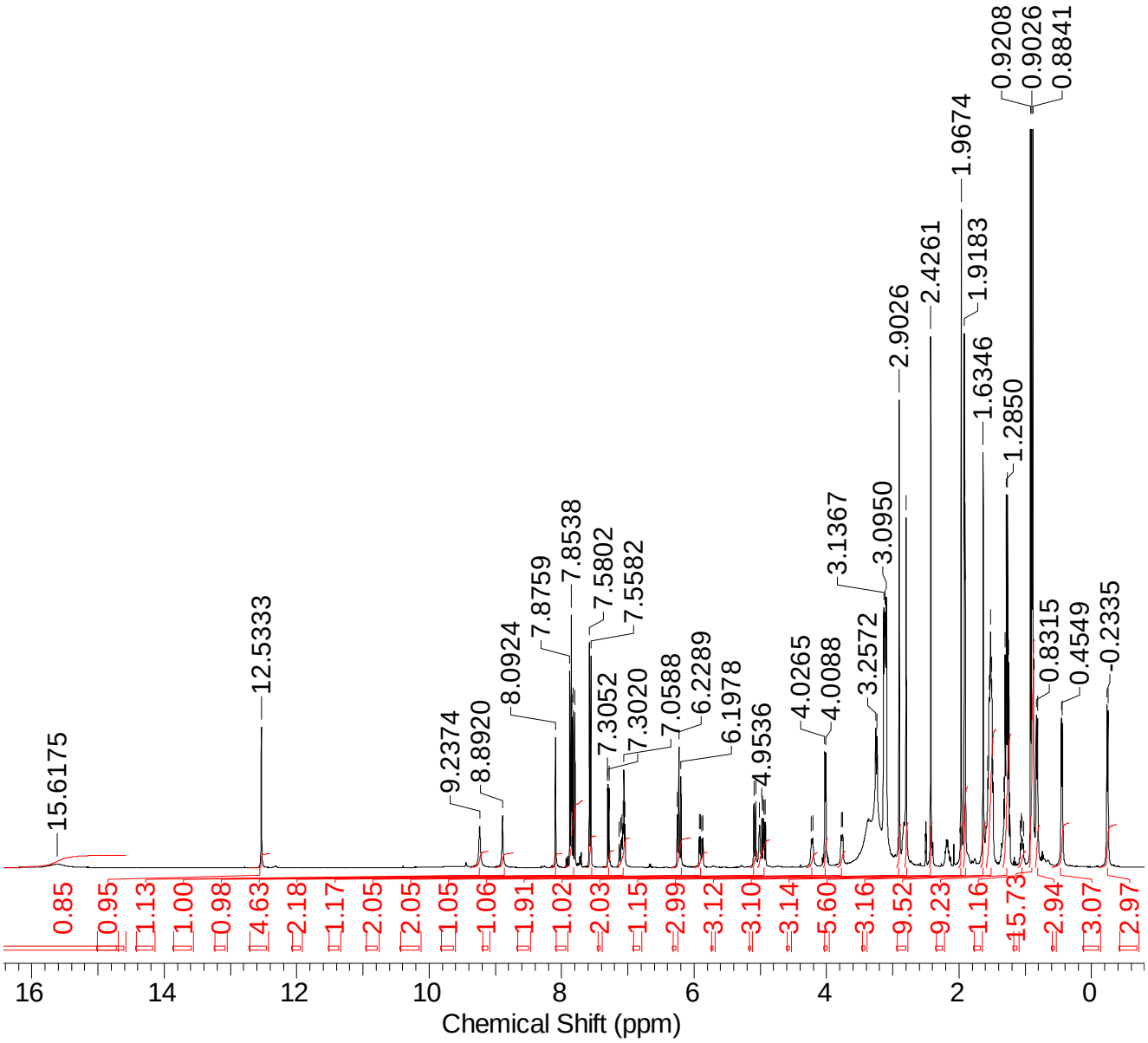


Figure S9 - $^{1}$H NMR of co-formulation ***f*** in DMSO-$d_6$ conducted at 298 K.

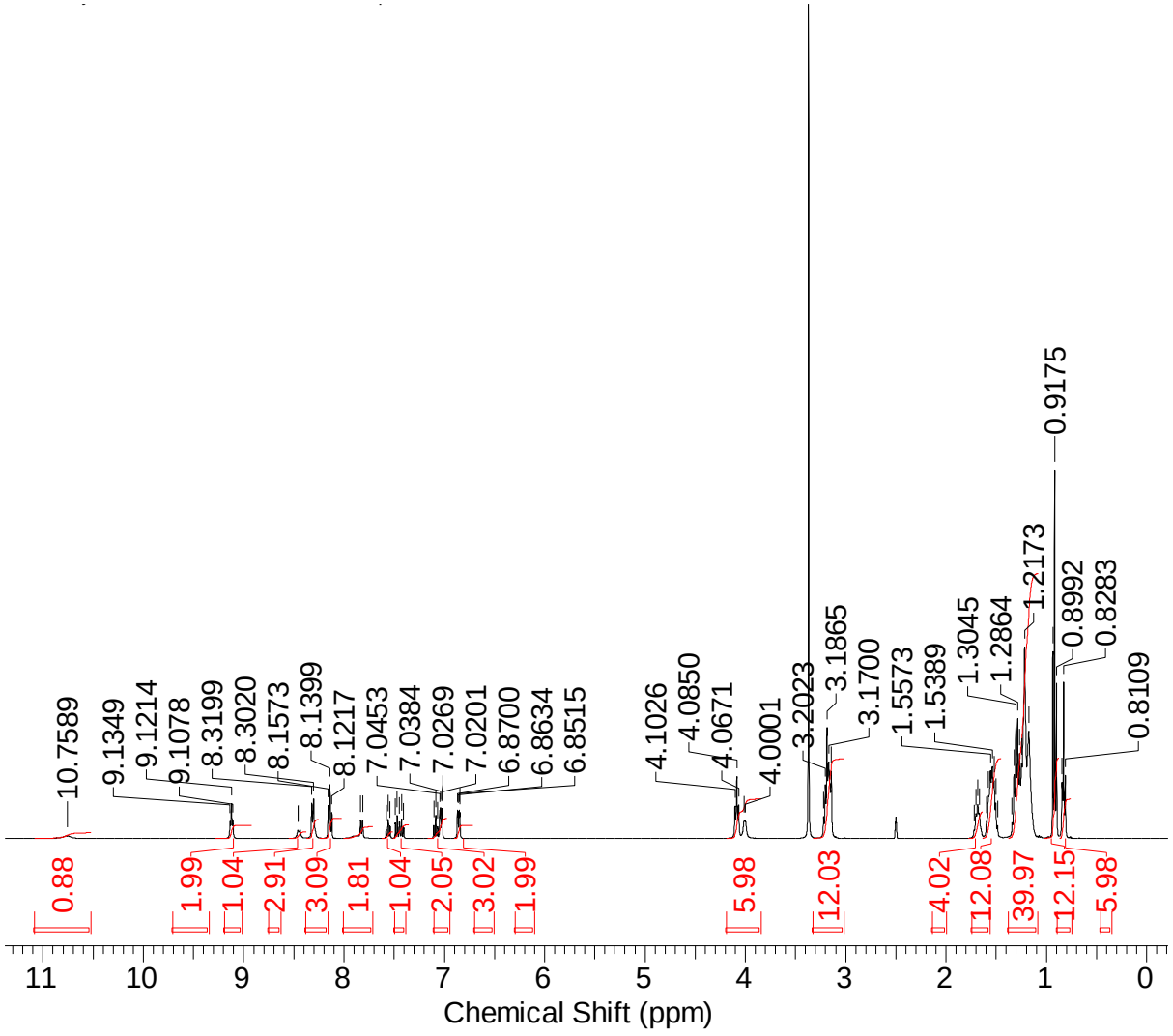


Figure S10 - $^{1}$H NMR of co-formulation ***g*** in DMSO-$d_6$ conducted at 298 K.

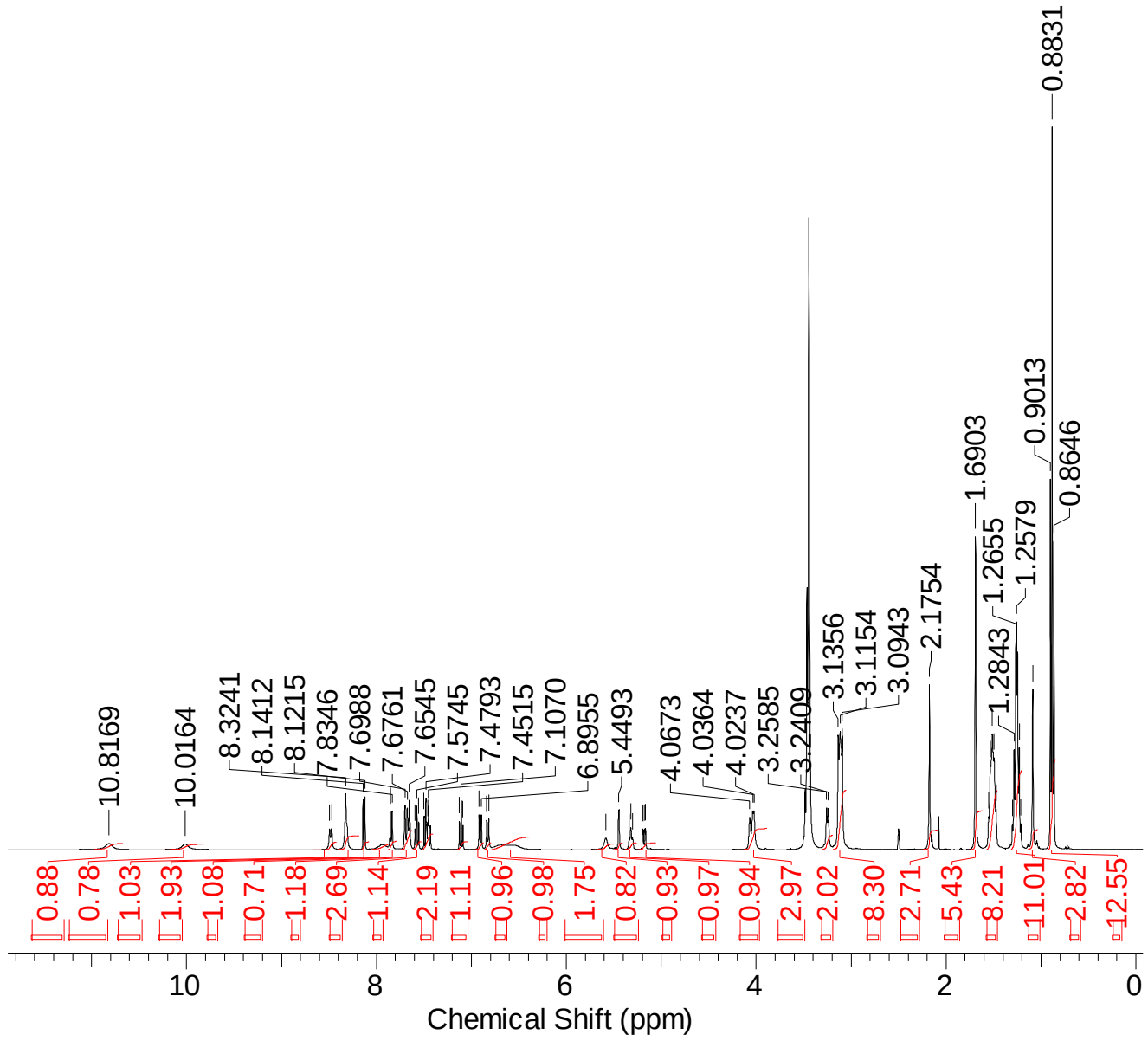


Figure S11 - $^{1}$H NMR of co-formulation ***h*** in DMSO-$d_6$ conducted at 298 K.

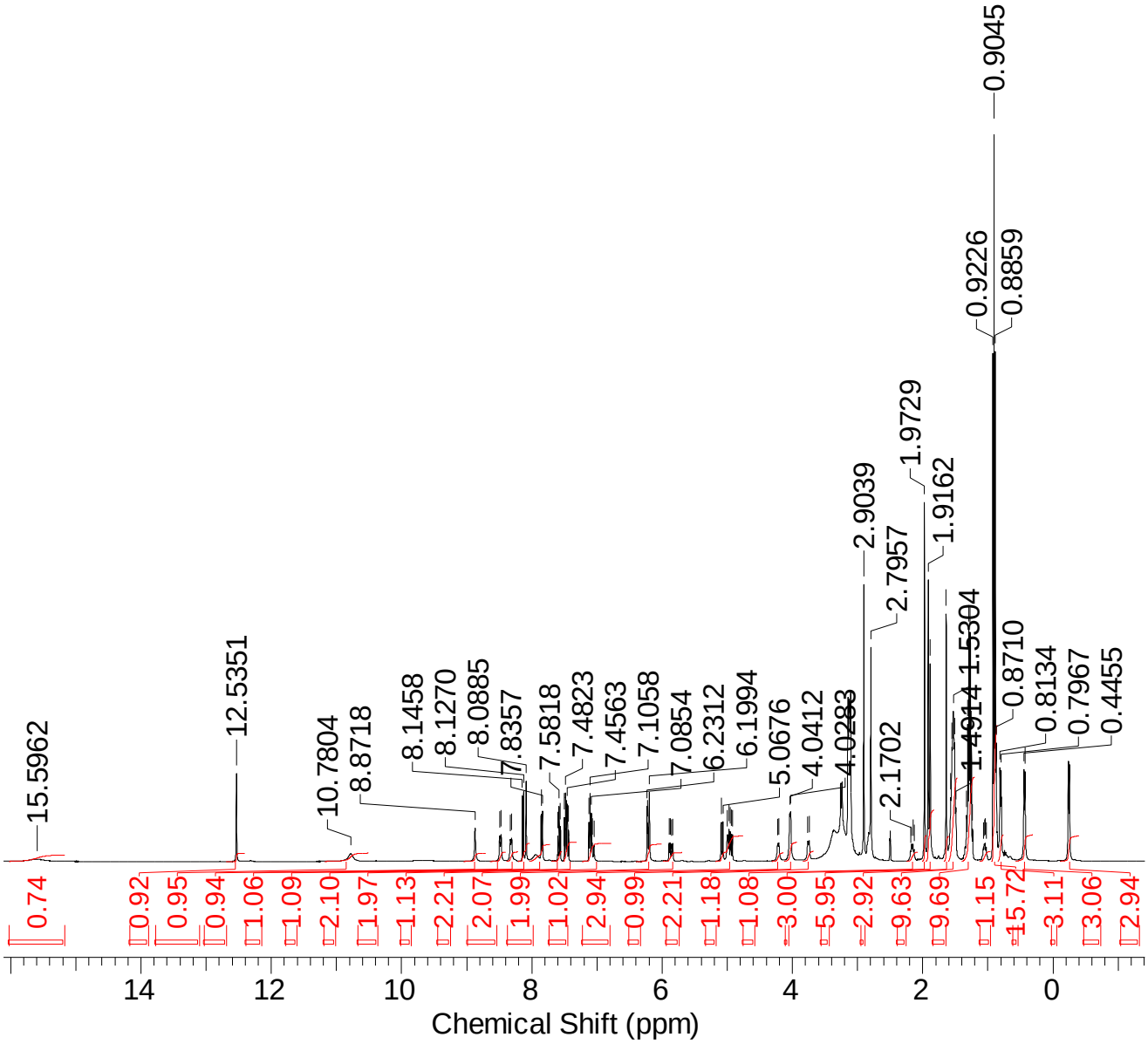


Figure S12 - $^{1}$H NMR of co-formulation ***i*** in DMSO-$d_6$ conducted at 298 K.

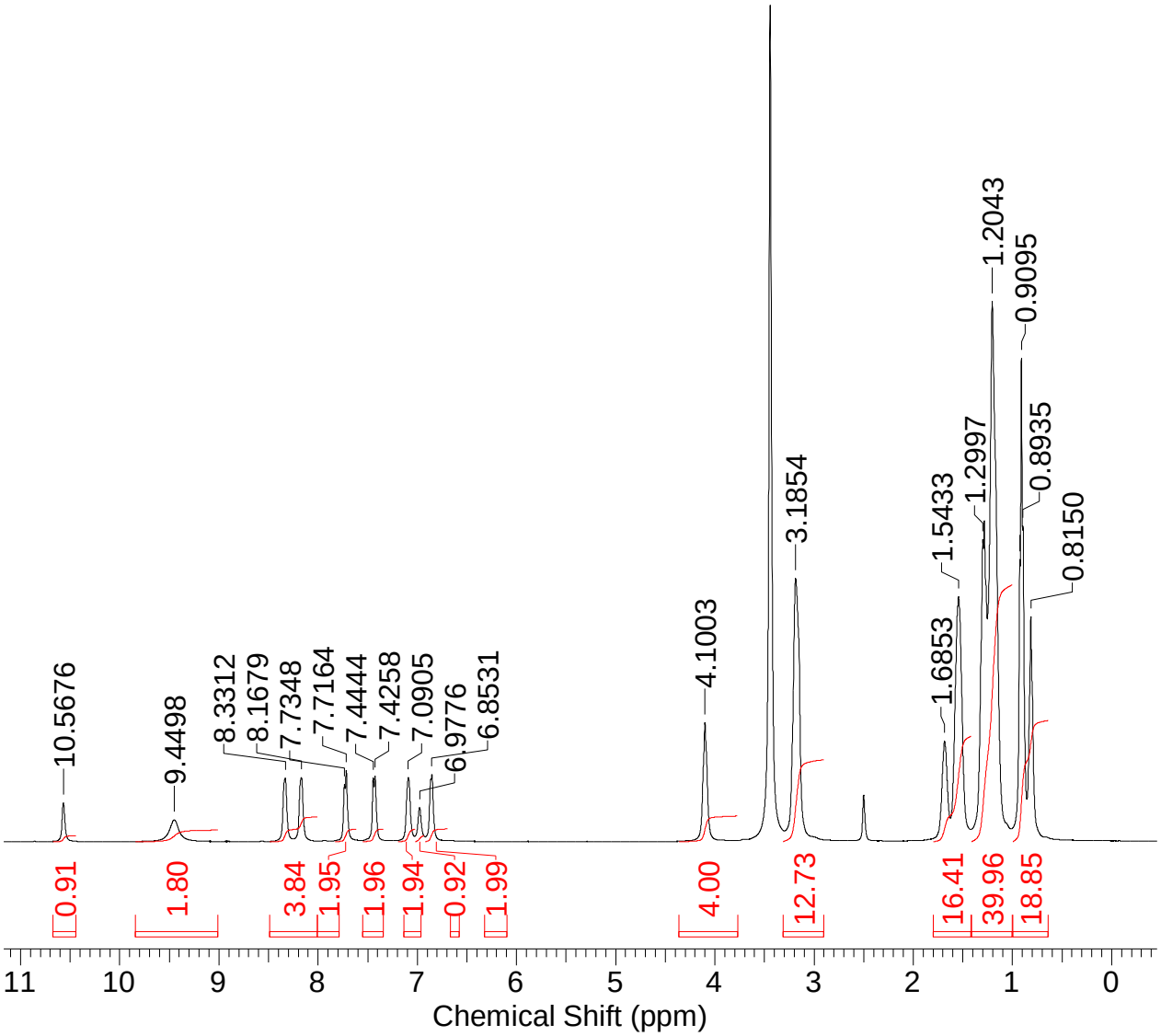


Figure S13 - $^{1}$H NMR of co-formulation ***j*** in DMSO-$d_6$ conducted at 298 K.

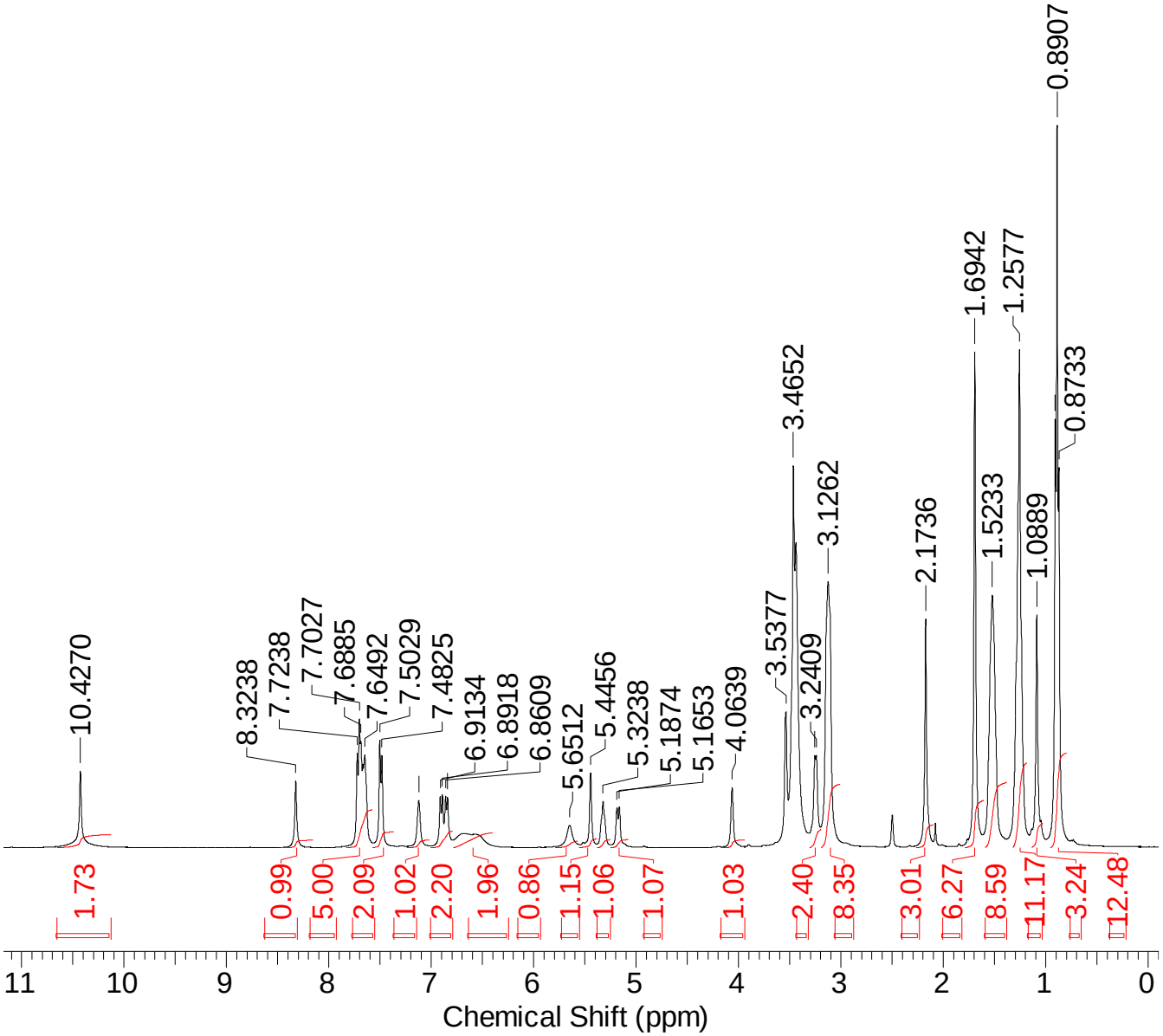


Figure S14 - $^{1}$H NMR of co-formulation ***k*** in DMSO-$d_6$ conducted at 298 K.

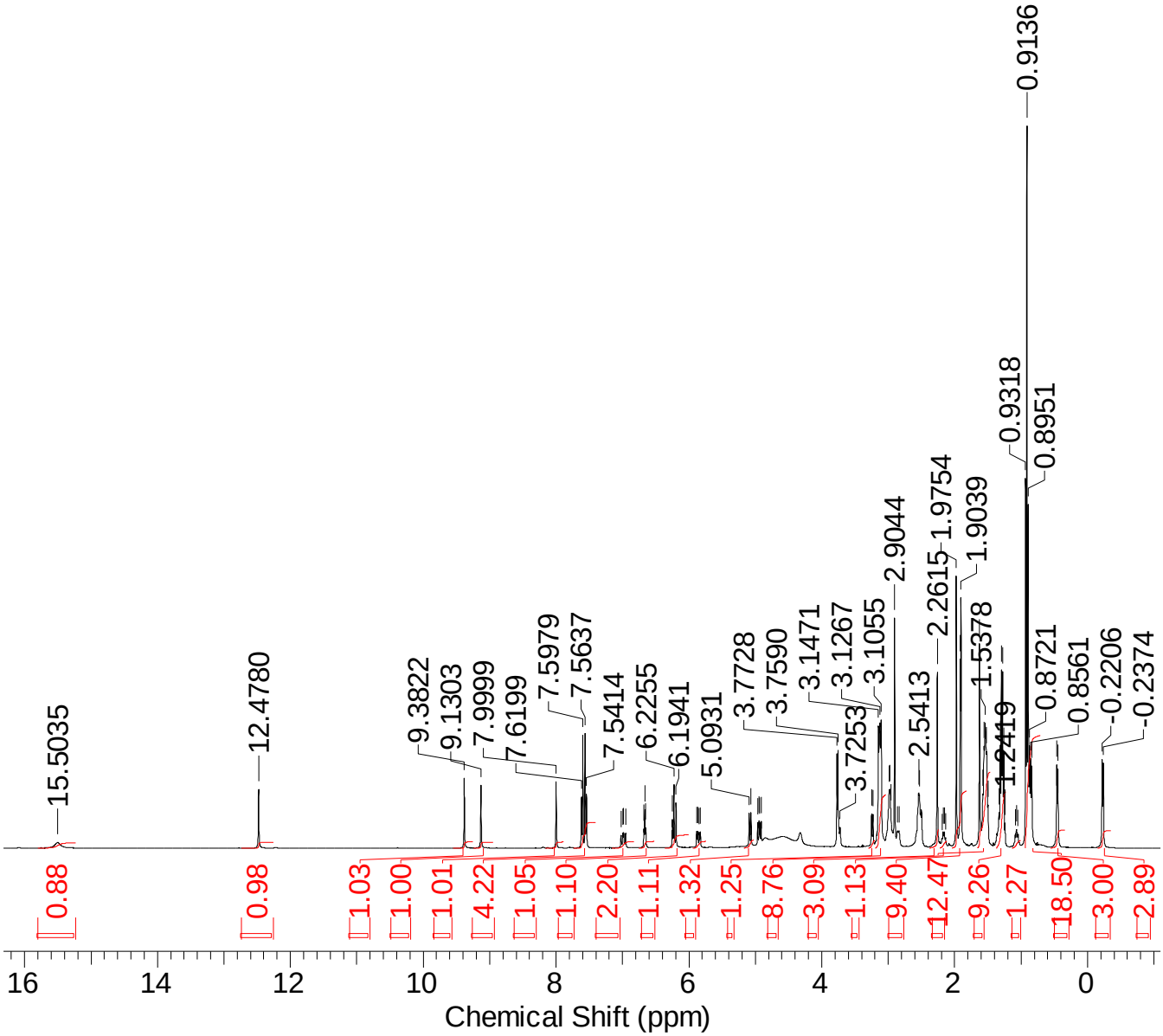


Figure S15 - $^{1}$H NMR of co-formulation ***I*** in DMSO-$d_6$ conducted at 298 K.

## $^1$H DOSY NMR experiments

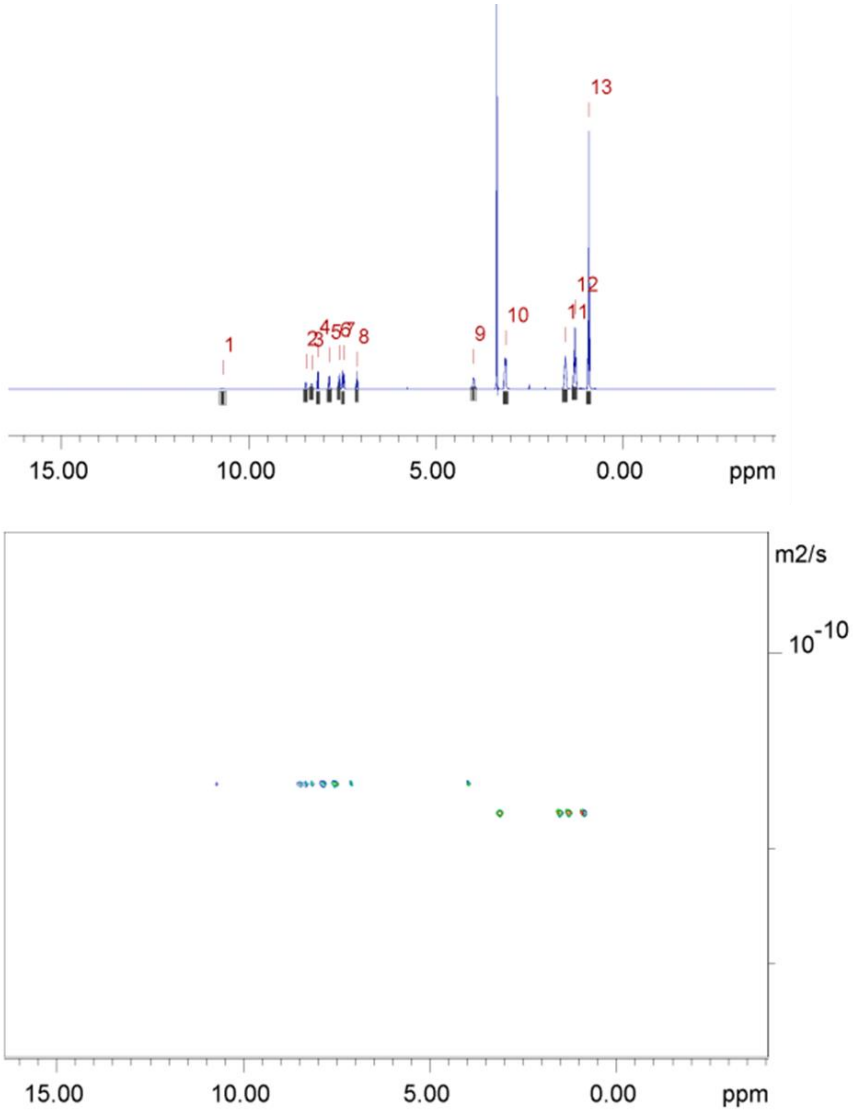


| Peak name | F2 [ppm] | Io | error | D [m2/s] | error |
|---|---|---|---|---|---|
| 1 | 10.691 | 2.03e+08 | 6.072e+04 | 1.60e-10 | 1.047e-13 |
| 2 | 8.474 | 6.98e+08 | 4.875e+04 | 1.59e-10 | 2.432e-14 |
| 3 | 8.316 | 6.45e+08 | 4.626e+04 | 1.59e-10 | 2.498e-14 |
| 4 | 8.143 | 7.51e+08 | 4.228e+04 | 1.59e-10 | 1.964e-14 |
| 5 | 7.842 | 8.99e+08 | 4.876e+04 | 1.59e-10 | 1.890e-14 |
| 6 | 7.590 | 7.91e+08 | 3.935e+04 | 1.59e-10 | 1.733e-14 |
| 7 | 7.477 | 1.62e+09 | 4.361e+04 | 1.59e-10 | 9.394e-15 |
| 8 | 7.107 | 8.06e+08 | 4.080e+04 | 1.59e-10 | 1.765e-14 |
| 9 | 3.991 | 1.22e+09 | 5.443e+04 | 1.59e-10 | 1.546e-14 |
| 10 | 3.137 | 3.93e+09 | 5.497e+04 | 1.77e-10 | 5.348e-15 |
| 11 | 1.547 | 4.42e+09 | 5.376e+04 | 1.75e-10 | 4.629e-15 |
| 12 | 1.292 | 5.61e+09 | 5.370e+04 | 1.76e-10 | 3.645e-15 |
| 13 | 0.915 | 9.26e+09 | 5.139e+04 | 1.76e-10 | 2.114e-15 |

Figure S16 - $^1$H DOSY NMR spectrum of SSA **3** (111.9 mM) in DMSO-$d_6$ at 298 K and a table reporting the diffusion constants calculated for each peak used to determine the hydrodynamic diameter of the anionic component of **3** ($d_H$ = 1.38 nm). Peaks 1-9 correspond to the anionic component of **3** while peaks 10-13 correspond to the cationic component of **3**.

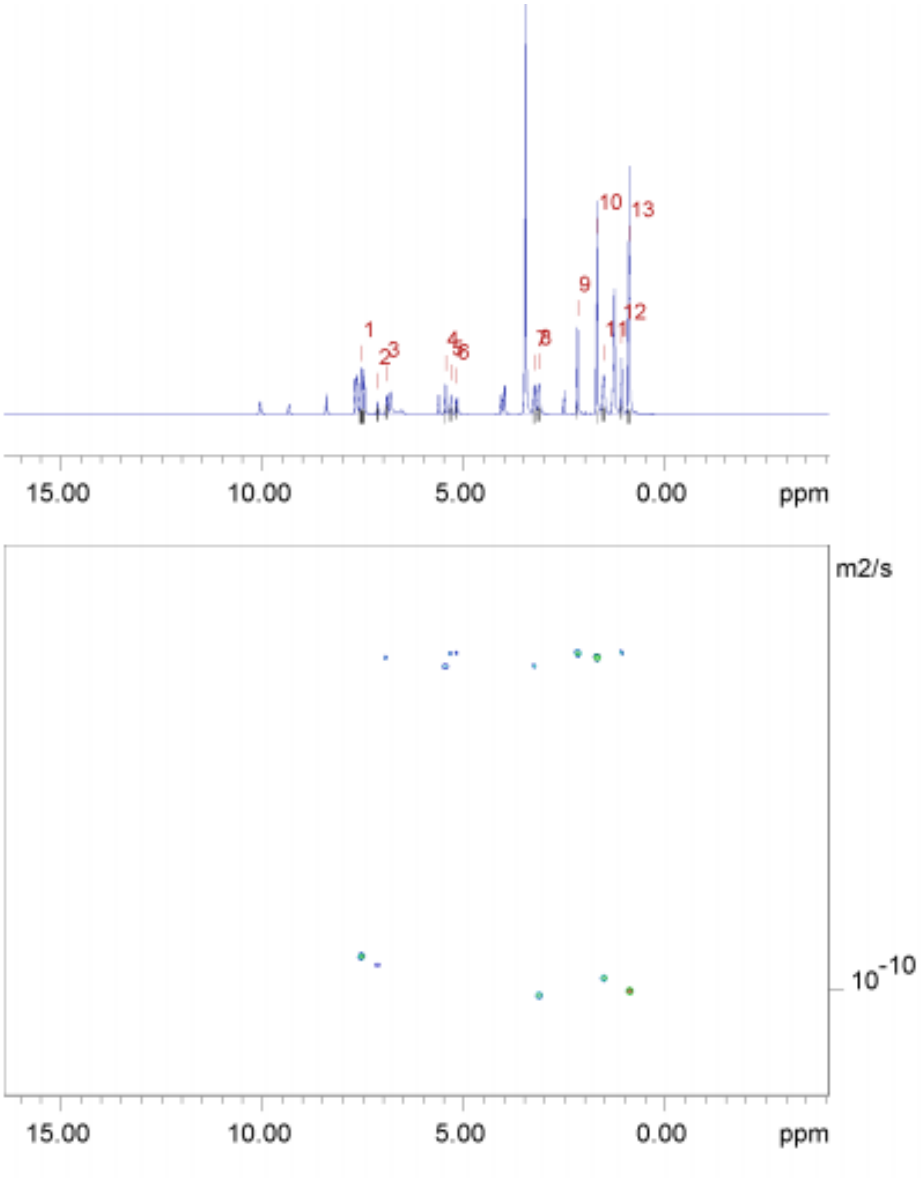


| Peak name | F2 [ppm] | Io | error | D [m2/s] | error |
|---|---|---|---|---|---|
| 1 | 7.521 | 8.23e+09 | 2.509e+05 | 9.46e-11 | 5.902e-15 |
| 2 | 7.133 | 1.02e+09 | 1.345e+05 | 9.57e-11 | 2.569e-14 |
| 3 | 6.912 | 1.78e+09 | 1.178e+05 | 5.58e-11 | 7.750e-15 |
| 4 | 5.450 | 1.62e+09 | 9.453e+04 | 5.69e-11 | 6.980e-15 |
| 5 | 5.317 | 2.02e+09 | 1.320e+05 | 5.57e-11 | 7.647e-15 |
| 6 | 5.174 | 1.32e+09 | 1.061e+05 | 5.55e-11 | 9.419e-15 |
| 7 | 3.247 | 2.70e+09 | 1.109e+05 | 5.67e-11 | 4.901e-15 |
| 8 | 3.135 | 4.31e+09 | 1.615e+05 | 1.01e-10 | 7.723e-15 |
| 9 | 2.174 | 4.47e+09 | 9.331e+04 | 5.56e-11 | 2.442e-15 |
| 10 | 1.690 | 9.88e+09 | 8.911e+04 | 5.58e-11 | 1.057e-15 |
| 11 | 1.526 | 5.97e+09 | 1.743e+05 | 9.77e-11 | 5.831e-15 |
| 12 | 1.083 | 2.61e+09 | 8.386e+04 | 5.56e-11 | 3.759e-15 |
| 13 | 0.896 | 2.31e+10 | 1.685e+05 | 1.01e-10 | 1.497e-15 |

Figure S17 - $^{1}$H DOSY NMR spectrum of co-formulation ***b*** (113.6 mM) in DMSO-$d_6$ at 298 K and a table reporting the diffusion constants calculated for each peak used to determine the hydrodynamic diameter of the anionic components of ***b*** ($d_H$ = 2.30 nm). Peaks 1 and 2 correspond to the anionic component of ***b*** while peaks 8, 11 and 13 correspond to the cationic component of ***b***. Peaks 3-7, 9-10 and 12 correspond to the drug component, novobiocin.

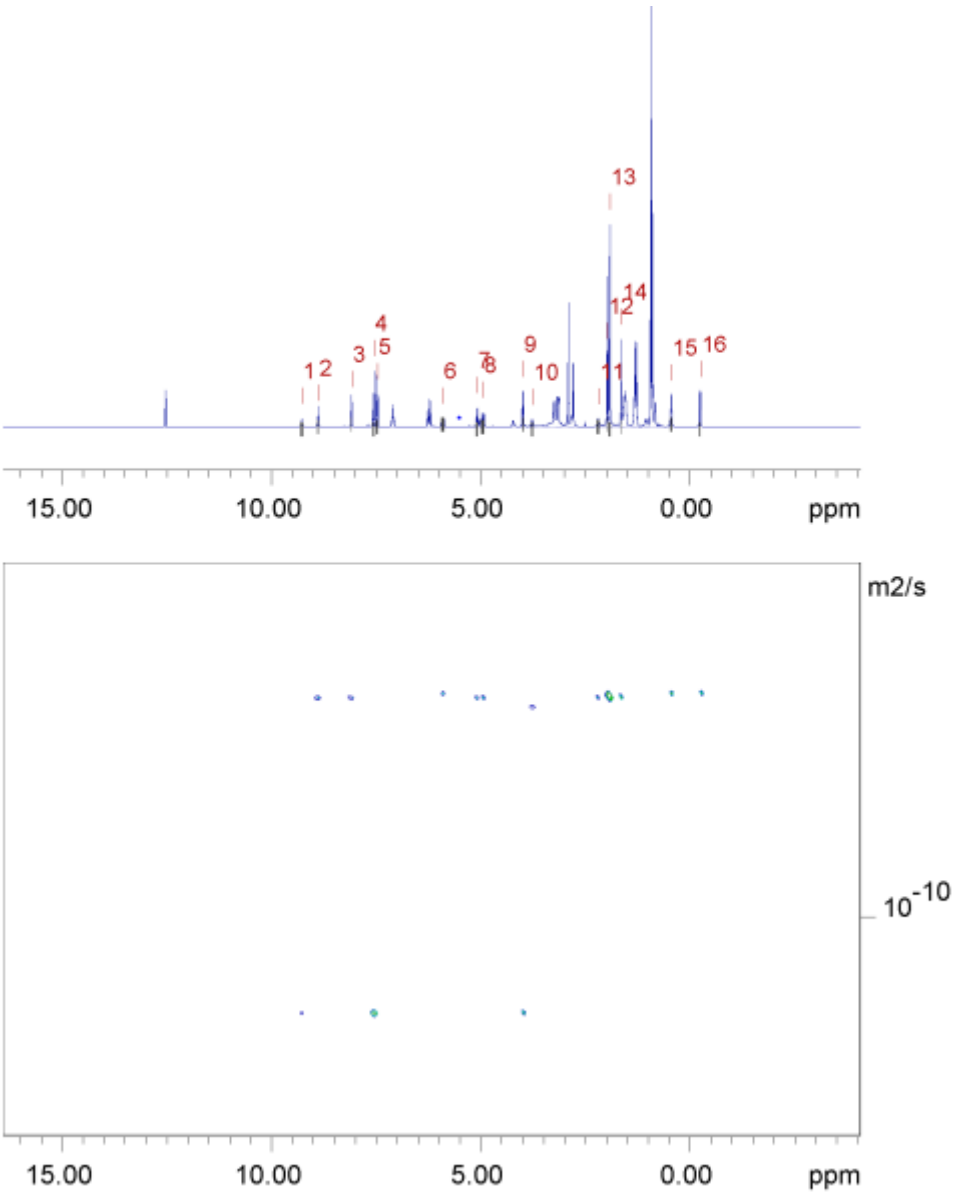


| Peak name | F2 [ppm] | Io | error | D [m2/s] | error |
|---|---|---|---|---|---|
| 1 | 9.277 | 6.02e+08 | 8.989e+04 | 1.15e-10 | 3.330e-14 |
| 2 | 8.888 | 8.50e+08 | 6.143e+04 | 7.25e-11 | 1.059e-14 |
| 3 | 8.087 | 7.15e+08 | 3.676e+04 | 7.24e-11 | 7.531e-15 |
| 4 | 7.558 | 2.26e+09 | 6.896e+04 | 1.15e-10 | 6.758e-15 |
| 5 | 7.474 | 2.38e+09 | 7.662e+04 | 1.15e-10 | 7.160e-15 |
| 6 | 5.907 | 1.02e+09 | 8.179e+04 | 7.23e-11 | 1.176e-14 |
| 7 | 5.093 | 1.01e+09 | 6.962e+04 | 7.25e-11 | 1.011e-14 |
| 8 | 4.947 | 1.19e+09 | 8.367e+04 | 7.28e-11 | 1.033e-14 |
| 9 | 3.994 | 1.67e+09 | 6.381e+04 | 1.15e-10 | 8.493e-15 |
| 10 | 3.770 | 6.22e+08 | 5.942e+04 | 7.38e-11 | 1.423e-14 |
| 11 | 2.192 | 9.73e+08 | 7.863e+04 | 7.28e-11 | 1.190e-14 |
| 12 | 1.973 | 3.30e+09 | 4.950e+04 | 7.23e-11 | 2.197e-15 |
| 13 | 1.916 | 6.01e+09 | 5.691e+04 | 7.25e-11 | 1.387e-15 |
| 14 | 1.643 | 1.99e+09 | 4.046e+04 | 7.26e-11 | 2.988e-15 |
| 15 | 0.448 | 2.21e+09 | 6.356e+04 | 7.20e-11 | 4.199e-15 |
| 16 | -0.243 | 1.77e+09 | 4.914e+04 | 7.21e-11 | 4.064e-15 |

Figure S18 - $^{1}$H DOSY NMR spectrum of co-formulation ***c*** (113.8 mM) in DMSO-$d_6$ at 298 K and a table reporting the diffusion constants calculated for each peak used to determine the hydrodynamic diameter of the anionic components of ***c*** ($d_H$ = 1.91 nm). Peaks 1, 4-5 and 9 correspond to the anionic component of ***c*** while peaks 2-3, 6-8 and 10-16 and 12 correspond to the drug component, rifampicin.

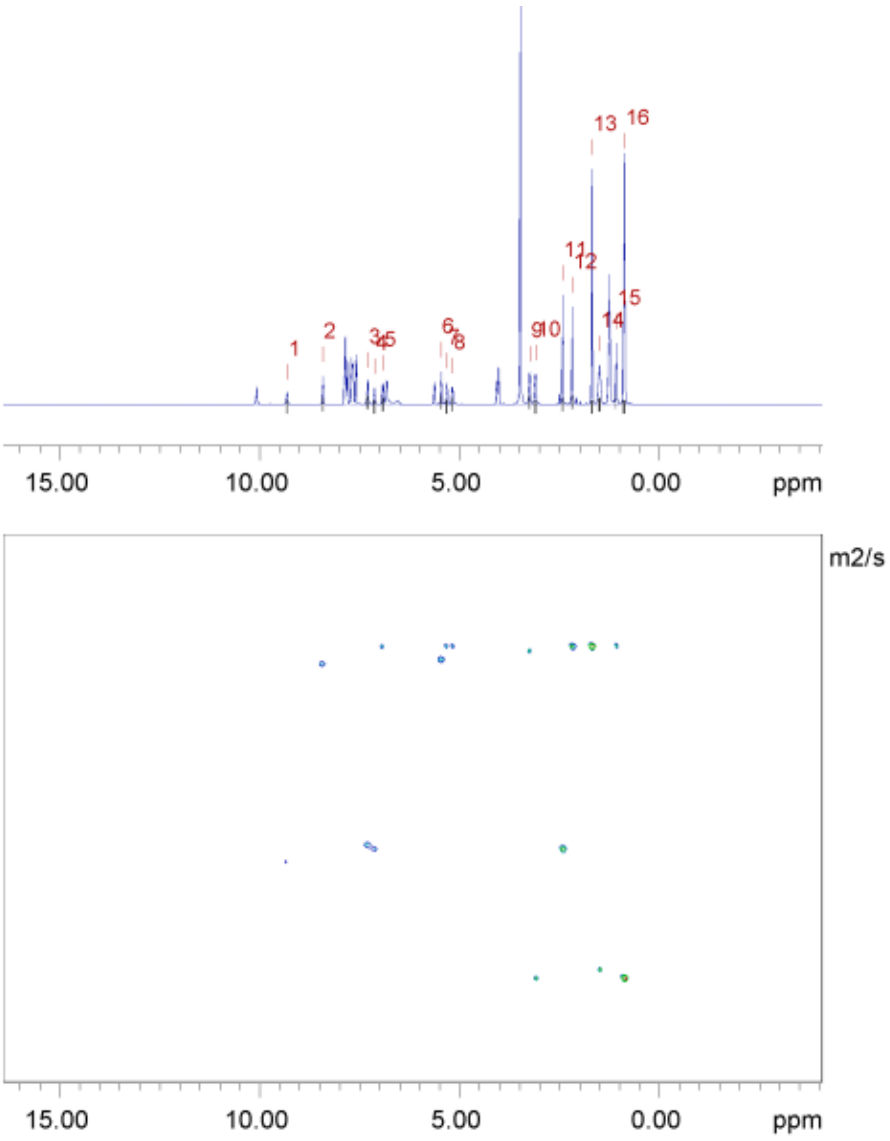


| Peak name | F2 [ppm] | Io | error | D [m2/s] | error |
|---|---|---|---|---|---|
| 1 | 9.315 | 9.58e+08 | 1.111e+05 | 7.12e-11 | 1.755e-14 |
| 2 | 8.421 | 1.69e+09 | 9.619e+04 | 5.04e-11 | 6.237e-15 |
| 3 | 7.299 | 2.06e+09 | 1.139e+05 | 6.90e-11 | 8.137e-15 |
| 4 | 7.128 | 1.36e+09 | 1.174e+05 | 6.97e-11 | 1.279e-14 |
| 5 | 6.918 | 2.17e+09 | 1.155e+05 | 4.92e-11 | 5.722e-15 |
| 6 | 5.458 | 1.99e+09 | 9.663e+04 | 5.03e-11 | 5.310e-15 |
| 7 | 5.318 | 1.87e+09 | 1.063e+05 | 4.89e-11 | 6.084e-15 |
| 8 | 5.185 | 1.62e+09 | 1.059e+05 | 4.90e-11 | 6.987e-15 |
| 9 | 3.246 | 3.05e+09 | 1.067e+05 | 4.96e-11 | 3.782e-15 |
| 10 | 3.101 | 4.37e+09 | 1.510e+05 | 8.68e-11 | 6.313e-15 |
| 11 | 2.422 | 6.12e+09 | 1.099e+05 | 6.97e-11 | 2.664e-15 |
| 12 | 2.185 | 5.70e+09 | 9.899e+04 | 4.89e-11 | 1.858e-15 |
| 13 | 1.689 | 1.36e+10 | 1.025e+05 | 4.90e-11 | 8.084e-16 |
| 14 | 1.500 | 5.80e+09 | 1.566e+05 | 8.55e-11 | 4.865e-15 |
| 15 | 1.084 | 2.58e+09 | 7.081e+04 | 4.92e-11 | 2.949e-15 |
| 16 | 0.880 | 2.43e+10 | 1.550e+05 | 8.73e-11 | 1.173e-15 |

Figure S19 - $^{1}$H DOSY NMR spectrum of co-formulation ***e*** (111.7 mM) in DMSO-$d_6$ at 298 K and a table reporting the diffusion constants calculated for each peak used to determine the hydrodynamic diameter of the anionic components of ***e*** ($d_H$ = 3.2 nm). Peaks 1, 3-4 and 11 correspond to the anionic component of ***e*** while peaks 10, 14 and 16 correspond to the cationic component of ***e***. Peaks 2, 5-9, 12-13 and 15 correspond to the drug component, novobiocin.

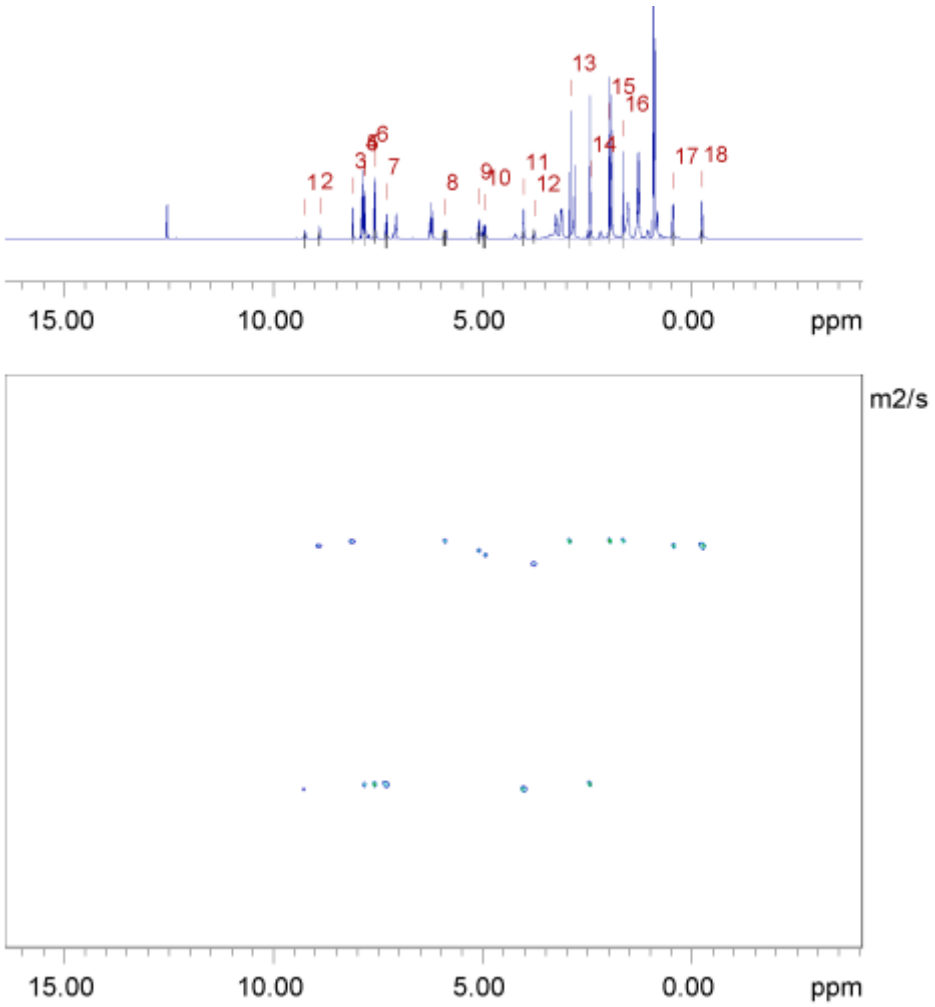


| Peak name | F2 [ppm] | Io | error | D [m2/s] | error |
|---|---|---|---|---|---|
| 1 | 9.249 | 6.91e+08 | 9.627e+04 | 8.89e-11 | 2.282e-14 |
| 2 | 8.903 | 8.99e+08 | 9.291e+04 | 6.76e-11 | 1.317e-14 |
| 3 | 8.101 | 9.83e+08 | 6.439e+04 | 6.73e-11 | 8.309e-15 |
| 4 | 7.832 | 7.04e+08 | 4.731e+04 | 8.85e-11 | 1.095e-14 |
| 5 | 7.809 | 1.46e+09 | 5.957e+04 | 8.86e-11 | 6.638e-15 |
| 6 | 7.577 | 3.36e+09 | 1.013e+05 | 8.86e-11 | 4.910e-15 |
| 7 | 7.303 | 1.72e+09 | 1.013e+05 | 8.84e-11 | 9.576e-15 |
| 8 | 5.902 | 1.44e+09 | 1.336e+05 | 6.74e-11 | 1.179e-14 |
| 9 | 5.092 | 1.35e+09 | 9.797e+04 | 6.79e-11 | 9.249e-15 |
| 10 | 4.957 | 1.29e+09 | 1.155e+05 | 6.83e-11 | 1.150e-14 |
| 11 | 4.026 | 2.38e+09 | 9.485e+04 | 8.91e-11 | 6.534e-15 |
| 12 | 3.775 | 8.73e+08 | 9.761e+04 | 6.89e-11 | 1.448e-14 |
| 13 | 2.913 | 3.76e+09 | 7.021e+04 | 6.73e-11 | 2.367e-15 |
| 14 | 2.435 | 3.92e+09 | 6.623e+04 | 8.85e-11 | 2.749e-15 |
| 15 | 1.976 | 3.93e+09 | 6.064e+04 | 6.73e-11 | 1.955e-15 |
| 16 | 1.643 | 2.19e+09 | 5.157e+04 | 6.72e-11 | 2.986e-15 |
| 17 | 0.457 | 2.53e+09 | 8.354e+04 | 6.75e-11 | 4.205e-15 |
| 18 | -0.236 | 2.64e+09 | 8.213e+04 | 6.76e-11 | 3.961e-15 |

Figure S20 - $^{1}$H DOSY NMR spectrum of co-formulation ***f*** (112.3 mM) in DMSO-$d_6$ at 298 K and a table reporting the diffusion constants calculated for each peak used to determine the hydrodynamic diameter of the anionic components of ***f*** ($d_H$ = 2.53 nm). Peaks 1, 4-7, 11 and 14 correspond to the anionic component of ***f*** while peaks 2-3, 8-10, 12-13 and 15-18 correspond to the drug component, rifampicin.

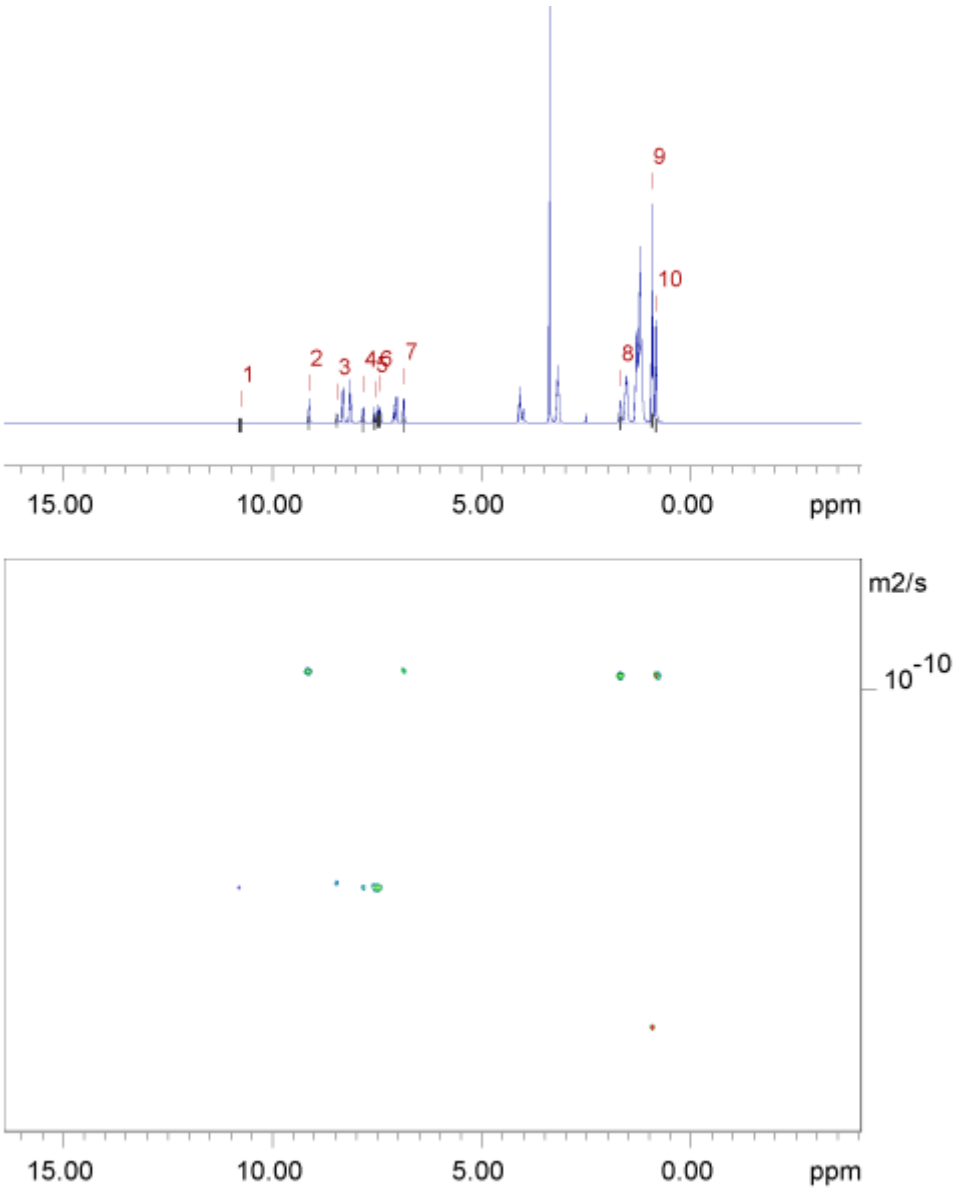


| Peak name | F2 [ppm] | Io | error | D [m2/s] | error |
|---|---|---|---|---|---|
| 1 | 10.768 | 2.39e+08 | 1.807e+05 | 1.40e-10 | 2.292e-13 |
| 2 | 9.129 | 1.70e+09 | 1.050e+05 | 9.73e-11 | 1.337e-14 |
| 3 | 8.457 | 6.71e+08 | 1.049e+05 | 1.39e-10 | 4.705e-14 |
| 4 | 7.832 | 9.00e+08 | 9.914e+04 | 1.39e-10 | 3.333e-14 |
| 5 | 7.562 | 1.18e+09 | 1.353e+05 | 1.39e-10 | 3.466e-14 |
| 6 | 7.460 | 2.64e+09 | 1.913e+05 | 1.39e-10 | 2.185e-14 |
| 7 | 6.864 | 2.17e+09 | 1.046e+05 | 9.74e-11 | 1.040e-14 |
| 8 | 1.693 | 2.45e+09 | 1.179e+05 | 9.76e-11 | 1.043e-14 |
| 9 | 0.926 | 1.49e+10 | 1.505e+05 | 1.75e-10 | 3.814e-15 |
| 10 | 0.831 | 6.87e+09 | 1.138e+05 | 9.82e-11 | 3.609e-15 |

Figure S21 - $^{1}$H DOSY NMR spectrum of co-formulation ***g*** (112.4 mM) in DMSO-$d_6$ at 298 K and a table reporting the diffusion constants calculated for each peak used to determine the hydrodynamic diameter of the anionic components of ***g*** ($d_H$ = 1.14 nm). Peaks 1 and 3-6 correspond to the anionic component of ***e*** while peak 9 corresponds to the cationic component of ***e***. Peaks 2, 7-8 and 10 correspond to the drug component, octenidine.

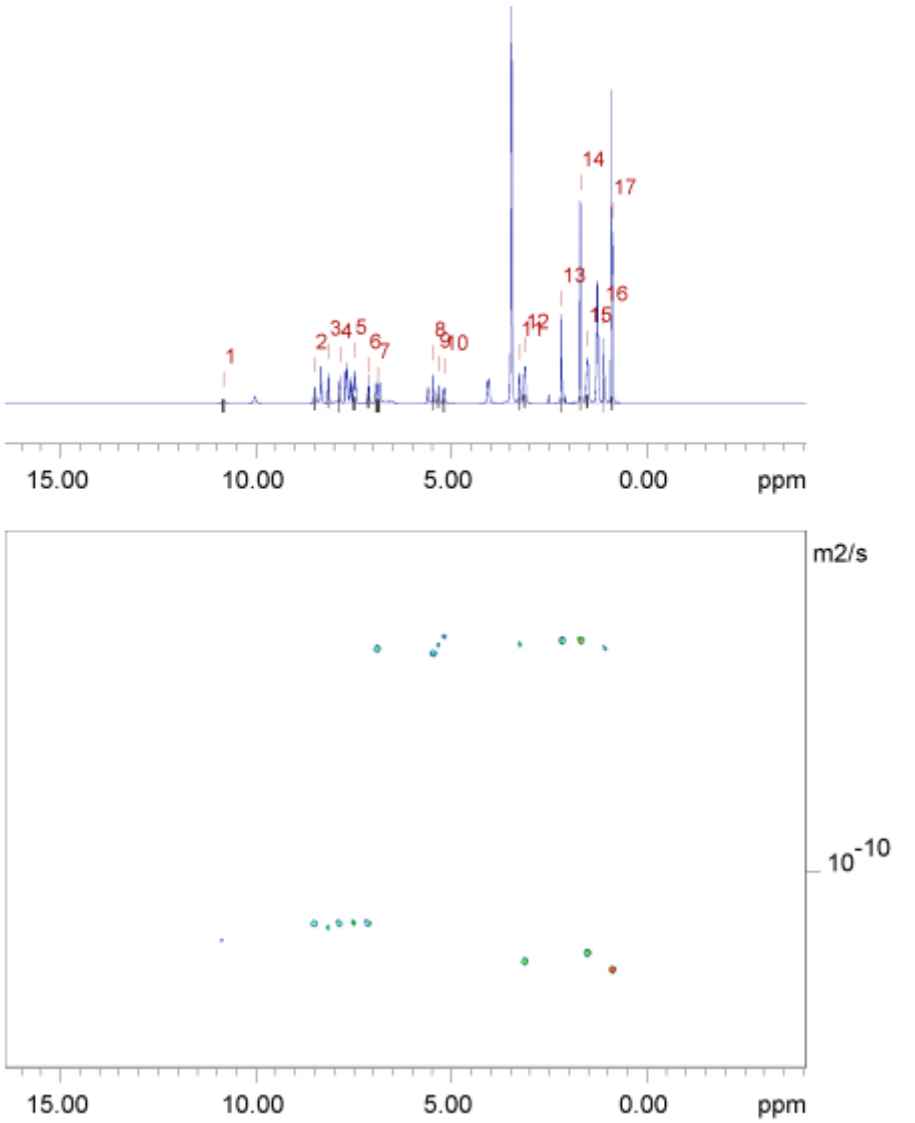


| Peak name | F2 [ppm] | Io | error | D [m2/s] | error |
|---|---|---|---|---|---|
| 1 | 10.835 | 4.34e+08 | 1.706e+05 | 1.13e-10 | 9.421e-14 |
| 2 | 8.496 | 1.65e+09 | 1.218e+05 | 1.10e-10 | 1.727e-14 |
| 3 | 8.145 | 1.99e+09 | 1.114e+05 | 1.11e-10 | 1.319e-14 |
| 4 | 7.858 | 1.85e+09 | 1.066e+05 | 1.10e-10 | 1.348e-14 |
| 5 | 7.480 | 4.31e+09 | 1.583e+05 | 1.09e-10 | 8.551e-15 |
| 6 | 7.122 | 1.98e+09 | 1.261e+05 | 1.10e-10 | 1.488e-14 |
| 7 | 6.881 | 3.57e+09 | 1.711e+05 | 6.74e-11 | 7.109e-15 |
| 8 | 5.458 | 1.40e+09 | 7.845e+04 | 6.79e-11 | 8.330e-15 |
| 9 | 5.333 | 1.45e+09 | 9.931e+04 | 6.68e-11 | 1.003e-14 |
| 10 | 5.193 | 1.30e+09 | 9.537e+04 | 6.62e-11 | 1.072e-14 |
| 11 | 3.261 | 2.63e+09 | 9.936e+04 | 6.69e-11 | 5.555e-15 |
| 12 | 3.127 | 4.92e+09 | 1.365e+05 | 1.17e-10 | 6.892e-15 |
| 13 | 2.185 | 4.13e+09 | 8.289e+04 | 6.63e-11 | 2.932e-15 |
| 14 | 1.697 | 1.05e+10 | 9.543e+04 | 6.63e-11 | 1.326e-15 |
| 15 | 1.523 | 6.54e+09 | 1.455e+05 | 1.16e-10 | 5.461e-15 |
| 16 | 1.100 | 1.94e+09 | 5.612e+04 | 6.76e-11 | 4.306e-15 |
| 17 | 0.895 | 2.18e+10 | 1.289e+05 | 1.19e-10 | 1.488e-15 |

Figure 22 - $^{1}$H DOSY NMR spectrum of co-formulation ***h*** (111.9 mM) in DMSO-$d_6$ at 298 K and a table reporting the diffusion constants calculated for each peak used to determine the hydrodynamic diameter of the anionic components of ***h*** ($d_H$ = 1.99 nm). Peaks 1-6 correspond to the anionic component of ***h*** while peaks 12, 15 and 17 correspond to the cationic component of ***h.*** Peaks 2, 7-11, 13-14 and 16 correspond to the drug component, novobiocin.

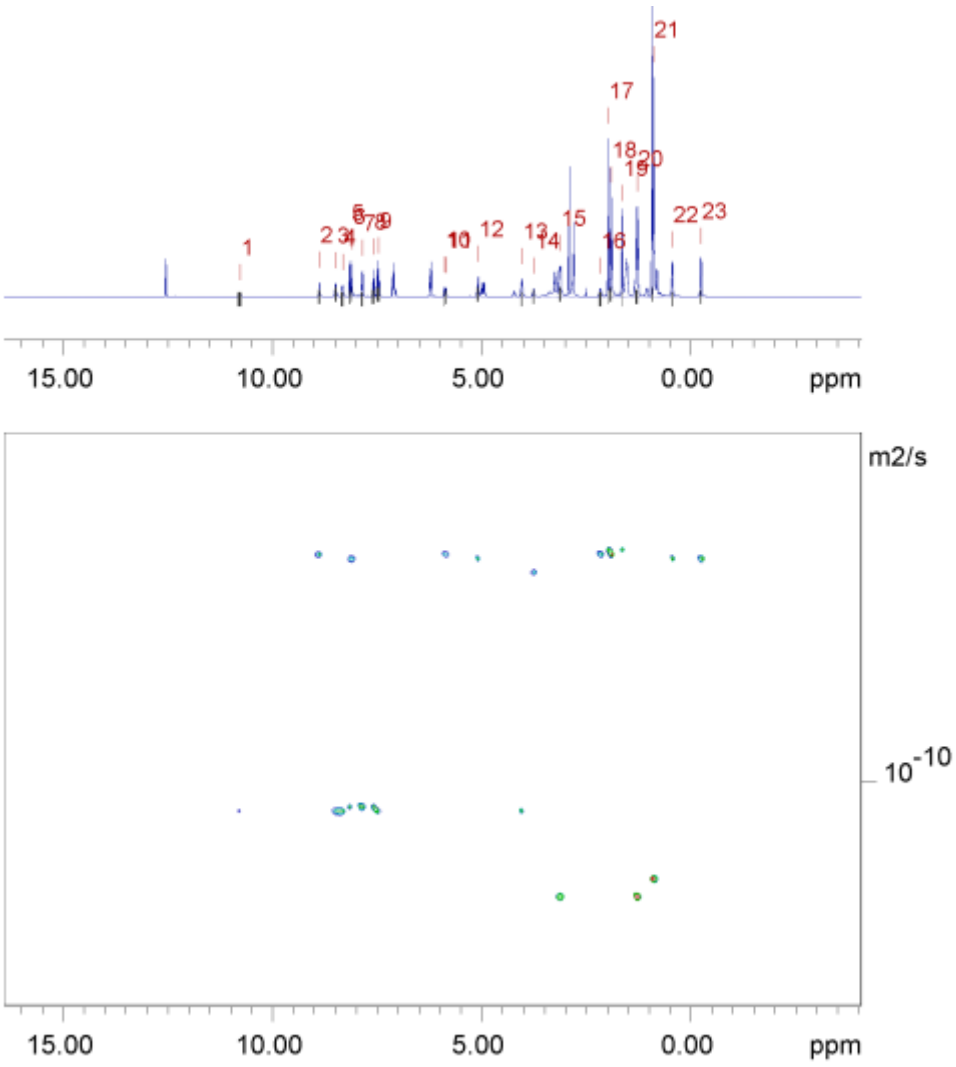
21
17
18
20
19
22
23
15
12
13
14
16
1
2
3
4
5
6
7
8
9
10
15.00
10.00
5.00
0.00
ppm
m2/s
10-10
15.00
10.00
5.00
0.00
ppm

| Peak name | F2 [ppm] | Io | error | D [m2/s] | error |
|---|---|---|---|---|---|
| 1 | 10.783 | 2.31e+08 | 1.245e+05 | 1.05e-10 | 1.017e-13 |
| 2 | 8.880 | 7.39e+08 | 8.608e+04 | 6.89e-11 | 1.464e-14 |
| 3 | 8.480 | 8.01e+08 | 8.587e+04 | 1.05e-10 | 2.018e-14 |
| 4 | 8.328 | 1.03e+09 | 1.028e+05 | 1.04e-10 | 1.869e-14 |
| 5 | 8.146 | 1.02e+09 | 6.752e+04 | 1.04e-10 | 1.236e-14 |
| 6 | 8.096 | 4.93e+08 | 3.402e+04 | 6.90e-11 | 8.688e-15 |
| 7 | 7.855 | 1.16e+09 | 7.555e+04 | 1.04e-10 | 1.219e-14 |
| 8 | 7.593 | 1.10e+09 | 9.144e+04 | 1.04e-10 | 1.554e-14 |
| 9 | 7.478 | 2.61e+09 | 1.153e+05 | 1.05e-10 | 8.306e-15 |
| 10 | 5.891 | 3.73e+08 | 5.629e+04 | 6.89e-11 | 1.899e-14 |
| 11 | 5.855 | 3.90e+08 | 5.888e+04 | 6.88e-11 | 1.895e-14 |
| 12 | 5.090 | 8.62e+08 | 6.993e+04 | 6.91e-11 | 1.022e-14 |
| 13 | 4.044 | 1.12e+09 | 7.561e+04 | 1.05e-10 | 1.265e-14 |
| 14 | 3.758 | 5.68e+08 | 7.072e+04 | 7.05e-11 | 1.599e-14 |
| 15 | 3.130 | 2.92e+09 | 9.613e+04 | 1.20e-10 | 7.110e-15 |
| 16 | 2.167 | 6.91e+08 | 8.140e+04 | 6.87e-11 | 1.477e-14 |
| 17 | 1.984 | 2.09e+09 | 3.800e+04 | 6.80e-11 | 2.254e-15 |
| 18 | 1.911 | 4.81e+09 | 7.398e+04 | 6.87e-11 | 1.928e-15 |
| 19 | 1.648 | 1.47e+09 | 3.807e+04 | 6.83e-11 | 3.232e-15 |
| 20 | 1.293 | 6.30e+09 | 1.047e+05 | 1.21e-10 | 3.611e-15 |
| 21 | 0.910 | 9.92e+09 | 7.863e+04 | 1.17e-10 | 1.665e-15 |
| 22 | 0.444 | 1.38e+09 | 5.363e+04 | 6.91e-11 | 4.909e-15 |
| 23 | -0.241 | 1.57e+09 | 5.637e+04 | 6.92e-11 | 4.526e-15 |

Figure S23 - $^{1}$H DOSY NMR spectrum of co-formulation ***i*** (112.8 mM) in DMSO-$d_6$ at 298 K and a table reporting the diffusion constants calculated for each peak used to determine the hydrodynamic diameter of the anionic components of ***i*** ($d_H$ = 2.09 nm). Peaks 1, 3-5, 7-9 and 13 correspond to the anionic component of ***i*** while peaks 15 and 20-21 correspond to the cationic component of ***i***. Peaks 2, 6, 10-12, 14, 16-19 and 22-23 correspond to the drug component, rifampicin.

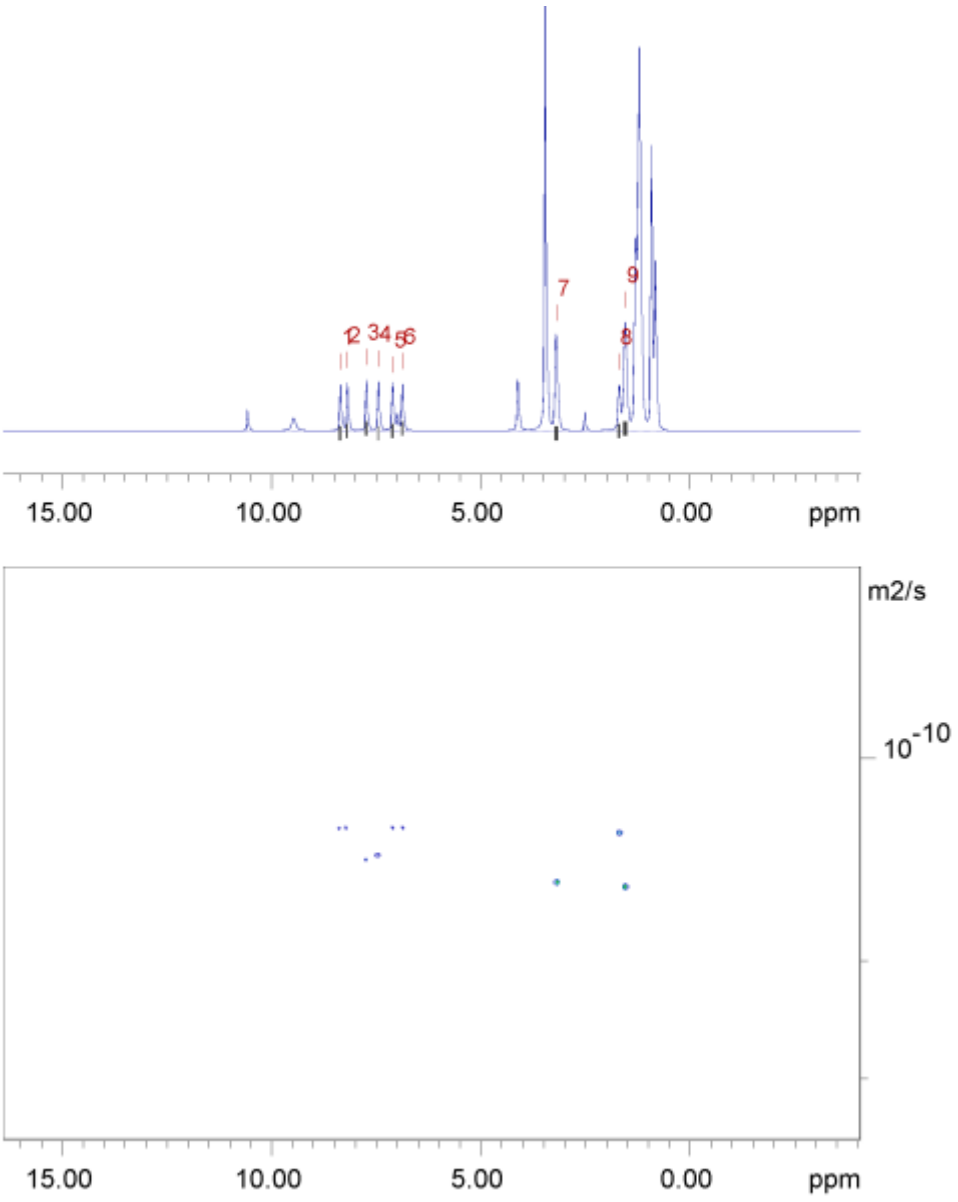


| Peak name | F2 [ppm] | Io | error | D [m2/s] | error |
|---|---|---|---|---|---|
| 1 | 8.356 | 4.56e+09 | 2.299e+05 | 1.27e-10 | 1.360e-14 |
| 2 | 8.192 | 4.07e+09 | 1.992e+05 | 1.26e-10 | 1.314e-14 |
| 3 | 7.738 | 4.61e+09 | 2.223e+05 | 1.41e-10 | 1.435e-14 |
| 4 | 7.450 | 4.06e+09 | 1.984e+05 | 1.40e-10 | 1.445e-14 |
| 5 | 7.107 | 4.45e+09 | 2.096e+05 | 1.28e-10 | 1.275e-14 |
| 6 | 6.875 | 4.38e+09 | 2.116e+05 | 1.26e-10 | 1.294e-14 |
| 7 | 3.194 | 1.63e+10 | 3.089e+05 | 1.53e-10 | 6.099e-15 |
| 8 | 1.696 | 5.65e+09 | 2.341e+05 | 1.29e-10 | 1.136e-14 |
| 9 | 1.552 | 1.98e+10 | 3.220e+05 | 1.56e-10 | 5.347e-15 |

Figure S24 - $^{1}$H DOSY NMR spectrum of co-formulation ***j*** (111.1 mM) in DMSO-$d_6$ at 298 K and a table reporting the diffusion constants calculated for each peak used to determine the hydrodynamic diameter of the anionic components of ***j*** ($d_H$ = 1.57 nm). Peaks 3 and 4 correspond to the anionic component of ***j*** while peaks 7 and 9 corresponds to the cationic component of ***j***. Peaks 1-2, 5-6 and 8 correspond to the drug component, octenidine.

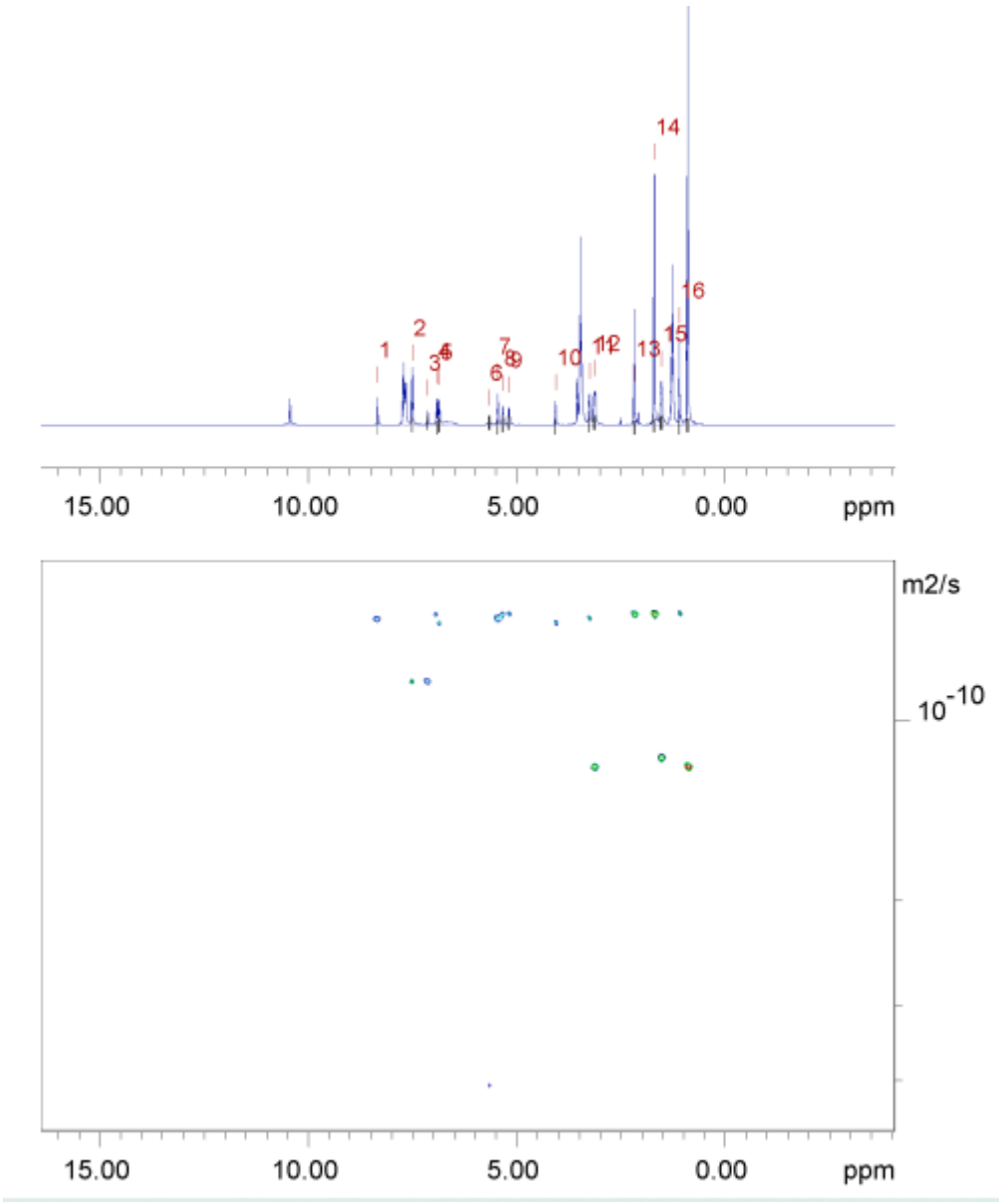
14
16
2
1
15
13
10
6
15.00
10.00
5.00
0.00
ppm
m2/s
$10^{-10}$
15.00
10.00
5.00
0.00
ppm

| Peak name | F2 [ppm] | Io | error | D [m2/s] | error |
|---|---|---|---|---|---|
| 1 | 8.337 | 1.22e+09 | 8.599e+04 | 6.78e-11 | 1.012e-14 |
| 2 | 7.503 | 3.57e+09 | 1.124e+05 | 8.53e-11 | 5.613e-15 |
| 3 | 7.138 | 1.19e+09 | 1.248e+05 | 8.59e-11 | 1.888e-14 |
| 4 | 6.913 | 1.77e+09 | 1.074e+05 | 6.60e-11 | 8.545e-15 |
| 5 | 6.860 | 1.97e+09 | 1.145e+05 | 6.91e-11 | 8.507e-15 |
| 6 | 5.661 | 7.51e+08 | 2.778e+05 | 4.11e-10 | 2.943e-13 |
| 7 | 5.458 | 1.68e+09 | 9.951e+04 | 6.79e-11 | 8.514e-15 |
| 8 | 5.334 | 2.01e+09 | 1.326e+05 | 6.60e-11 | 9.258e-15 |
| 9 | 5.188 | 1.67e+09 | 1.184e+05 | 6.60e-11 | 9.962e-15 |
| 10 | 4.073 | 1.70e+09 | 1.135e+05 | 6.81e-11 | 9.661e-15 |
| 11 | 3.259 | 2.70e+09 | 1.051e+05 | 6.78e-11 | 5.606e-15 |
| 12 | 3.135 | 5.89e+09 | 1.764e+05 | 1.18e-10 | 7.308e-15 |
| 13 | 2.176 | 5.47e+09 | 1.206e+05 | 6.58e-11 | 3.089e-15 |
| 14 | 1.700 | 1.22e+10 | 1.130e+05 | 6.60e-11 | 1.304e-15 |
| 15 | 1.532 | 7.05e+09 | 1.735e+05 | 1.16e-10 | 5.887e-15 |
| 16 | 1.097 | 2.96e+09 | 7.419e+04 | 6.63e-11 | 3.537e-15 |
| 17 | 0.899 | 2.45e+10 | 1.592e+05 | 1.20e-10 | 1.602e-15 |

Figure S25 - $^{1}$H DOSY NMR spectrum of co-formulation ***k*** (112.0 mM) in DMSO-$d_6$ at 298 K and a table reporting the diffusion constants calculated for each peak used to determine the hydrodynamic diameter of the anionic components of ***k*** ($d_H$ = 2.56 nm). Peaks 2 and 3 correspond to the anionic component of ***k*** while peaks 12, 15 and 17 correspond to the cationic component of ***k.*** Peaks 1, 4-5, 7-11, 13-14 and 16 correspond to the drug component, novobiocin.

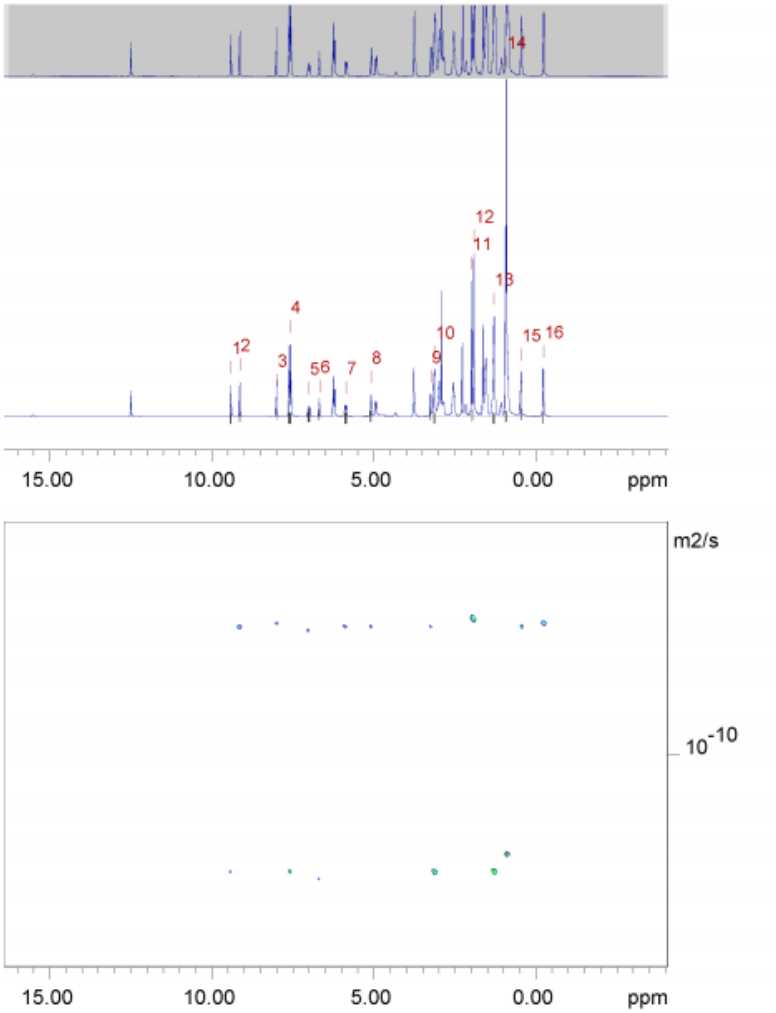


| Peak name | F2 [ppm] | Io | error | D [m2/s] | error |
|---|---|---|---|---|---|
| 1 | 9.408 | 1.51e+09 | 1.373e+05 | 1.27e-10 | 2.159e-14 |
| 2 | 9.132 | 1.76e+09 | 1.323e+05 | 7.78e-11 | 1.121e-14 |
| 3 | 8.002 | 1.44e+09 | 9.378e+04 | 7.73e-11 | 9.710e-15 |
| 4 | 7.590 | 9.75e+09 | 2.334e+05 | 1.27e-10 | 5.688e-15 |
| 5 | 7.000 | 1.69e+09 | 1.930e+05 | 7.83e-11 | 1.716e-14 |
| 6 | 6.681 | 1.25e+09 | 1.349e+05 | 1.28e-10 | 2.588e-14 |
| 7 | 5.865 | 1.80e+09 | 1.685e+05 | 7.77e-11 | 1.398e-14 |
| 8 | 5.088 | 1.81e+09 | 1.329e+05 | 7.78e-11 | 1.097e-14 |
| 9 | 3.246 | 1.27e+09 | 1.018e+05 | 7.78e-11 | 1.197e-14 |
| 10 | 3.127 | 6.50e+09 | 1.748e+05 | 1.26e-10 | 6.348e-15 |
| 11 | 1.983 | 4.70e+09 | 8.064e+04 | 7.62e-11 | 2.522e-15 |
| 12 | 1.916 | 8.68e+09 | 9.356e+04 | 7.67e-11 | 1.593e-15 |
| 13 | 1.298 | 1.22e+10 | 1.807e+05 | 1.26e-10 | 3.489e-15 |
| 14 | 0.916 | 2.57e+10 | 1.619e+05 | 1.22e-10 | 1.444e-15 |
| 15 | 0.461 | 3.61e+09 | 1.146e+05 | 7.74e-11 | 4.732e-15 |
| 16 | -0.229 | 2.91e+09 | 9.806e+04 | 7.71e-11 | 4.995e-15 |

Figure S26 - $^{1}$H DOSY NMR spectrum of co-formulation ***I*** (111.2 mM) in DMSO-$d_6$ at 298 K and a table reporting the diffusion constants calculated for each peak used to determine the hydrodynamic diameter of the anionic components of ***I*** ($d_H$ = 1.72 nm). Peaks 1, 3-5, 7-9 and 13 correspond to the anionic component of ***I*** while peaks 15 and 20-21 correspond to the cationic component of ***I***. Peaks 2, 6, 10-12, 14, 16-19 and 22-23 correspond to the drug component, rifampicin.

## Quantitative $^{1}$H NMR experiments

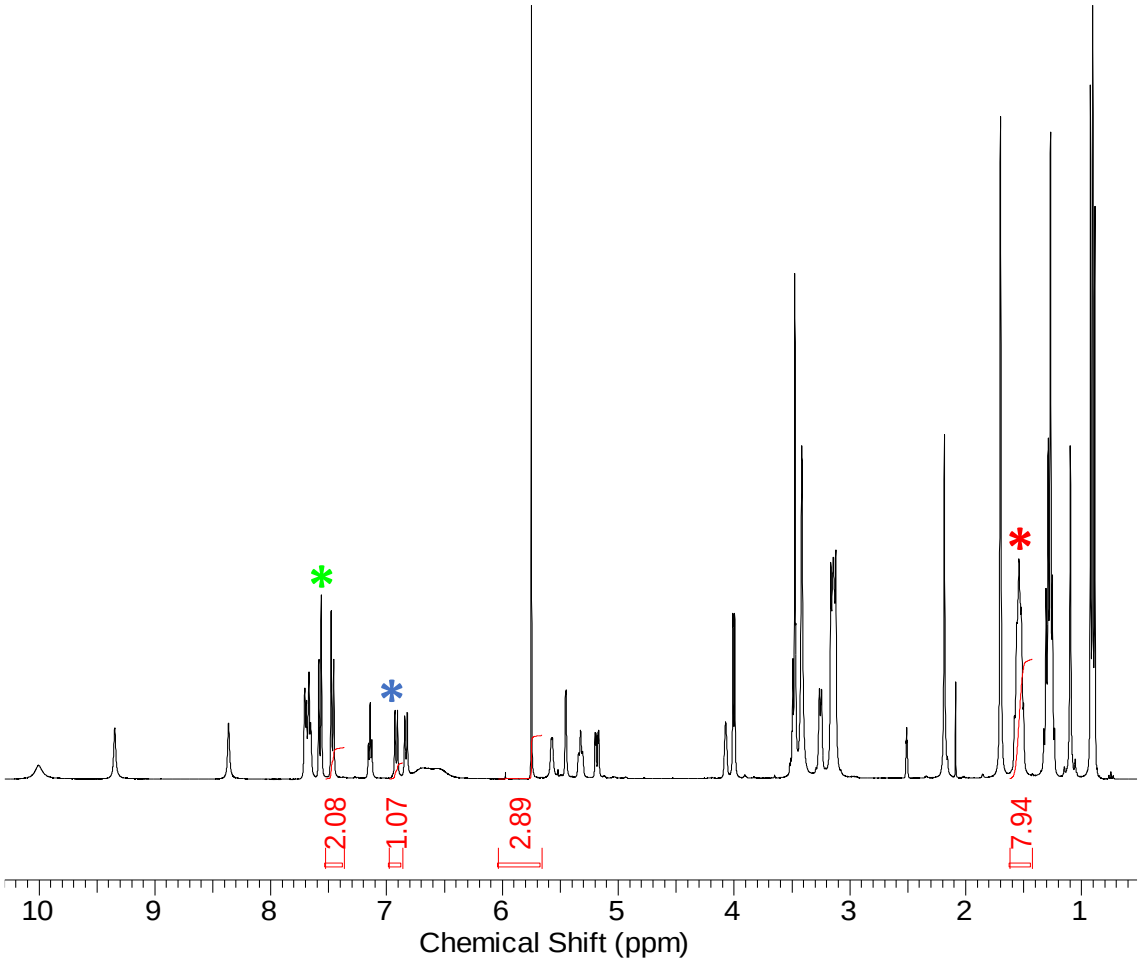


Figure S27 - $^{1}$H NMR spectrum with a delay ($d_1$ = 60 s) of co-formulation ***b*** (110.7 mM) in DMSO-$d_6$/ 1.0 % DCM. Comparative integration indicated 0 % of the sample has become NMR silent. (Novobiocin*, anionic component of the SSA*, TBA counter cation*).

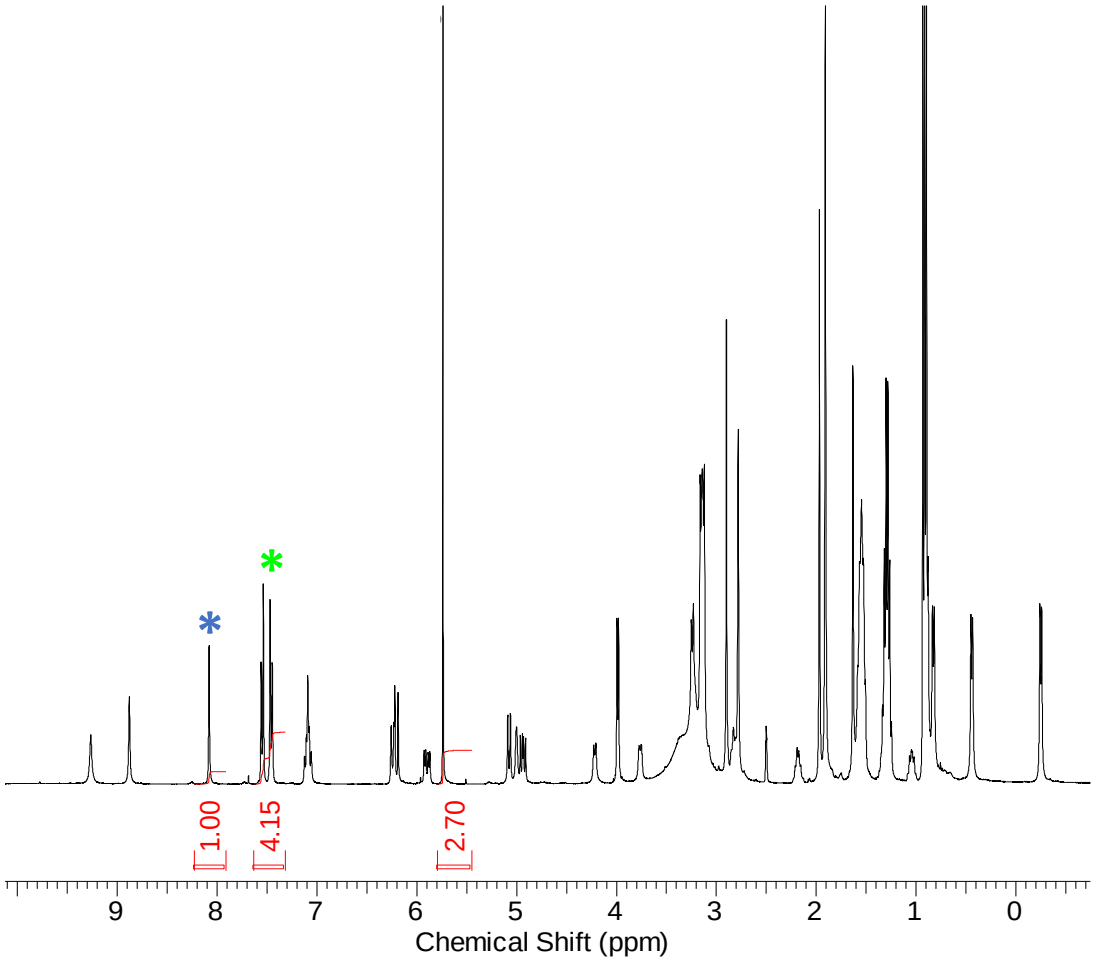


Figure S28 – $^{1}$H NMR spectrum with a delay ($d_1$ = 60 s) of co-formulation ***c*** (118.5 mM) in DMSO-$d_6$/ 1.0 % DCM. Comparative integration indicated 0 % of the sample has become NMR silent. (Rifampicin* and anionic component of the SSA*).

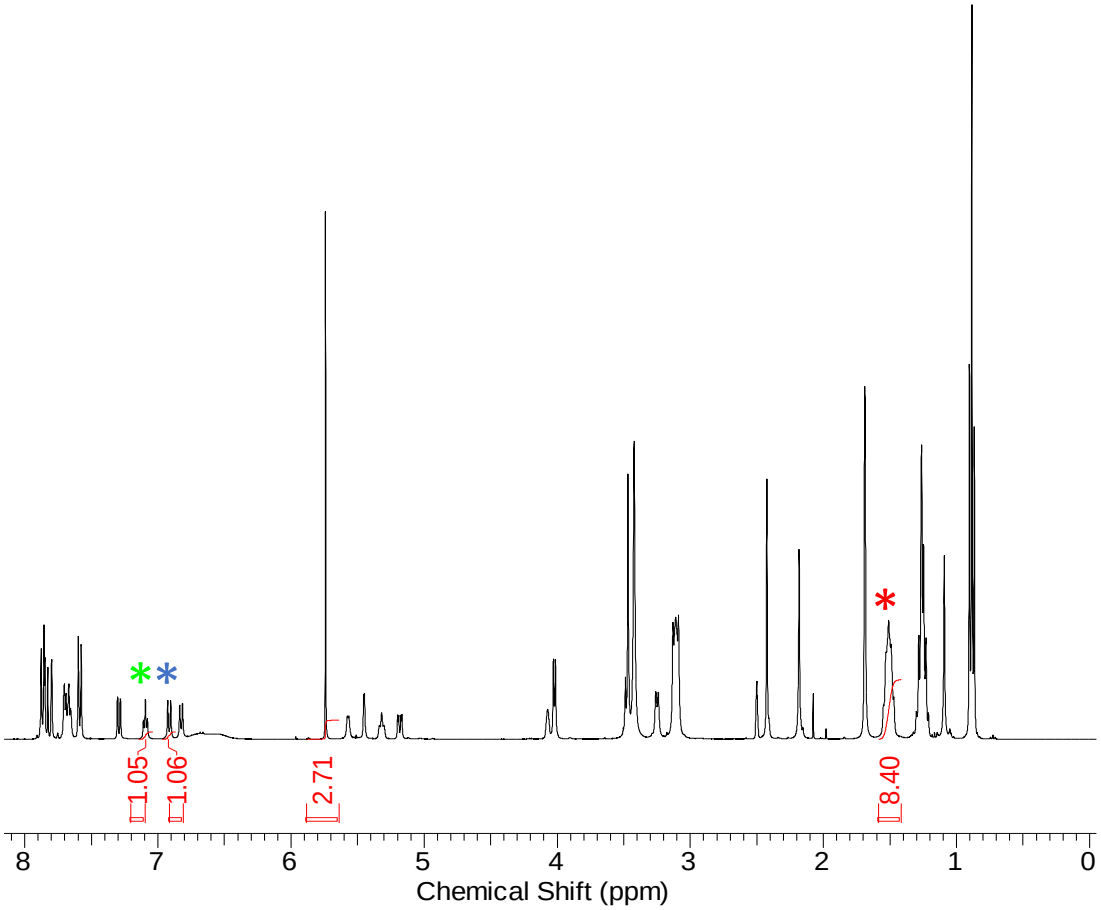


Figure S29 – $^{1}$H NMR spectrum with a delay ($d_1$ = 60 s) of co-formulation ***e*** (118.1 mM) in DMSO-$d_6$/ 1.0 % DCM. Comparative integration indicated 0 % of the sample has become NMR silent. (Novobiocin*, anionic component of the SSA*, TBA counter cation*).

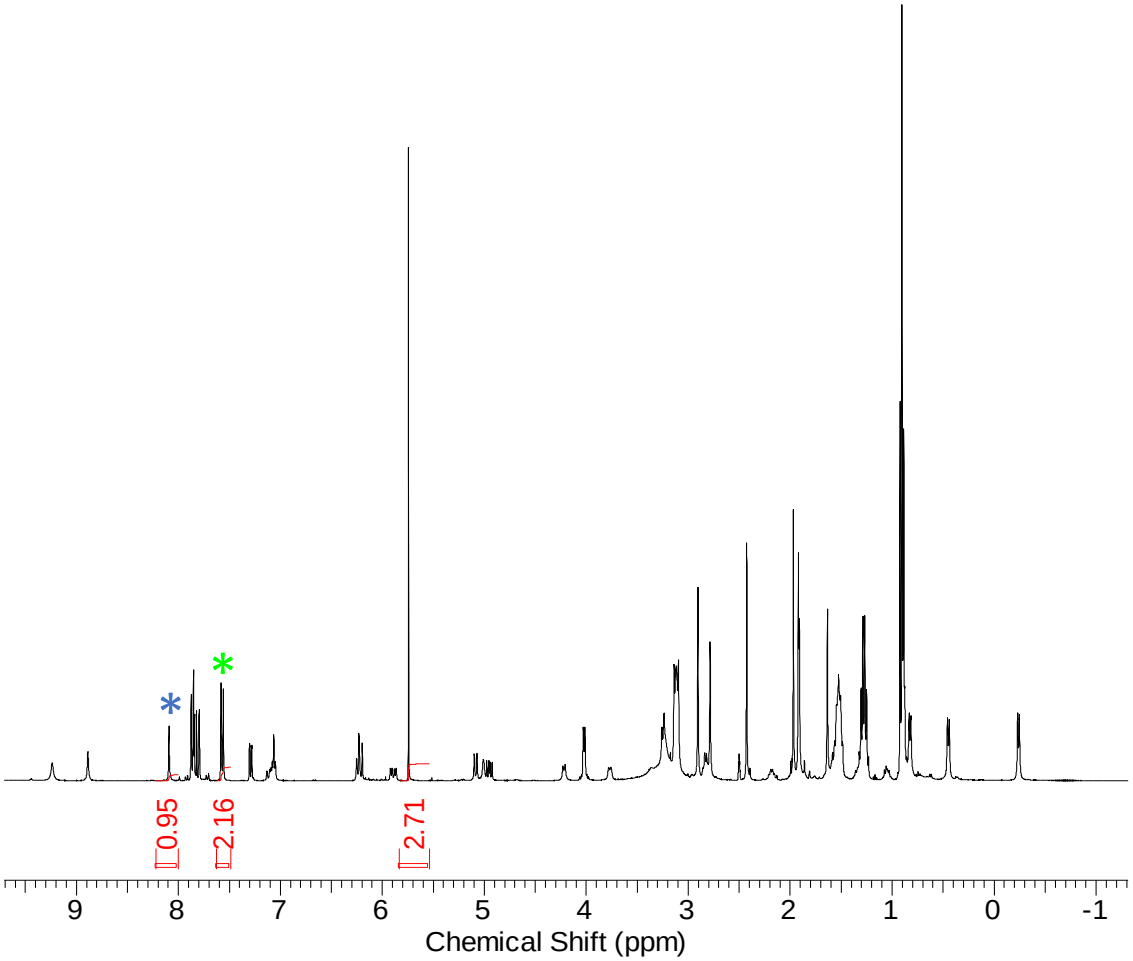


Figure S30 - $^{1}$H NMR spectrum with a delay ($d_1$ = 60 s) of co-formulation **f** (118.1 mM) in DMSO-$d_6$/ 1.0 % DCM. Comparative integration indicated 0 % of the sample has become NMR silent. (Rifampicin* and anionic component of the SSA*).

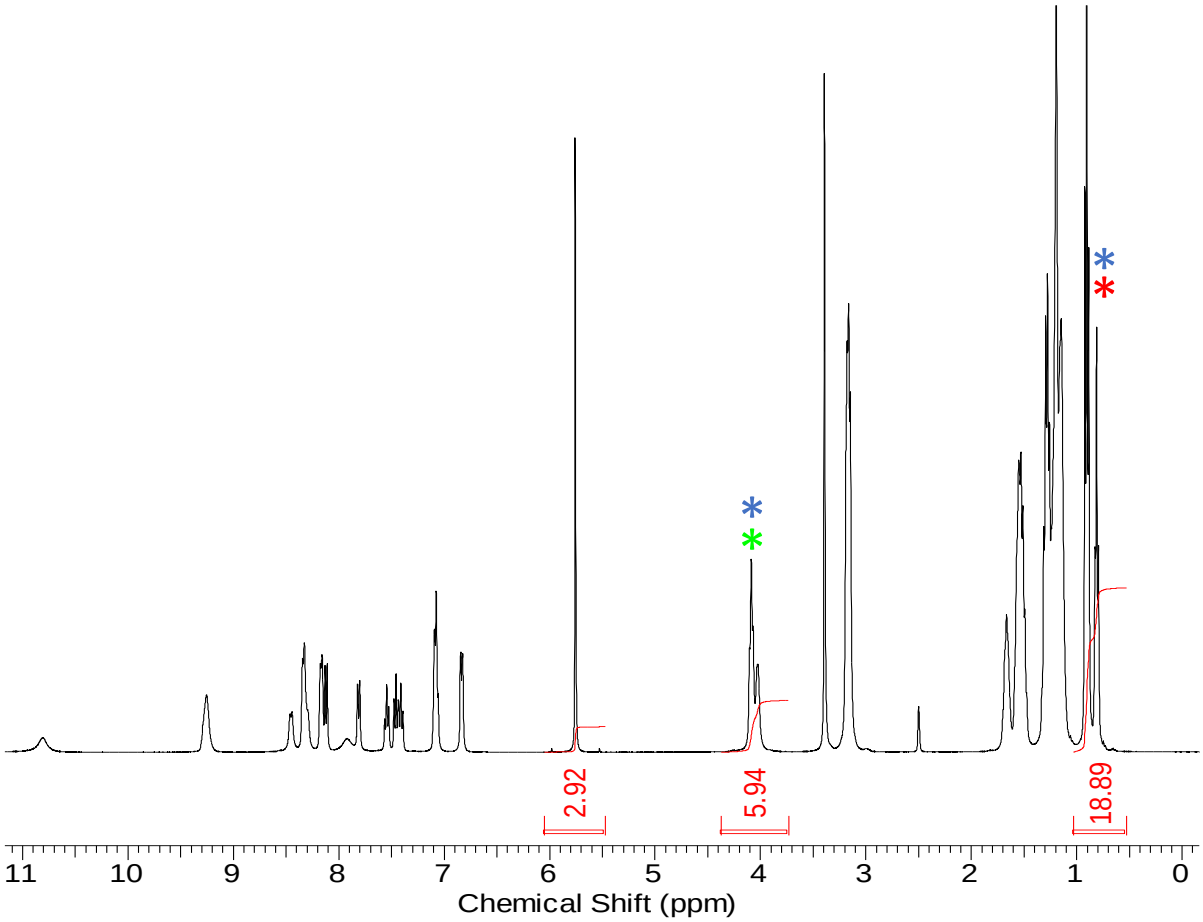


Figure S31 - $^{1}$H NMR spectrum with a delay ($d_1$ = 60 s) of co-formulation ***g*** (109.6 mM) in DMSO-$d_6$/ 1.0 % DCM. Comparative integration indicated 0 % of the sample has become NMR silent. (Octenidine*, anionic component of the SSA*, TBA counter cation*).

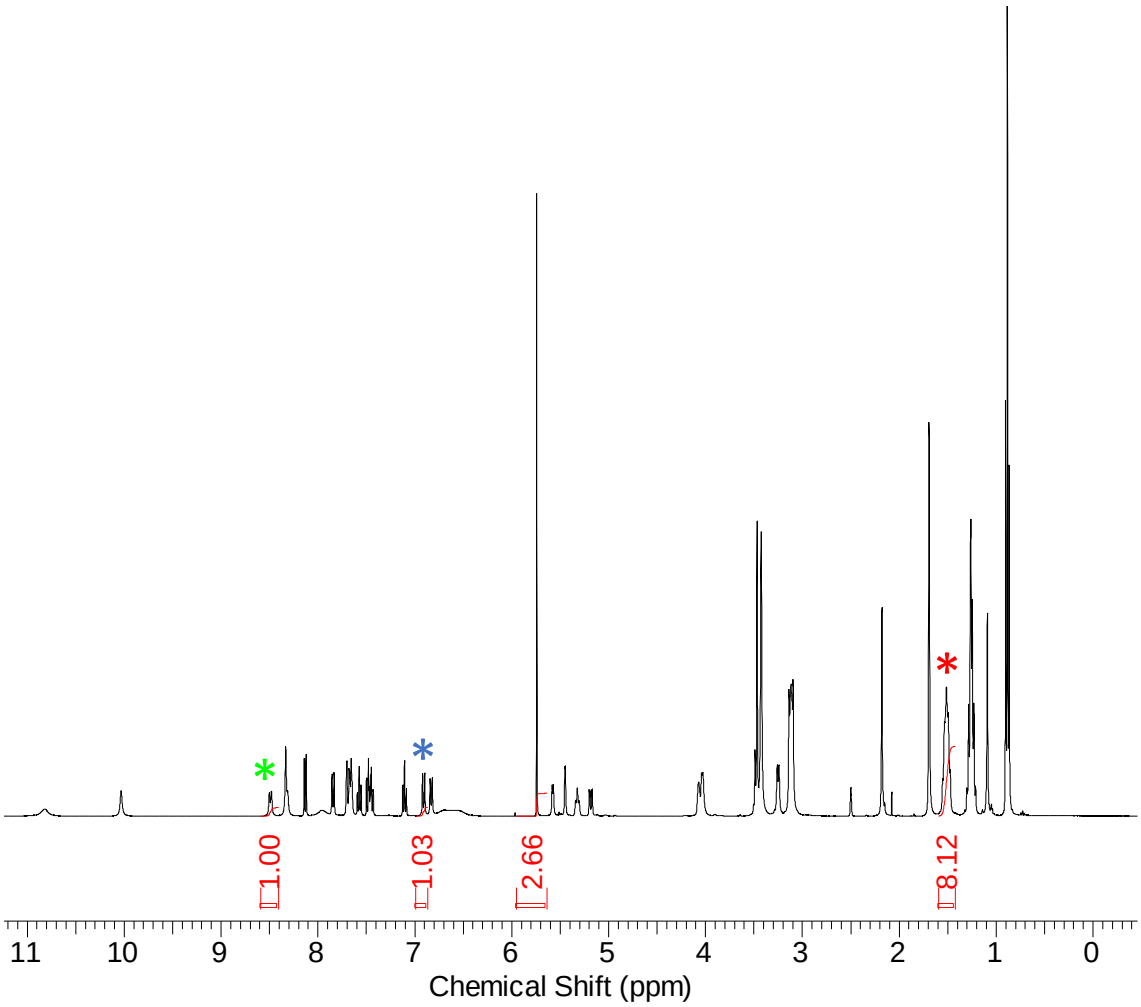


Figure S32 - $^{1}$H NMR spectrum with a delay ($d_1$ = 60 s) of co-formulation ***h*** (111.9 mM) in DMSO-$d_6$/ 1.0 % DCM. Comparative integration indicated 0 % of the sample has become NMR silent. (Novobiocin*, anionic component of the SSA*, TBA counter cation*).

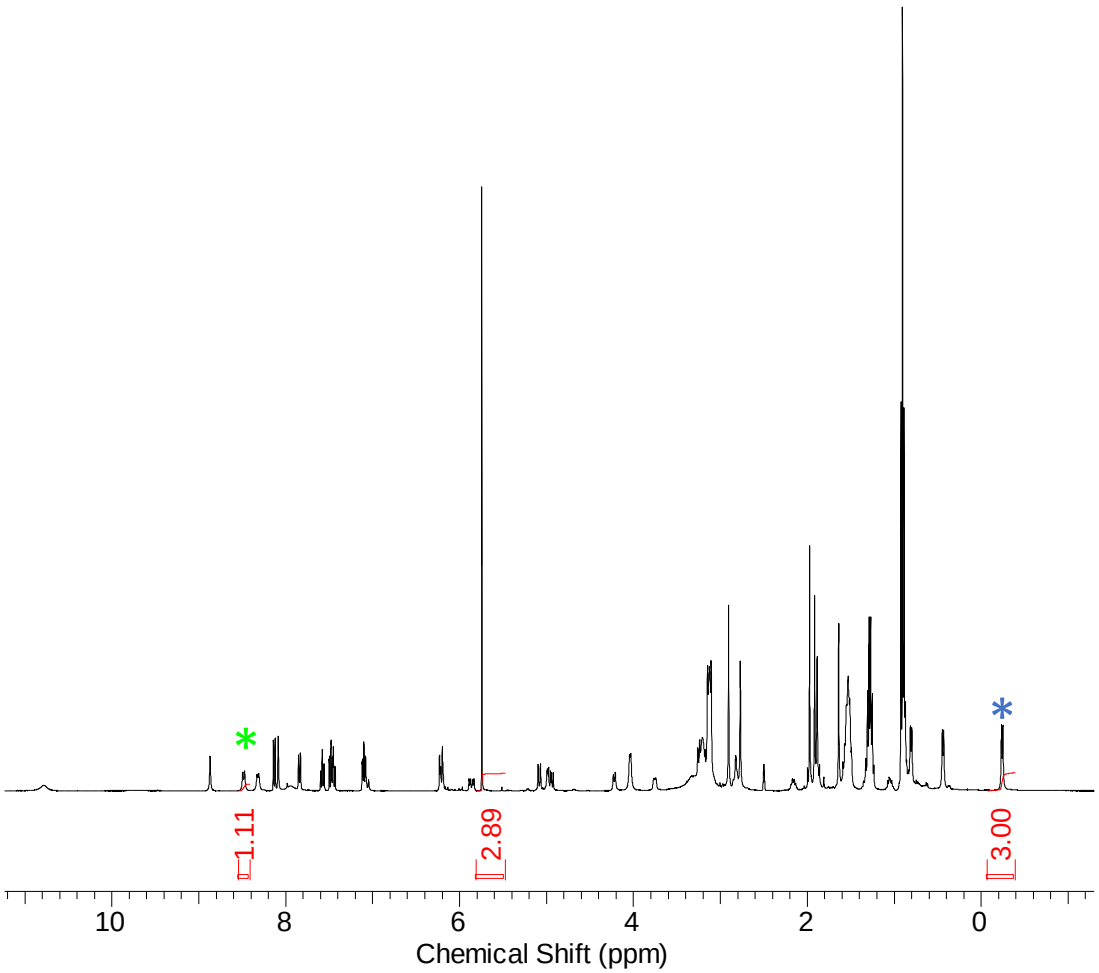


Figure S33 - $^{1}$H NMR spectrum with a delay ($d_1$ = 60 s) of co-formulation ***i*** (118.1 mM) in DMSO-$d_6$/ 1.0 % DCM. Comparative integration indicated 0 % of the sample has become NMR silent. (Rifampicin* and anionic component of the SSA*).

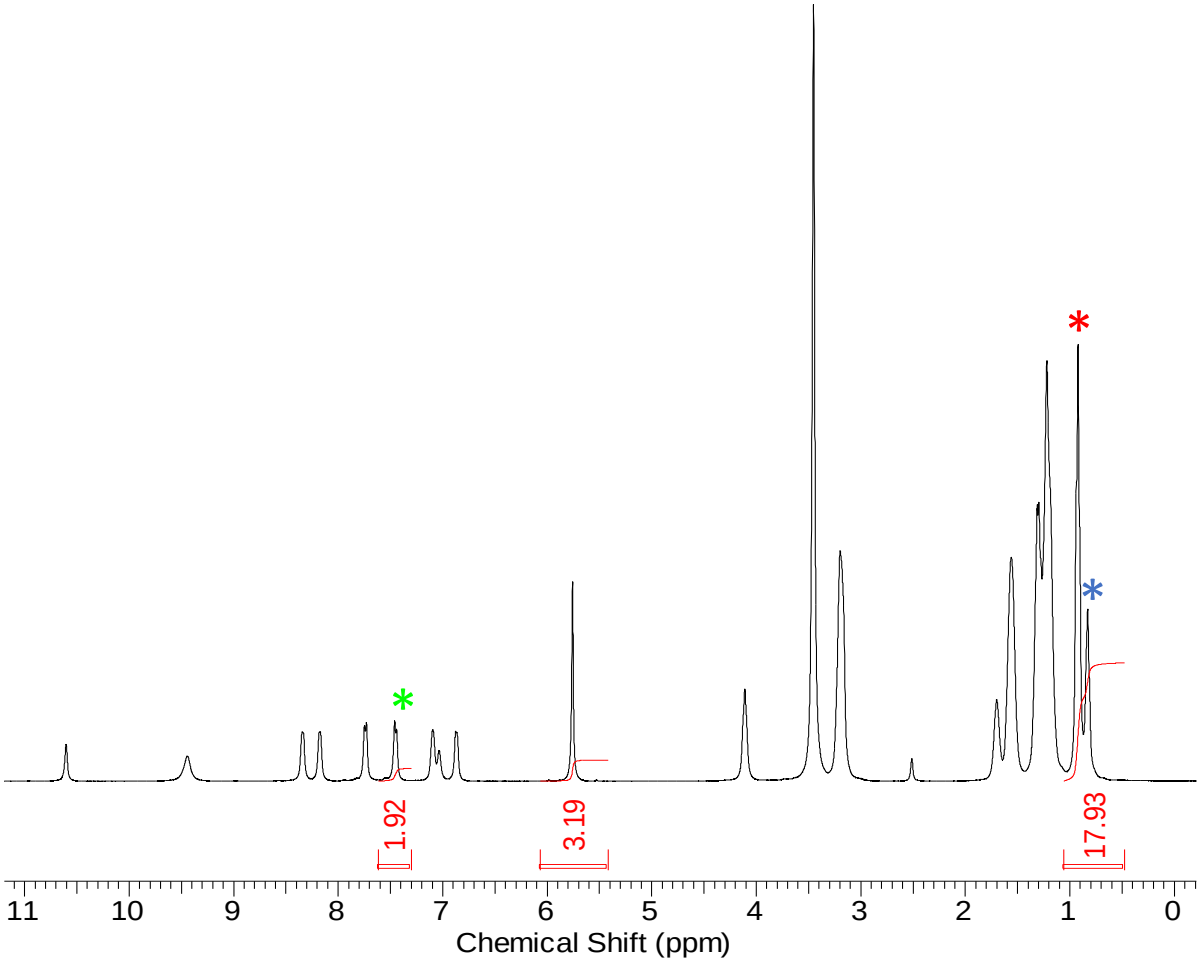


Figure S34 - $^{1}$H NMR spectrum with a delay ($d_1$ = 60 s) of co-formulation ***j*** (100.3 mM) in DMSO-$d_6$/ 1.0 % DCM. Comparative integration indicated 0 % of the sample has become NMR silent. (Octenidine*, anionic component of the SSA*, TBA counter cation*).

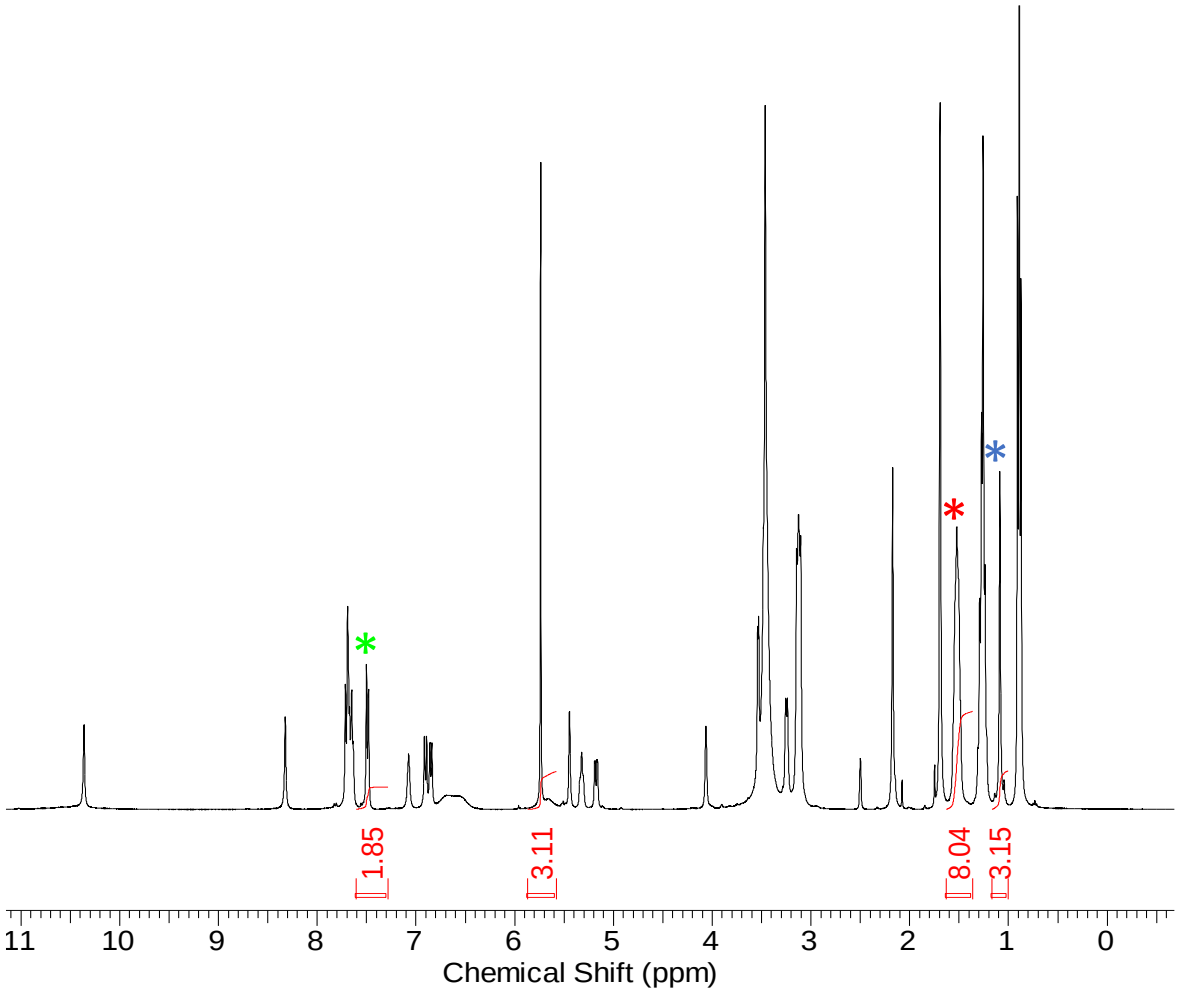


Figure S35 - $^{1}$H NMR spectrum with a delay ($d_1$ = 60 s) of co-formulation ***k*** (102.9 mM) in DMSO-$d_6$/ 1.0 % DCM. Comparative integration indicated 0 % of the sample has become NMR silent. (Novobiocin*, anionic component of the SSA*, TBA counter cation*).

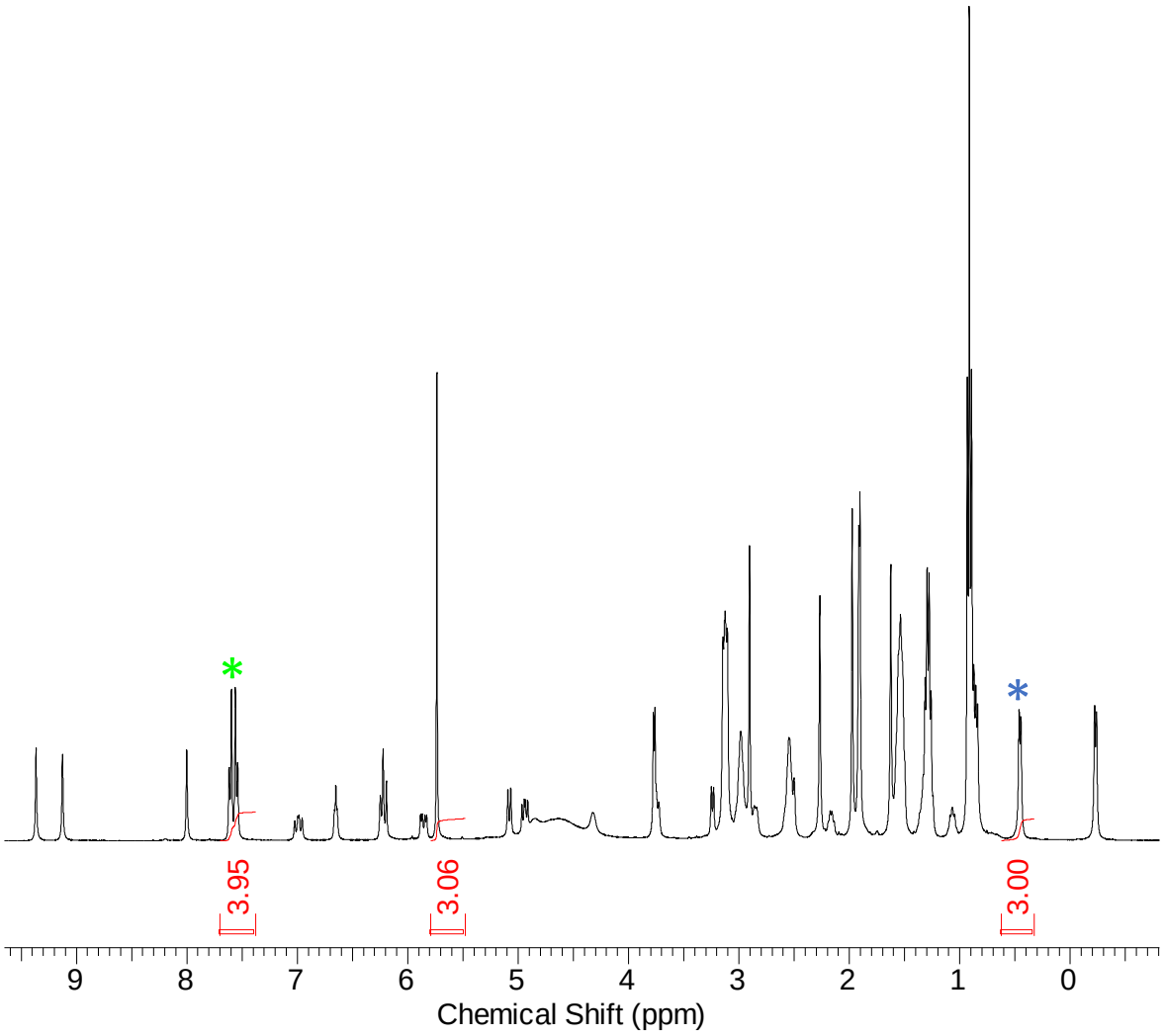


Figure S36 - $^{1}$H NMR spectrum with a delay ($d_1$ = 60 s) of co-formulation ***I*** (104.6 mM) in DMSO-$d_6$/ 1.0 % DCM. Comparative integration indicated 0 % of the sample has become NMR silent. (Rifampicin* and anionic component of the SSA*).

## $^1$H NMR self-association studies

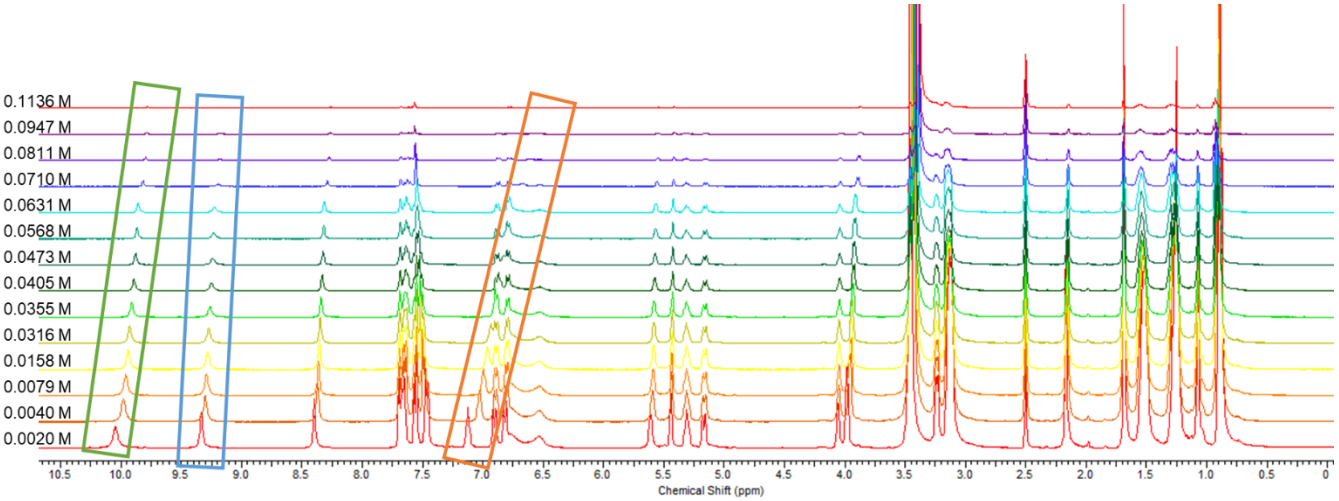


Figure S37 - $^1$H NMR stack plot of co-formulation ***b*** in DMSO-$d_6$ 0.5 % $H_2O$ solution. Samples were prepared in series with an aliquot of the most concentrated solution undergoing serial dilution.

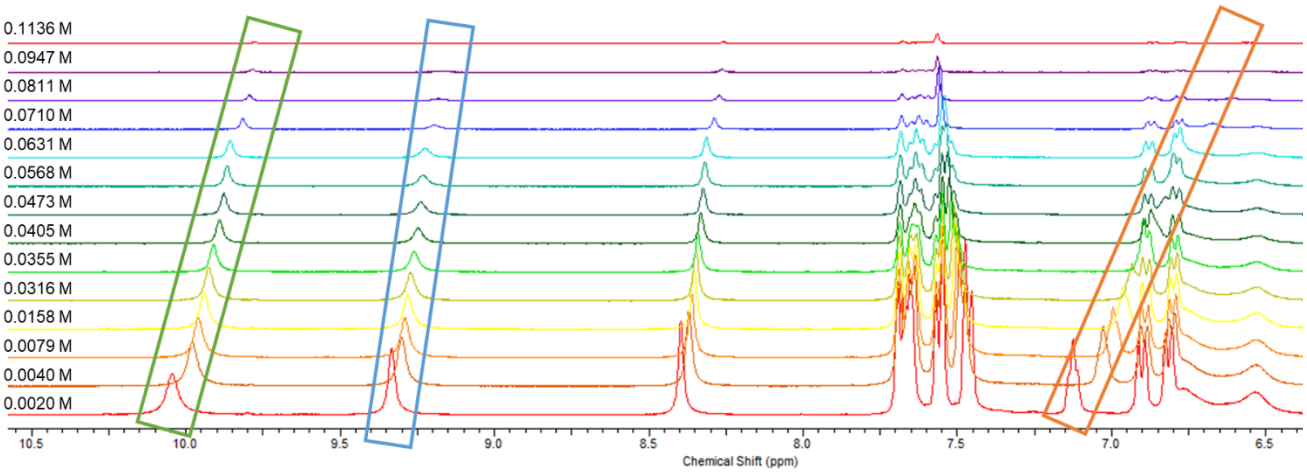


Figure S38 – Enlarged $^1$H NMR stack plot of co-formulation ***b*** in DMSO-$d_6$ 0.5 % $H_2O$ solution. Samples were prepared in series with an aliquot of the most concentrated solution undergoing serial dilution.

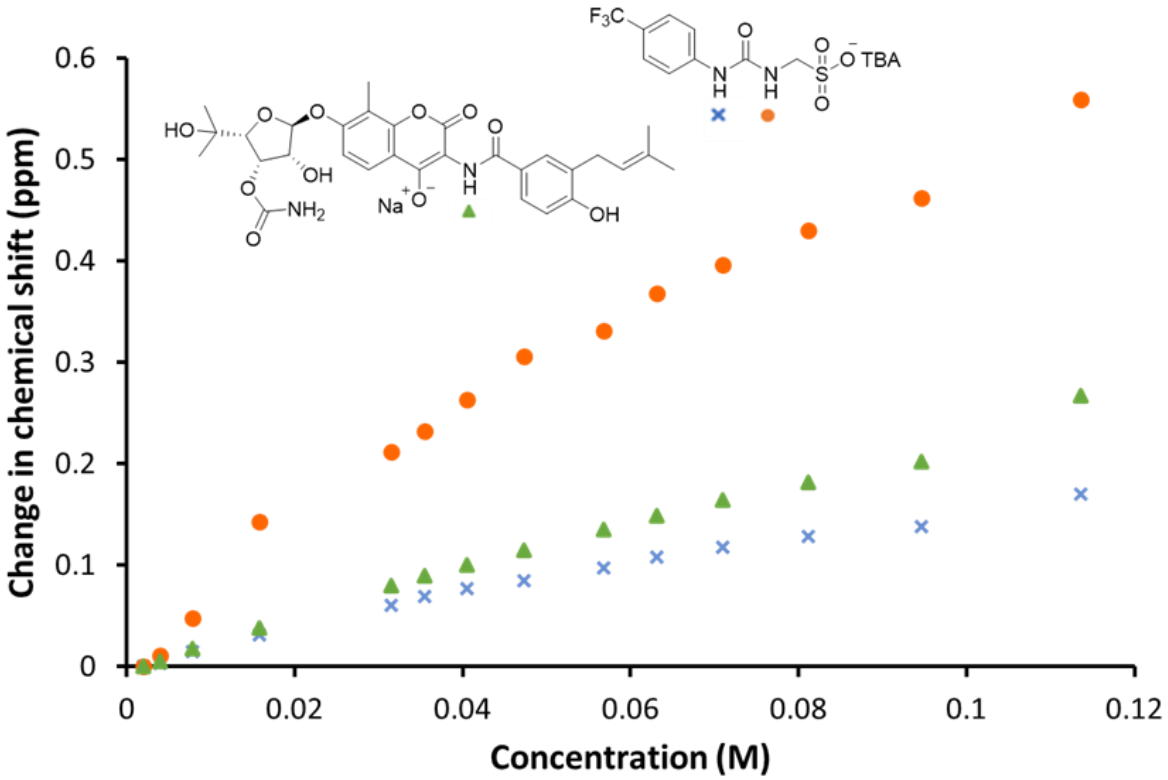


Figure S39 - Graph illustrating the $^{1}$H NMR down-field change in chemical shift of SSA (**1**) urea and appropriate co-formulant NH resonances with increasing concentration of co-formulation ***b*** in DMSO-$d_6$ 0.5 % $H_2O$ (298 K).

## Self-association constant calculation

Co-formulation ***b*** - Dilution study in DMSO-$d_6$ 5 % $H_2O$. Values calculated from data gathered from SSA (**1**) NH urea resonances.

*Equal K/Dimerization model*

$K_e$ = 4.44 $M^{-1}$ ± 2.4373 %  $K_{dim}$ = 2.22 $M^{-1}$ ± 1.2186 %

http://app.supramolecular.org/bindfit/view/d528c451-f9ed-4fe4-bf73-f39aa5c592bf

*CoEK model*

$K_e$ = 2.02 $M^{-1}$ ± 29.3231 %  $K_{dim}$ = 1.01 $M^{-1}$ ± 14.6615 %  ρ = 1.70 ± 37.0358 %

http://app.supramolecular.org/bindfit/view/5ddfdfe5-b8e5-47be-ba51-def3ad11860e

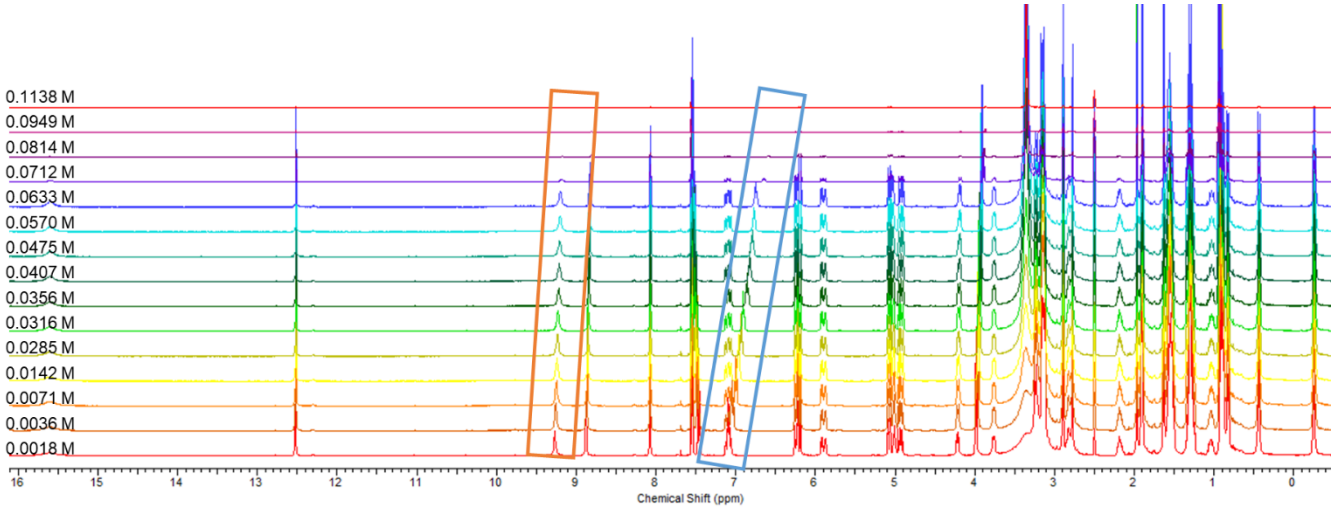


Figure S40 - $^{1}$H NMR stack plot of co-formulation ***c*** in DMSO-$d_6$ 0.5 % $H_2O$ solution. Samples were prepared in series with an aliquot of the most concentrated solution undergoing serial dilution.

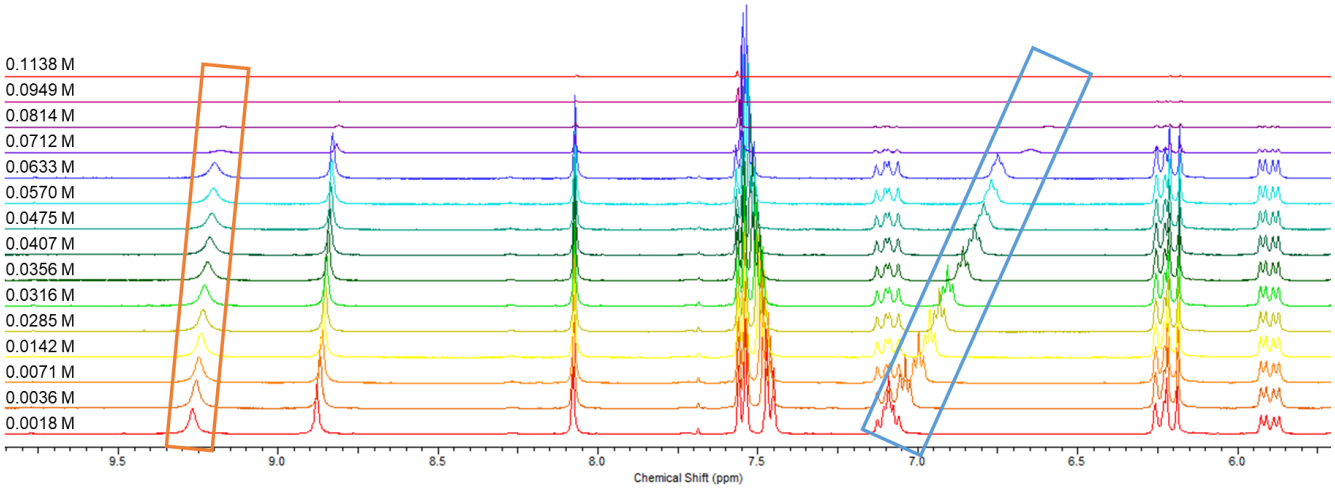


Figure S41 – Enlarged $^{1}$H NMR stack plot of co-formulation ***c*** in DMSO-$d_6$ 0.5 % $H_2O$ solution. Samples were prepared in series with an aliquot of the most concentrated solution undergoing serial dilution.

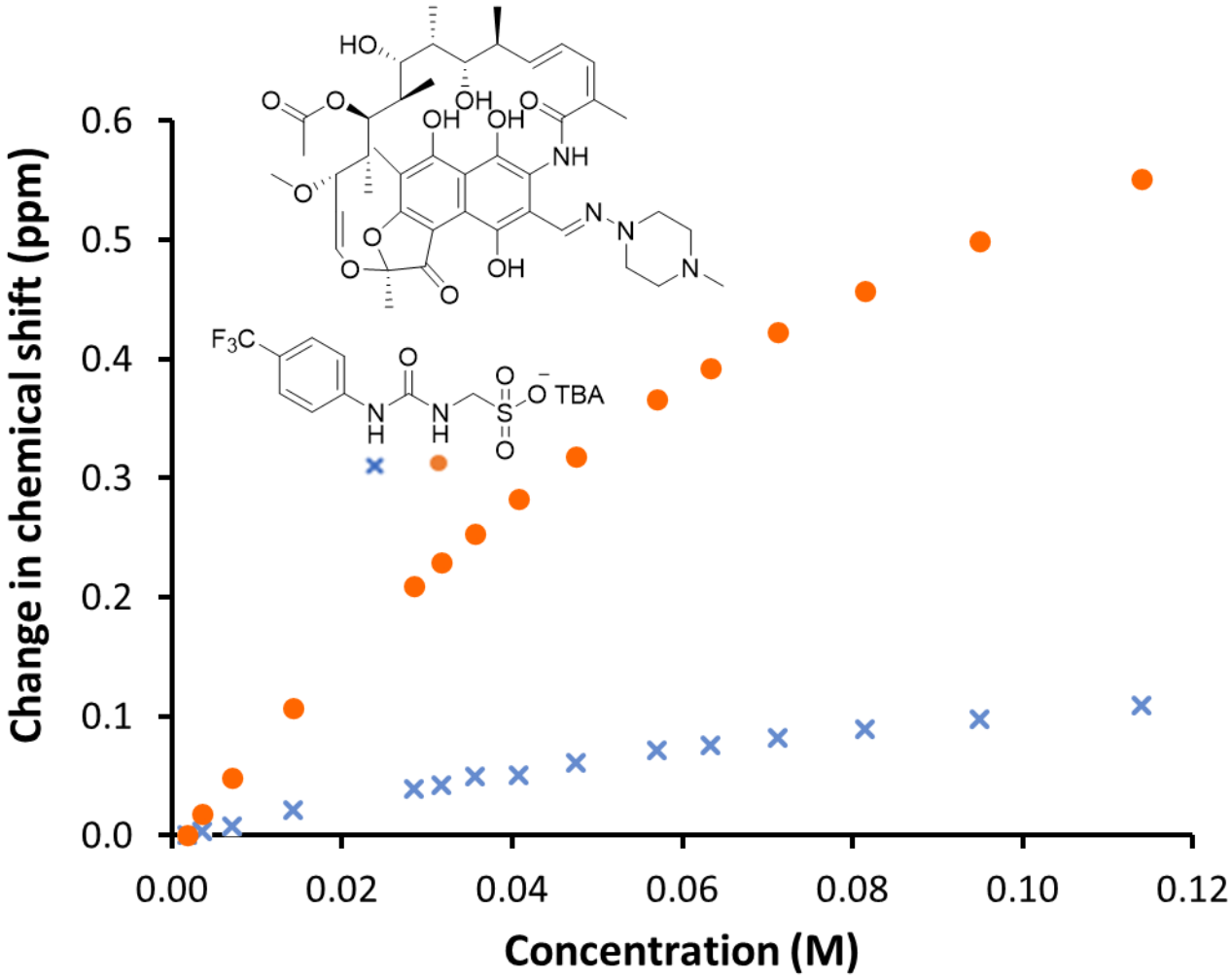


Figure S42 - Graph illustrating the $^{1}$H NMR down-field change in chemical shift of SSA (**1**) urea with increasing concentration of co-formulation ***c*** in DMSO-$d_6$ 0.5 % $H_2O$ (298 K)..

## Self-association constant calculation

Co-formulation ***c*** - Dilution study in DMSO-$d_6$ 5 % $H_2O$. Values calculated from data gathered from SSA (**1**) NH urea resonances.

*Equal K/Dimerization model*

$K_e$ = 5.78 $M^{-1}$ ± 0.5468 %  $K_{dim}$ = 2.89 $M^{-1}$ ± 0.2734 %

http://app.supramolecular.org/bindfit/view/128fcf54-1d84-4c76-b841-506e2dd801fa

*CoEK model*

$K_e$ = 12.34 $M^{-1}$ ± 0.7699 %  $K_{dim}$ = 6.17 $M^{-1}$ ± 0.3849 %  ρ = 0.55 ± 2.1754 %

http://app.supramolecular.org/bindfit/view/e75b12af-e538-4af5-85f2-b0c654c2e343

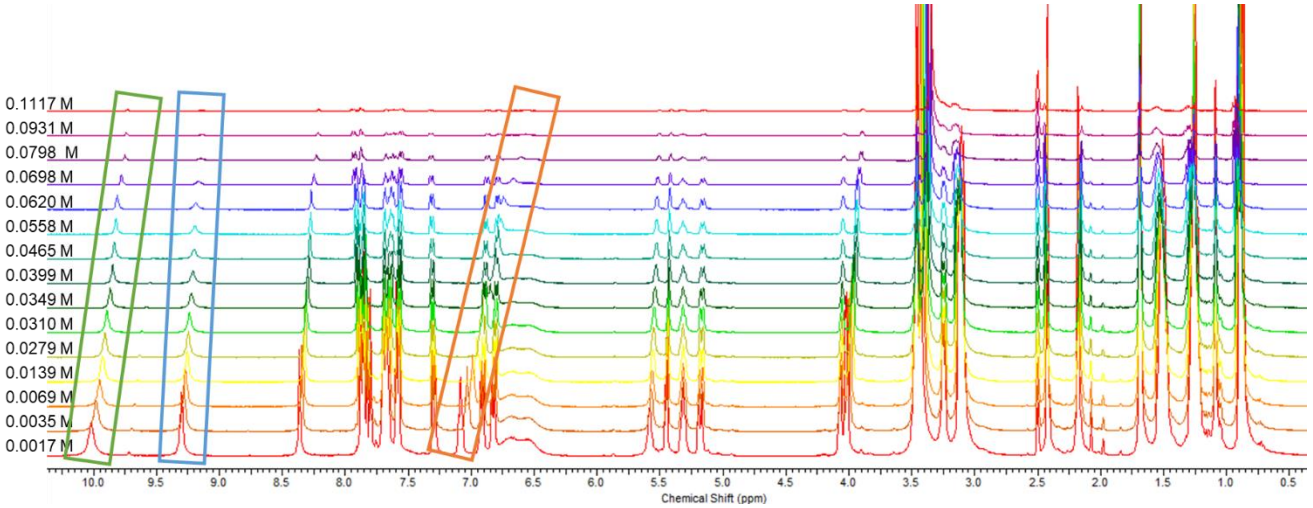


Figure S43 - $^{1}$H NMR stack plot of co-formulation ***e*** in DMSO-$d_6$ 0.5 % $H_2O$ solution. Samples were prepared in series with an aliquot of the most concentrated solution undergoing serial dilution.

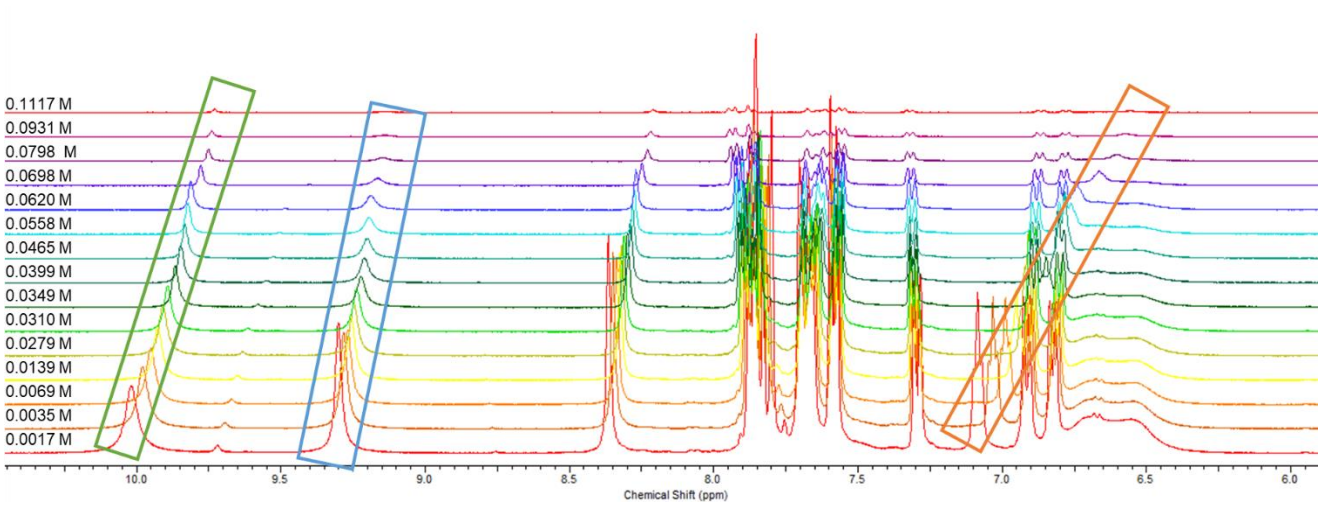


Figure S44 – Enlarged $^{1}$H NMR stack plot of co-formulation ***e*** in DMSO-$d_6$ 0.5 % $H_2O$ solution. Samples were prepared in series with an aliquot of the most concentrated solution undergoing serial dilution.

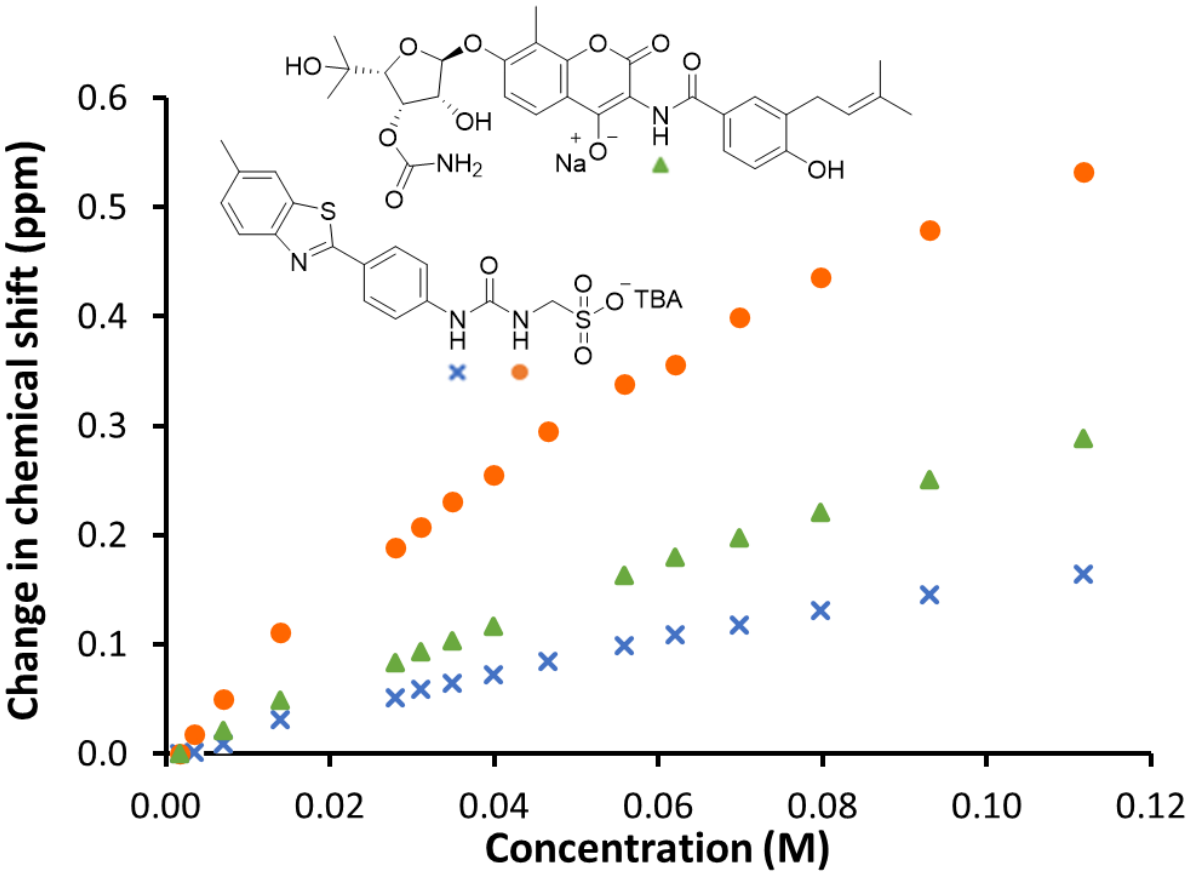


Figure S45 - Graph illustrating the $^{1}$H NMR down-field change in chemical shift of SSA (**2**) urea and appropriate co-formulant NH resonances with increasing concentration of co-formulation **e** in DMSO-$d_6$ 0.5 % $H_2O$ (298 K).

## Self-association constant calculation

Co-formulation ***e*** - Dilution study in DMSO-$d_6$ 5 % $H_2O$. Values calculated from data gathered from SSA (**2**) NH urea resonances.

*Equal K/Dimerization model*

$K_e$ = 4.14 $M^{-1}$ ± 0.8909 %  $K_{dim}$ = 2.07 $M^{-1}$ ± 0.4454 %

http://app.supramolecular.org/bindfit/view/1e3ce722-9bcf-4c91-82dd-973c24a00099

*CoEK model*

$K_e$ = 3.17 $M^{-1}$ ± 7.0724 %  $K_{dim}$ = 1.59 $M^{-1}$ ± 3.5362 %  ρ = 1.18 ± 9.9785 %

http://app.supramolecular.org/bindfit/view/4c23c35a-32cc-4aa1-9fc8-d839cfaafa88

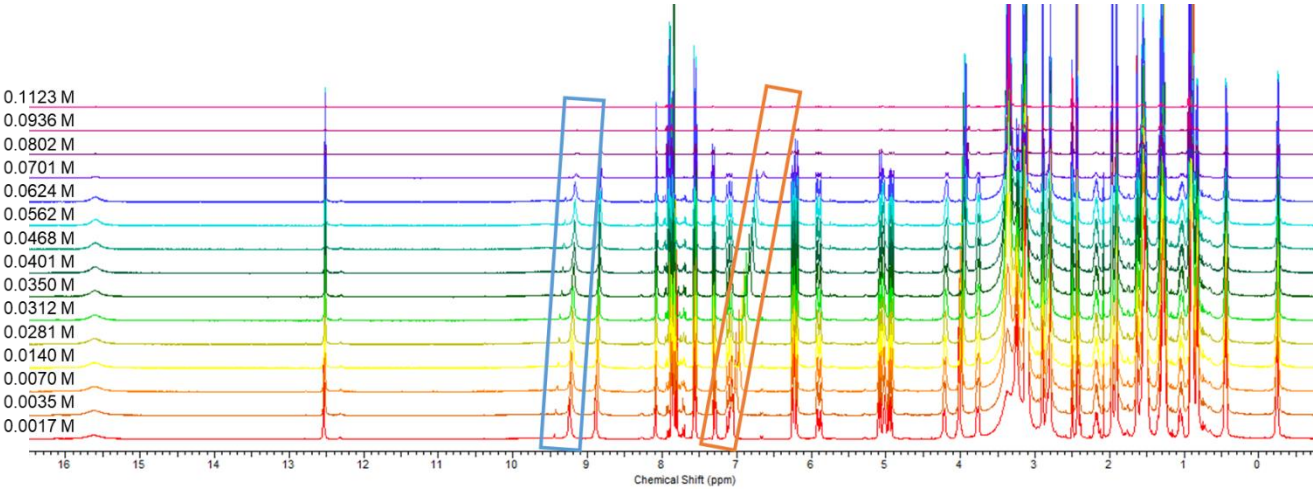


Figure S46 - $^{1}$H NMR stack plot of co-formulation ***f*** in DMSO-$d_6$ 0.5 % $H_2O$ solution. Samples were prepared in series with an aliquot of the most concentrated solution undergoing serial dilution.

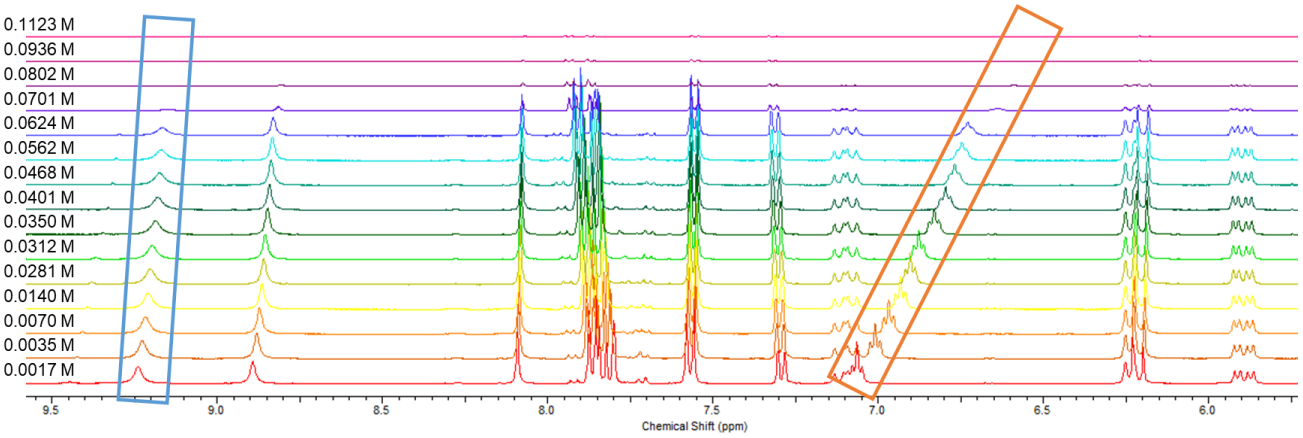


Figure S47 – Enlarged $^{1}$H NMR stack plot of co-formulation ***f*** in DMSO-$d_6$ 0.5 % $H_2O$ solution. Samples were prepared in series with an aliquot of the most concentrated solution undergoing serial dilution.

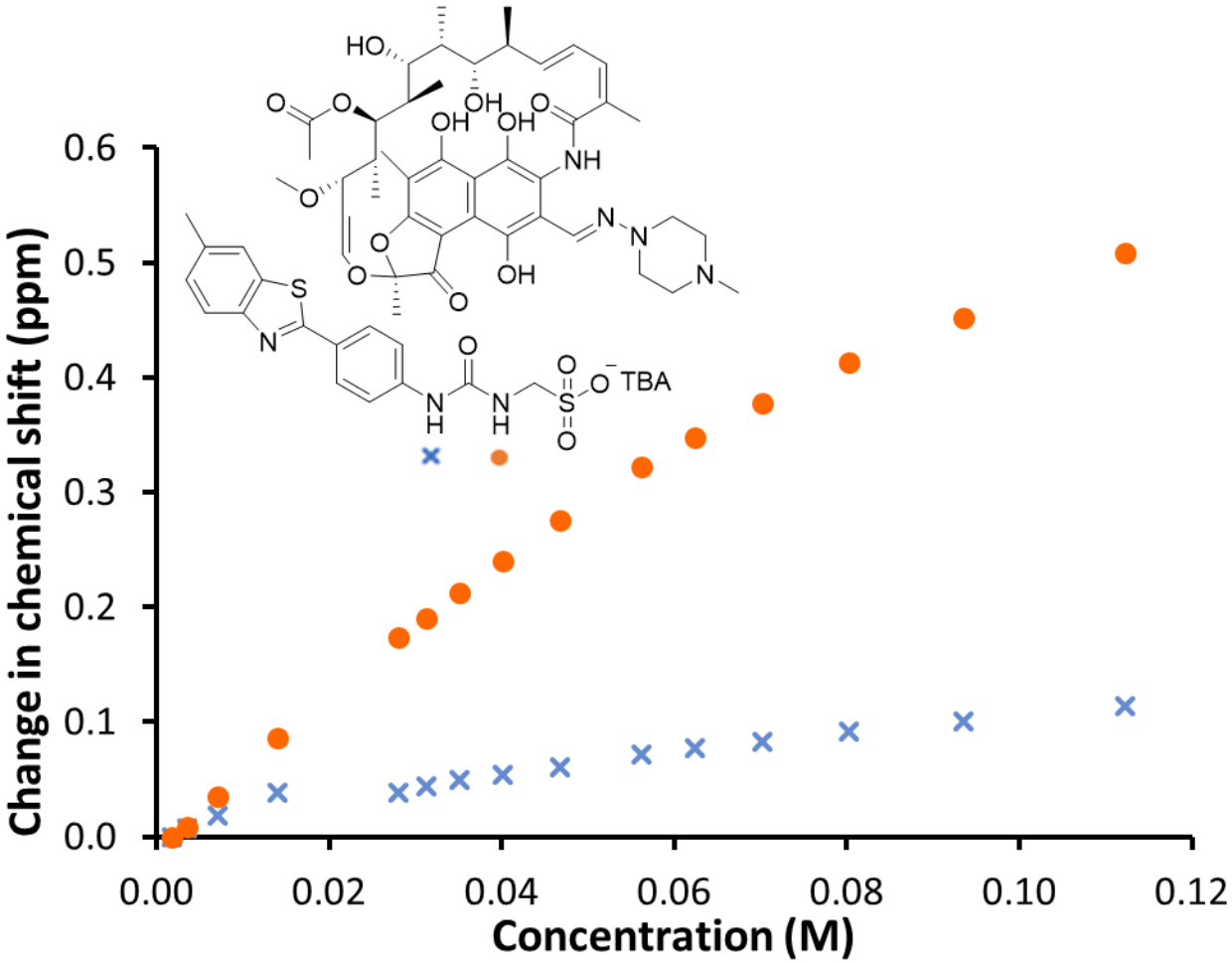


Figure S48 - Graph illustrating the $^{1}$H NMR down-field change in chemical shift of SSA (**2**) urea with increasing concentration of co-formulation ***f*** in DMSO-$d_6$ 0.5 % $H_2O$ (298 K).

## Self-association constant calculation

Co-formulation ***f*** - Dilution study in DMSO-$d_6$ 5 % $H_2O$. Values calculated from data gathered from SSA (**2**) NH urea resonances.

*Equal K/Dimerization model*

$K_e$ = 4.06 $M^{-1}$ ± 1.0701 %  $K_{dim}$ = 2.03 $M^{-1}$ ± 0.5351 %

http://app.supramolecular.org/bindfit/view/abc8136b-927a-49bb-b2f7-ea2de7deb2db

*CoEK model*

$K_e$ = 10.39 $M^{-1}$ ± 2.7627 %  $K_{dim}$ = 5.19 $M^{-1}$ ± 1.3813 %  ρ = 0.52 ± 7.1161 %

http://app.supramolecular.org/bindfit/view/09420342-ea5a-48b5-aeef-92529c0aa3ac

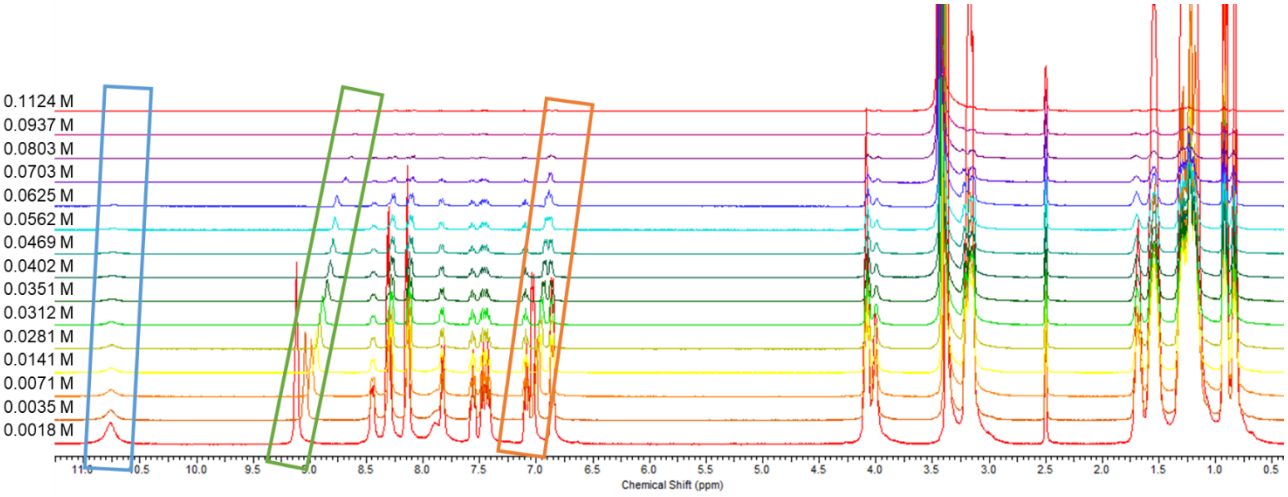


Figure S49 - $^{1}$H NMR stack plot of co-formulation ***g*** in DMSO-$d_6$ 0.5 % $H_2O$ solution. Samples were prepared in series with an aliquot of the most concentrated solution undergoing serial dilution.

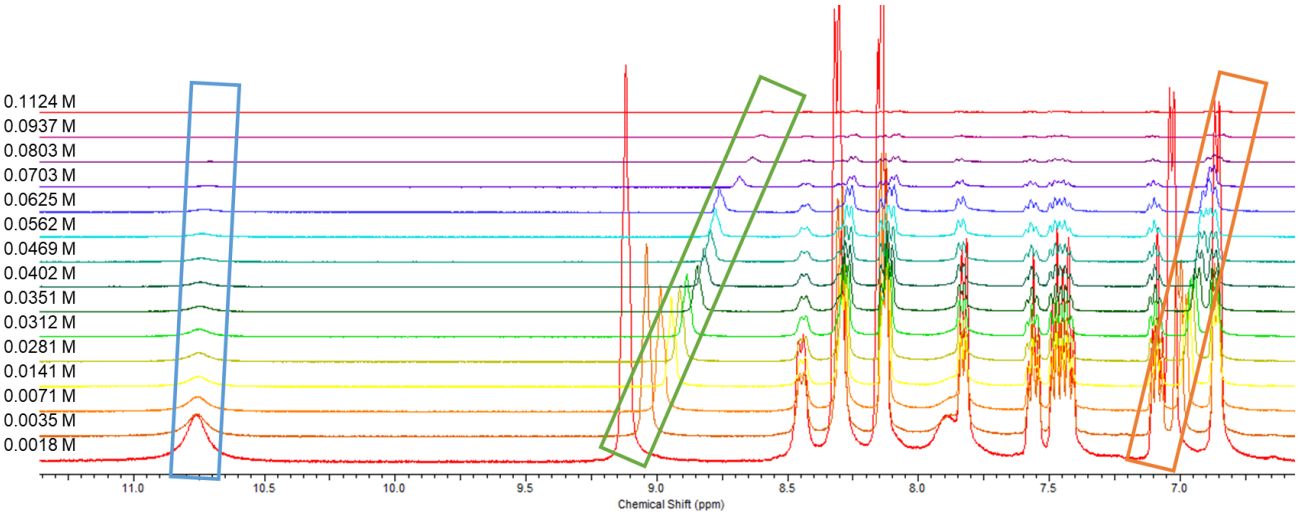


Figure S50 – Enlarged $^{1}$H NMR stack plot of co-formulation ***g*** in DMSO-$d_6$ 0.5 % $H_2O$ solution. Samples were prepared in series with an aliquot of the most concentrated solution undergoing serial dilution.

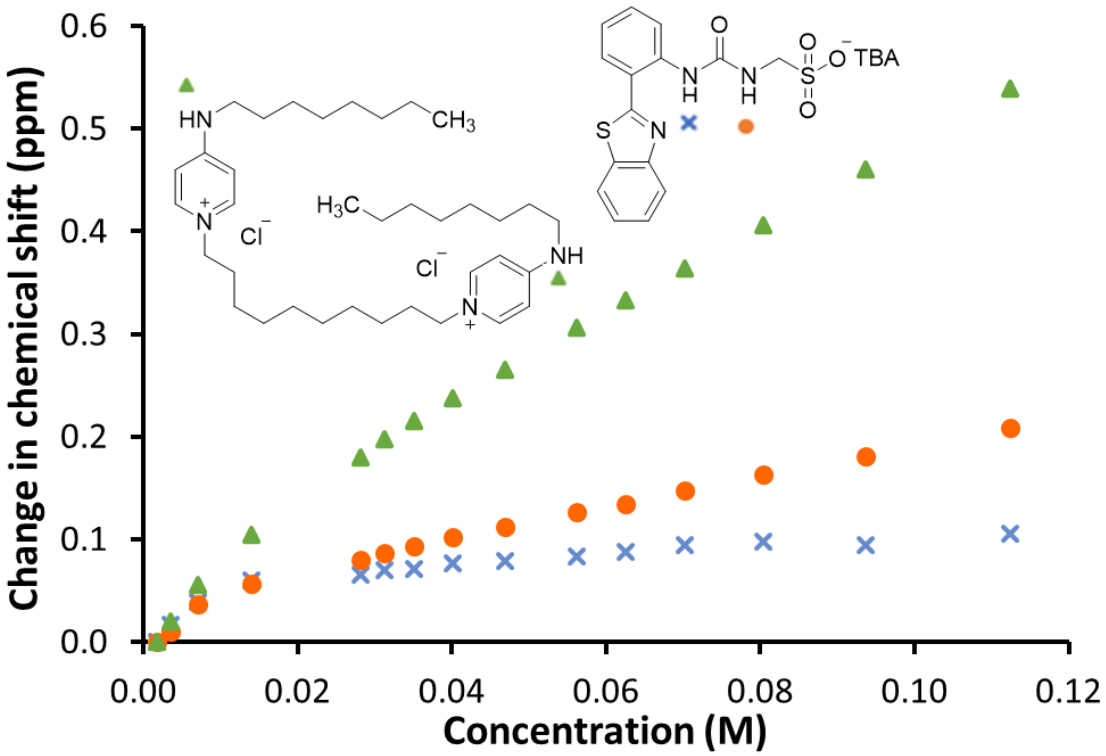


Figure S51 - Graph illustrating the $^{1}$H NMR down-field change in chemical shift of SSA (**3**) urea and appropriate co-formulant NH resonances with increasing concentration of co-formulation **g** in DMSO-$d_6$ 0.5 % $H_2O$ (298 K).

## Self-association constant calculation

Co-formulation ***g*** - Dilution study in DMSO-$d_6$ 5 % $H_2O$. Values calculated from data gathered from SSA (**3**) NH urea resonances.

*Equal K/Dimerization model*

$K_e$ = 7.81 $M^{-1}$ ± 6.1958 %  $K_{dim}$ = 3.91 $M^{-1}$ ± 3.0879 %

http://app.supramolecular.org/bindfit/view/1d3fc1ee-462a-443a-ae55-7750fd96893f

*CoEK model*

$K_e$ = 3.59 $M^{-1}$ ± 45.2451 %  $K_{dim}$ = 1.80 $M^{-1}$ ± 22.6225 %  ρ = 1.77 ± 63.8361 %

http://app.supramolecular.org/bindfit/view/219d4bd1-121d-4e51-8835-175a1e5b6add

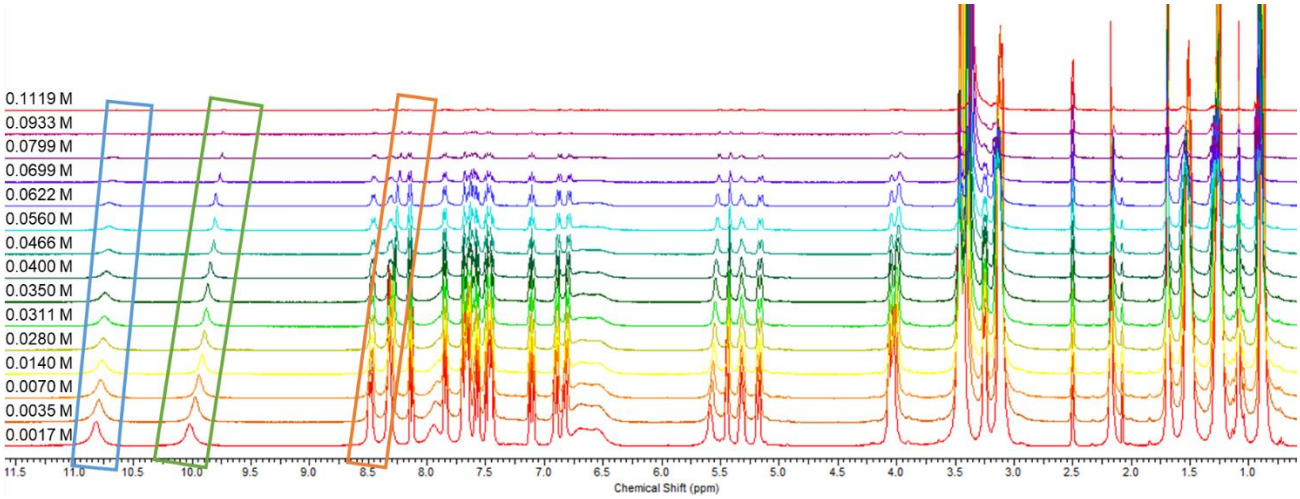


Figure S52 - $^{1}$H NMR stack plot of co-formulation ***h*** in DMSO-$d_6$ 0.5 % $H_2O$ solution. Samples were prepared in series with an aliquot of the most concentrated solution undergoing serial dilution.

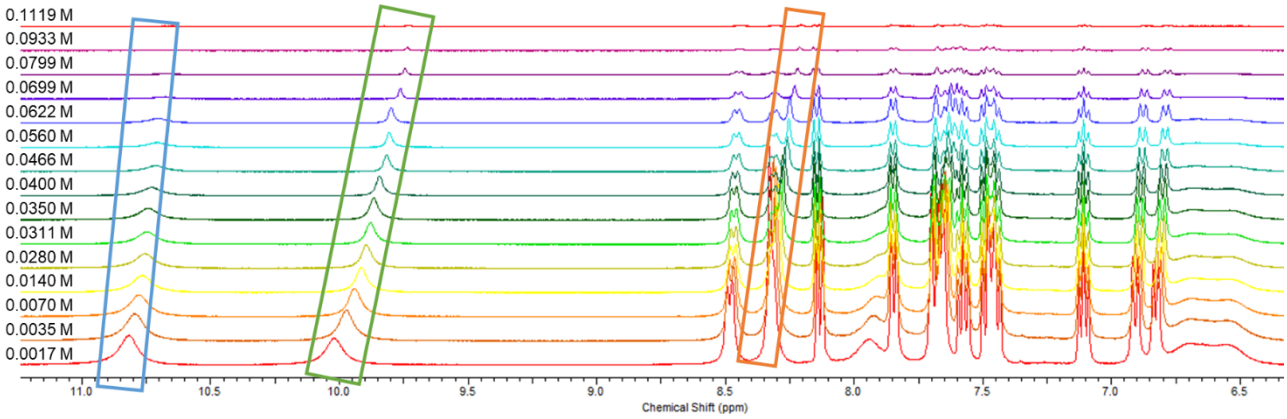


Figure S53 - Enlarged $^{1}$H NMR stack plot of co-formulation **h** in DMSO-$d_6$ 0.5 % $H_2O$ solution. Samples were prepared in series with an aliquot of the most concentrated solution undergoing serial dilution.

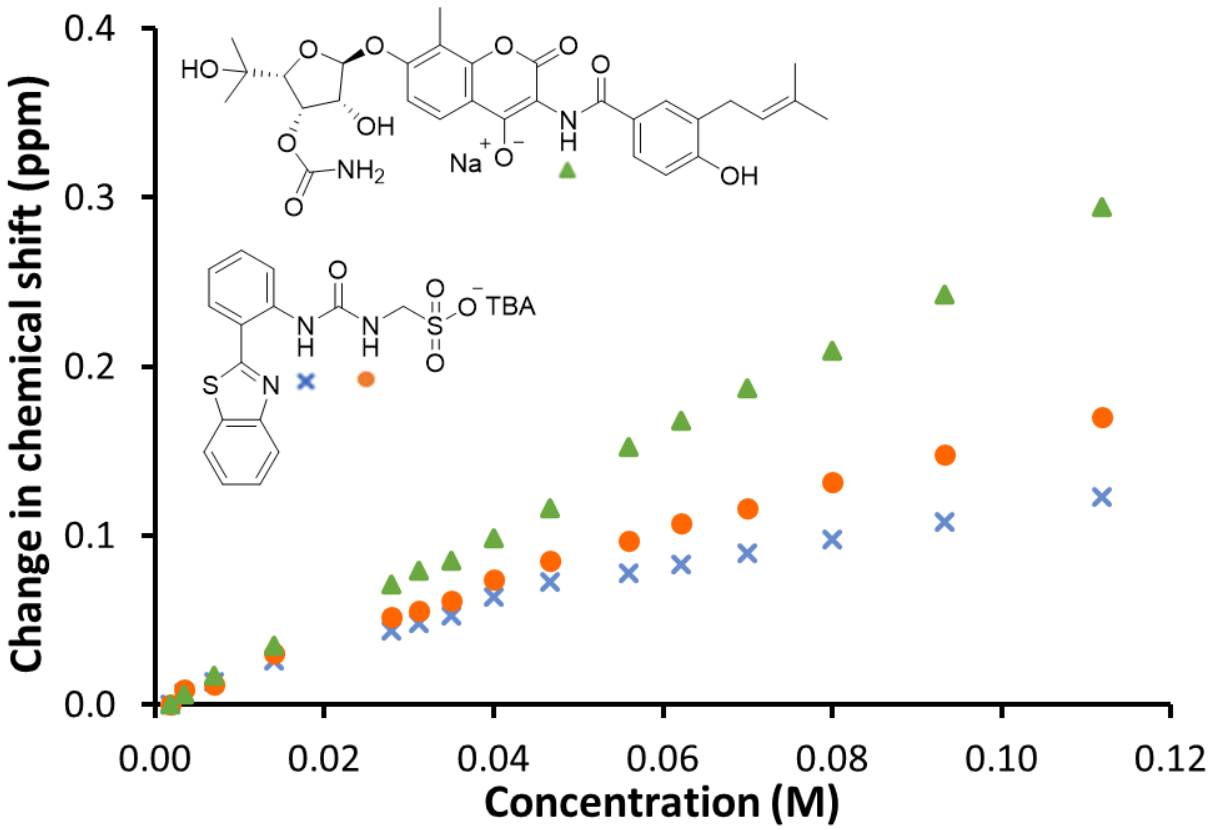


Figure S54 - Graph illustrating the $^{1}$H NMR down-field change in chemical shift of SSA (**3**) urea and appropriate co-formulant NH resonances with increasing concentration of co-formulation ***h*** in DMSO-$d_6$ 0.5 % $H_2O$ (298 K).

## Self-association constant calculation

Co-formulation ***h*** - Dilution study in DMSO-$d_6$ 5 % $H_2O$. Values calculated from data gathered from SSA (**3**) NH urea resonances.

*Equal K/Dimerization model*

$K_e$ = 2.63 $M^{-1}$ ± 1.7535 %  $K_{dim}$ = 1.31 $M^{-1}$ ± 0.8767 %

http://app.supramolecular.org/bindfit/view/1d3fc1ee-462a-443a-ae55-7750fd96893f

*CoEK model*

$K_e$ = 1.23 $M^{-1}$ ± 32.4964 %  $K_{dim}$ = 0.62 $M^{-1}$ ± 16.2482 %  ρ = 1.62 ± 37.8928 %

http://app.supramolecular.org/bindfit/view/219d4bd1-121d-4e51-8835-175a1e5b6add

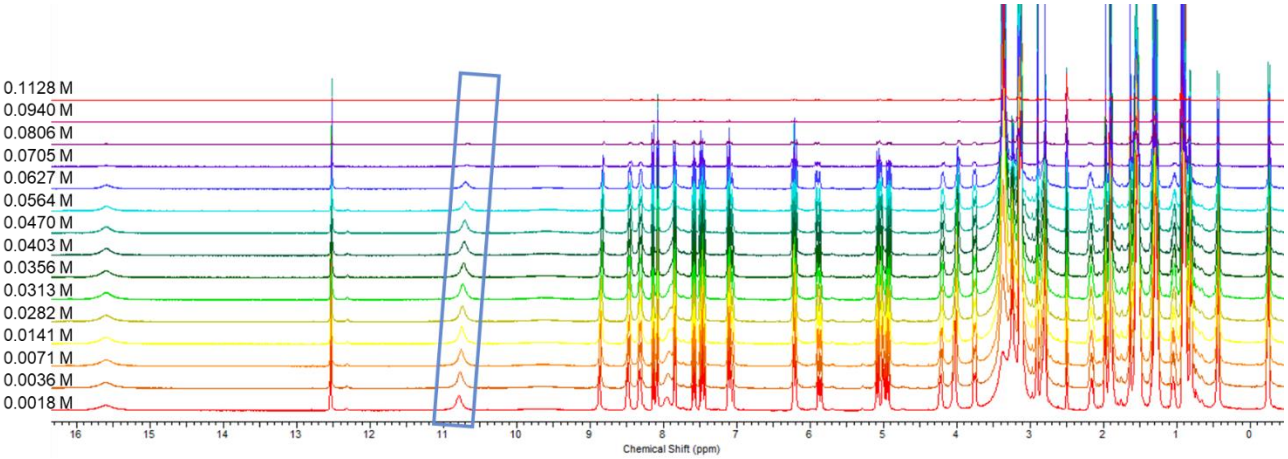


Figure S55 - $^{1}$H NMR stack plot of co-formulation ***i*** in DMSO-$d_6$ 0.5 % $H_2O$ solution. Samples were prepared in series with an aliquot of the most concentrated solution undergoing serial dilution.

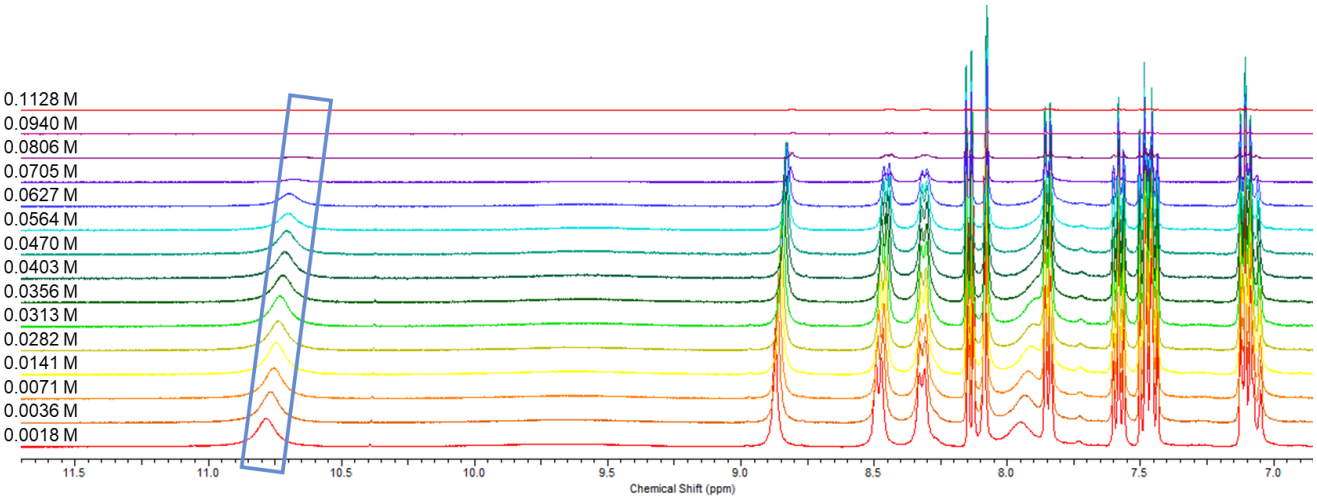


Figure S56 – Enlarged $^{1}$H NMR stack plot of co-formulation ***i*** in DMSO-$d_6$ 0.5 % $H_2O$ solution. Samples were prepared in series with an aliquot of the most concentrated solution undergoing serial dilution.

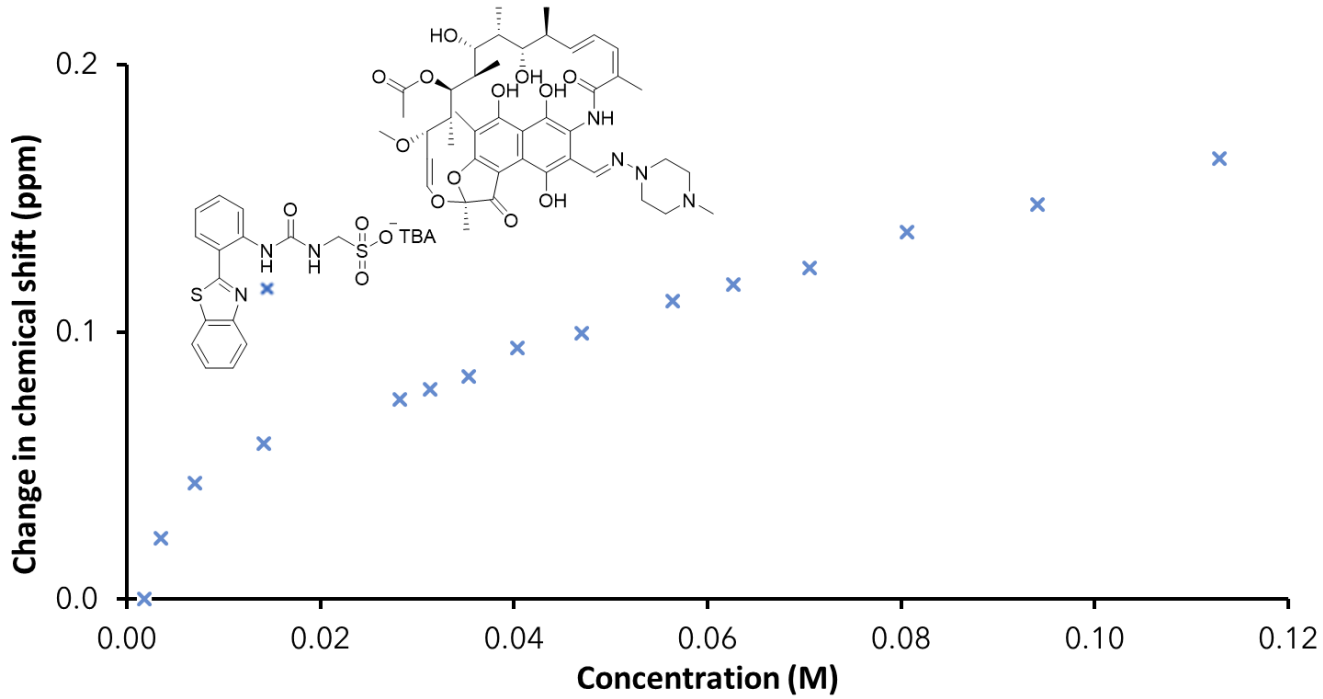


Figure S57 - Graph illustrating the $^{1}$H NMR down-field change in chemical shift of SSA (**3**) urea and appropriate co-formulant NH resonances with increasing concentration of co-formulation ***i*** in DMSO-$d_6$ 0.5 % $H_2O$ (298 K).

## Self-association constant calculation

Co-formulation ***i*** - Dilution study in DMSO-$d_6$ 5 % $H_2O$. Values calculated from data gathered from a single SSA (**3**) NH urea resonance.

*Equal K/Dimerization model*

$K_e$ = 8.17 $M^{-1}$ ± 7.7895 %  $K_{dim}$ = 4.09 $M^{-1}$ ± 3.8948 %

http://app.supramolecular.org/bindfit/view/b48e0b8d-253e-4047-847d-d41aacb47b7a

*CoEK model*

$K_e$ = 3.80 $M^{-1}$ ± 55.5630 %  $K_{dim}$ = 1.90 $M^{-1}$ ± 27.7815 %  ρ = 1.77 ± 79.6074 %

http://app.supramolecular.org/bindfit/view/4be487b0-6863-4881-88a7-d8304669766c

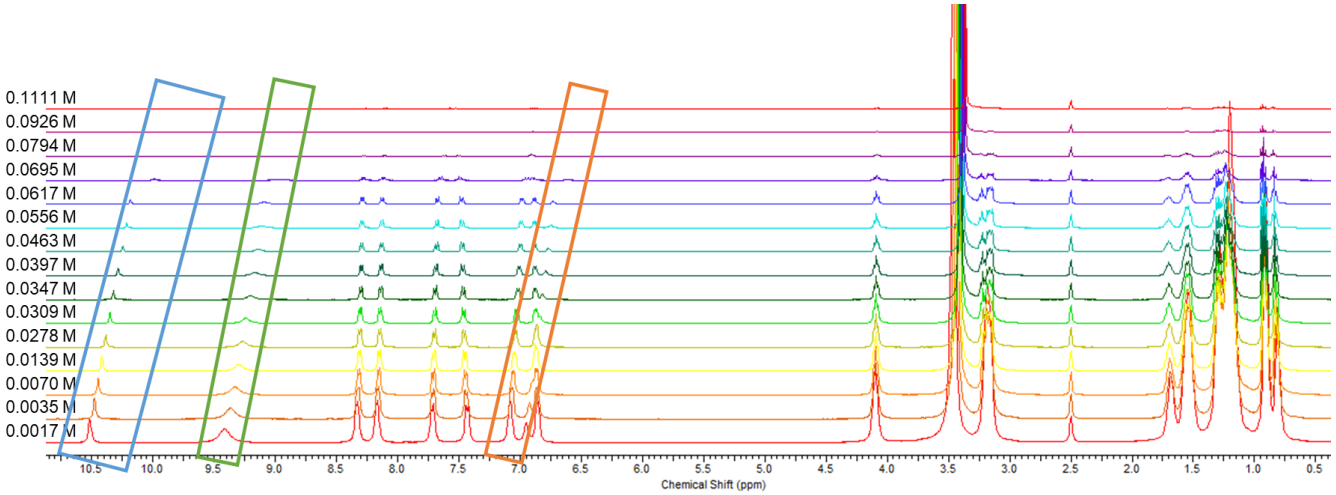


Figure S58 - $^{1}$H NMR stack plot of co-formulation ***j*** in DMSO-$d_6$ 0.5 % $H_2O$ solution. Samples were prepared in series with an aliquot of the most concentrated solution undergoing serial dilution.

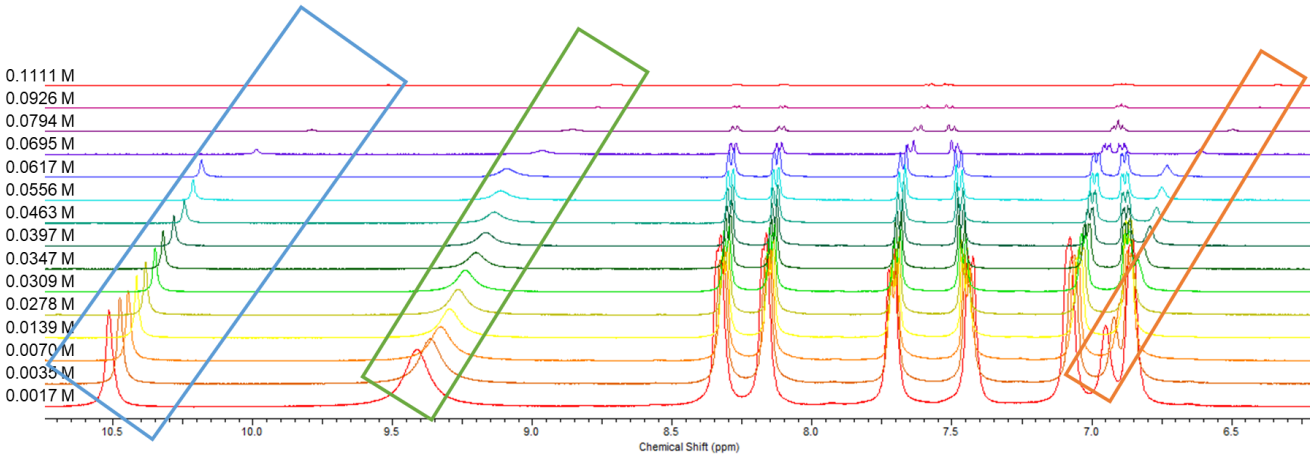


Figure S59 – Enlarged $^{1}$H NMR stack plot of co-formulation ***j*** in DMSO-$d_6$ 0.5 % $H_2O$ solution. Samples were prepared in series with an aliquot of the most concentrated solution undergoing serial dilution.

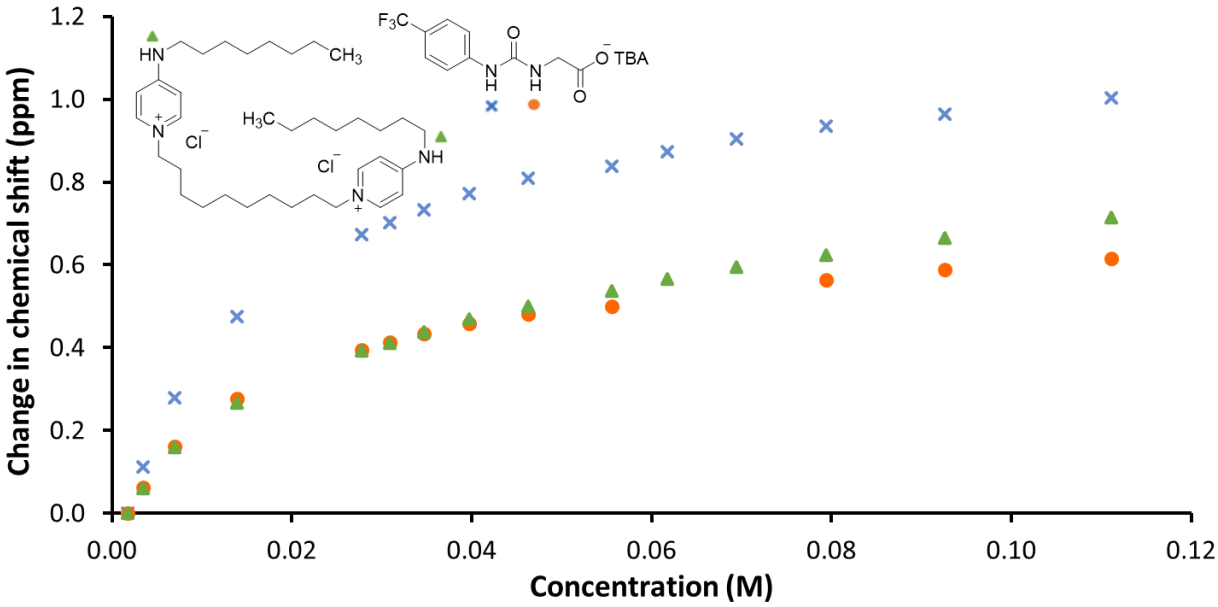


Figure S60 - Graph illustrating the $^{1}$H NMR down-field change in chemical shift of SSA (**4**) urea and appropriate co-formulant NH resonances with increasing concentration of co-formulation ***j*** in DMSO-$d_6$ 0.5 % $H_2O$ (298 K).

## Self-association constant calculation

Co-formulation ***j*** - Dilution study in DMSO-$d_6$ 5 % $H_2O$. Values calculated from data gathered from a single SSA (**4**) NH urea resonance.

*Equal K/Dimerization model*

$K_e$ = 78.18 $M^{-1}$ ± 1.2112 %  $K_{dim}$ = 39.09 $M^{-1}$ ± 0.6056 %

http://app.supramolecular.org/bindfit/view/23183f48-d5fc-4d1a-afa7-f904f88b887b

*CoEK model*

$K_e$ = 81.59 $M^{-1}$ ± 1.1801 %  $K_{dim}$ = 40.80 $M^{-1}$ ± 0.5900 %  ρ = 0.84 ± 3.8983 %

http://app.supramolecular.org/bindfit/view/dc86b128-752c-437e-86d3-ab349697afac

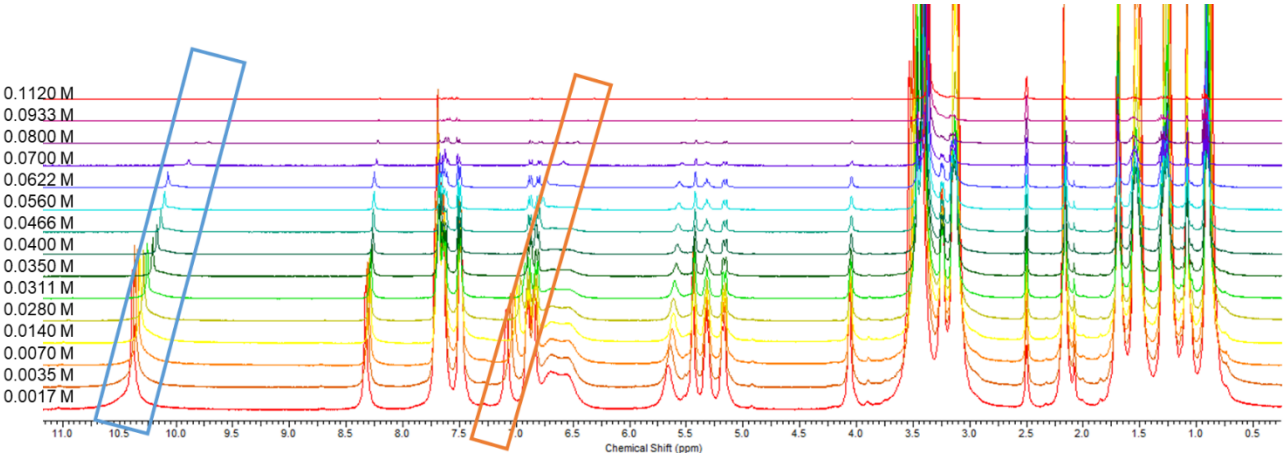


Figure S61 - $^{1}$H NMR stack plot of co-formulation **k** in DMSO-$d_6$ 0.5 % $H_2O$ solution. Samples were prepared in series with an aliquot of the most concentrated solution undergoing serial dilution.

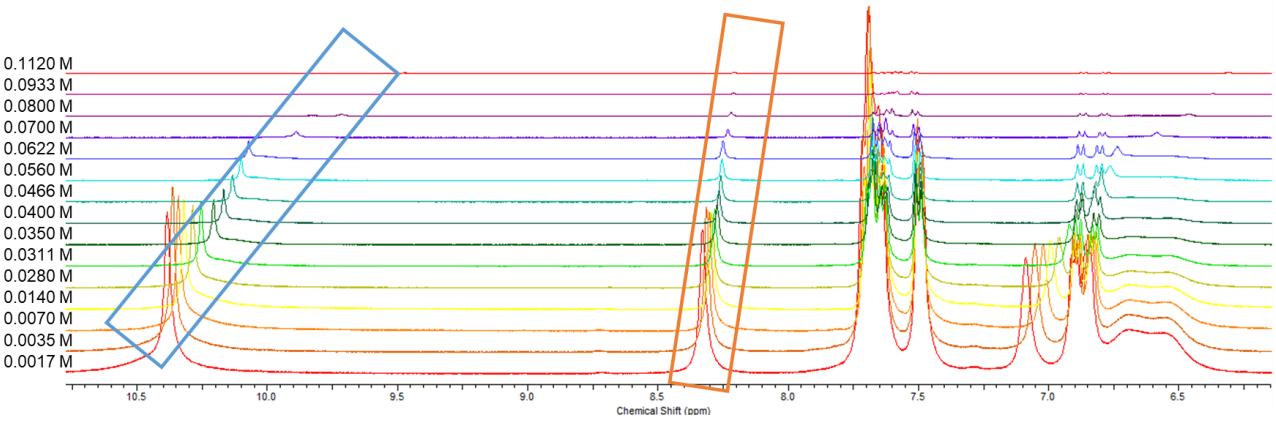


Figure S62 – Enlarged $^{1}$H NMR stack plot of co-formulation ***k*** in DMSO-$d_6$ 0.5 % $H_2O$ solution. Samples were prepared in series with an aliquot of the most concentrated solution undergoing serial dilution.

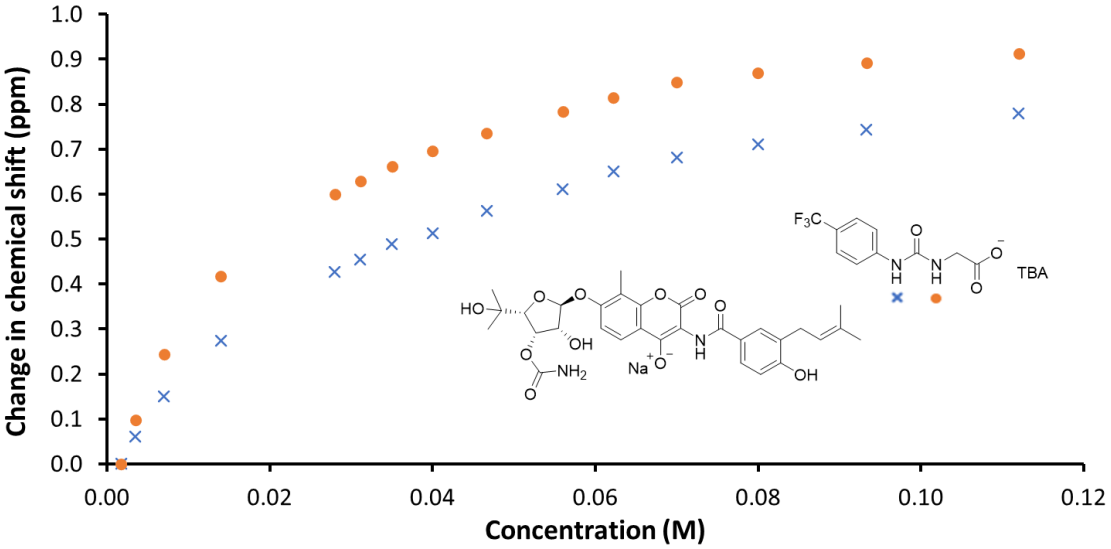


Figure S63 - Graph illustrating the $^{1}$H NMR down-field change in chemical shift of SSA (**4**) urea and appropriate co-formulant NH resonances with increasing concentration of co-formulation ***k*** in DMSO-$d_6$ 0.5 % $H_2O$ (298 K).

## Self-association constant calculation

Co-formulation ***k*** - Dilution study in DMSO-$d_6$ 5 % $H_2O$. Values calculated from data gathered from SSA (**4**) NH urea resonances.

*Equal K/Dimerization model*

$K_e$ = 41.90 $M^{-1}$ ± 3.1148 %  $K_{dim}$ = 20.95 $M^{-1}$ ± 1.5574 %

http://app.supramolecular.org/bindfit/view/efb348f6-f123-492f-9a9d-632c43cabdac

*CoEK model*

$K_e$ = 42.06 $M^{-1}$ ± 3.3053 %  $K_{dim}$ = 21.03 $M^{-1}$ ± 1.6526 %  ρ = 0.99 ± 12.5209 %

http://app.supramolecular.org/bindfit/view/f5957374-1a78-4b1b-8bd2-044b20adffae

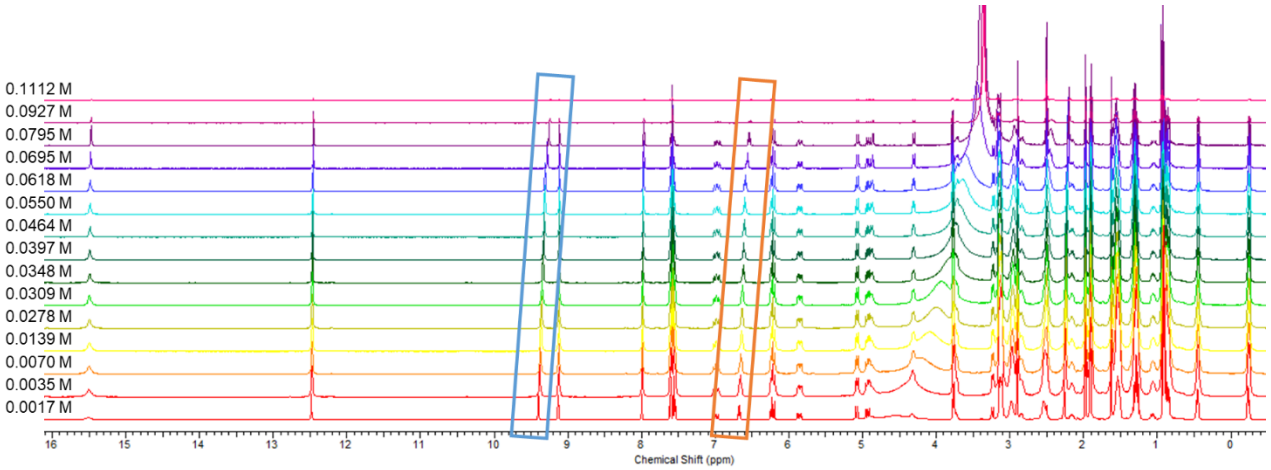


Figure S64 - $^{1}$H NMR stack plot of co-formulation ***I*** in DMSO-$d_6$ 0.5 % $H_2O$ solution. Samples were prepared in series with an aliquot of the most concentrated solution undergoing serial dilution.

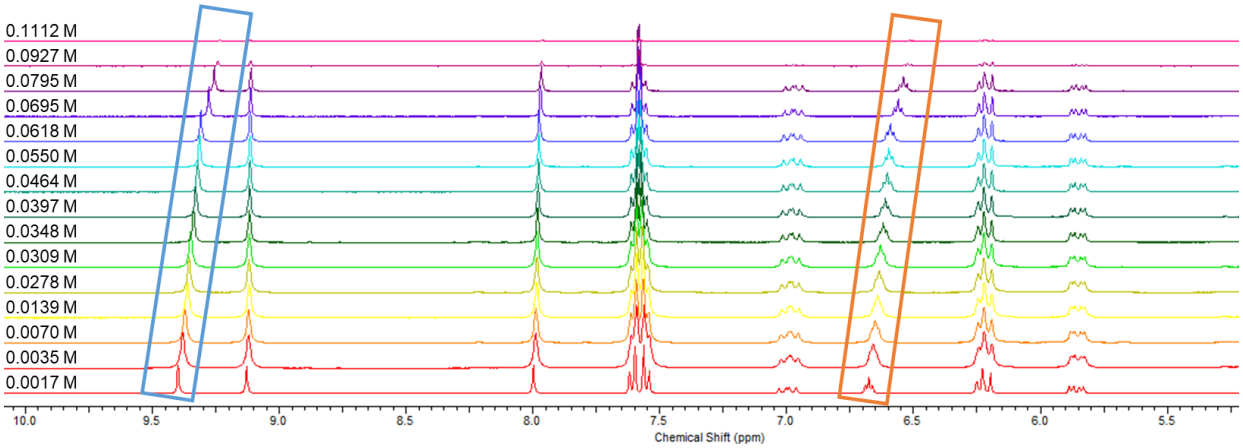


Figure S65 – Enlarged $^{1}$H NMR stack plot of co-formulation ***I*** in DMSO-$d_6$ 0.5 % $H_2O$ solution. Samples were prepared in series with an aliquot of the most concentrated solution undergoing serial dilution.

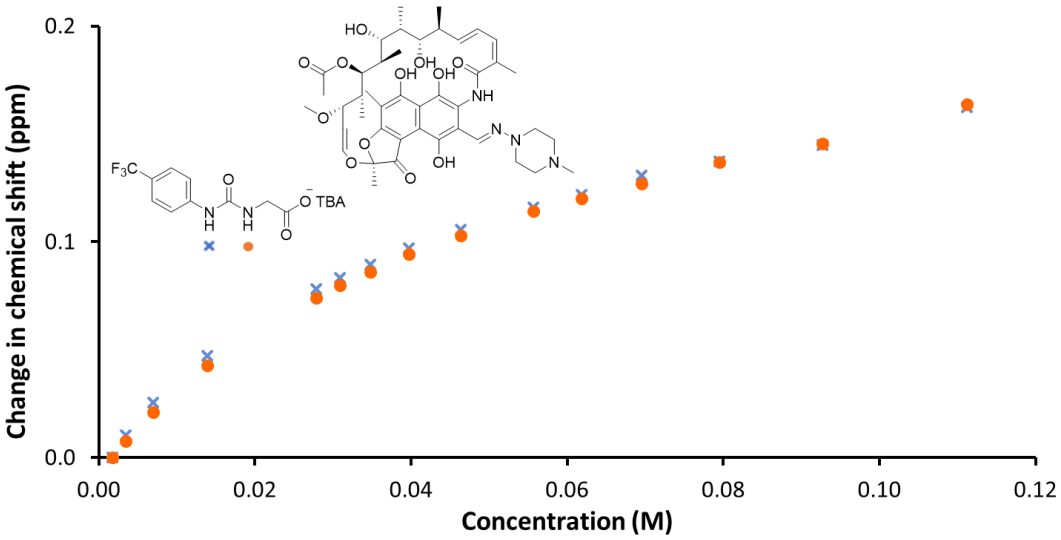


Figure S66 - Graph illustrating the $^{1}$H NMR down-field change in chemical shift of SSA (**4**) urea and appropriate co-formulant NH resonances with increasing concentration of co-formulation ***I*** in DMSO-$d_6$ 0.5 % $H_2O$ (298 K).

## Self-association constant calculation

Co-formulation ***i*** - Dilution study in DMSO-$d_6$ 5 % $H_2O$. Values calculated from data gathered from a single SSA (**4**) NH urea resonance.

*Equal K/Dimerization model*

$K_e$ = 13.23 $M^{-1}$ ± 1.2414 %  $K_{dim}$ = 6.62 $M^{-1}$ ± 0.6207 %

http://app.supramolecular.org/bindfit/view/54ae6033-228a-49fc-a0be-7a4cbfa2477c

*CoEK model*

$K_e$ = 5.44 $M^{-1}$ ± 5.8420 %  $K_{dim}$ = 2.72 $M^{-1}$ ± 2.9210 %  ρ = 1.96 ± 9.1254 %

http://app.supramolecular.org/bindfit/view/8ced8d04-5a65-41f1-9f90-1766f092c834

## Dynamic light scattering

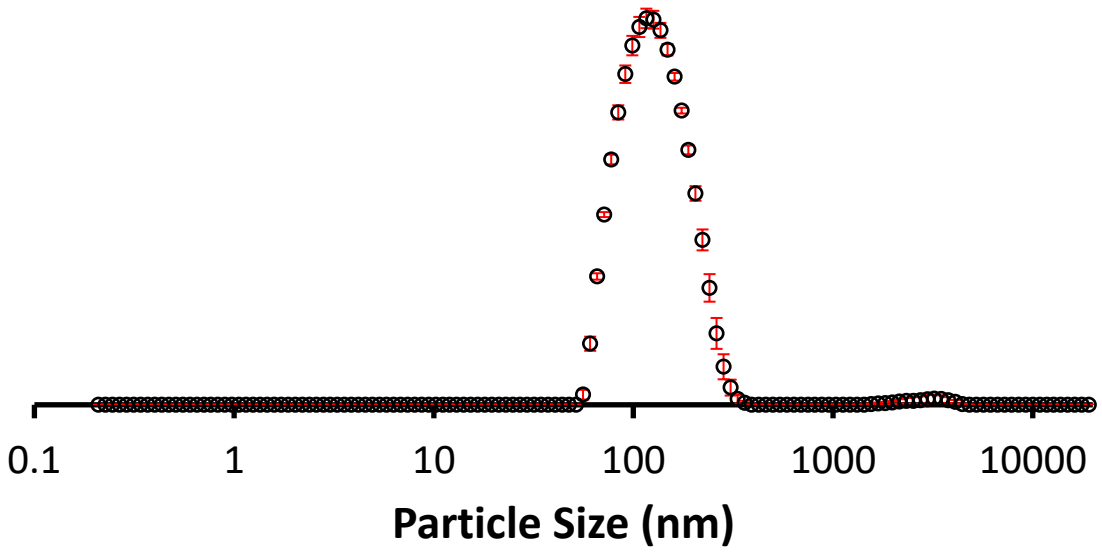


Figure S67 - The average intensity particle size distribution calculated using 9 DLS runs for co-formulation ***b*** (0.56 mM) in an EtOH: $H_2O$ (1:19) solution at 298 K.

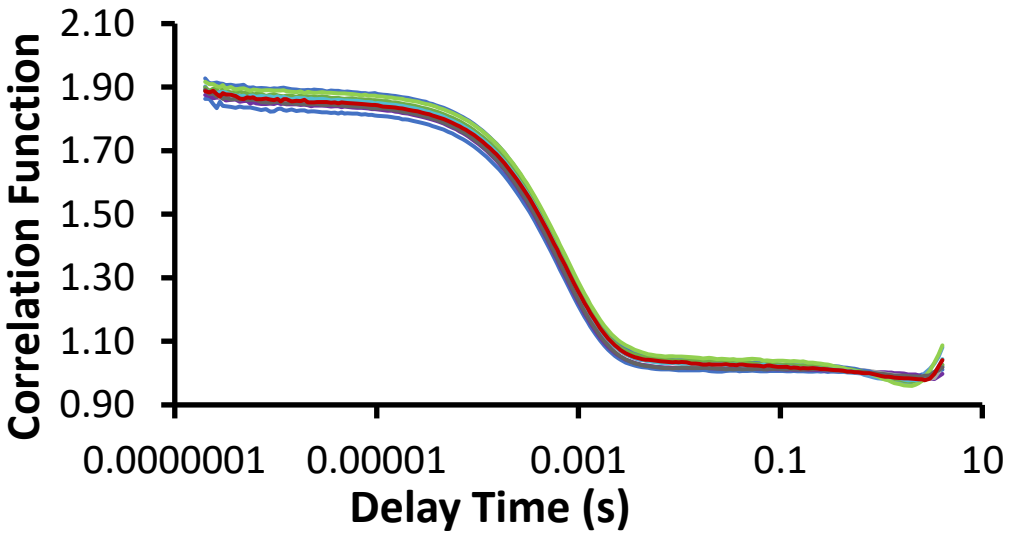


Figure S68 - Correlation function data for 9 DLS runs of co-formulation ***b*** (0.56 mM) in an EtOH: $H_2O$ (1:19) solution at 298 K.

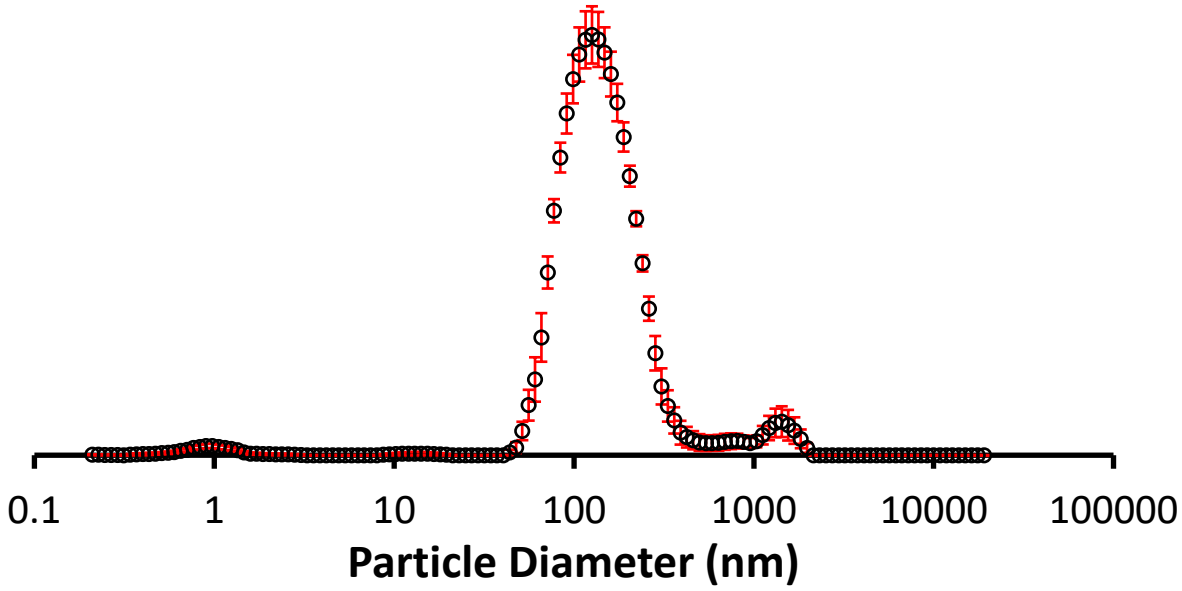


Figure S69 - The average intensity particle size distribution calculated using 9 DLS runs for co-formulation ***c*** (0.56 mM) in an EtOH: $H_2O$ (1:19) solution at 298 K.

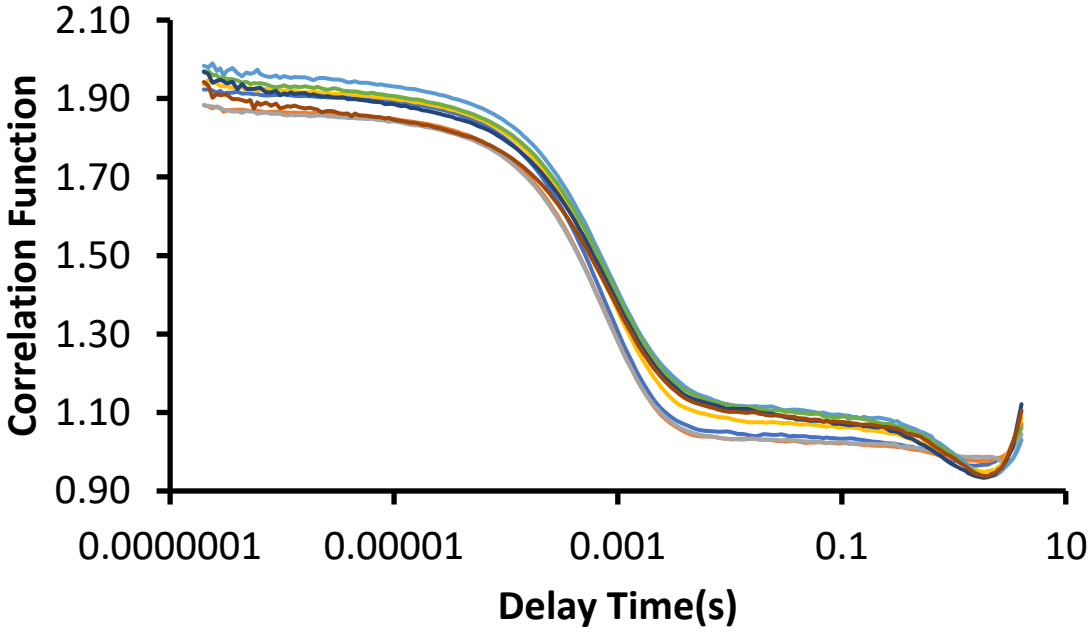


Figure S70 - Correlation function data for 9 DLS runs of co-formulation ***c*** (0.56 mM) in an EtOH: $H_2O$ (1:19) solution at 298 K.

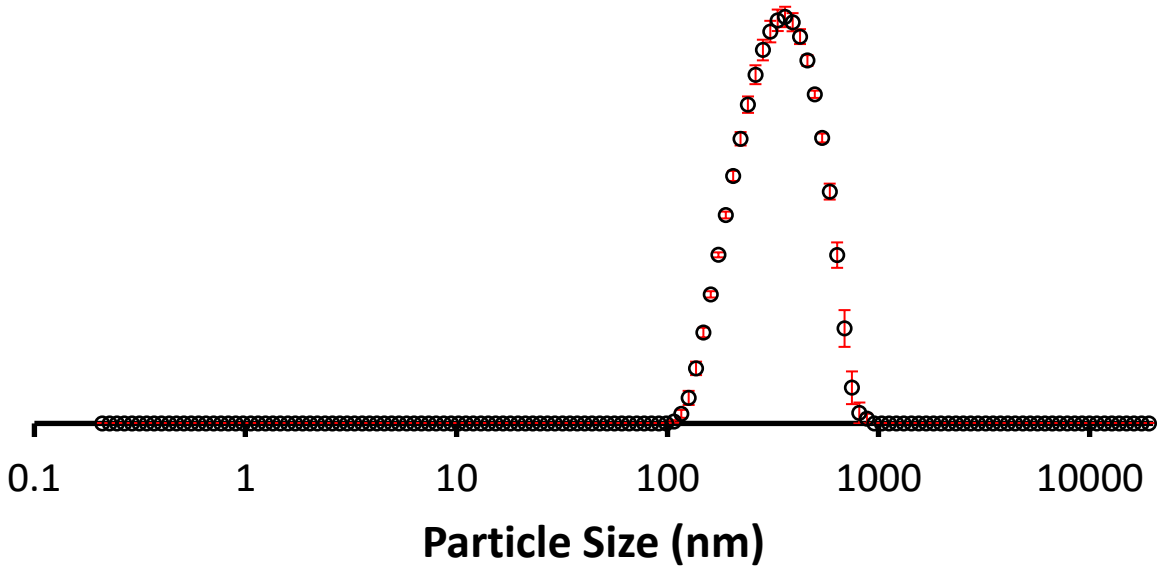


Figure S71 - The average intensity particle size distribution calculated using 9 DLS runs for co-formulation ***d*** (0.56 mM) in an EtOH: $H_2O$ (1:19) solution at 298 K.

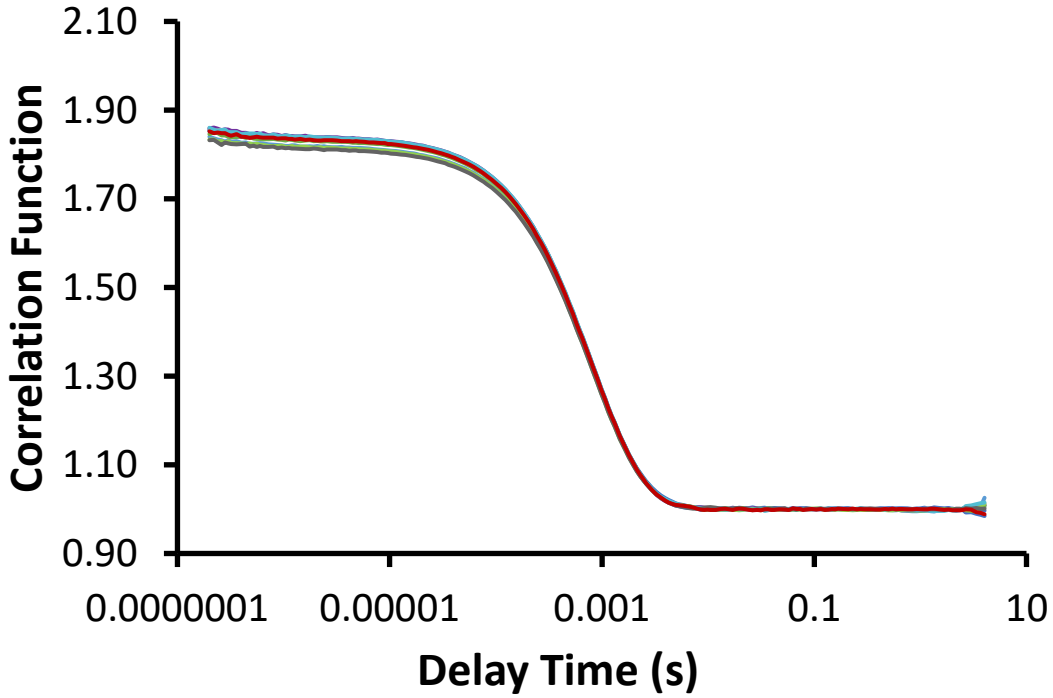


Figure S72 - Correlation function data for 9 DLS runs of co-formulation ***d*** (0.56 mM) in an EtOH: $H_2O$ (1:19) solution at 298 K.

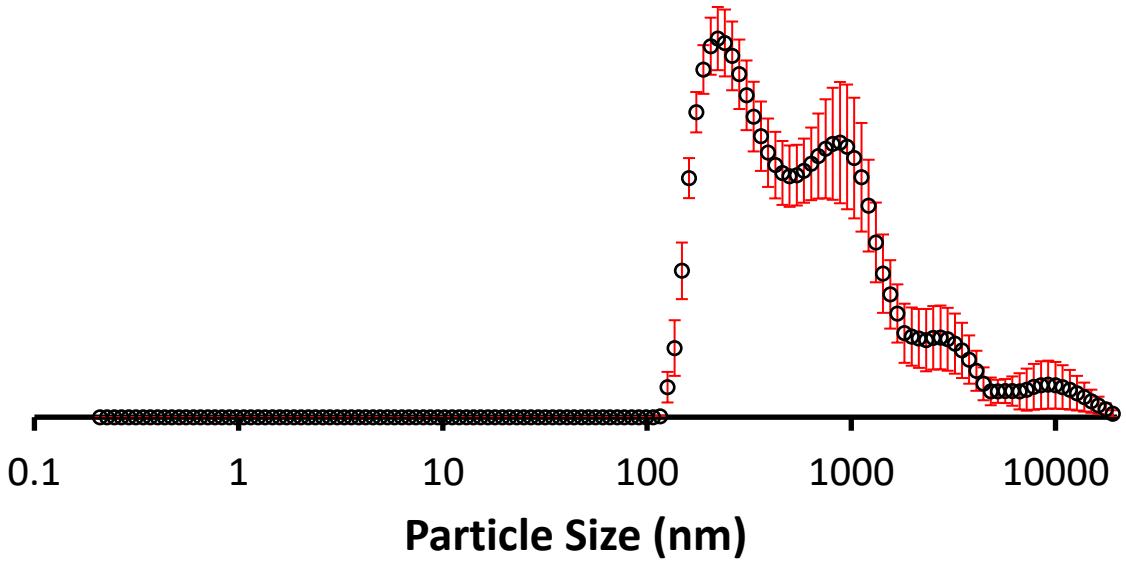


Figure S73 - The average intensity particle size distribution calculated using 9 DLS runs for co-formulation ***e*** (0.56 mM) in an EtOH: $H_2O$ (1:19) solution at 298 K.

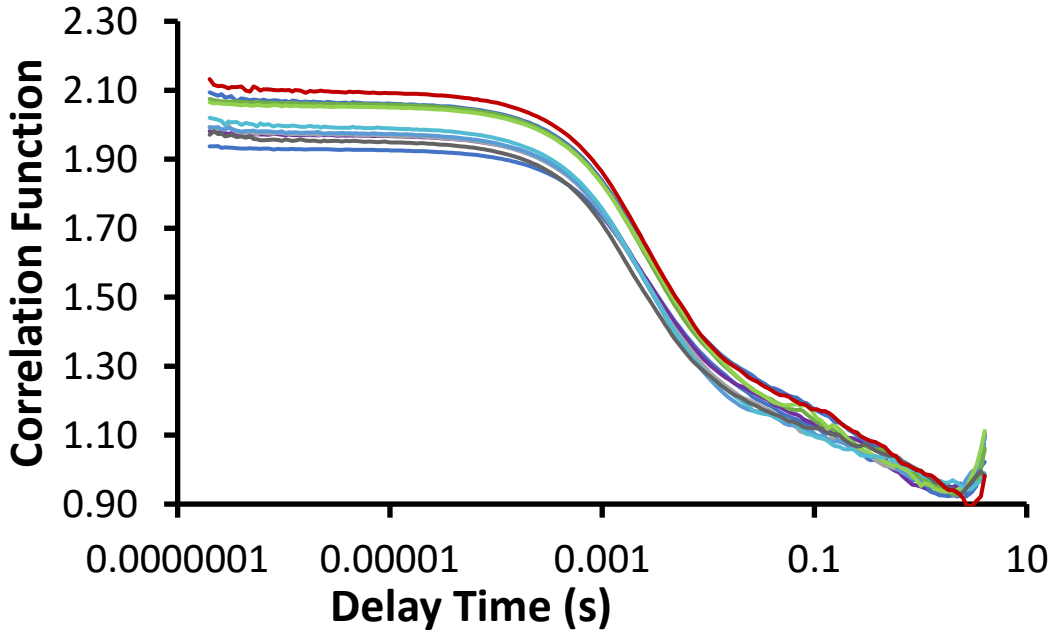


Figure S74 - Correlation function data for 9 DLS runs of co-formulation ***e*** (0.56 mM) in an EtOH: $H_2O$ (1:19) solution at 298 K.

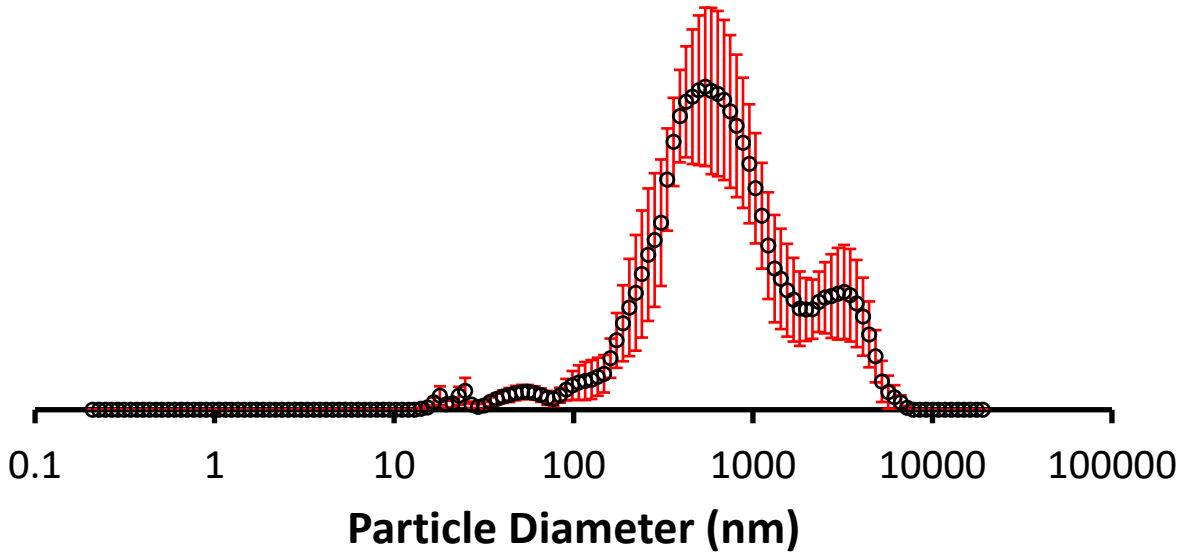


Figure S75 - The average intensity particle size distribution calculated using 9 DLS runs for co-formulation ***f*** (0.56 mM) in an EtOH: $H_2O$ (1:19) solution at 298 K.

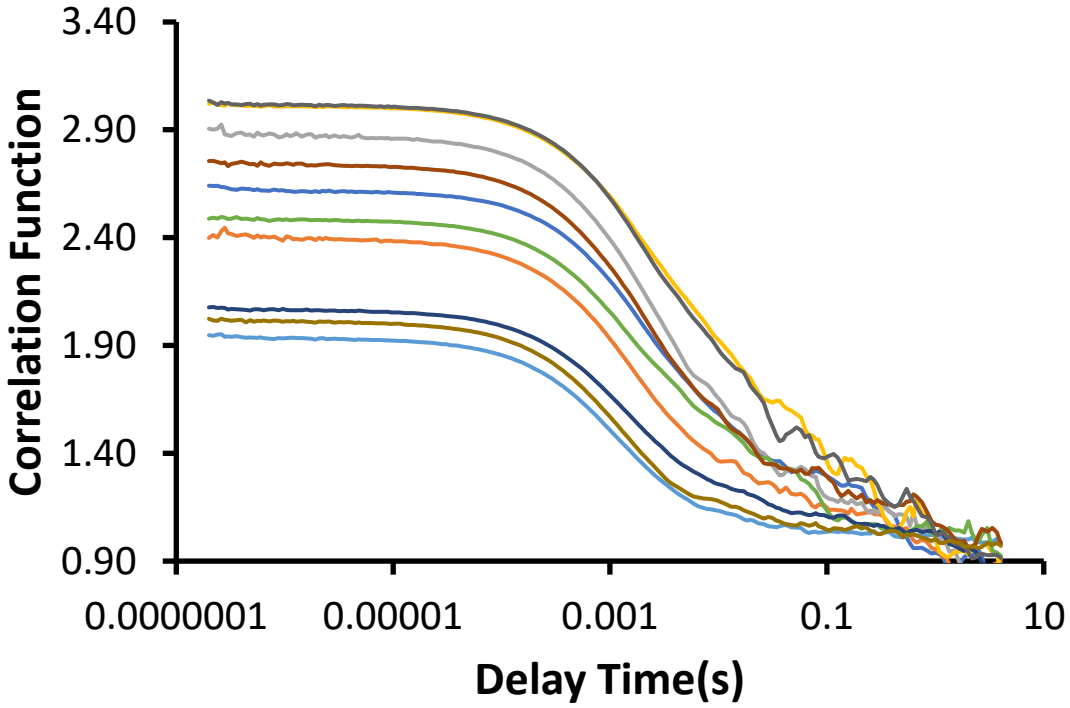


Figure S76 - Correlation function data for 9 DLS runs of co-formulation ***f*** (0.56 mM) in an EtOH: $H_2O$ (1:19) solution at 298 K.

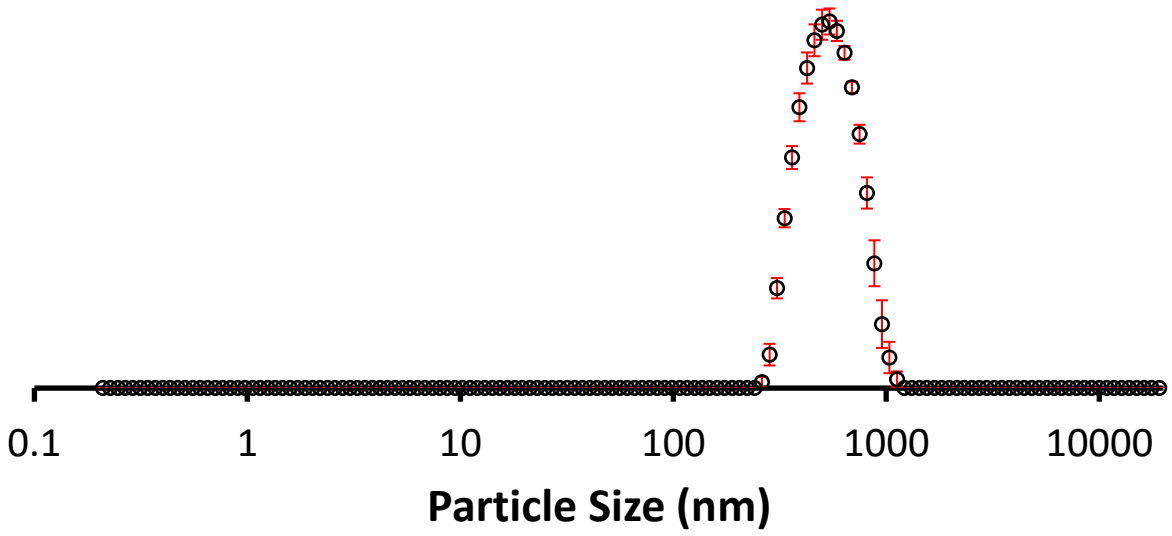


Figure S77 - The average intensity particle size distribution calculated using 9 DLS runs for co-formulation ***g*** (0.56 mM) in an EtOH: $H_2O$ (1:19) solution at 298 K.

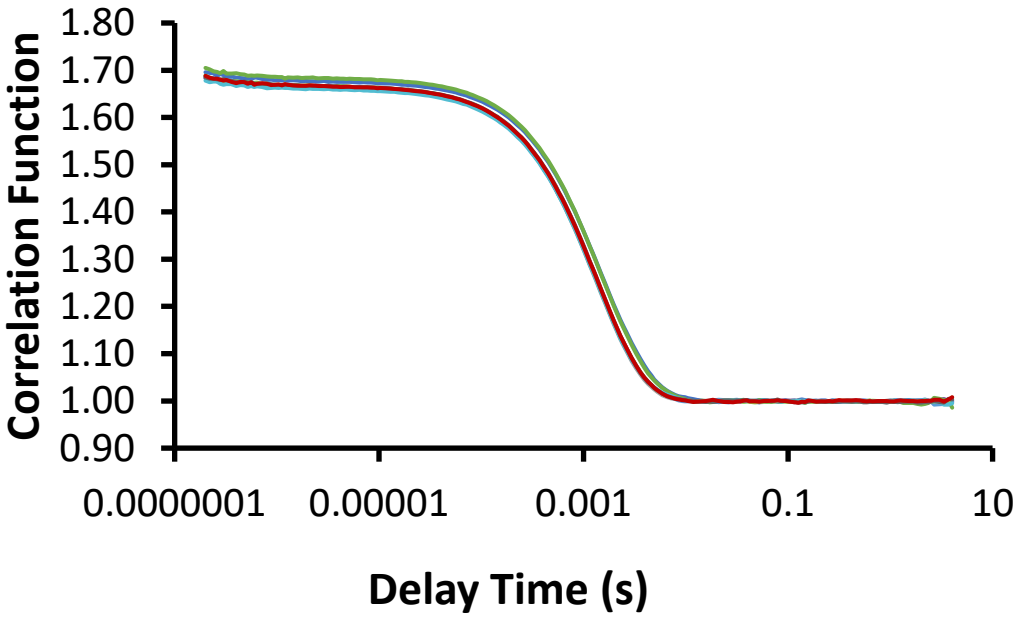


Figure S78 - Correlation function data for 9 DLS runs of co-formulation ***g*** (0.56 mM) in an EtOH: $H_2O$ (1:19) solution at 298 K.

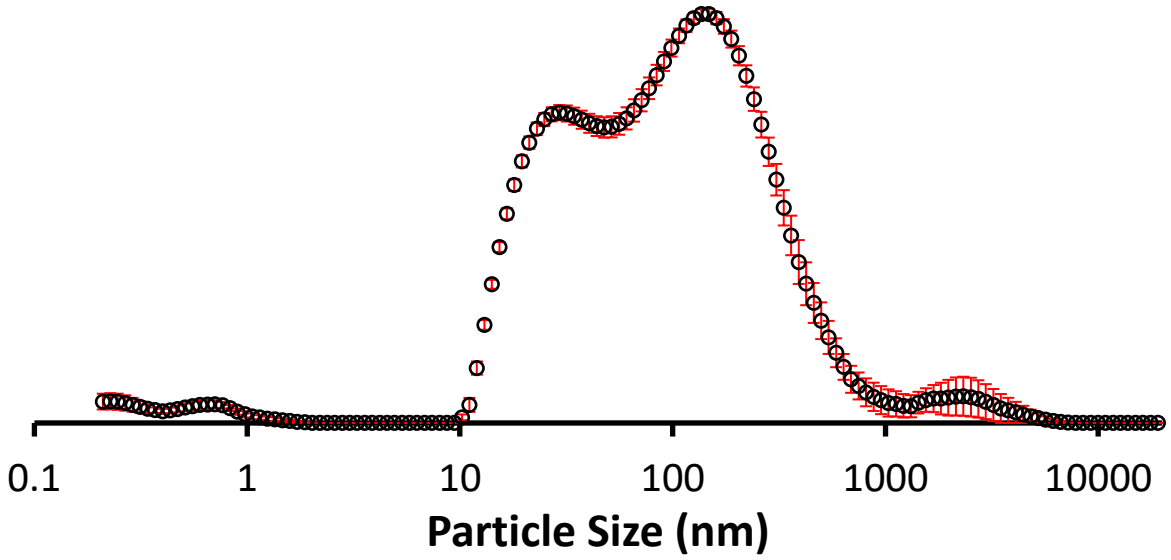


Figure S79 - The average intensity particle size distribution calculated using 9 DLS runs for co-formulation ***h*** (0.56 mM) in an EtOH: $H_2O$ (1:19) solution at 298 K.

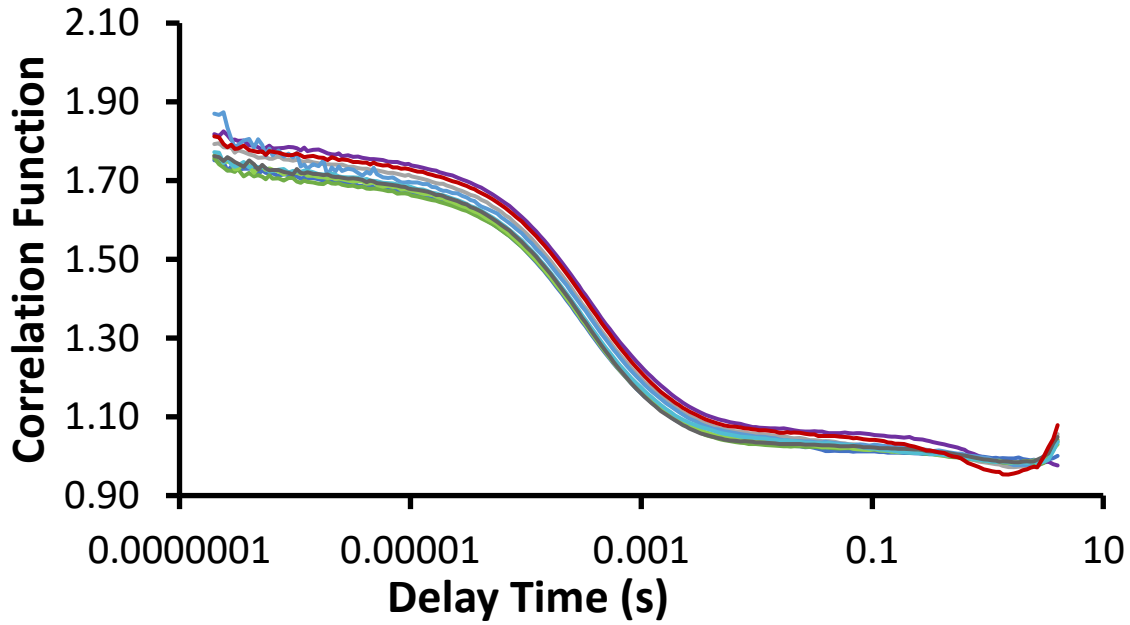


Figure S80 - Correlation function data for 9 DLS runs of co-formulation ***h*** (0.56 mM) in an EtOH: $H_2O$ (1:19) solution at 298 K.

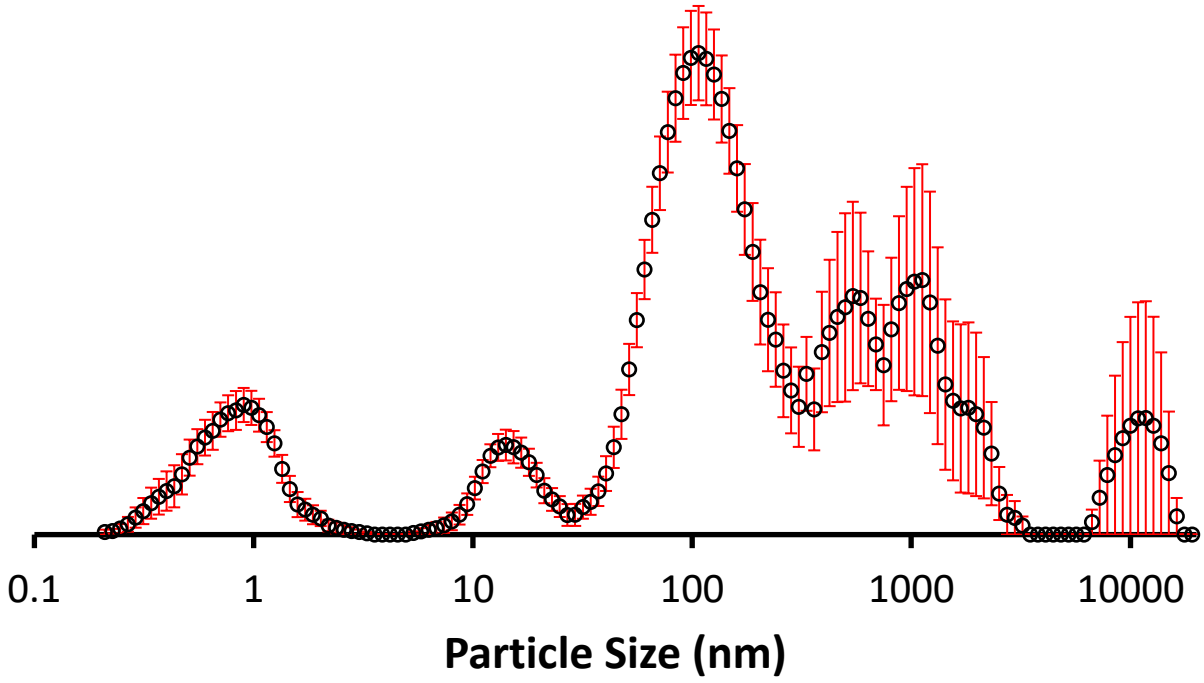


Figure S81 - The average intensity particle size distribution calculated using 9 DLS runs for co-formulation ***i*** (0.56 mM) in an EtOH: $H_2O$ (1:19) solution at 298 K.

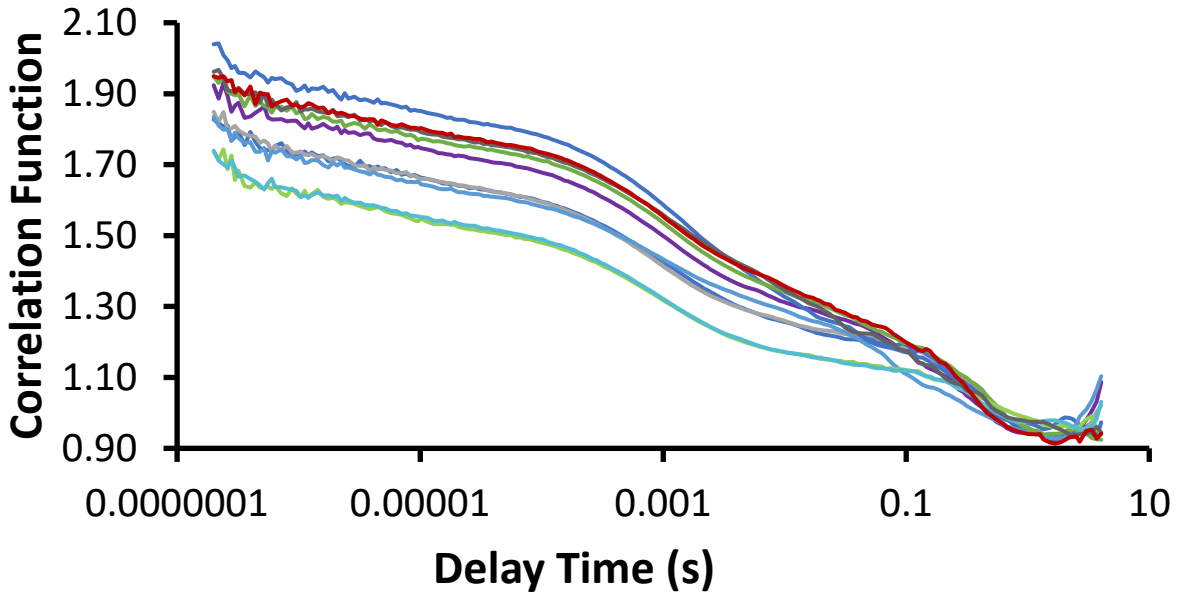


Figure S82 - Correlation function data for 9 DLS runs of co-formulation ***i*** (0.56 mM) in an EtOH: $H_2O$ (1:19) solution at 298 K.

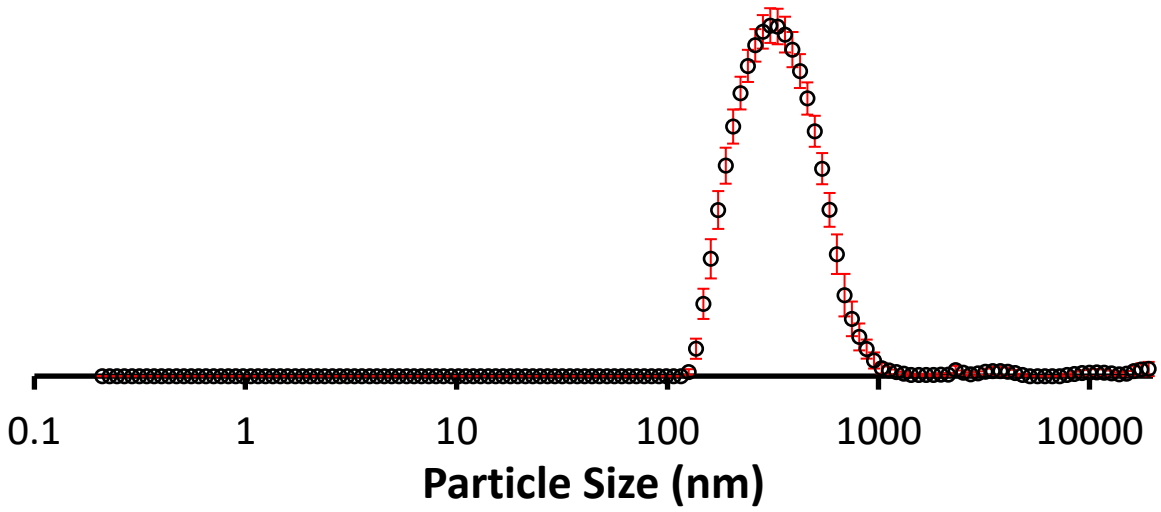


Figure S83 - The average intensity particle size distribution calculated using 9 DLS runs for co-formulation ***j*** (0.56 mM) in an EtOH: $H_2O$ (1:19) solution at 298 K.

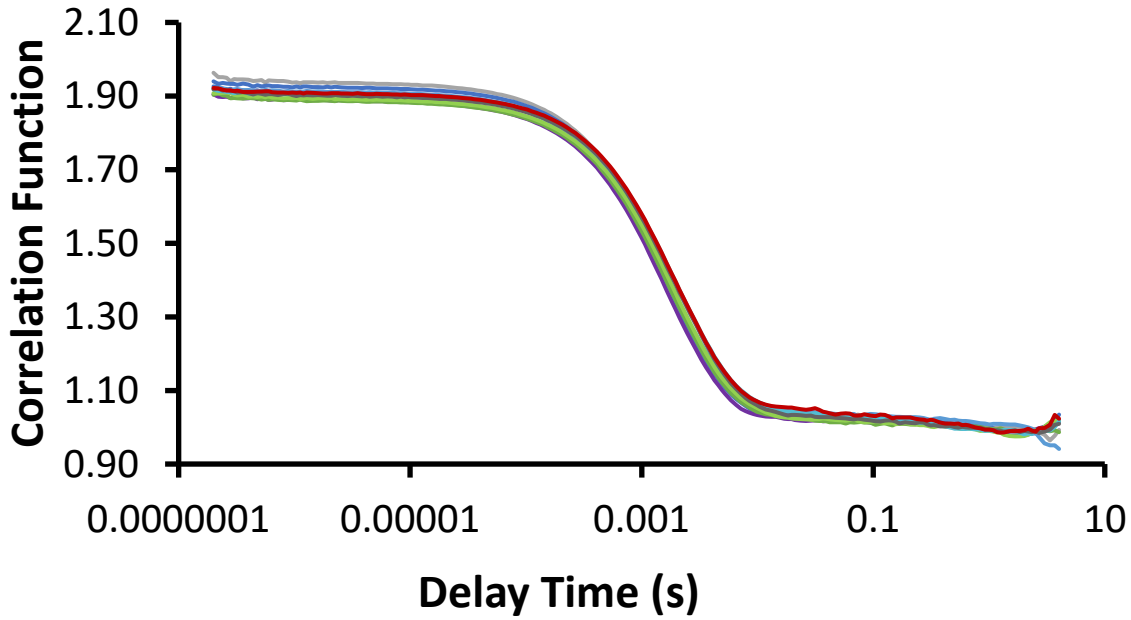


Figure S84 - Correlation function data for 9 DLS runs of co-formulation ***j*** (0.56 mM) in an EtOH: $H_2O$ (1:19) solution at 298 K.

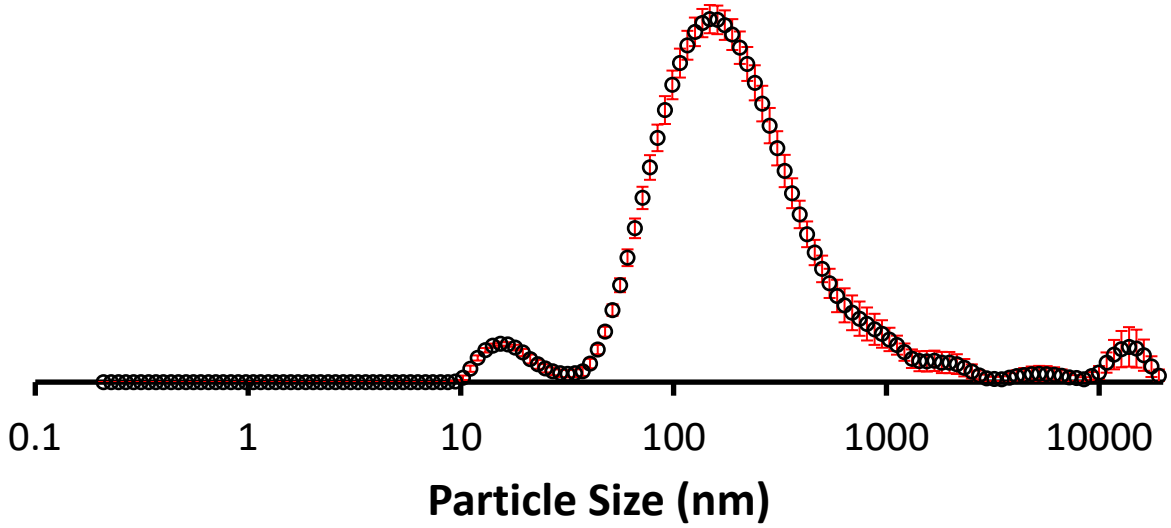


Figure S85 - The average intensity particle size distribution calculated using 9 DLS runs for co-formulation ***k*** (0.56 mM) in an EtOH: $H_2O$ (1:19) solution at 298 K.

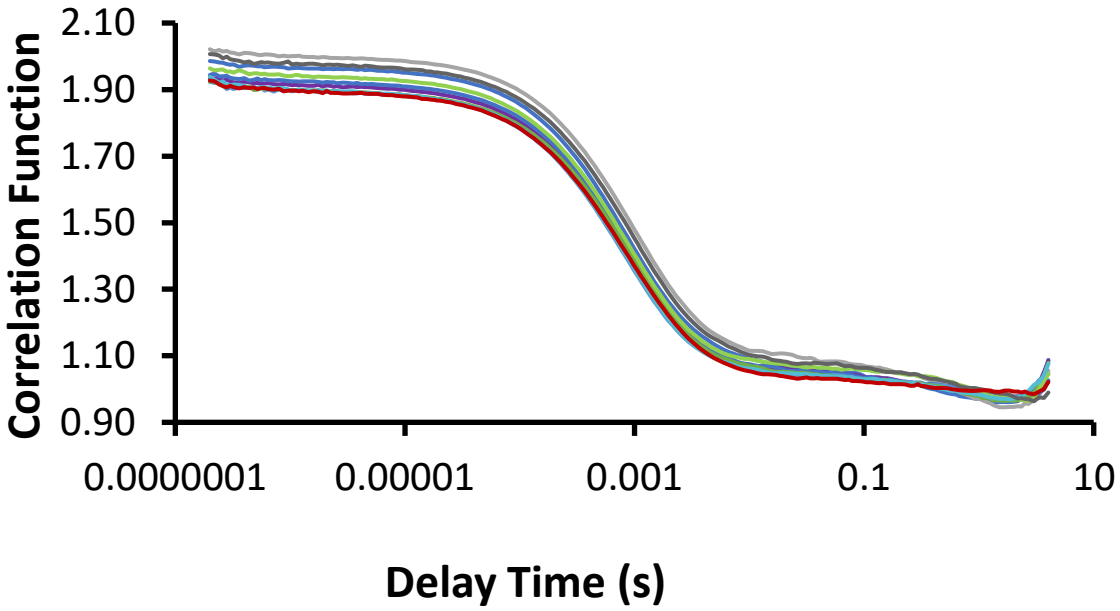


Figure S86 - Correlation function data for 9 DLS runs of co-formulation ***k*** (0.56 mM) in an EtOH: $H_2O$ (1:19) solution at 298 K.

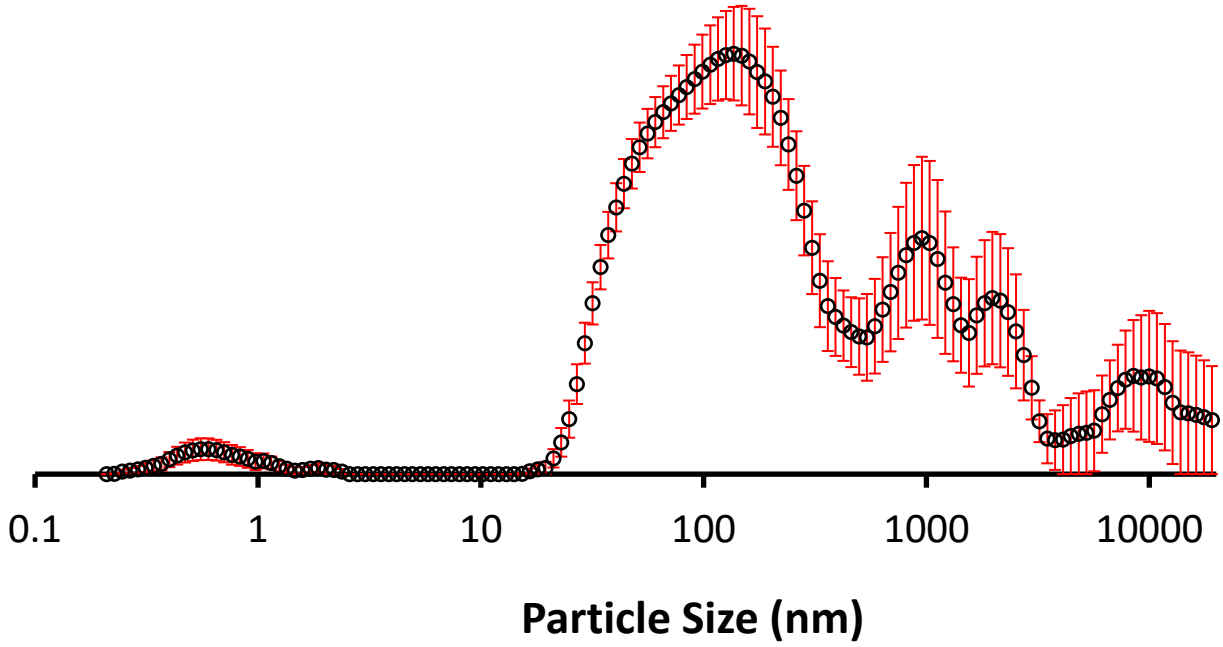


Figure S87 - The average intensity particle size distribution calculated using 9 DLS runs for co-formulation ***I*** (0.56 mM) in an EtOH: $H_2O$ (1:19) solution at 298 K.

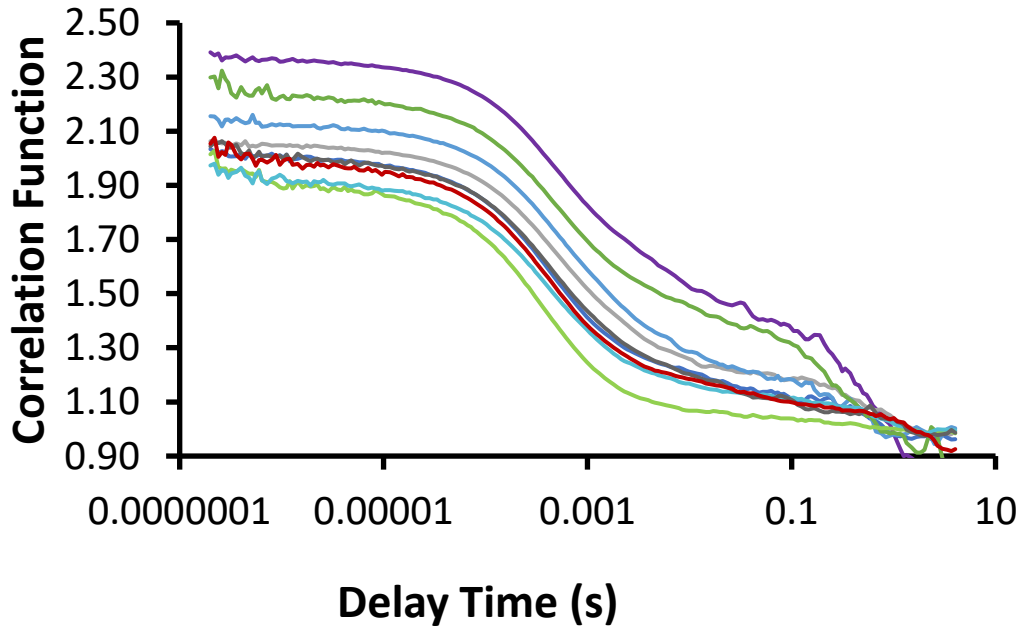


Figure S88 - Correlation function data for 9 DLS runs of co-formulation ***I*** (0.56 mM) in an EtOH: $H_2O$ (1:19) solution at 298 K.

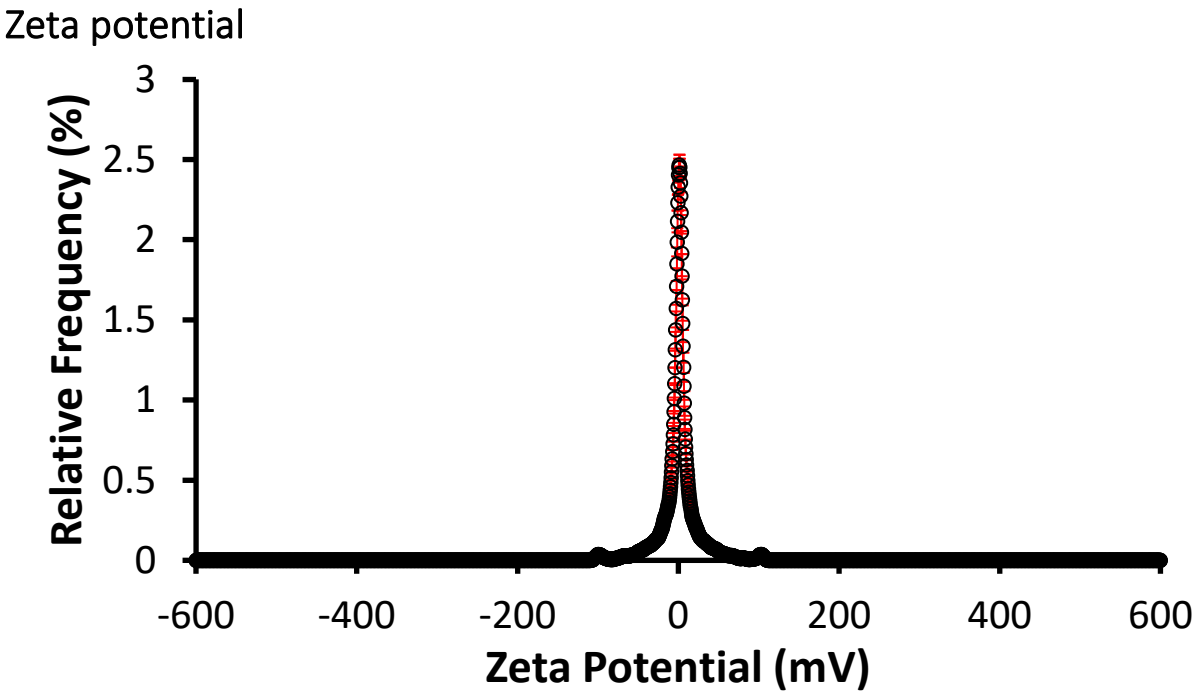


Figure S89 - The average zeta potential distribution calculated using 9 runs for co-formulation ***b*** (0.56 mM) in an EtOH:$H_2O$ (1:19) solution at 298 K.

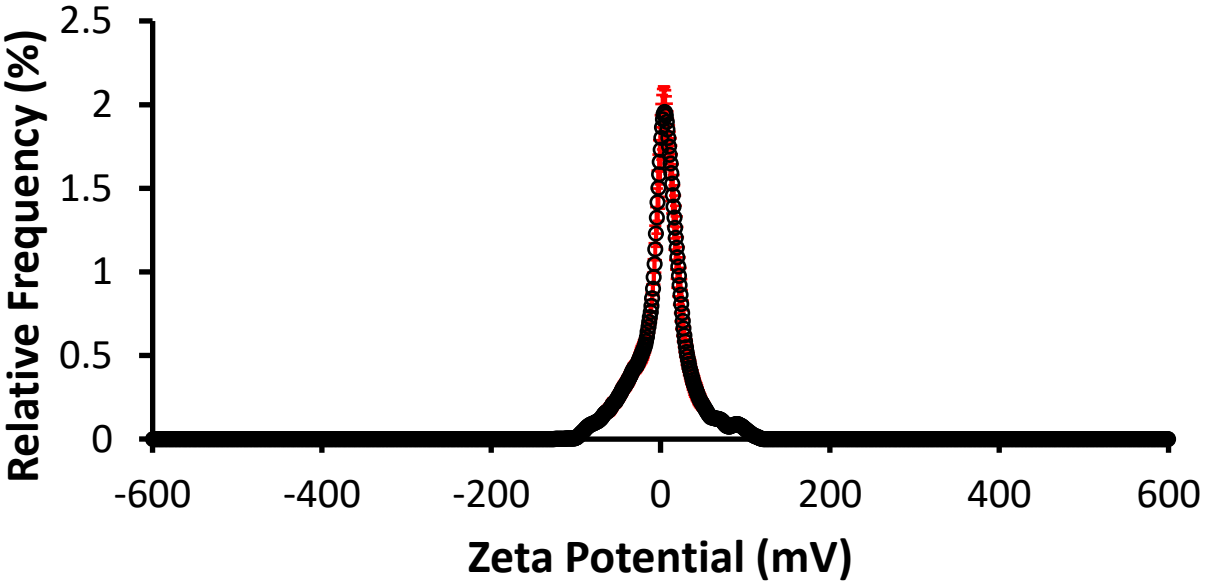


Figure S90 - The average zeta potential distribution calculated using 9 runs for co-formulation **c** (0.56 mM) in an EtOH:$H_2O$ (1:19) solution at 298 K.

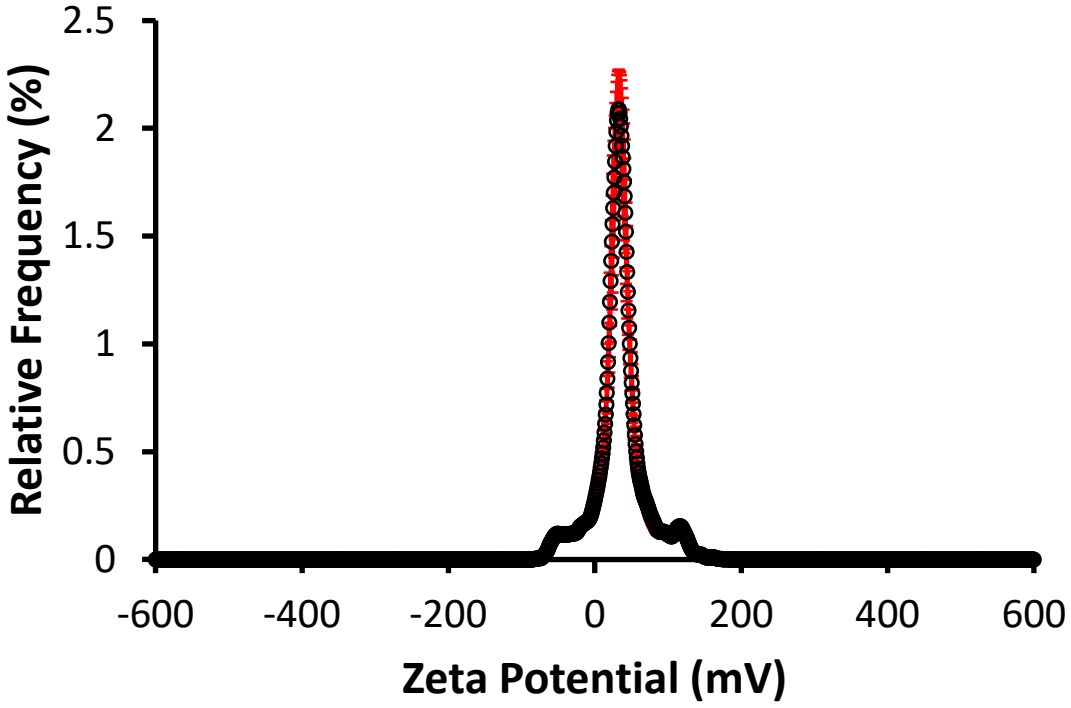


Figure S91 - The average zeta potential distribution calculated using 9 runs for co-formulation ***d*** (0.56 mM) in an EtOH:$H_2O$ (1:19) solution at 298 K.

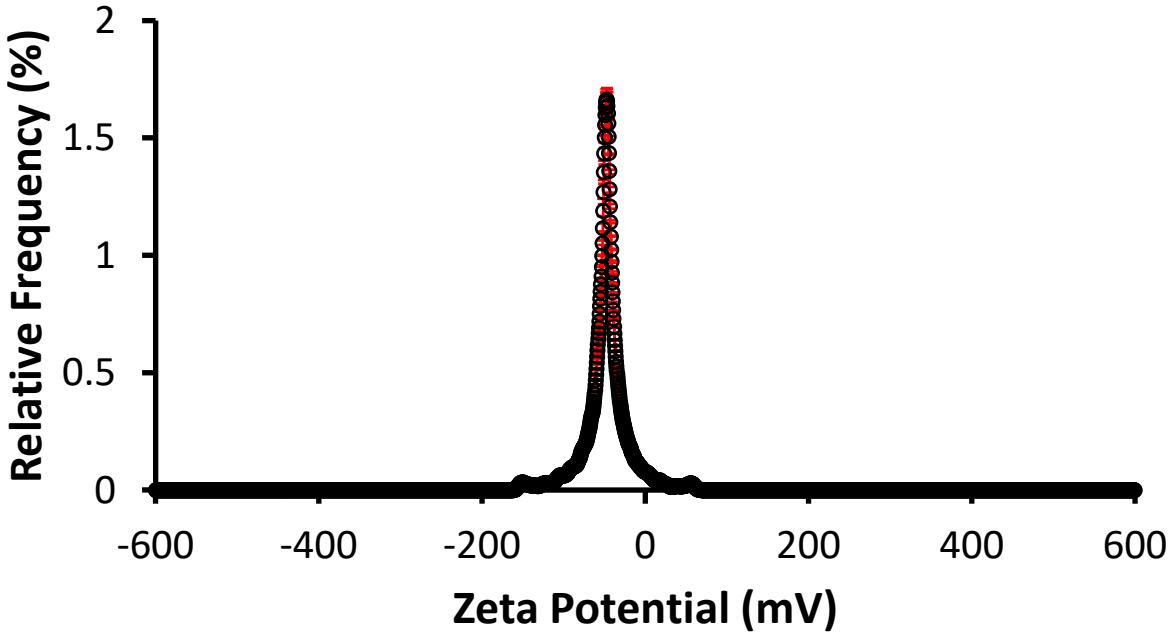


Figure S92 - The average zeta potential distribution calculated using 9 runs for co-formulation ***e*** (0.56 mM) in an EtOH:$H_2O$ (1:19) solution at 298 K.

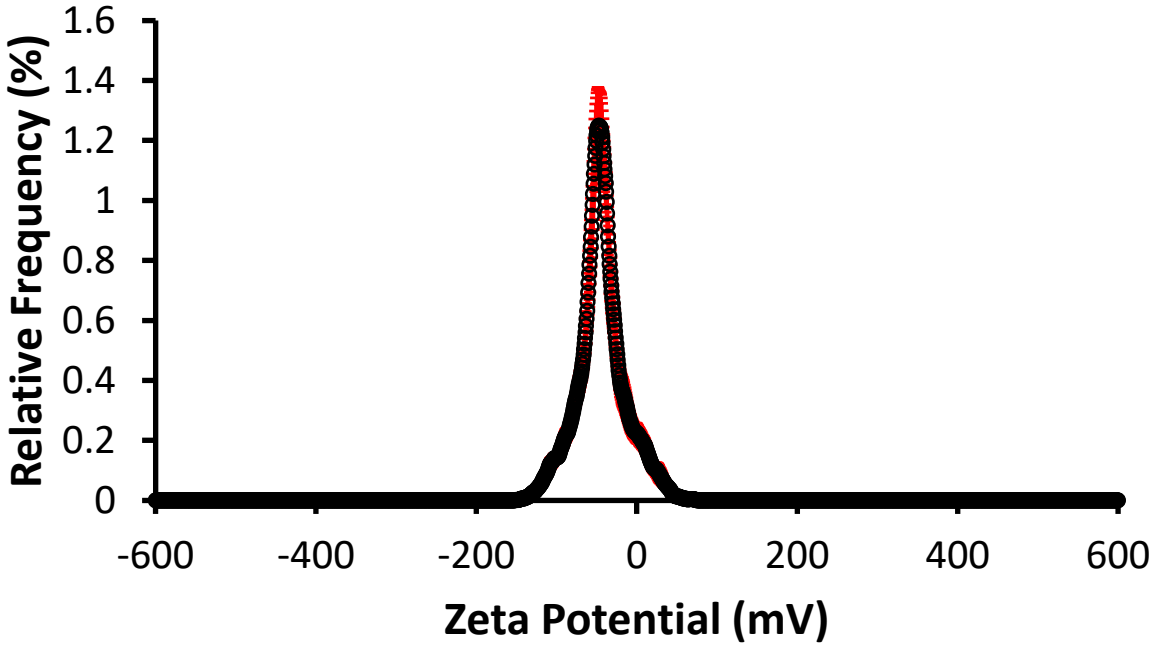


Figure S93 - The average zeta potential distribution calculated using 9 runs for co-formulation ***f*** (0.56 mM) in an EtOH:$H_2O$ (1:19) solution at 298 K.

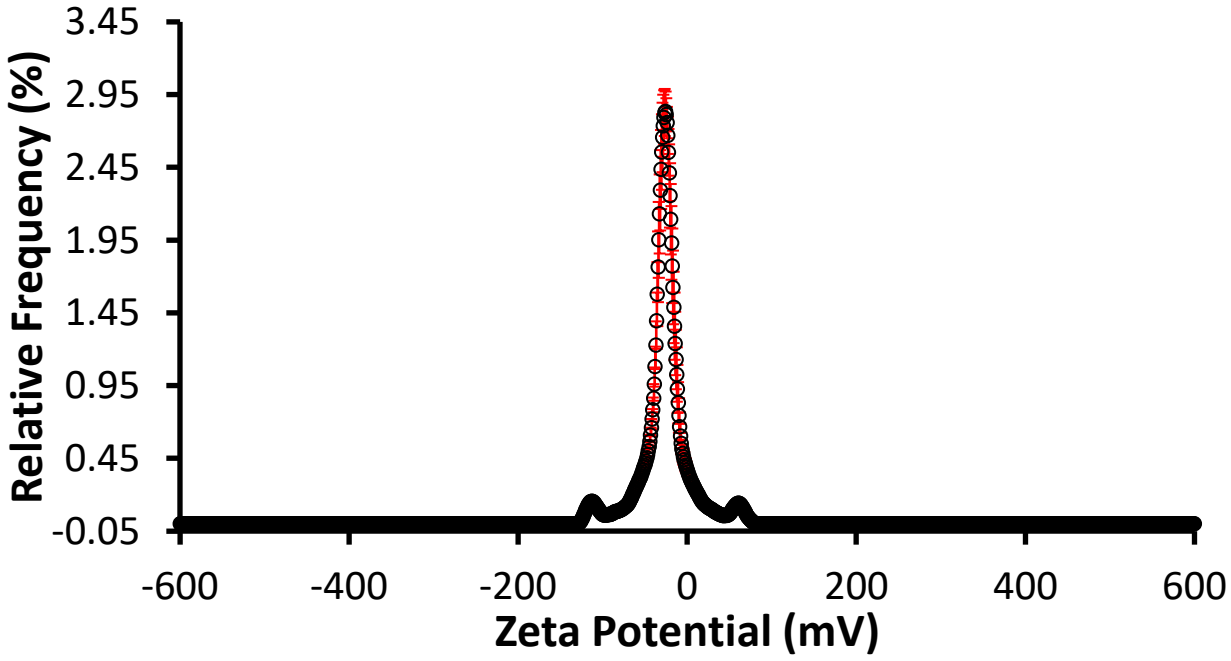


Figure S94 - The average zeta potential distribution calculated using 9 runs for co-formulation ***g*** (0.56 mM) in an EtOH:$H_2O$ (1:19) solution at 298 K.

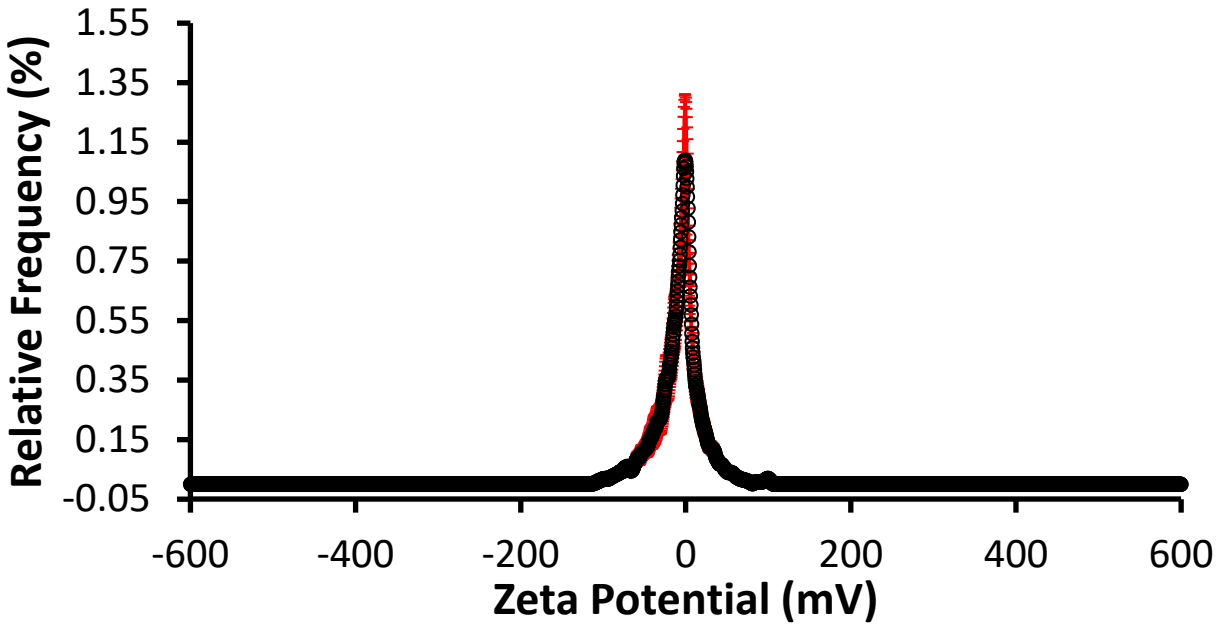


Figure S95 - The average zeta potential distribution calculated using 9 runs for co-formulation ***h*** (0.56 mM) in an EtOH:$H_2O$ (1:19) solution at 298 K.

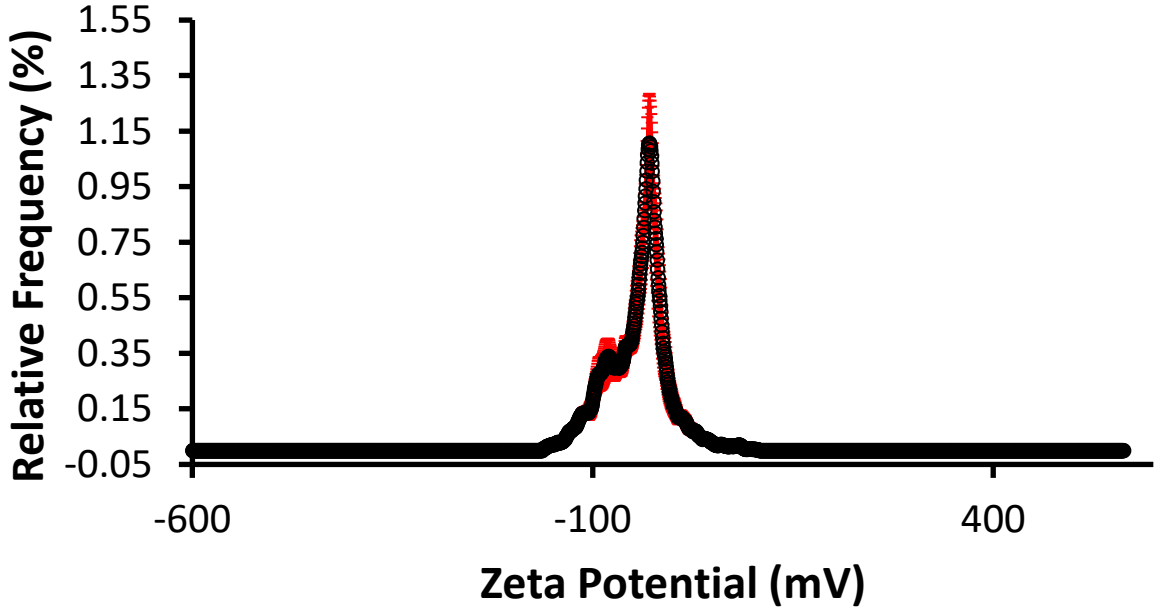


Figure S96 - The average zeta potential distribution calculated using 9 runs for co-formulation ***i*** (0.56 mM) in an EtOH:$H_2O$ (1:19) solution at 298 K.

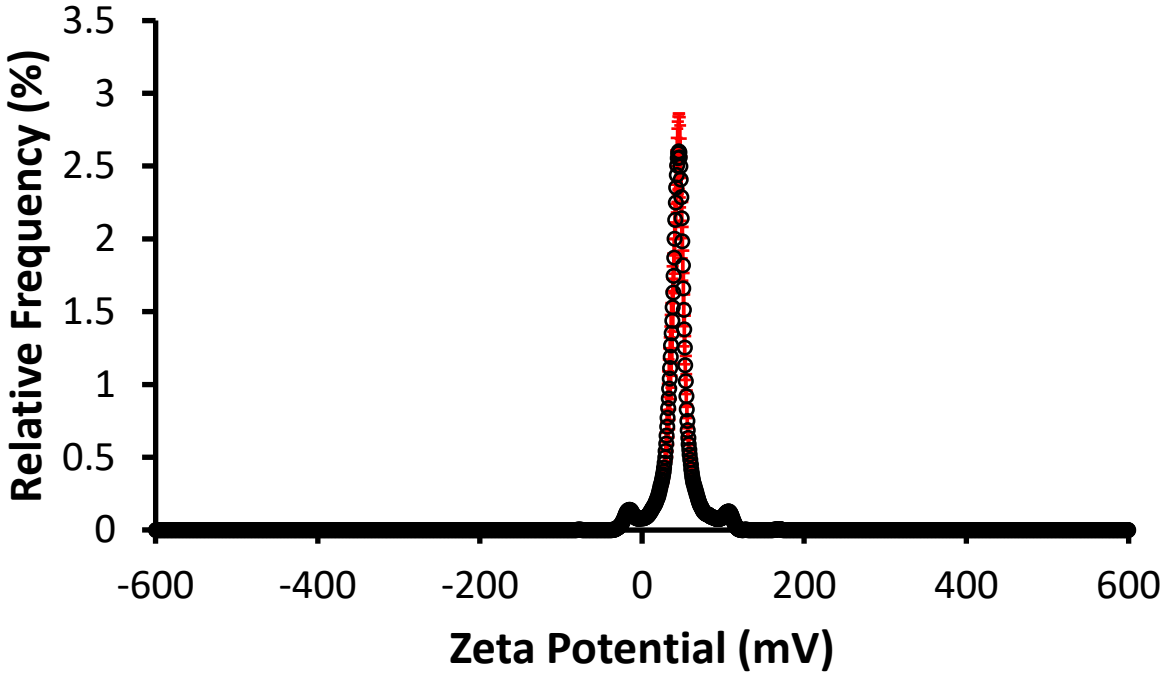


Figure S97 - The average zeta potential distribution calculated using 9 runs for co-formulation ***j*** (0.56 mM) in an EtOH:$H_2O$ (1:19) solution at 298 K.

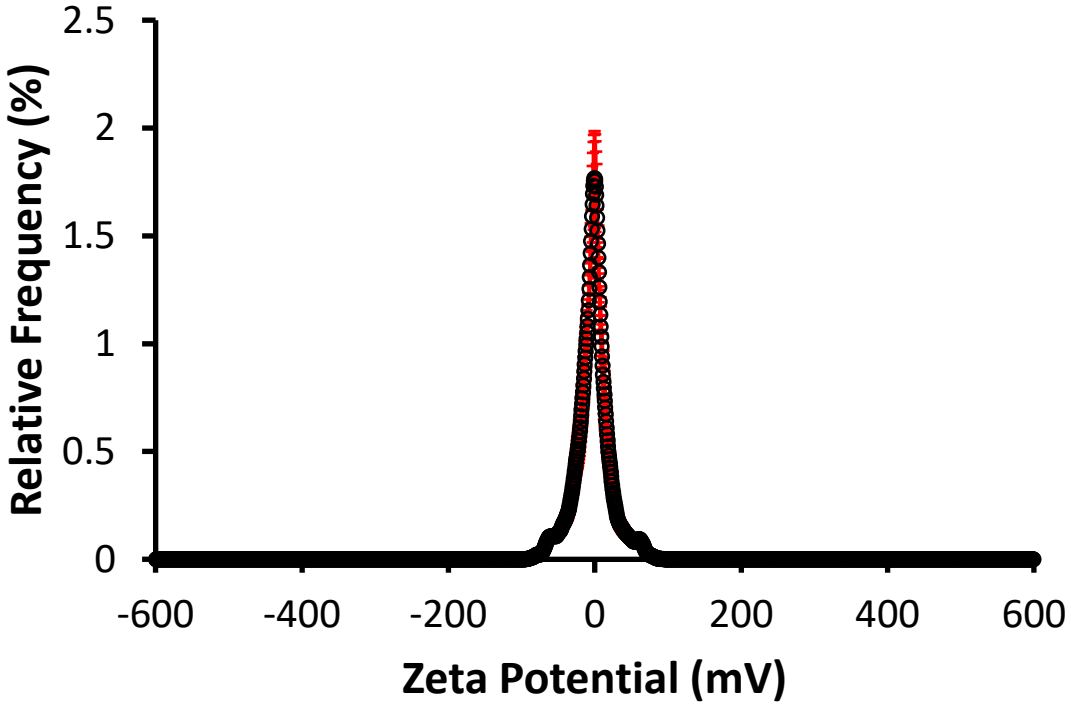


Figure S98 - The average zeta potential distribution calculated using 9 runs for co-formulation ***k*** (0.56 mM) in an EtOH:$H_2O$ (1:19) solution at 298 K.

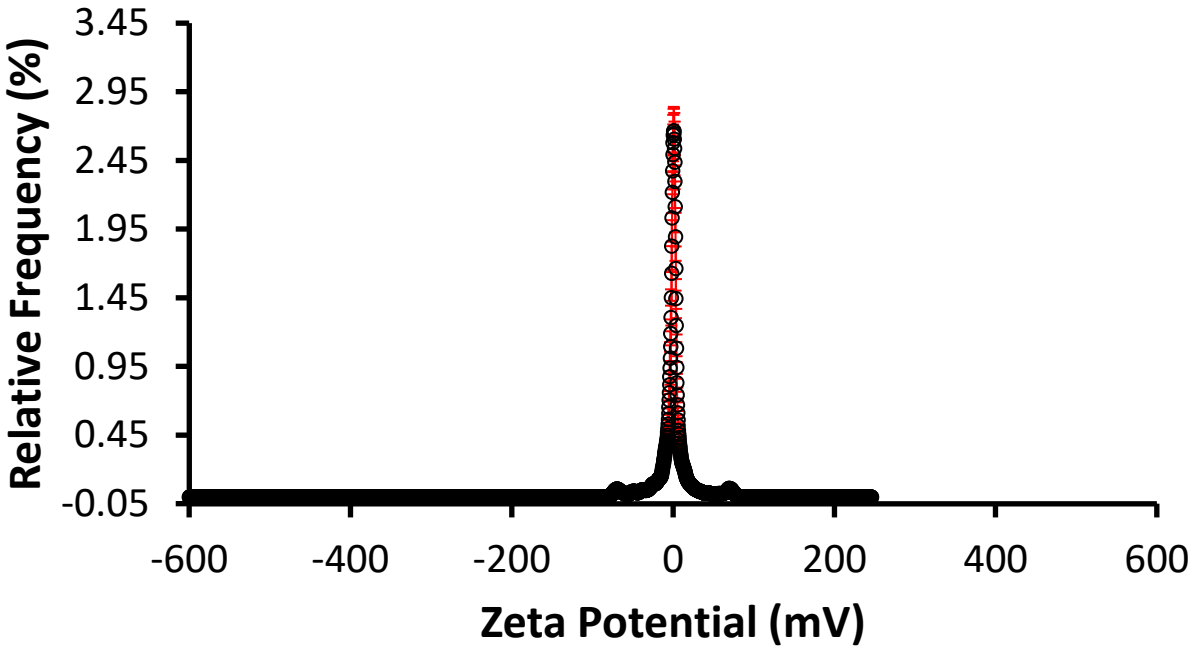


Figure S99 - The average zeta potential distribution calculated using 9 runs for co-formulation ***l*** (0.56 mM) in an EtOH:$H_2O$ (1:19) solution at 298 K.

## Surface Tension measurements and Critical micelle concentrations (CMC) determination

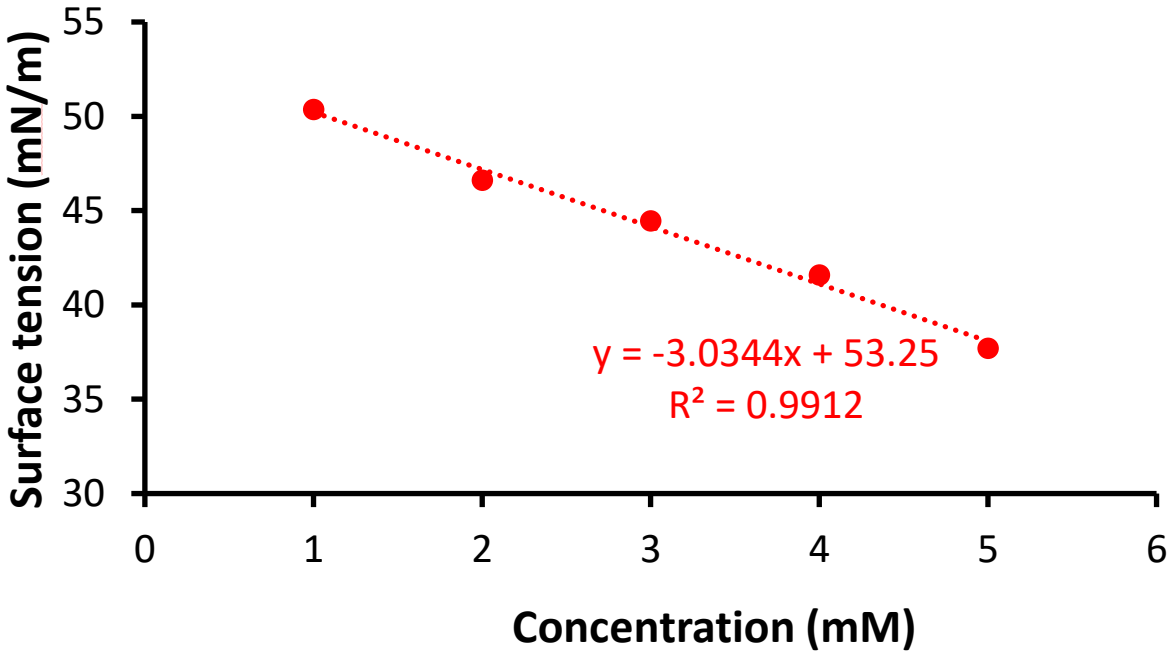


Figure S100 - Calculation of CMC for co-formulation ***b*** in an EtOH:$H_2O$ 1:19 mixture using surface tension measurements. A CMC could not be calculated as solubility limits were reached.

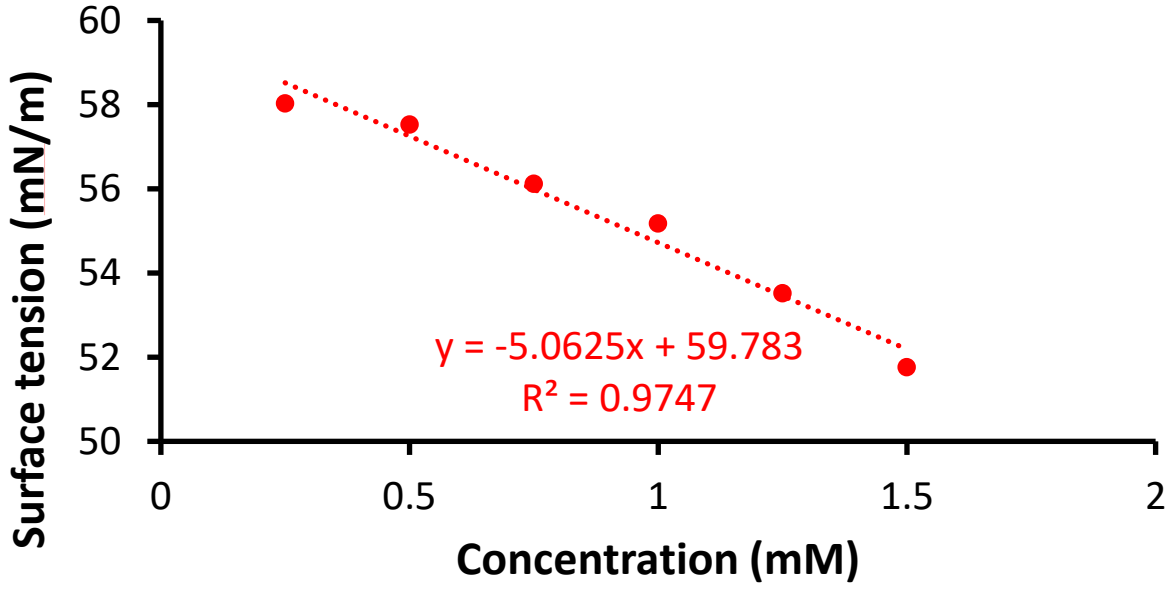


Figure S101 - Calculation of CMC for co-formulation ***c*** in an EtOH:$H_2O$ 1:19 mixture using surface tension measurements. A CMC could not be calculated as solubility limits were reached.

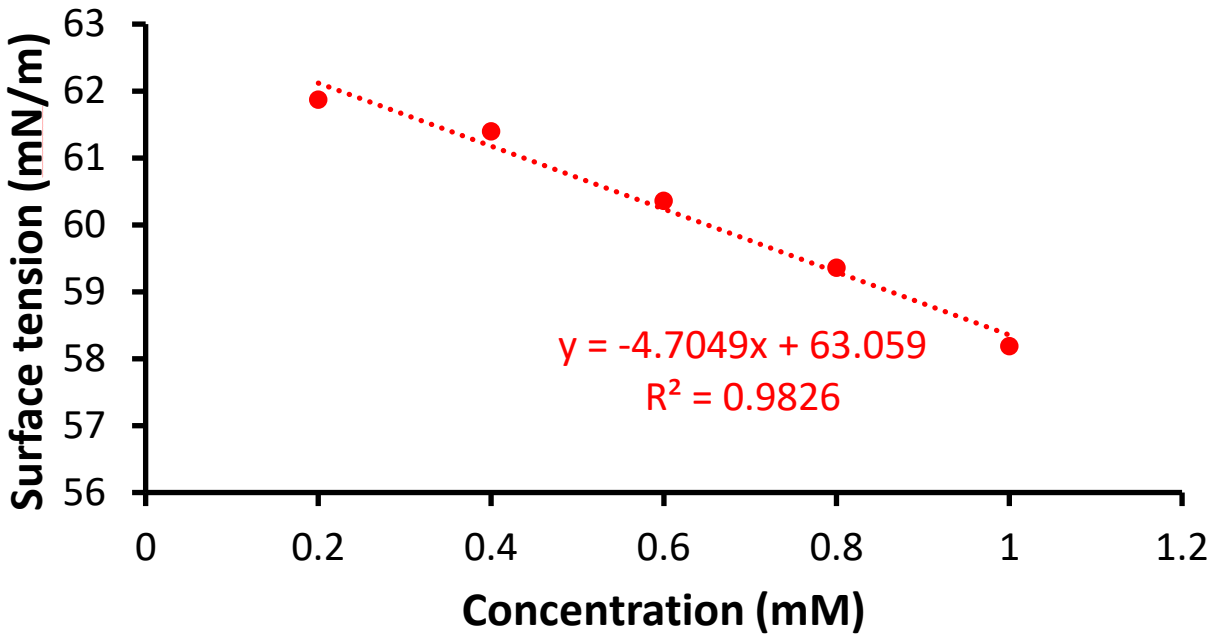


Figure S102 - Calculation of CMC for co-formulation ***d*** in an EtOH:$H_2O$ 1:19 mixture using surface tension measurements. A CMC could not be calculated as solubility limits were reached.

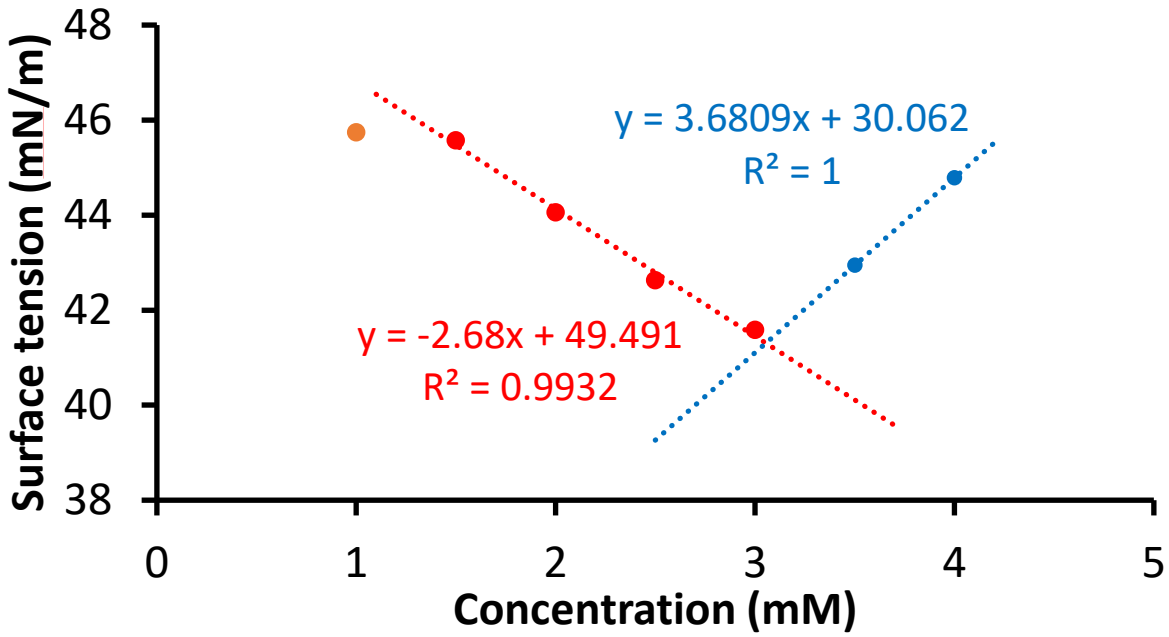


Figure S103 – Calculation of CMC (3.1 mM) for co-formulation ***e*** in an EtOH:$H_2O$ 1:19 mixture using surface tension measurements.

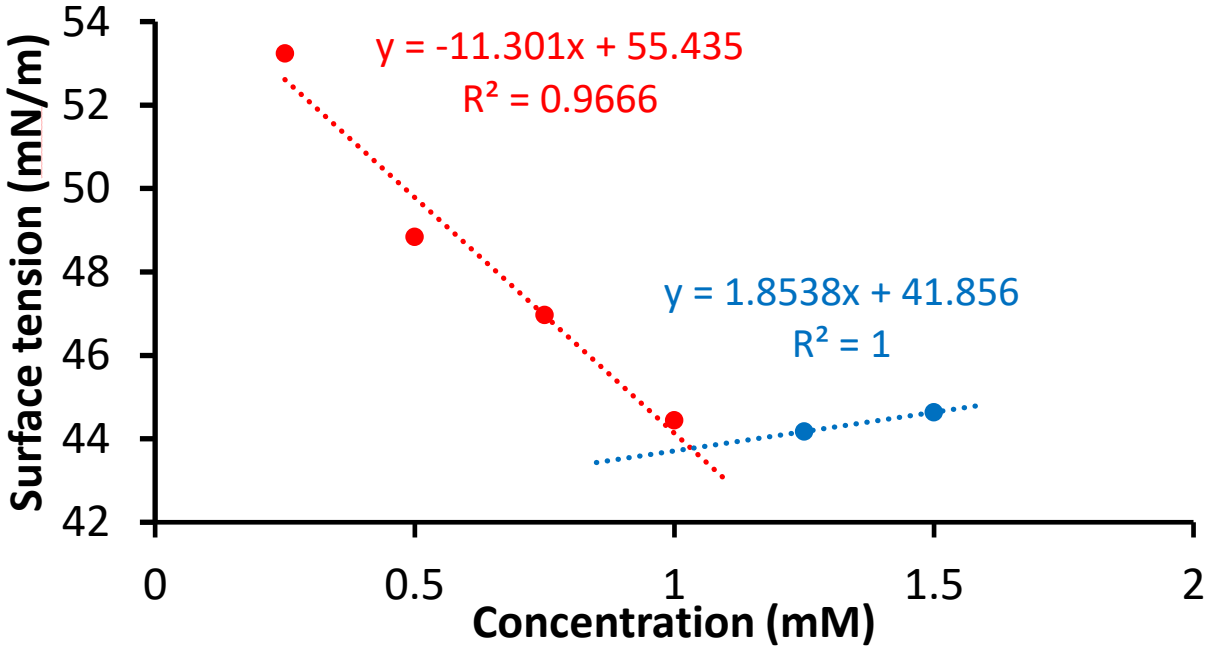


Figure S104 - Calculation of CMC (1.0 mM) for co-formulation ***f*** in an EtOH:$H_2O$ 1:19 mixture using surface tension measurements.

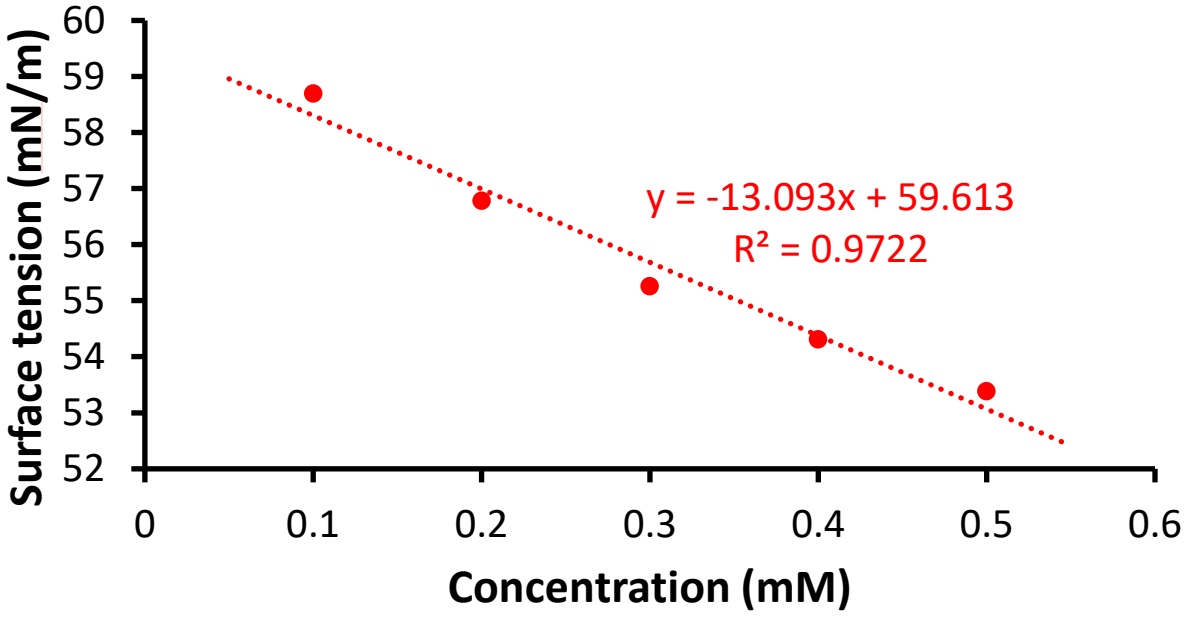


Figure S105 - Calculation of CMC for co-formulation ***g*** in an EtOH:$H_2O$ 1:19 mixture using surface tension measurements. A CMC could not be calculated as solubility limits were reached.

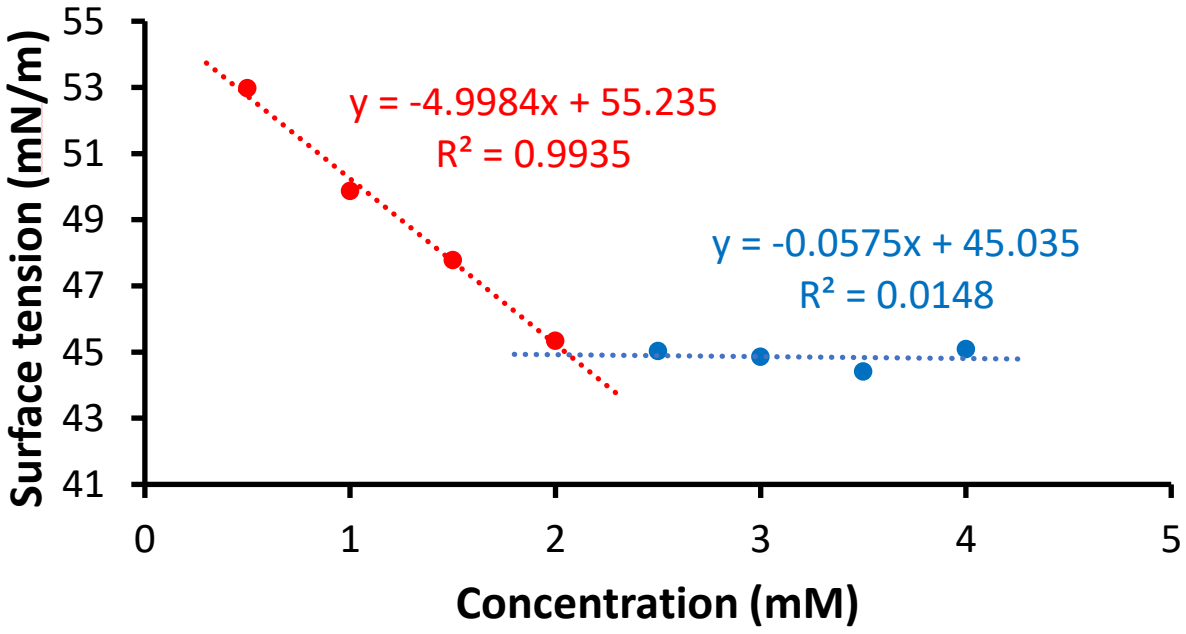


Figure S106 - Calculation of CMC (2.1 mM) for co-formulation ***h*** in an EtOH:$H_2O$ 1:19 mixture using surface tension measurements.

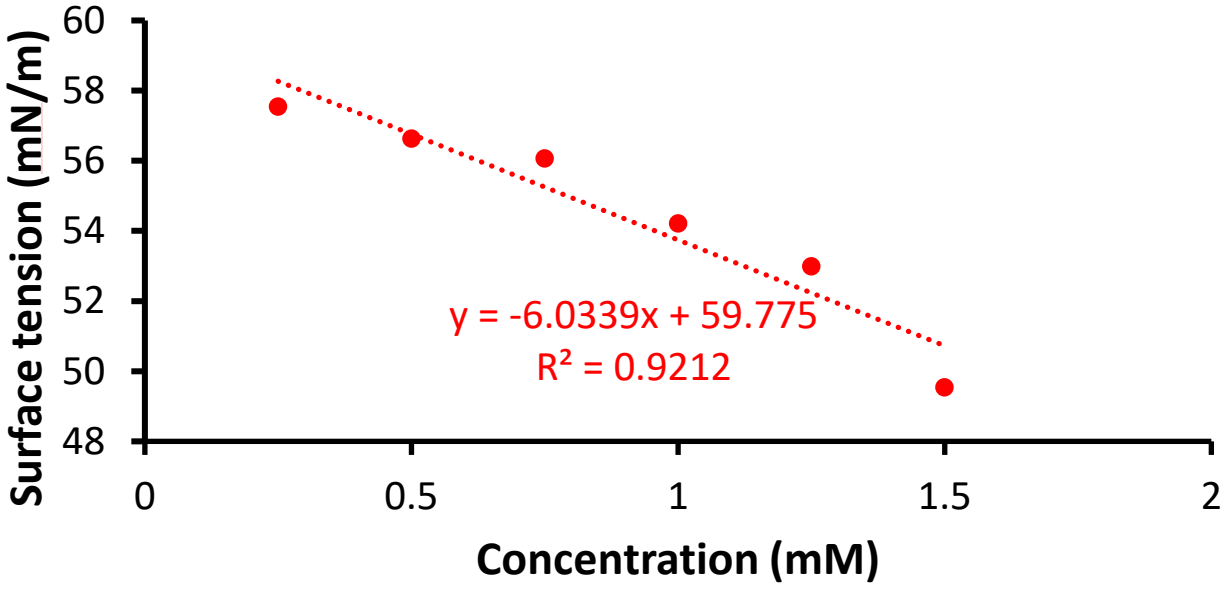


Figure S107 - Calculation of CMC for co-formulation ***i*** in an EtOH:$H_2O$ 1:19 mixture using surface tension measurements. A CMC could not be calculated as solubility limits were reached.

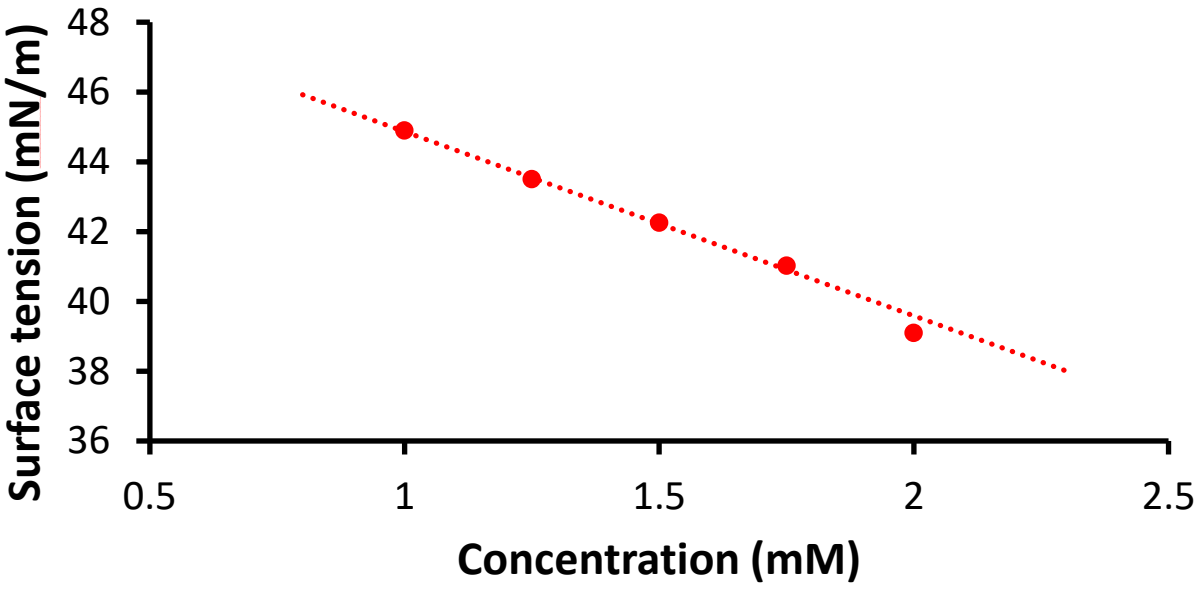


Figure S108 - Calculation of CMC for co-formulation ***j*** in an EtOH:$H_2O$ 1:19 mixture using surface tension measurements. A CMC could not be calculated as solubility limits were reached.

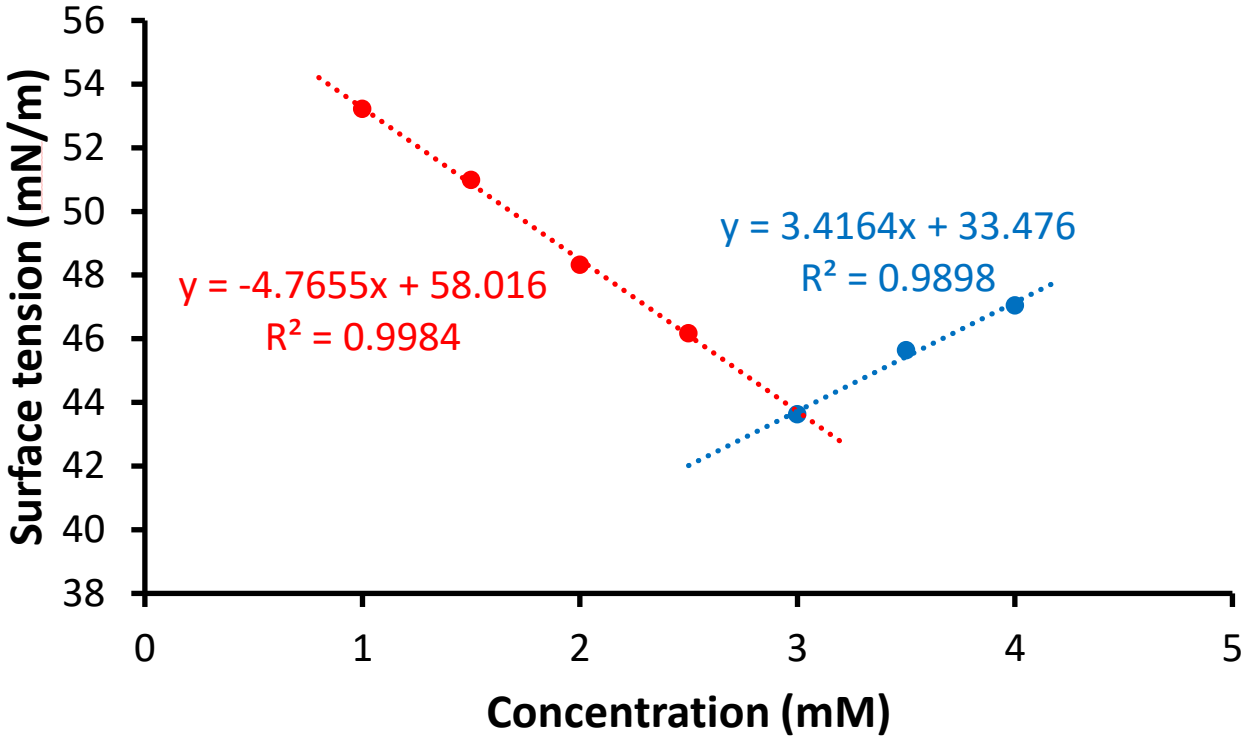


Figure S109 - Calculation of CMC (3.0 mM) for co-formulation ***k*** in an EtOH:$H_2O$ 1:19 mixture using surface tension measurements.

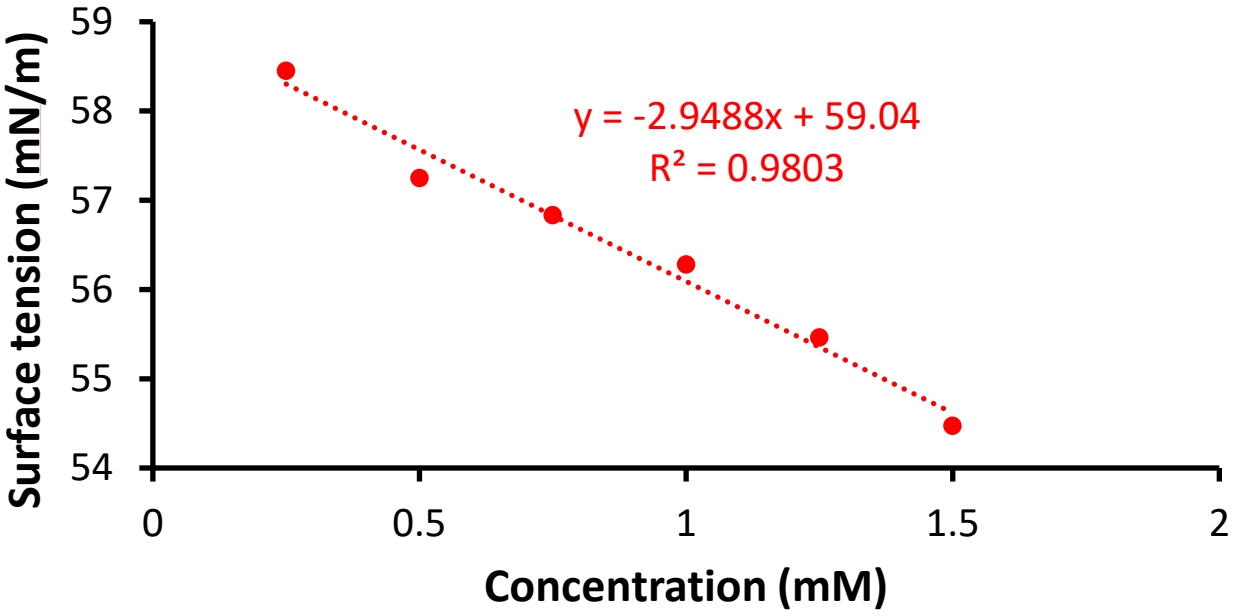


Figure S110 - Calculation of CMC for co-formulation ***l*** in an EtOH:$H_2O$ 1:19 mixture using surface tension measurements. A CMC could not be calculated as solubility limits were reached.

# Single Crystal

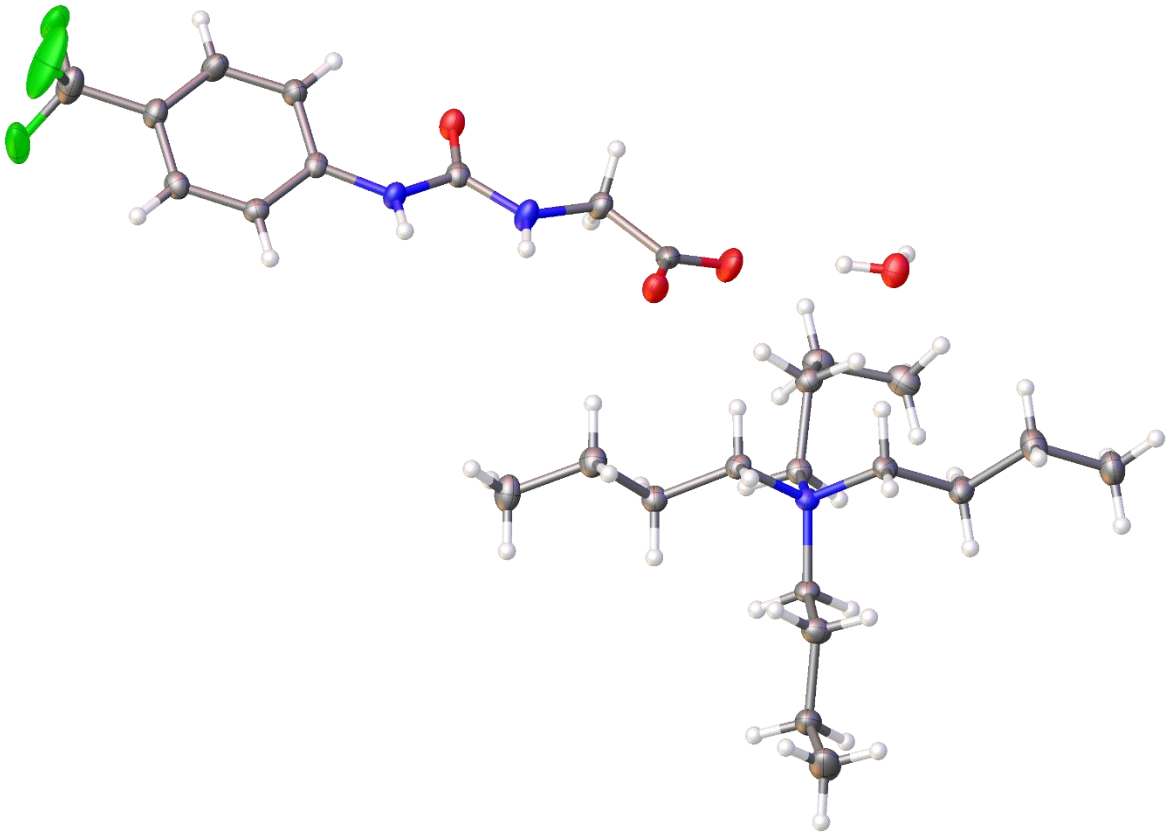

Figure S111 - Single crystal X-ray structure of **4**: red = oxygen; yellow = sulfur; blue = nitrogen; white = hydrogen; grey = carbon. CCDC 2122929, $C_{26}H_{46}F_3N_3O_4$ (M = 642.83): triclinic, space group P -1, a = 8.8423(3) Å, b = 9.1649(3) Å, c = 18.9396(7) Å, α = 81.398(3)°, β = 82.114(3)°, γ = 67.226(3)°, V = 1394.03(9) Å$^3$, Z = 2, T = 100(1) K, CuK\α = 1.54184 Å, Dcalc = 1.243 g/cm$^3$, 23887 reflections measured (9.482 ≤ 2Θ ≤ 144.000), 5395 unique ($R_{int}$ = 0.0320**,** $R_{sigma}$ = 0.0208) which were used in all calculations. The final $R_1$ was 0.0384 (I > 2σ(I)) and $wR_2$ was 0.0980 (all data). Internal angle of anion:anion hydrogen bonded dimerisation = 180.00(12)

Table S2 - Hydrogen bond distances and angles observed for **4**, calculated from the single crystal X-ray structure shown above.

| Hydrogen bond donor | Hydrogen bond acceptor | Hydrogen bond length (D•••A) (Å) | Hydrogen bond angle (D-H•••A) (°) |
|---|---|---|---|
| N1 | O2 | 2.9675(14) | 144.75(7) |
| N2 | O2 | 2.7426(13) | 156.24(7) |
| O4 | O1 | 2.7443(13) | 171.08(7) |
| O4 | O3 | 2.7973(12) | 168.74(7) |

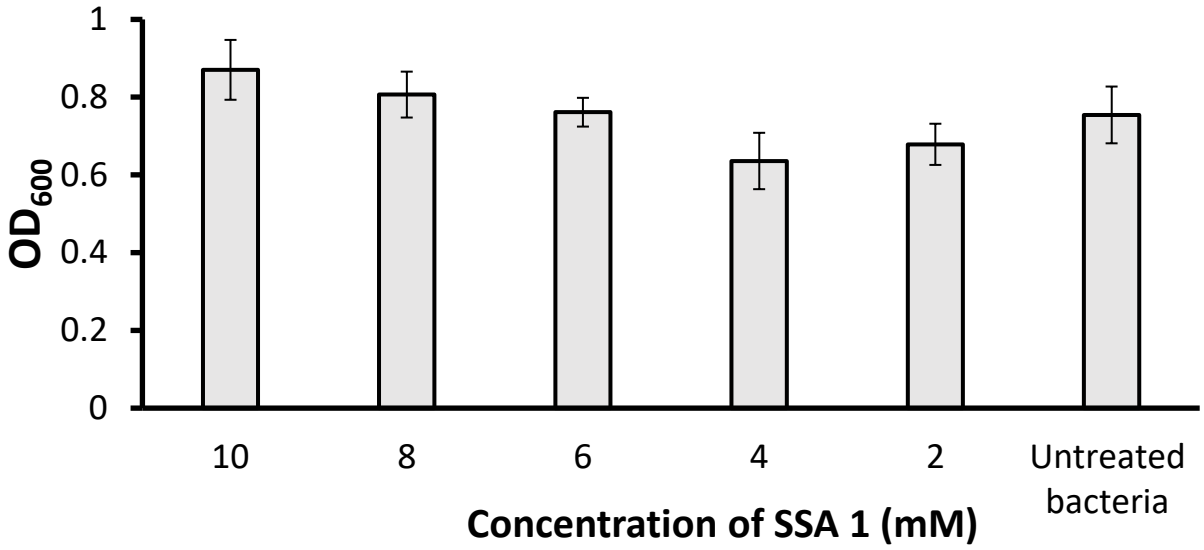


Figure S112 – Determination of MIC of SSA **1** against *P. aeruginosa* PA01.

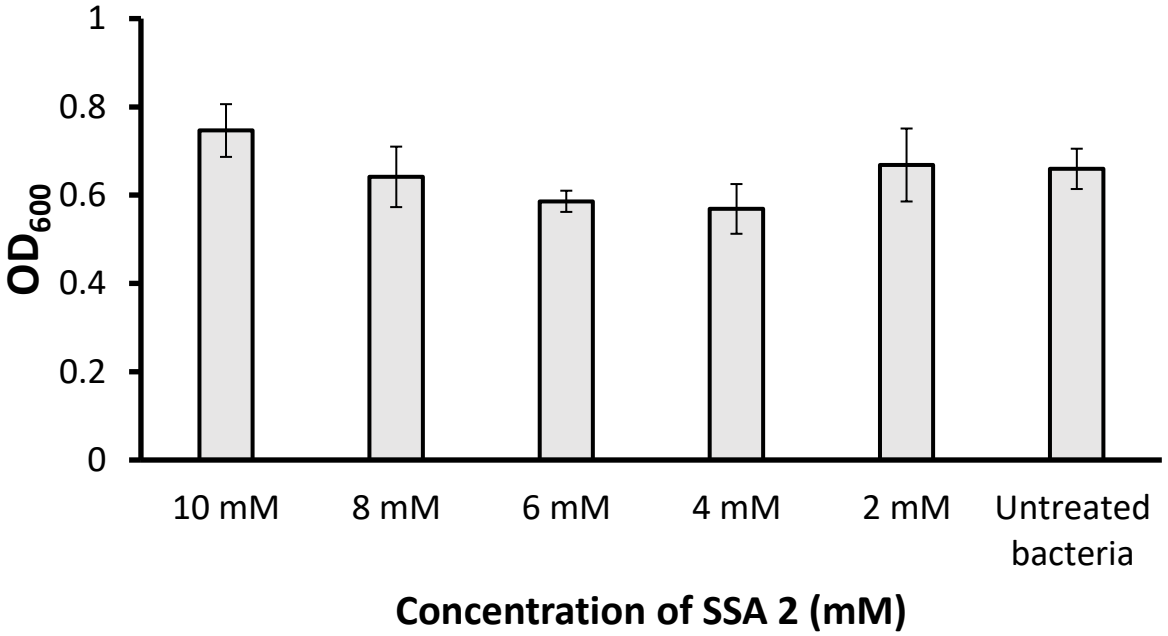


Figure S113 - Determination of MIC of SSA **2** against *P. aeruginosa* PA01.

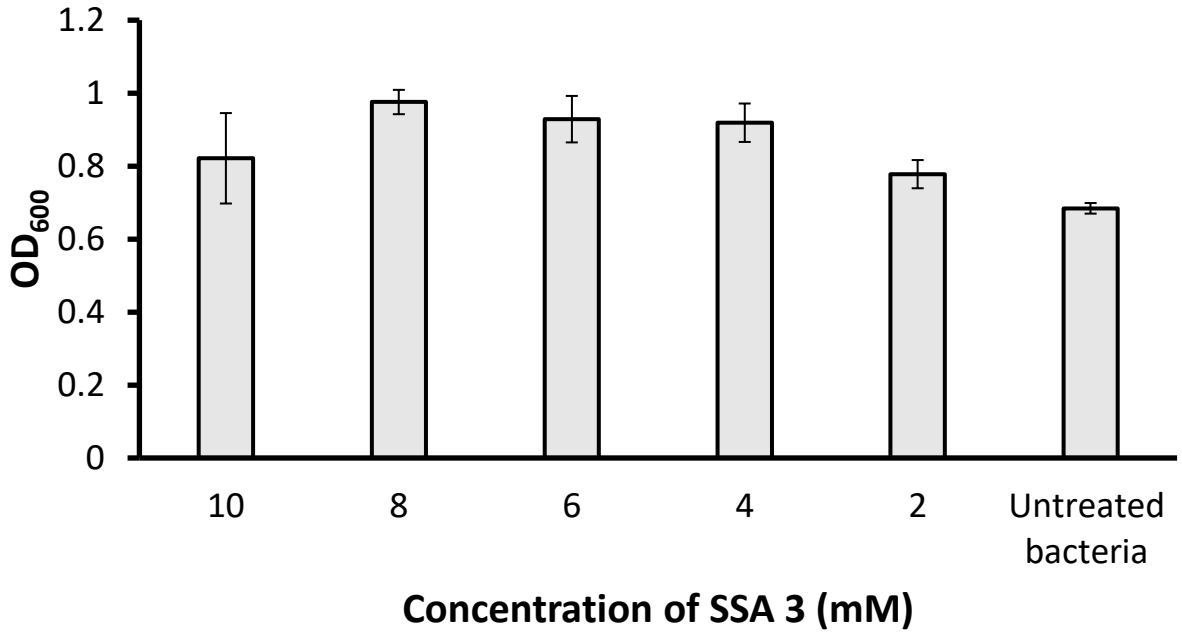


Figure S114 - Determination of MIC of SSA **3** against *P. aeruginosa* PA01.

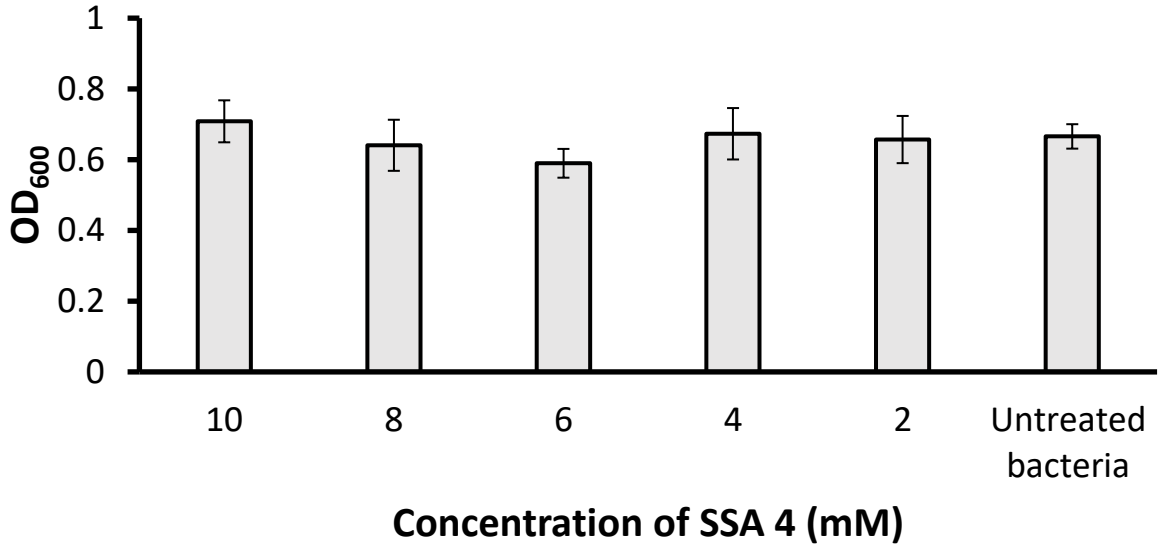


Figure S115 - Determination of MIC of SSA **4** against *P. aeruginosa* PA01.

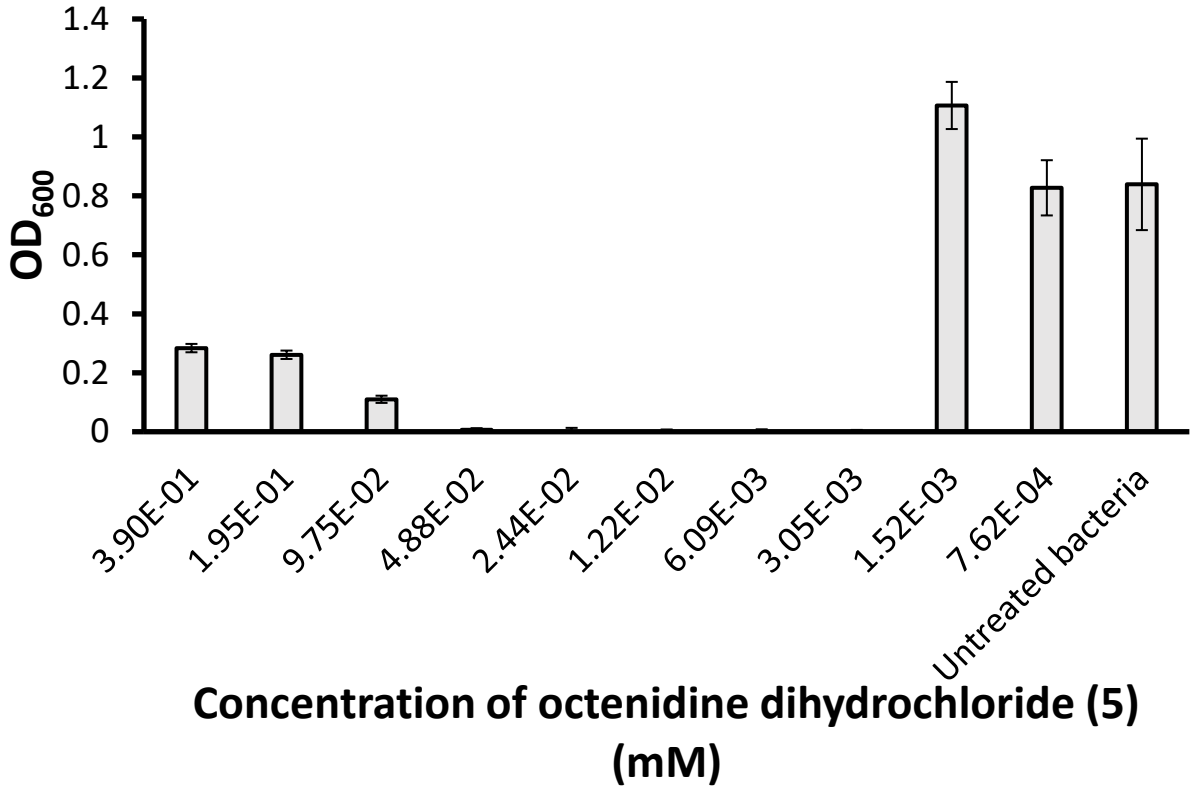


Figure S116 - Determination of MIC of octenidine dihydrochloride (**5**) against *P. aeruginosa* PAO1. At higher concentrations, compound clouding caused increase in OD.

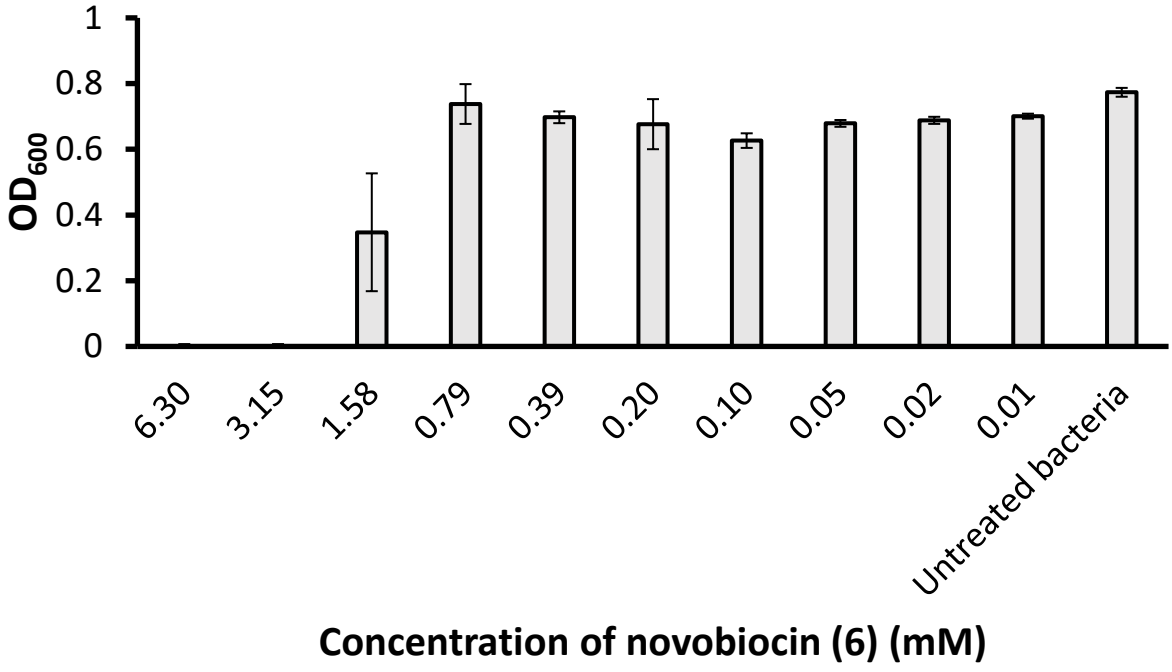


Figure S117 - Determination of MIC of novobiocin (**6**) against *P. aeruginosa* PAO1.

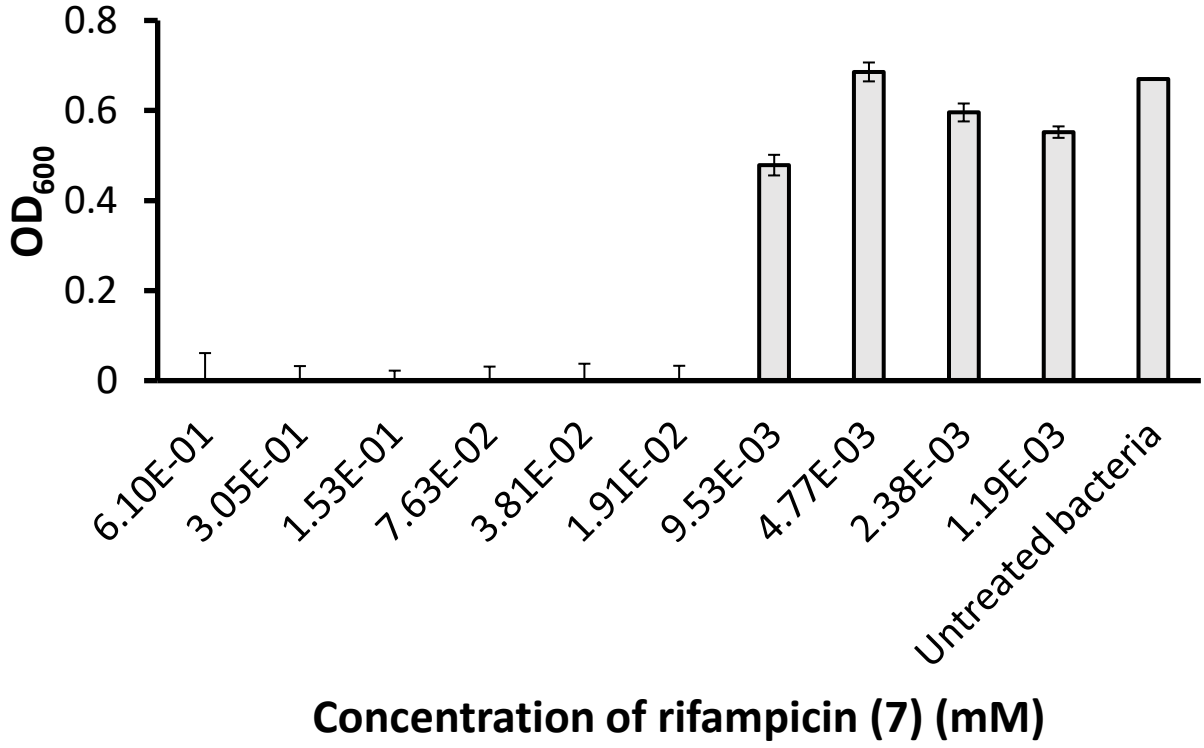


Figure S118 - Determination of MIC of rifampicin (**7**) against *P. aeruginosa* PAO1.

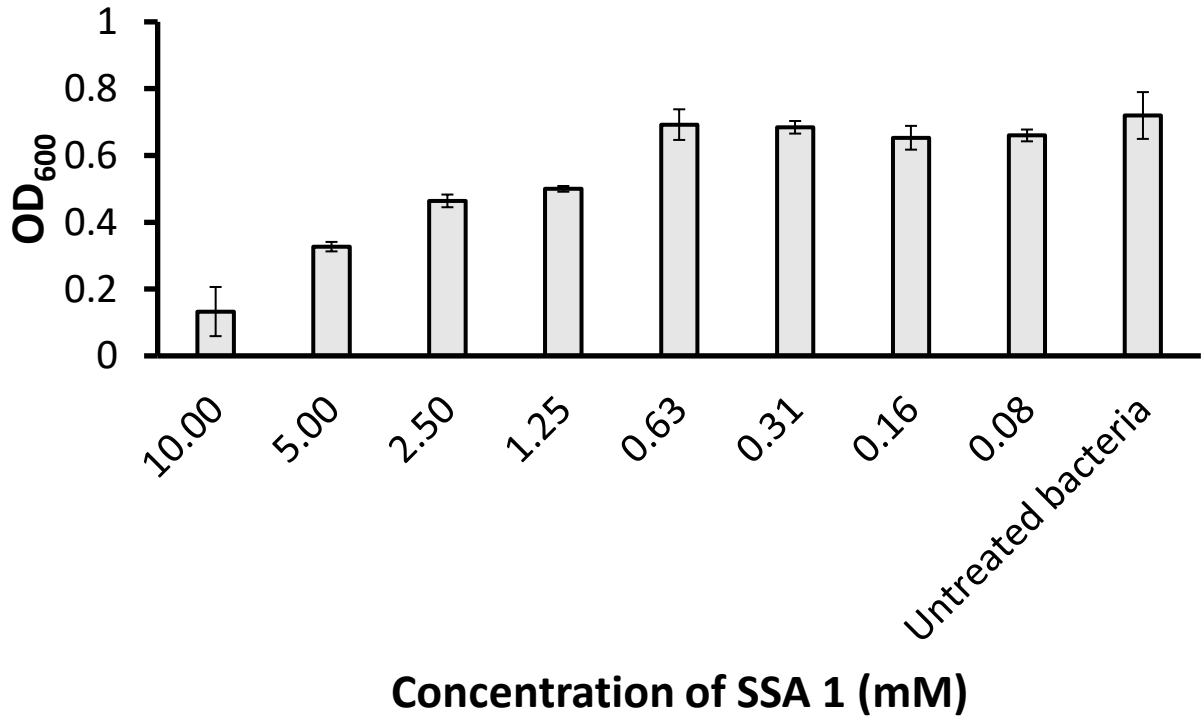


Figure S119 - Determination of MIC of SSA **1** against *E. coli* DH10β.

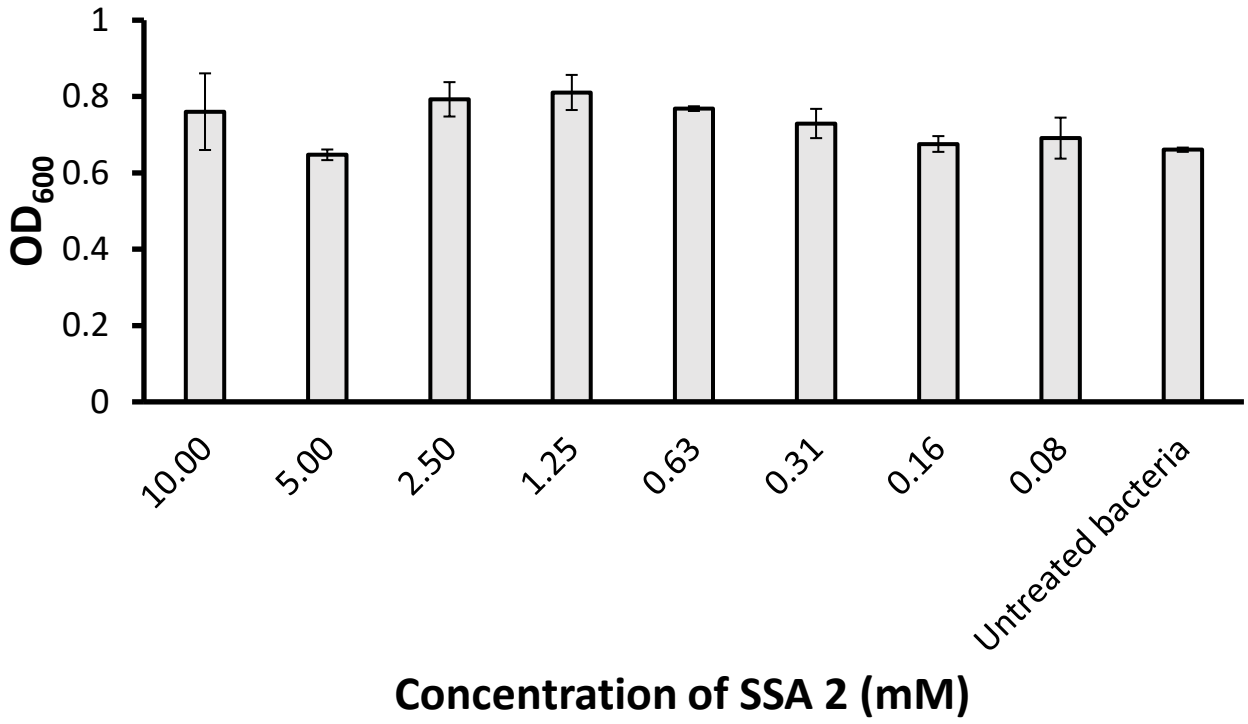


Figure S120 – Determination of MIC of SSA **2** against *E. coli* DH10β.

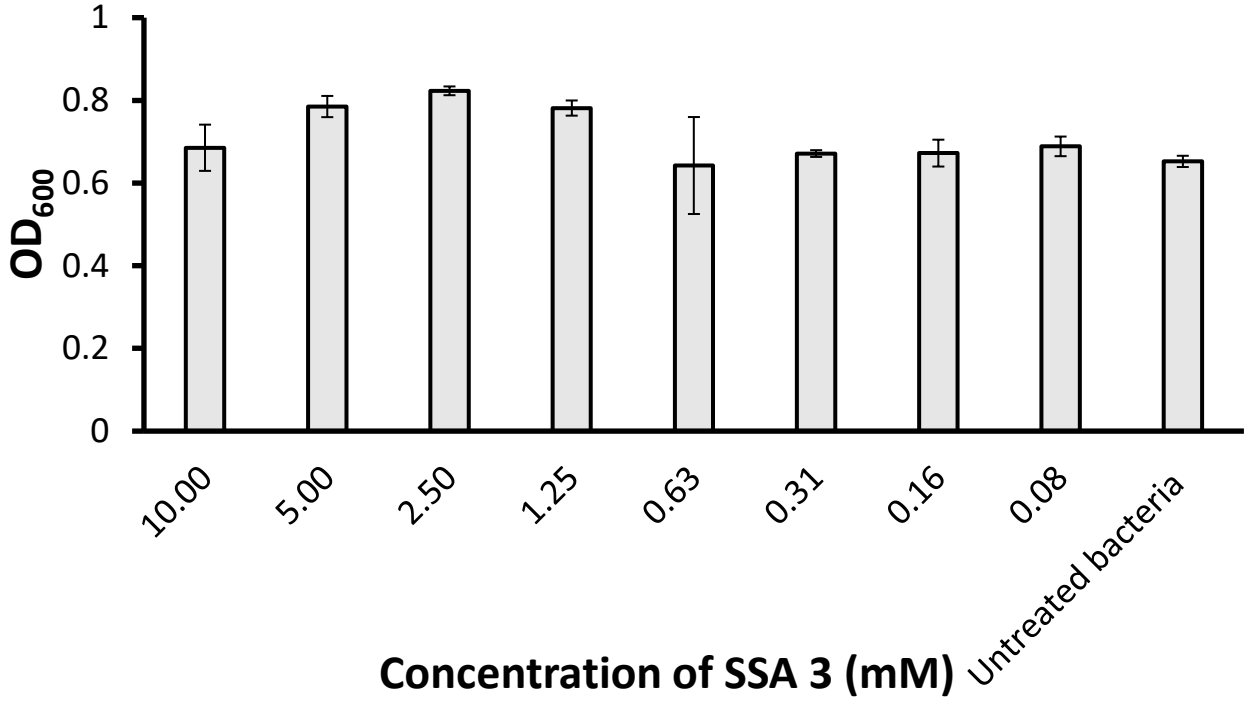


Figure S121 – Determination of MIC of SSA **3** against *E. coli* DH10β.

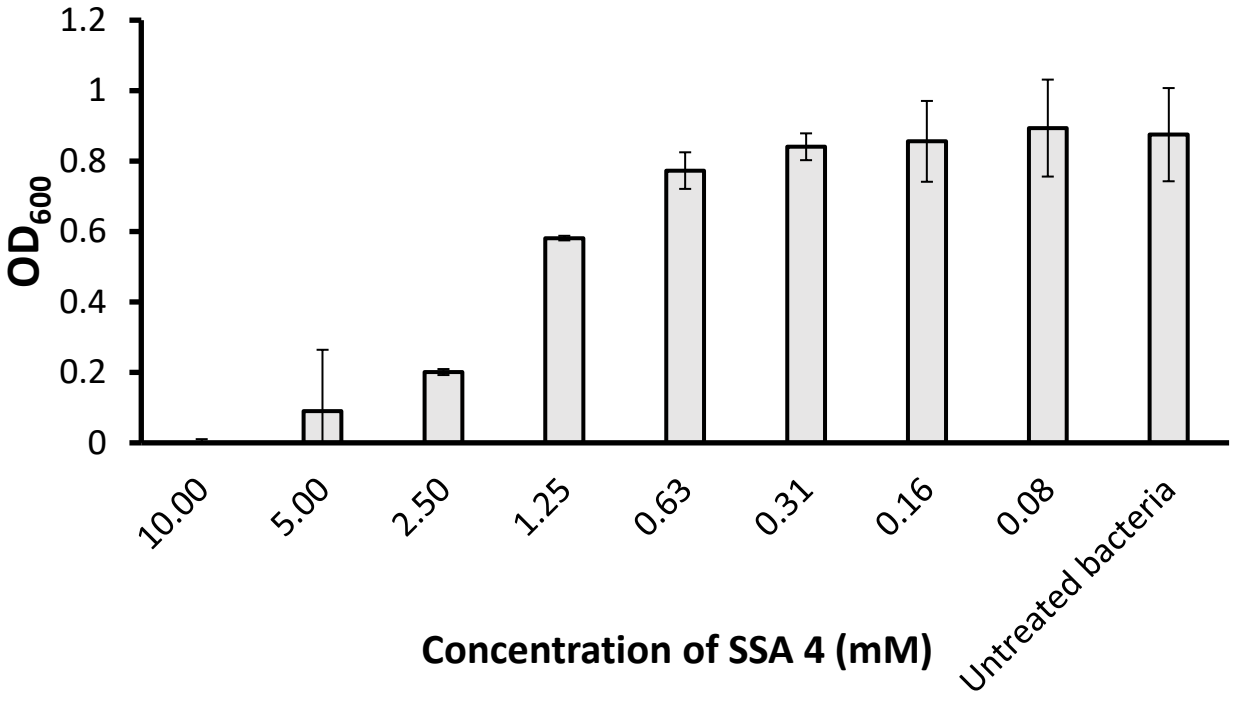


Figure S122 – Determination of MIC of SSA **4** against *E. coli* DH10β.

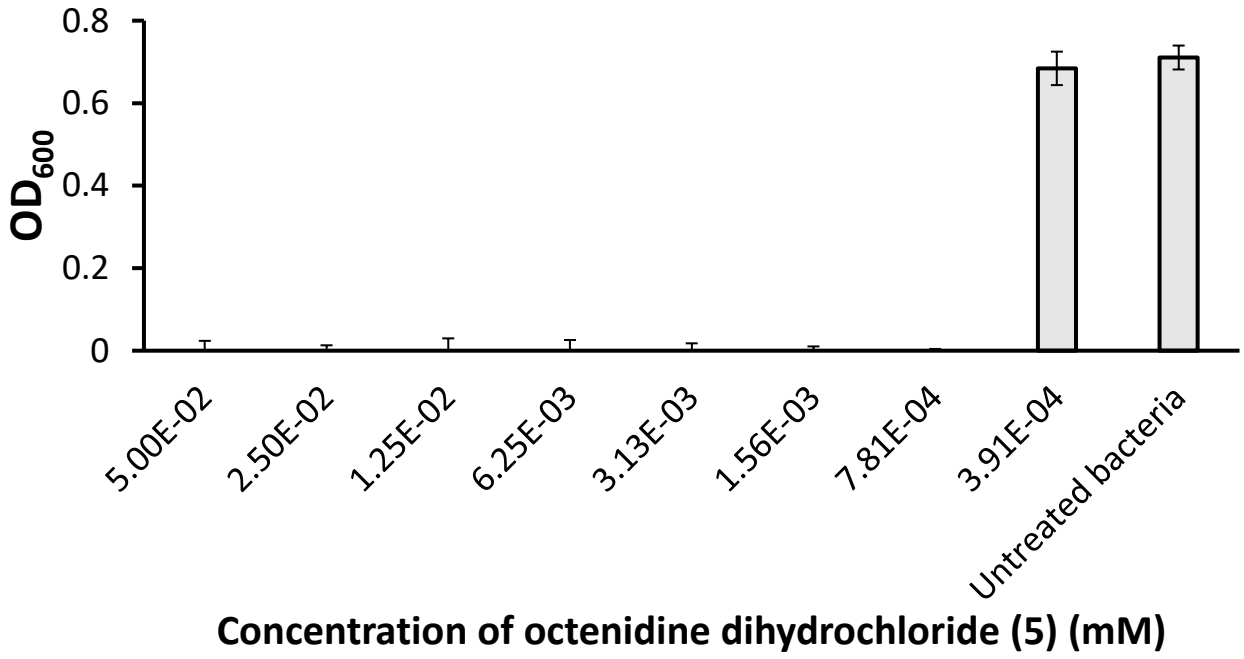


Figure S123 - Determination of MIC against octenidine dihydrochloride (**5**) for *E. coli* DH10β.

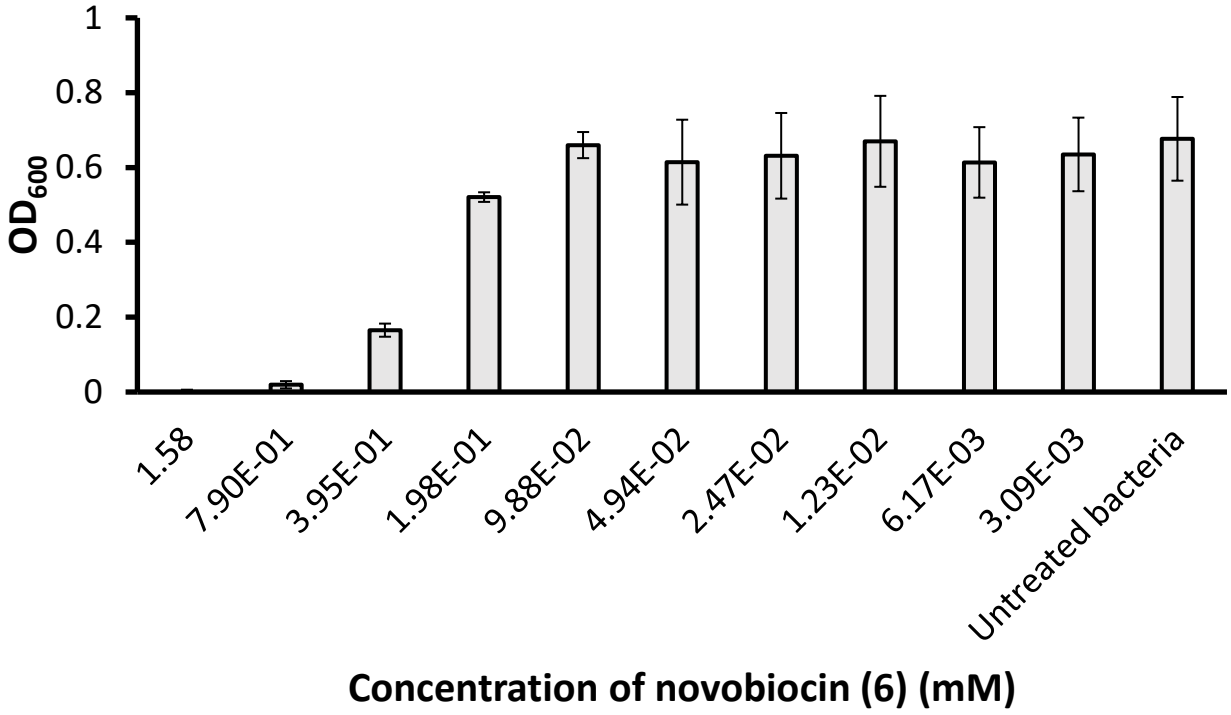


Figure S124 - Determination of MIC against novobiocin (**6**) for *E. coli* DH10β.

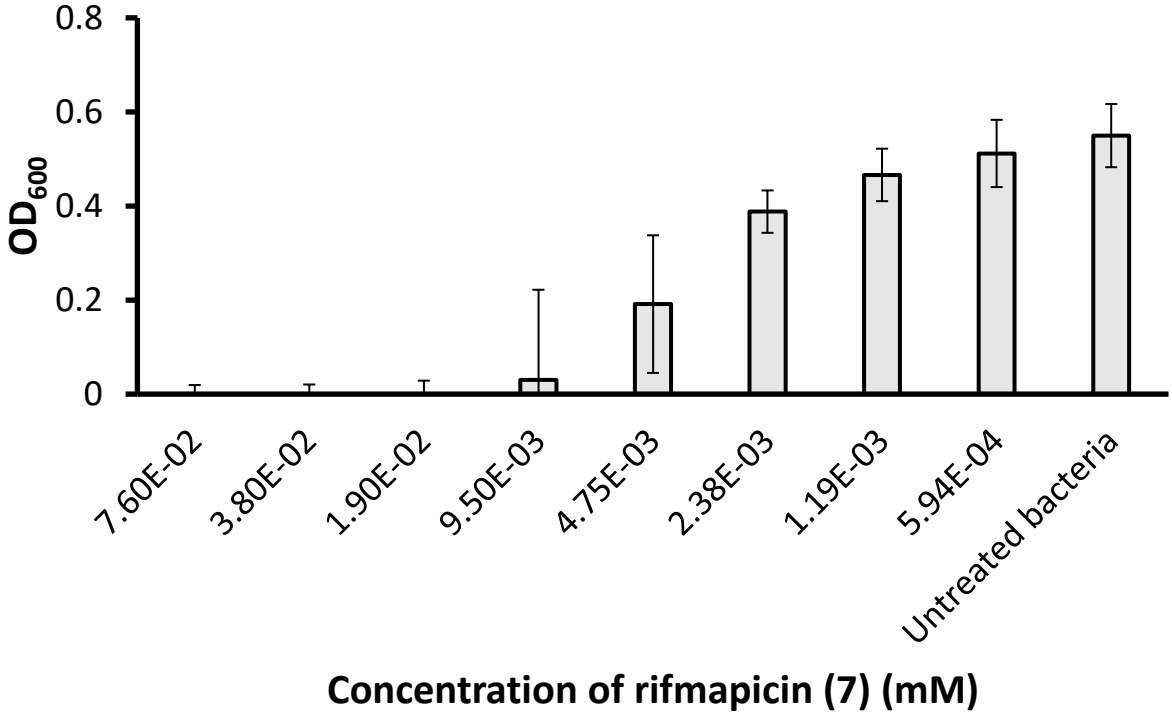


Figure S125 - Determination of MIC against rifampicin (**7**) for *E. coli* DH10β.

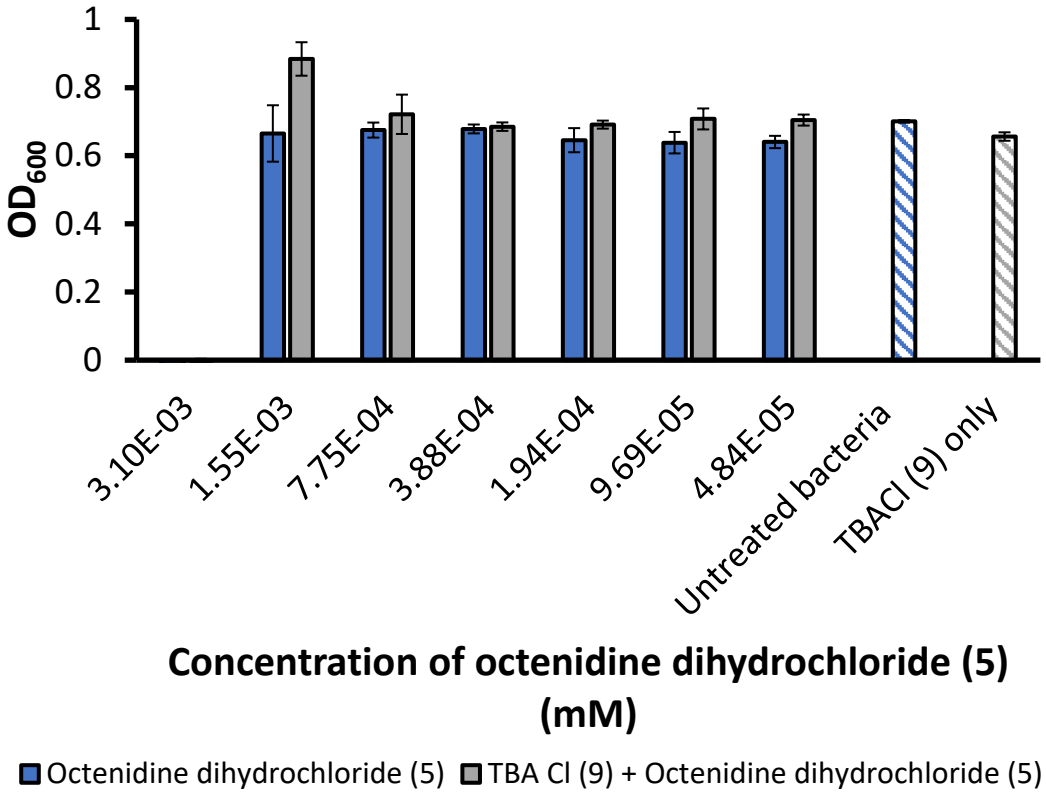


Figure S126 – A control experiment where TBACl (**9**) at 8 mM was incubated with *P. aeruginosa* PA01 for ≈ 10 minutes before being added to a well containing octenidine dihydrochloride (**5**) at varying concentrations.

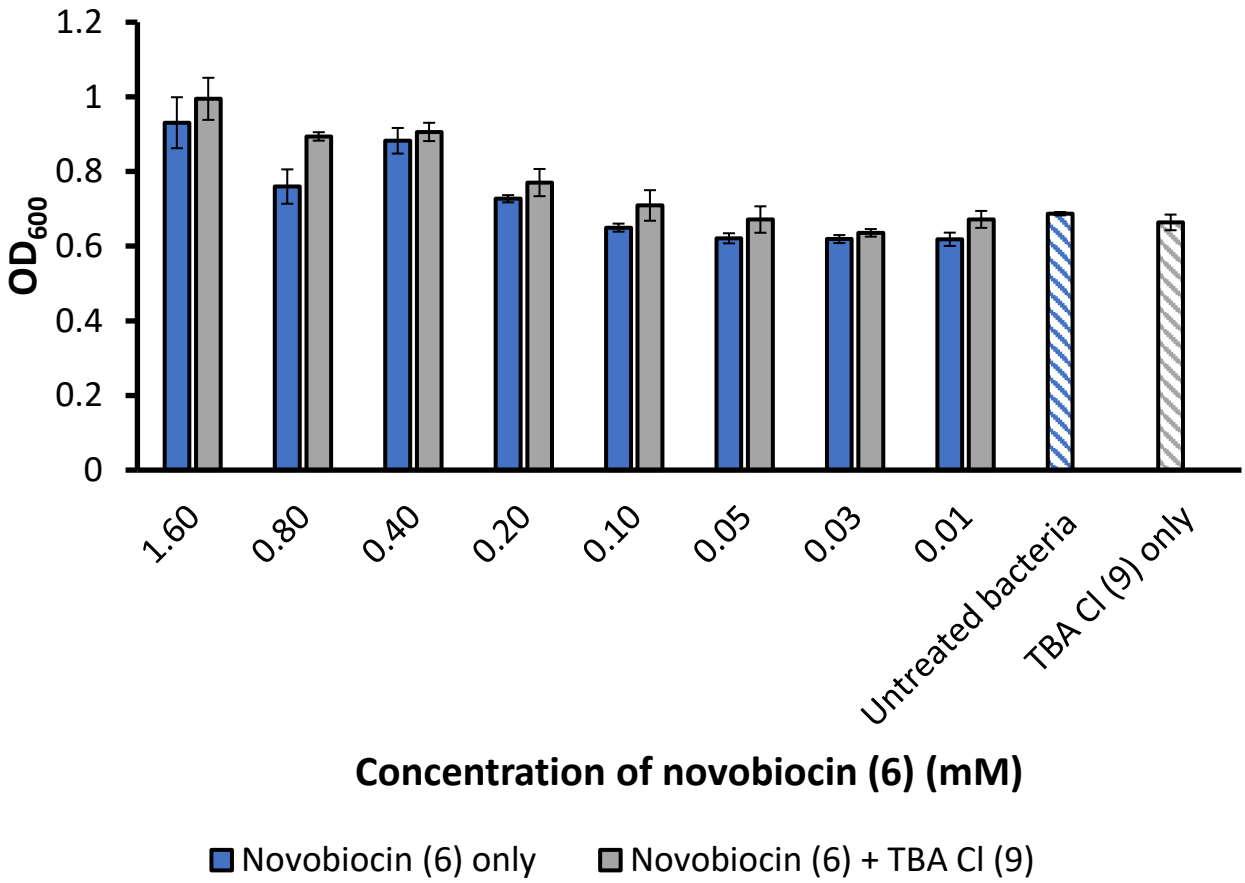


Figure S127 - A control experiment where TBACl (**9**) at 8 mM was incubated with *P. aeruginosa* PA01 for ≈ 10 minutes before being added to a well containing novobiocin (**6**) at varying concentrations.

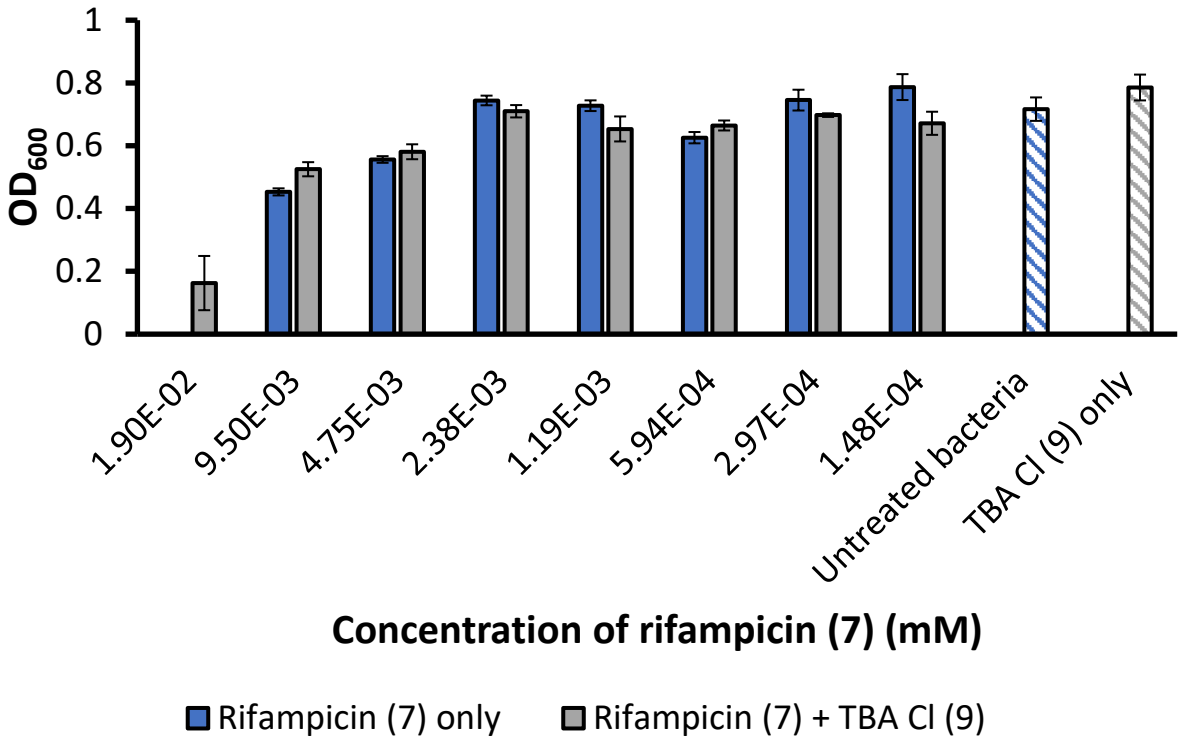


Figure S128 - A control experiment where TBACl (**9**) at 8 mM was incubated with *P. aeruginosa* PA01 for ≈ 10 minutes before being added to a well containing rifampicin (**7**) at varying concentrations.

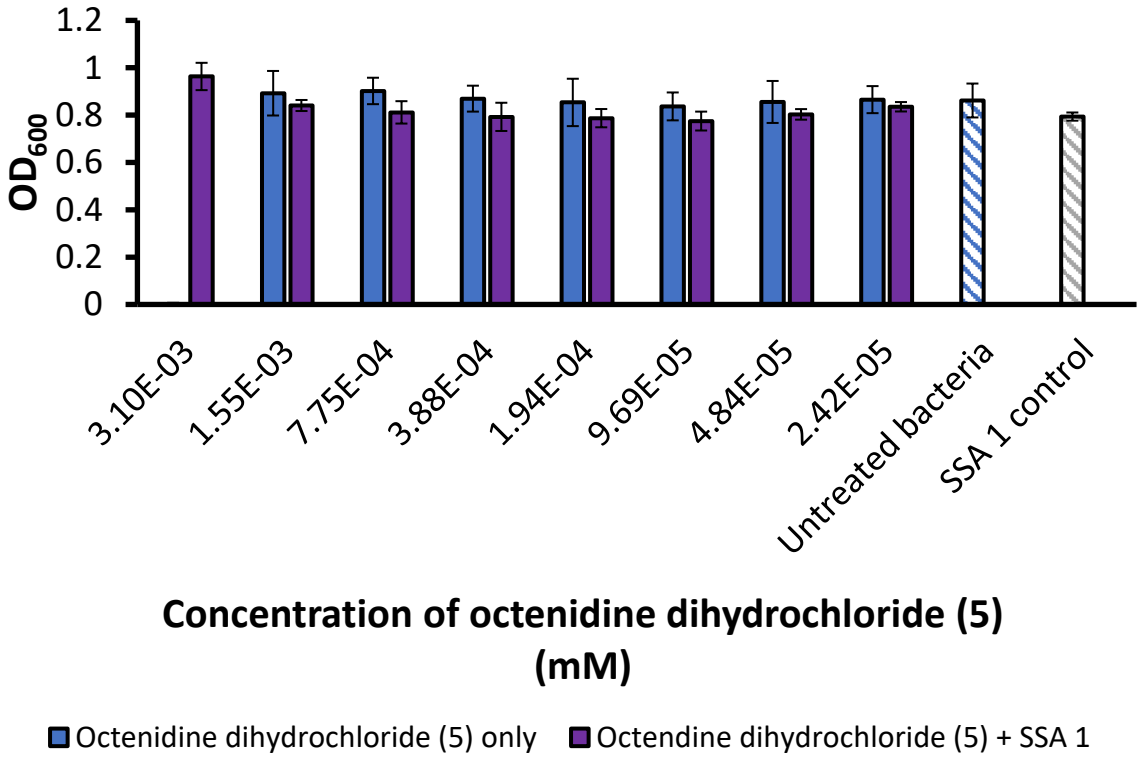


Figure S129 - SSA **1** (8 mM) was incubated with *P. aeruginosa* PA01 for ≈ 10 minutes before being added to a well containing octenidine dihydrochloride (**5**) at varying concentrations.

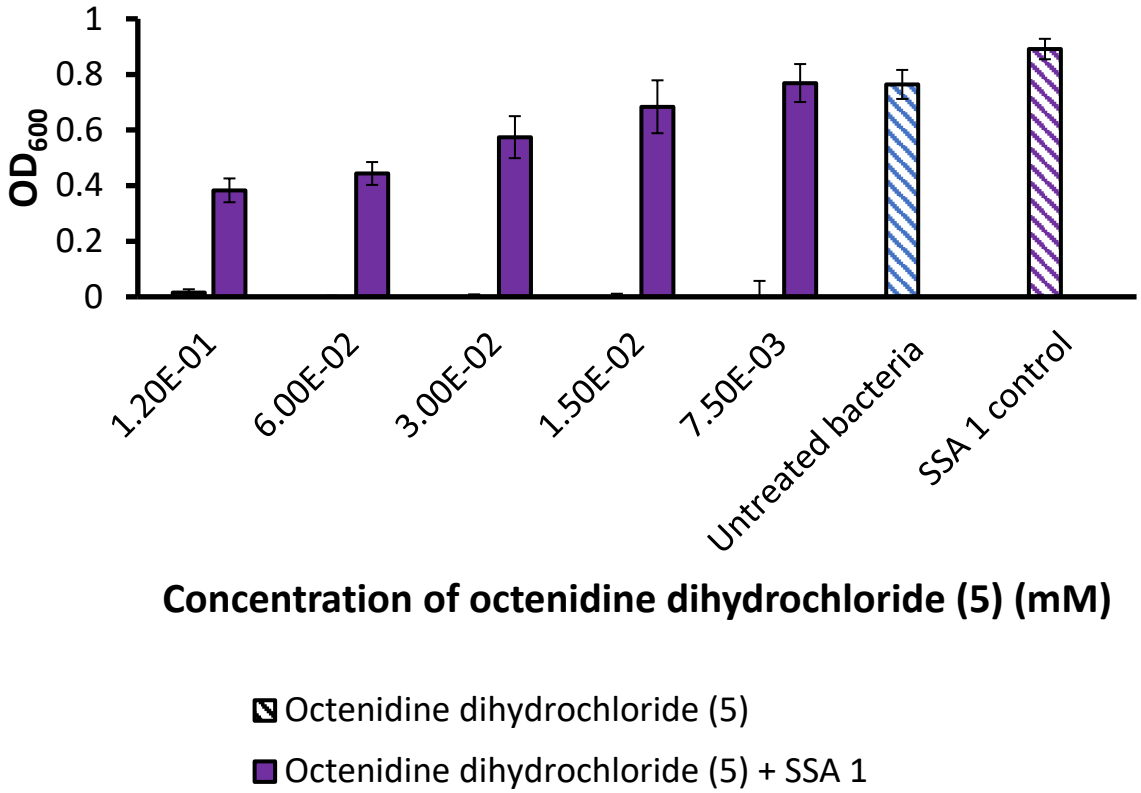


Figure S130 - SSA **1** (8 mM) was incubated with *P. aeruginosa* PA01 for ≈ 10 minutes before being added to a well containing octenidine dihydrochloride (**5**) at varying concentrations. Concentration of octenidine dihydrochloride (**5**) was increased until solubility limit was reached to further investigate antagonism.

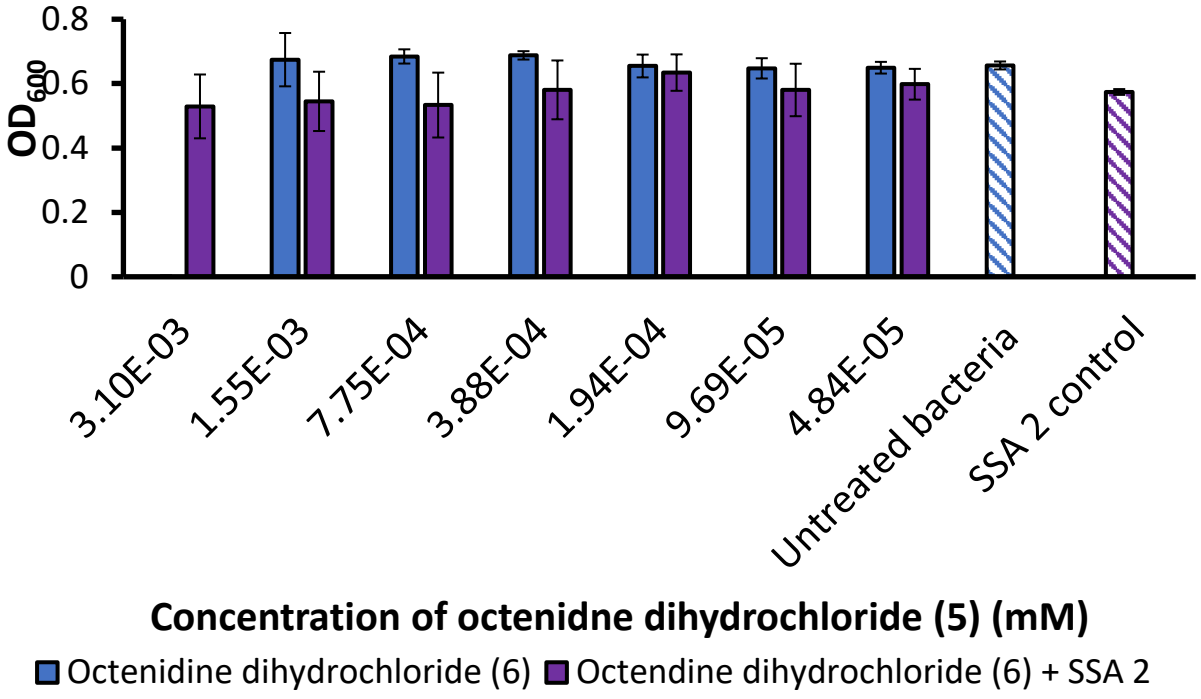


Figure S131 - SSA **2** (8 mM) was incubated with *P. aeruginosa* PA01 for ≈ 10 minutes before being added to a well containing octenidine dihydrochloride (**5**) at varying concentrations.

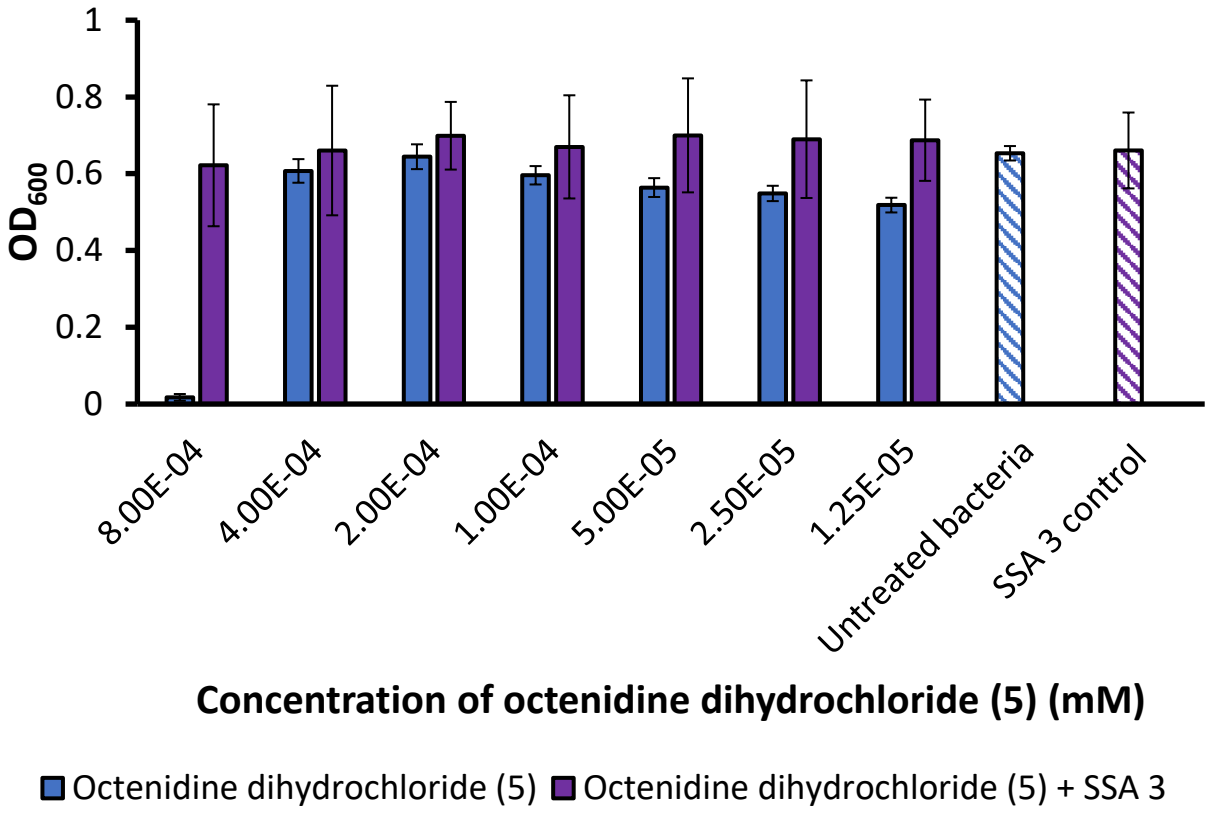


Figure S132 - SSA **3** (8 mM) was incubated with *P. aeruginosa* PA01 for ≈ 10 minutes before being added to a well containing octenidine dihydrochloride (**5**) at varying concentrations.

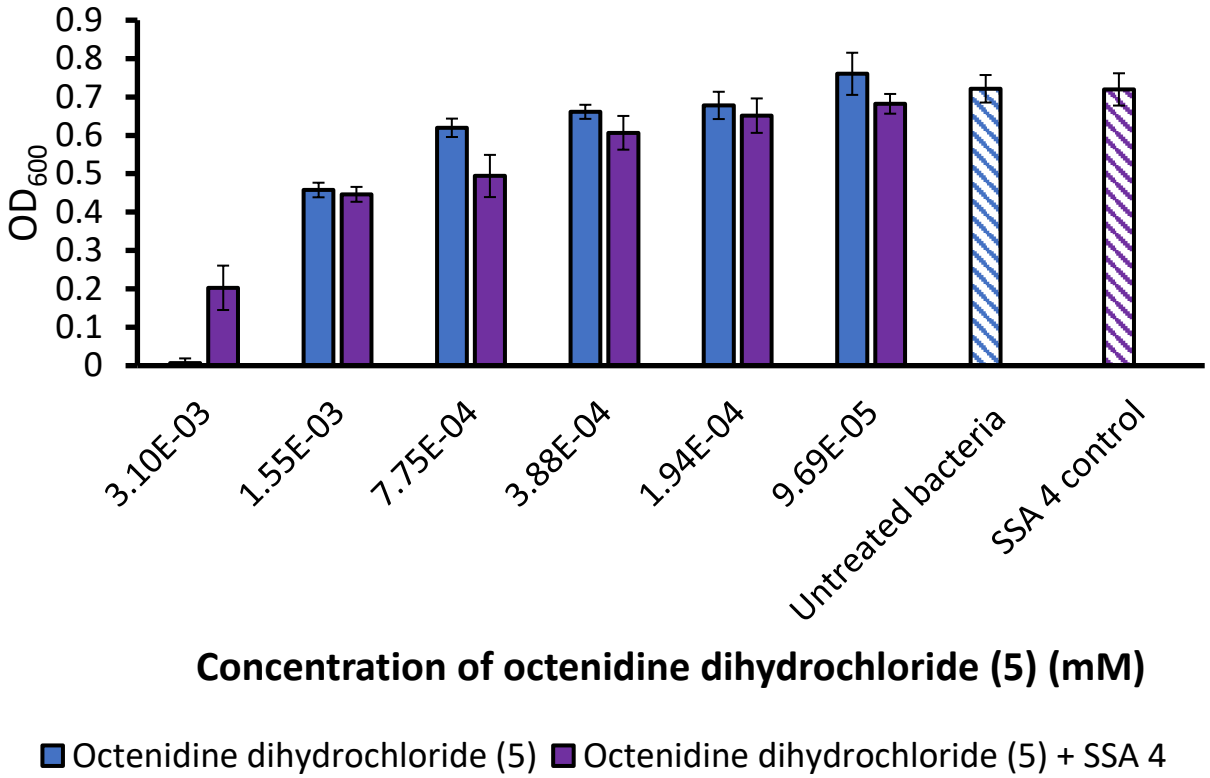


Figure S133 - SSA **4** (8 mM) was incubated with *P. aeruginosa* PA01 for ≈ 10 minutes before being added to a well containing octenidine dihydrochloride (**5**) at varying concentrations.

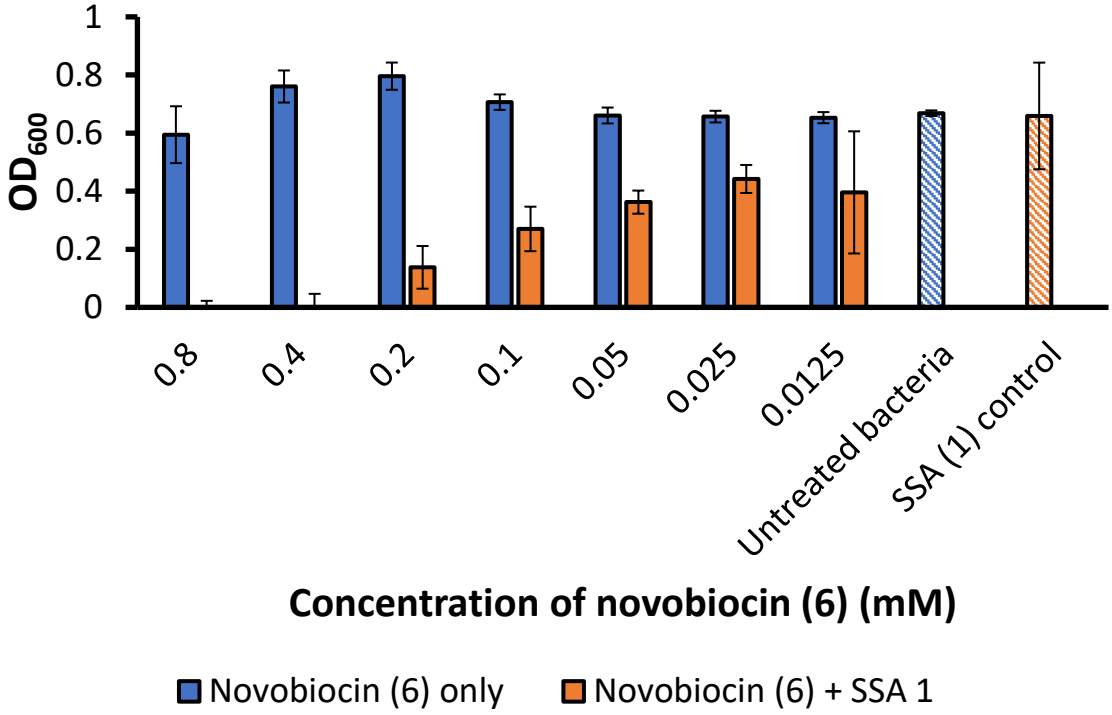


Figure S134 - SSA **1** (8 mM) was incubated with *P. aeruginosa* PA01 for ≈ 10 minutes before being added to a well containing novobiocin (**6**) at varying concentrations.

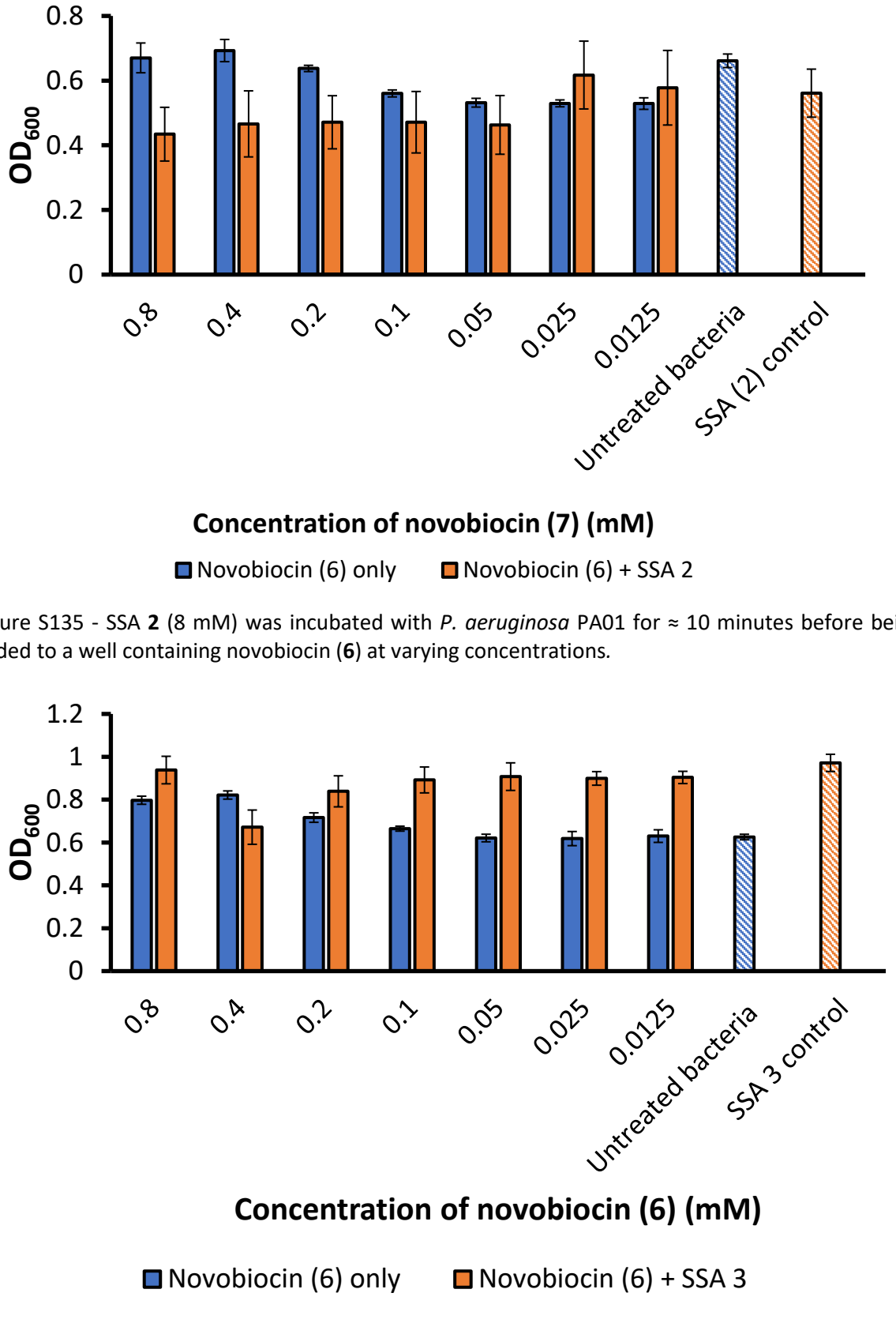


Figure S135 - SSA **2** (8 mM) was incubated with *P. aeruginosa* PA01 for ≈ 10 minutes before being added to a well containing novobiocin (**6**) at varying concentrations.




Figure S136 - SSA **3** (8 mM) was incubated with *P. aeruginosa* PA01 for ≈ 10 minutes before being added to a well containing novobiocin (**6**) at varying concentrations.

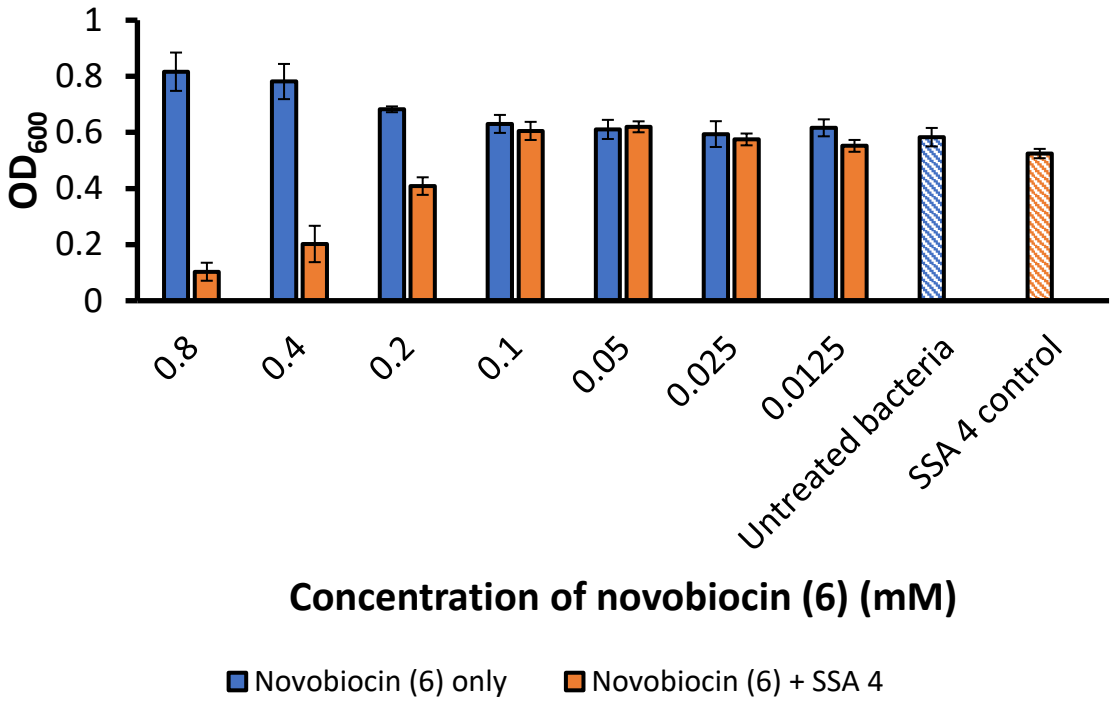


Figure S137 - SSA **4** (8 mM) was incubated with *P. aeruginosa* PA01 for ≈ 10 minutes before being added to a well containing novobiocin (**6**) at varying concentrations.

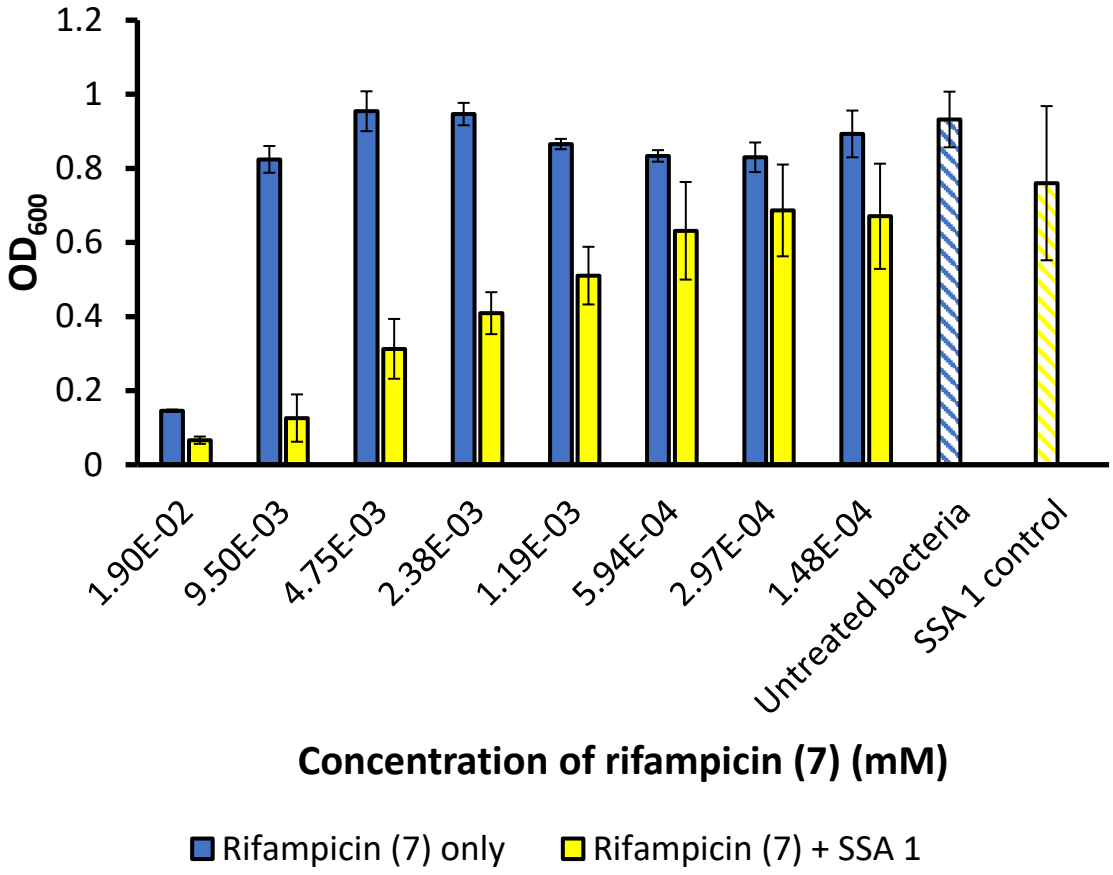


Figure S138 – SSA **1** (8 mM) was incubated with *P. aeruginosa* PA01 for ≈ 10 minutes before being added to a well containing rifampicin (**7**) at varying concentrations.

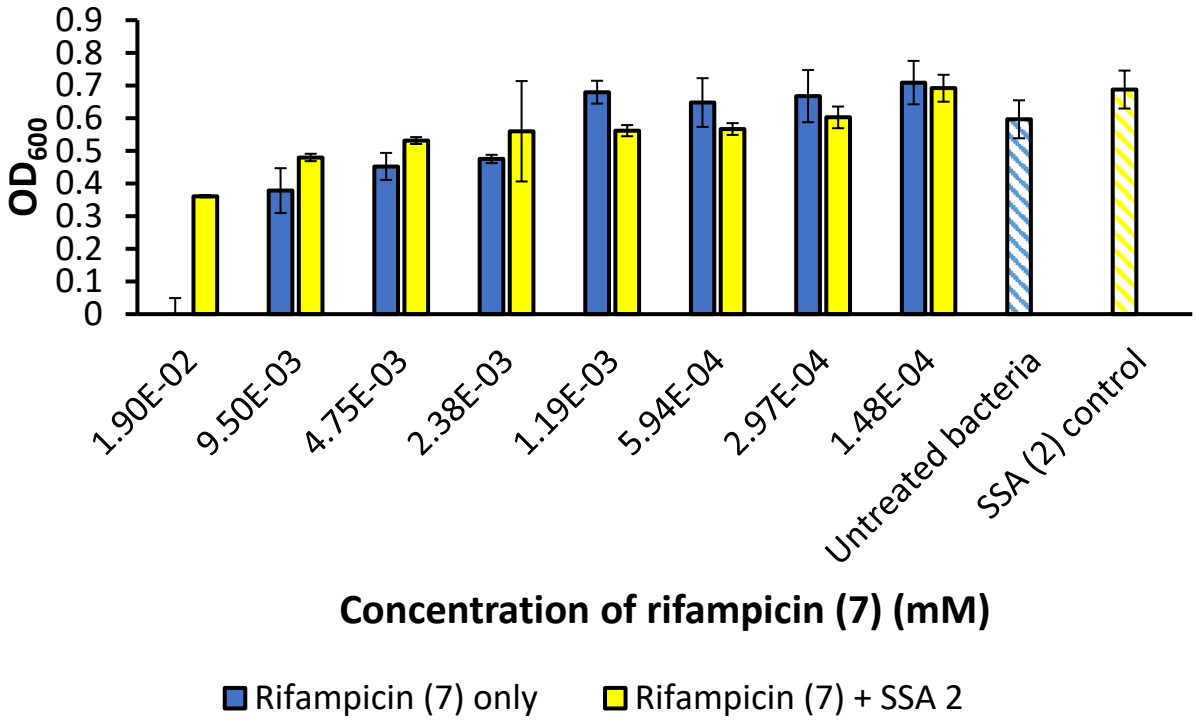


Figure S139 - SSA **2** (8 mM) was incubated with *P. aeruginosa* PA01 for ≈ 10 minutes before being added to a well containing rifampicin (**7**) at varying concentrations.

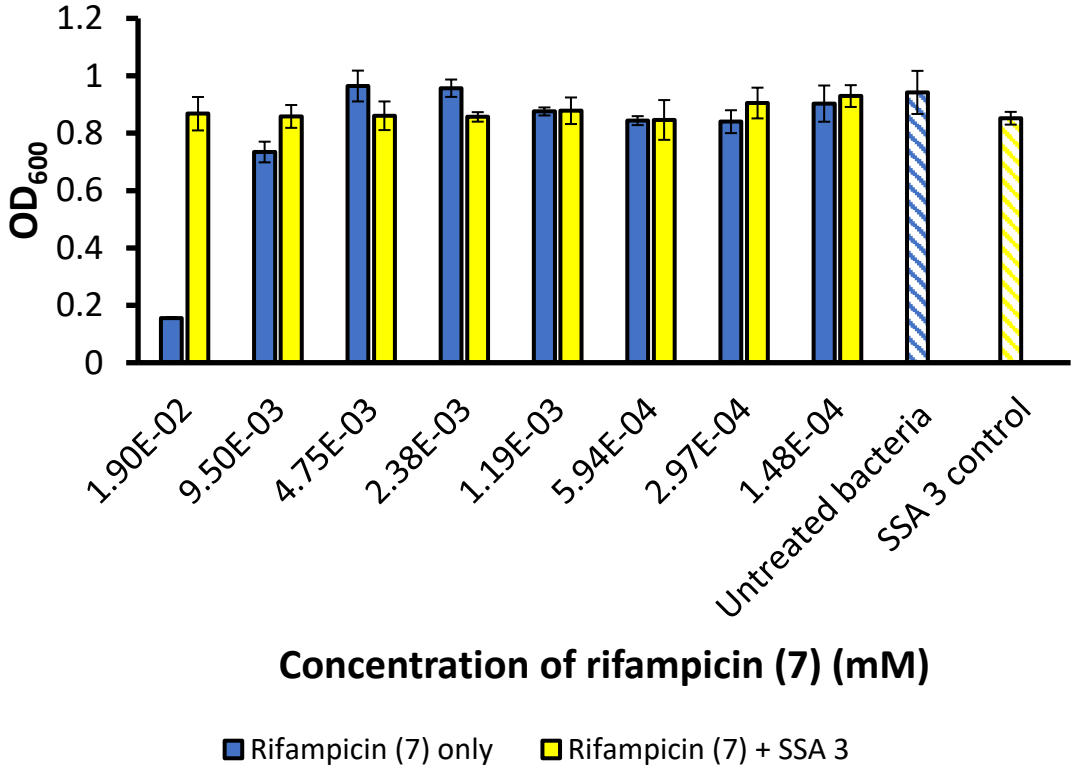


Figure 140 - SSA **3** (8 mM) was incubated with *P. aeruginosa* PA01 for ≈ 10 minutes before being added to a well containing rifampicin (**8**) at varying concentrations.

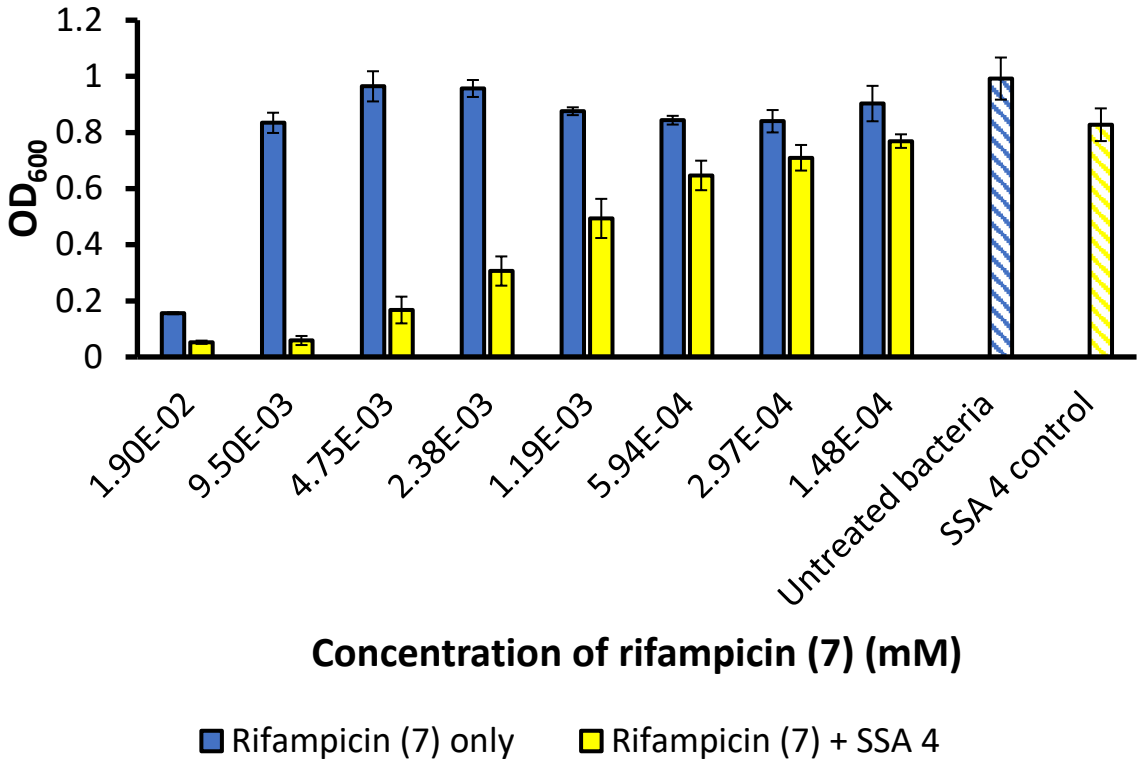


Figure S141 - SSA **4** (8 mM) was incubated with *P. aeruginosa* PA01 for ≈ 10 minutes before being added to a well containing rifampicin (**7**) at varying concentrations.

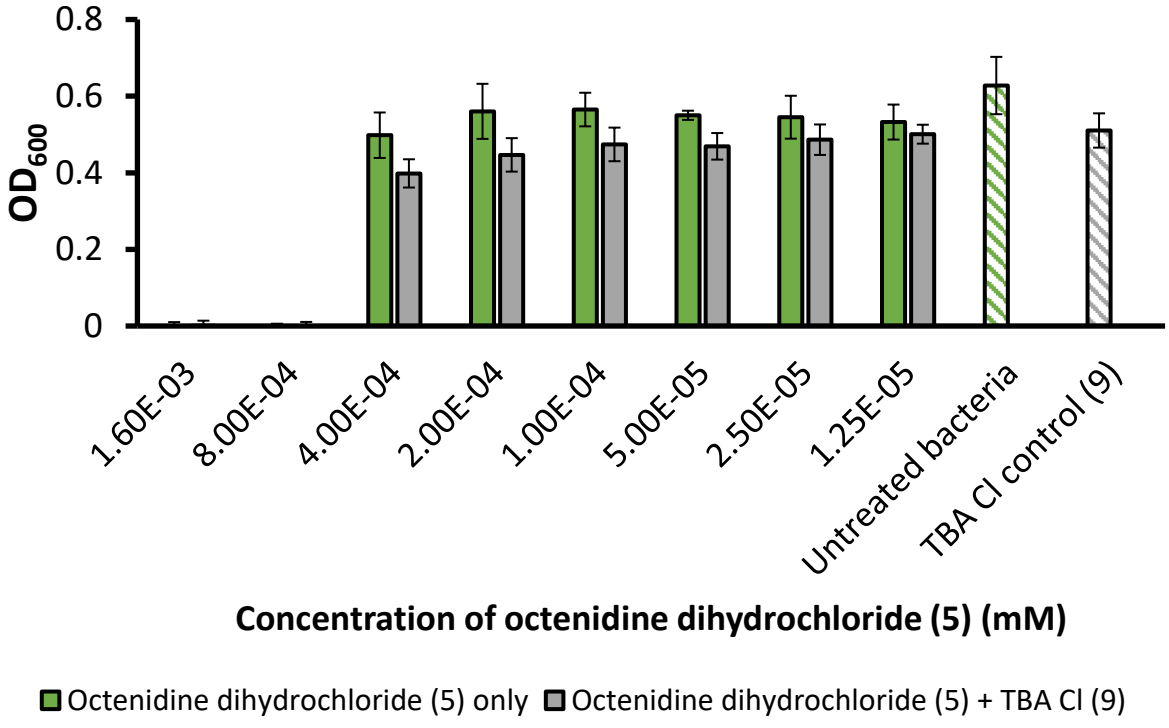


Figure S142 - A control experiment where TBACl (**9**) at 8 mM was incubated with *E. coli* DH10β for ≈ 10 minutes before being added to a well containing octenidine dihydrochloride (**5**) at varying concentrations.

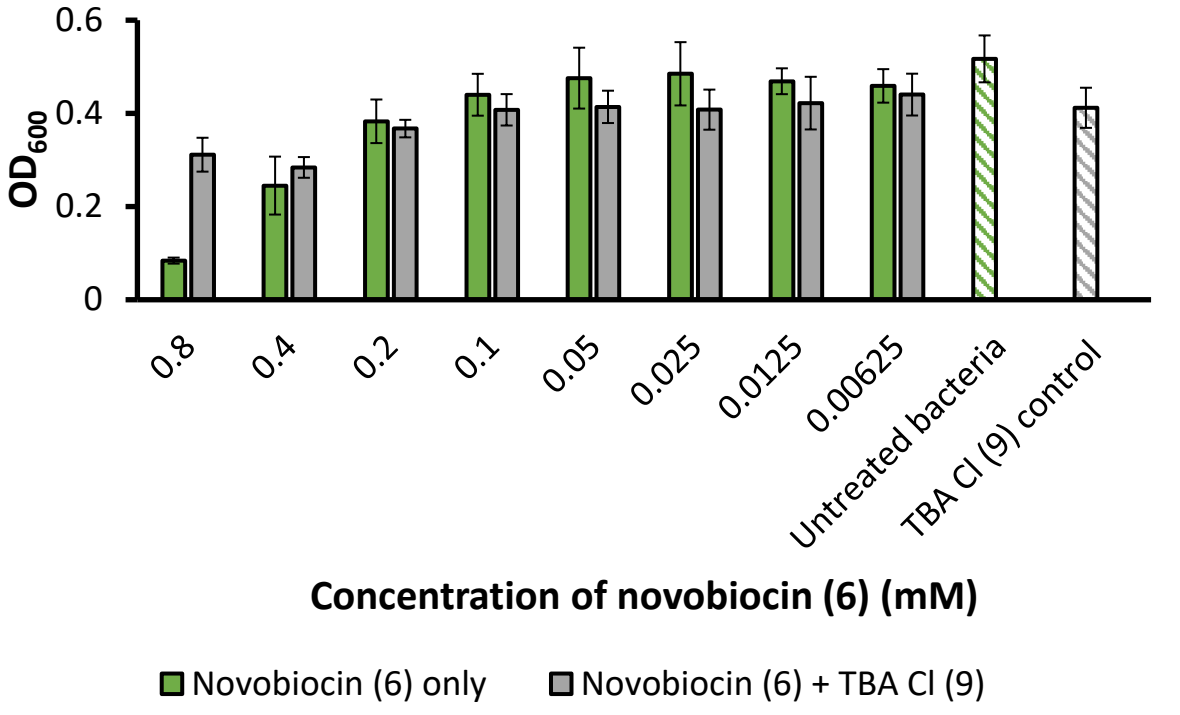


Figure S143 - A control experiment where TBACl (**9**) at 8 mM was incubated with *E. coli* DH10β for ≈ 10 minutes before being added to a well containing novobiocin (**6**) at varying concentrations.

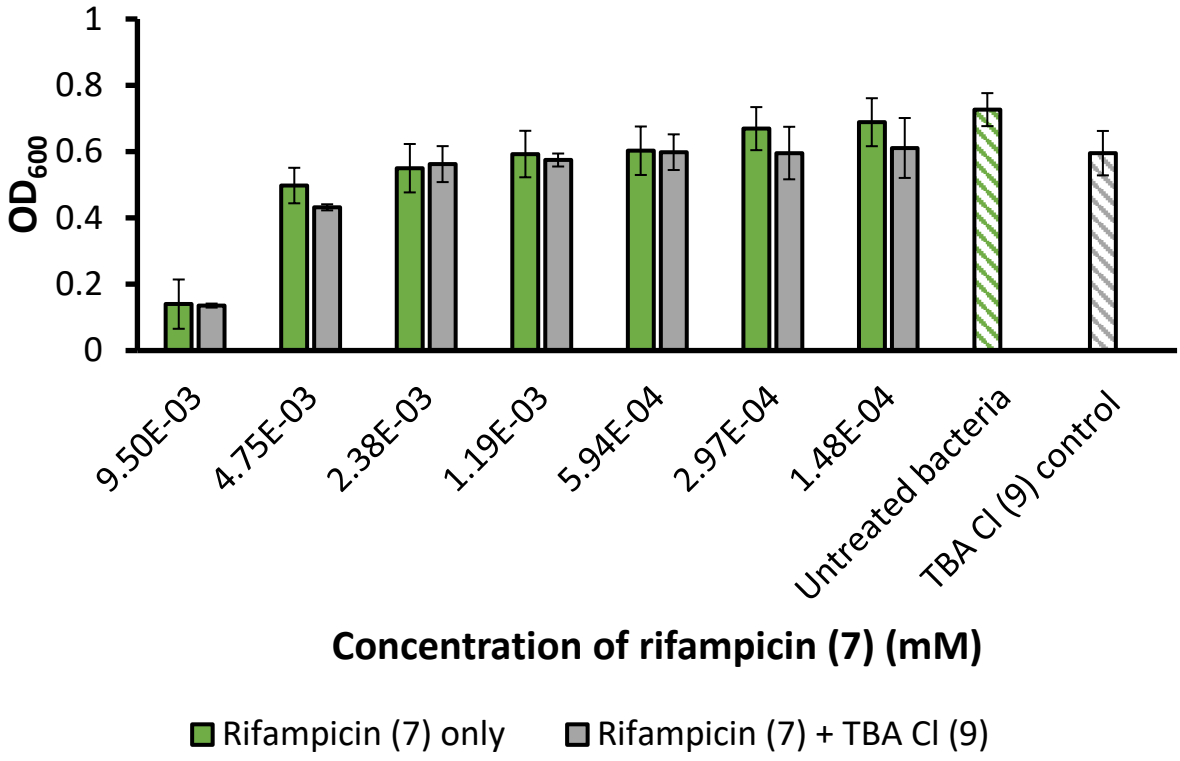


Figure S144 - A control experiment where TBACl (**9**) at 8 mM was incubated with *E. coli* DH10β for ≈ 10 minutes before being added to a well containing rifampicin (**7**) at varying concentrations.

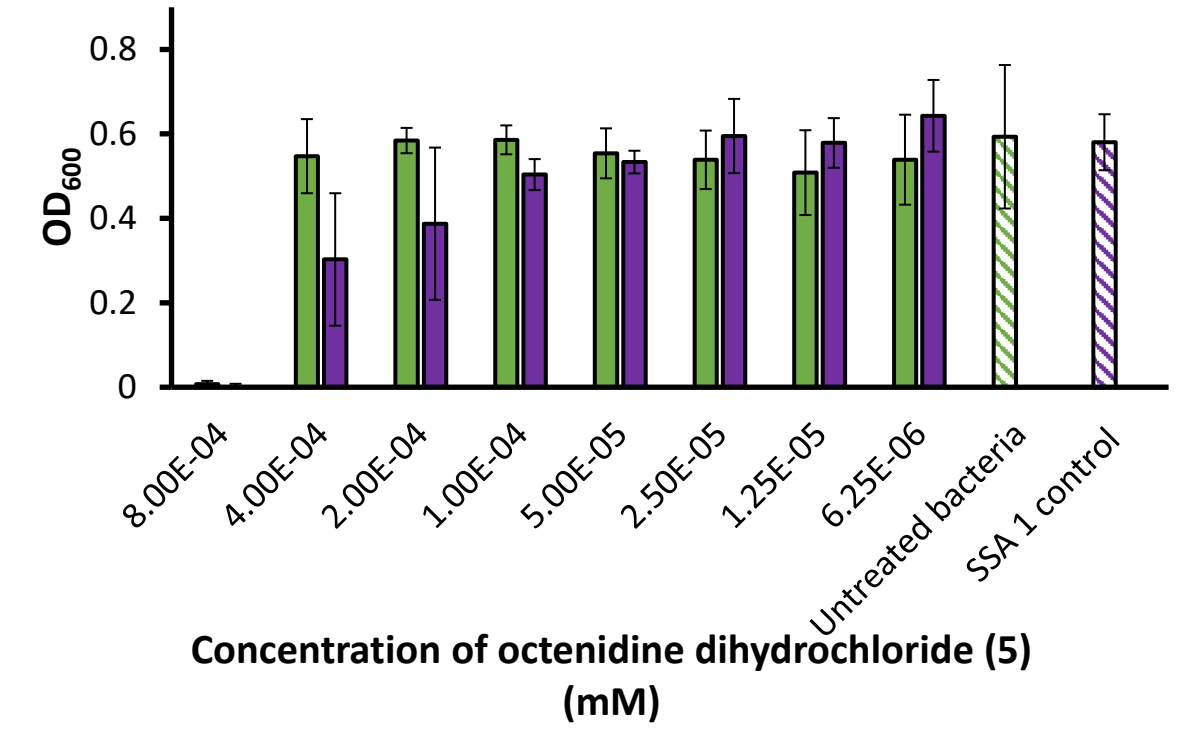


Figure S145 - SSA **1** (0.63 mM) was incubated with *E. coli* DH10β for ≈ 10 minutes before being added to a well containing octenidine dihydrochloride (**5**) at varying concentrations.

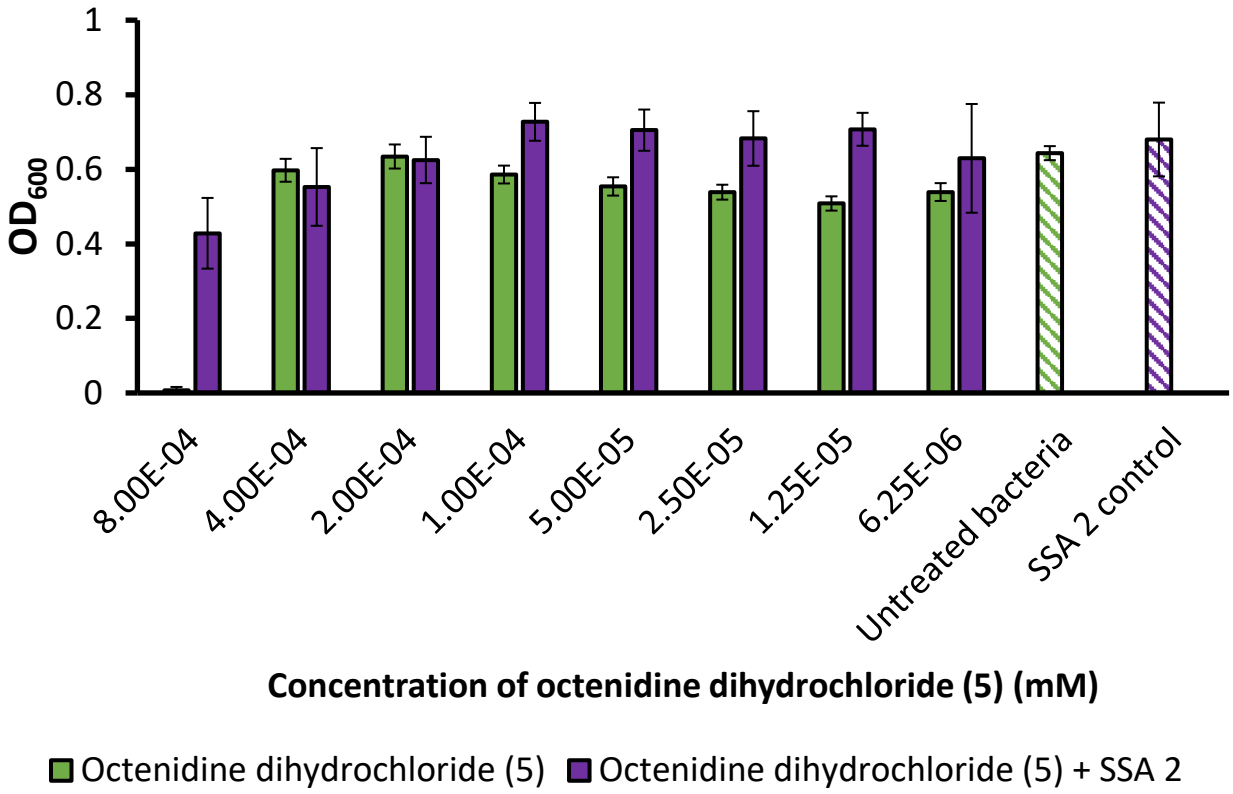


Figure S146 - SSA **2** (8 mM) was incubated with *E. coli* DH10β for ≈ 10 minutes before being added to a well containing octenidine dihydrochloride (**5**) at varying concentrations.

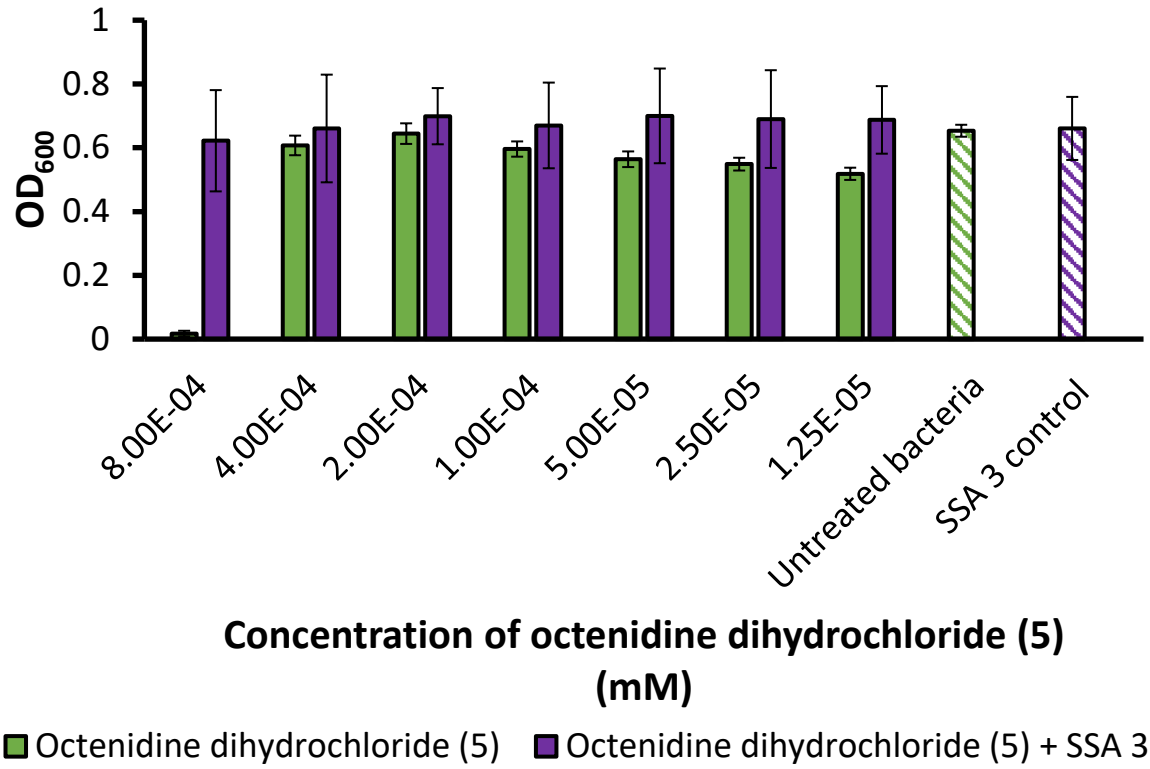


Figure S147 - SSA **3** (8 mM) was incubated with *E. coli* DH10β for ≈ 10 minutes before being added to a well containing octenidine dihydrochloride (**5**) at varying concentrations.

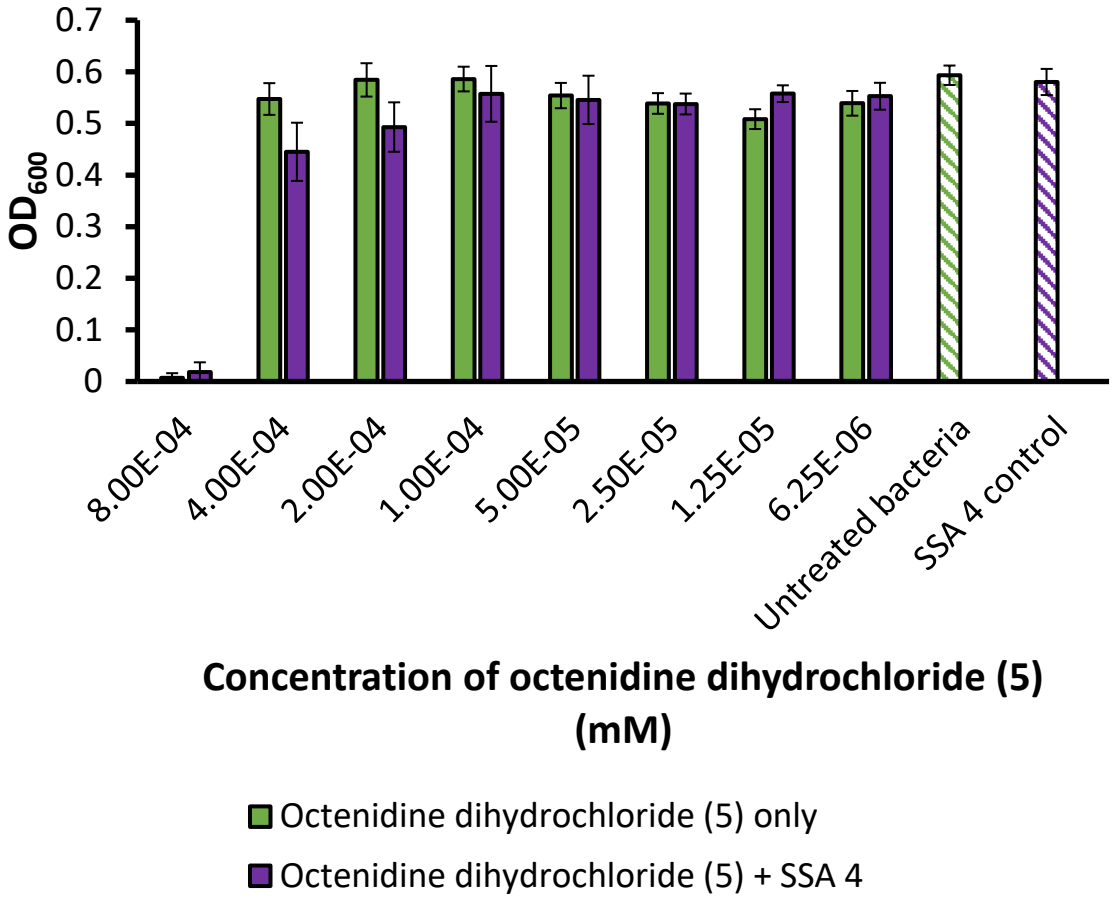


Figure S148 - SSA **4** (0.63 mM) was incubated with *E. coli* DH10β for ≈ 10 minutes before being added to a well containing octenidine dihydrochloride (**5**) at varying concentrations.

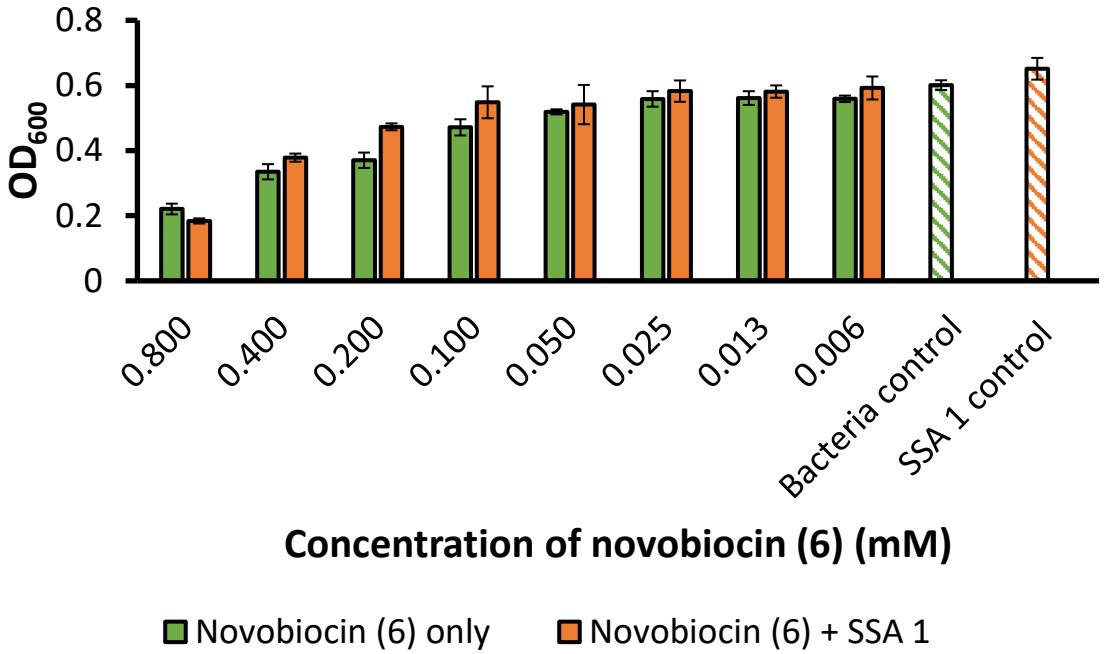


Figure S149 - SSA **1** (0.63 mM) was incubated with *E. coli* DH10β for ≈ 10 minutes before being added to a well containing novobiocin (**6**) at varying concentrations.

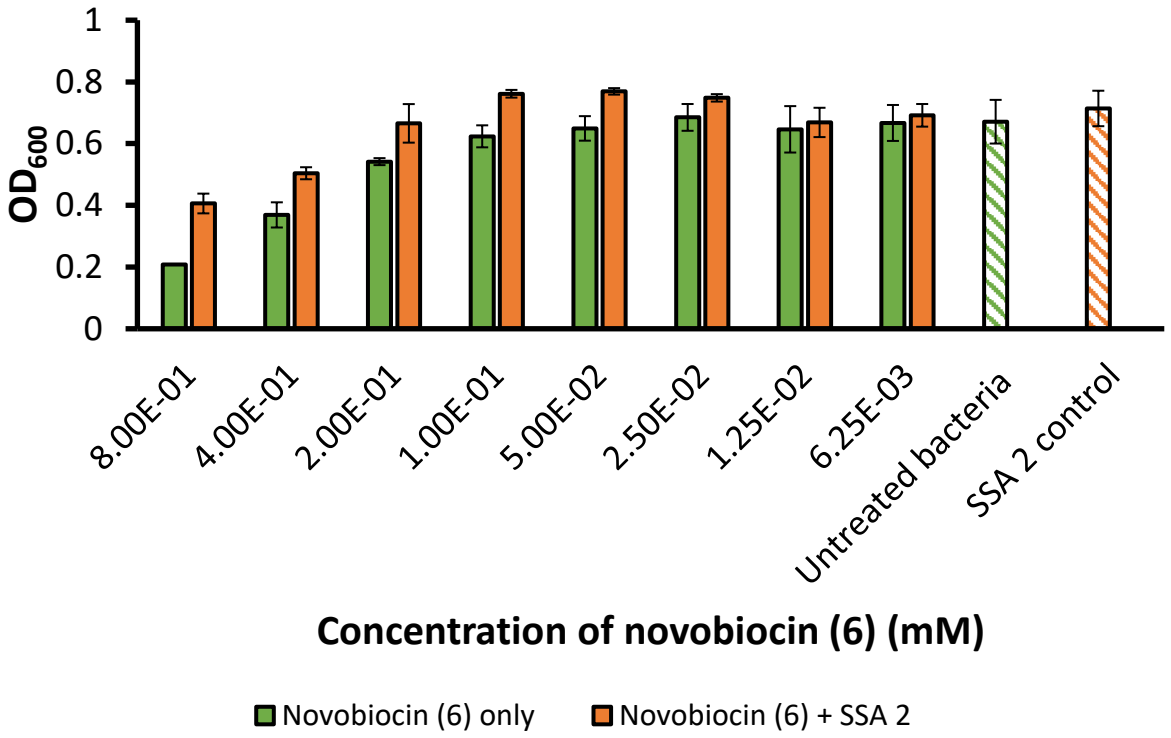


Figure S150 - SSA **2** (8 mM) was incubated with *E. coli* DH10β for ≈ 10 minutes before being added to a well containing novobiocin (**6**) at varying concentrations.

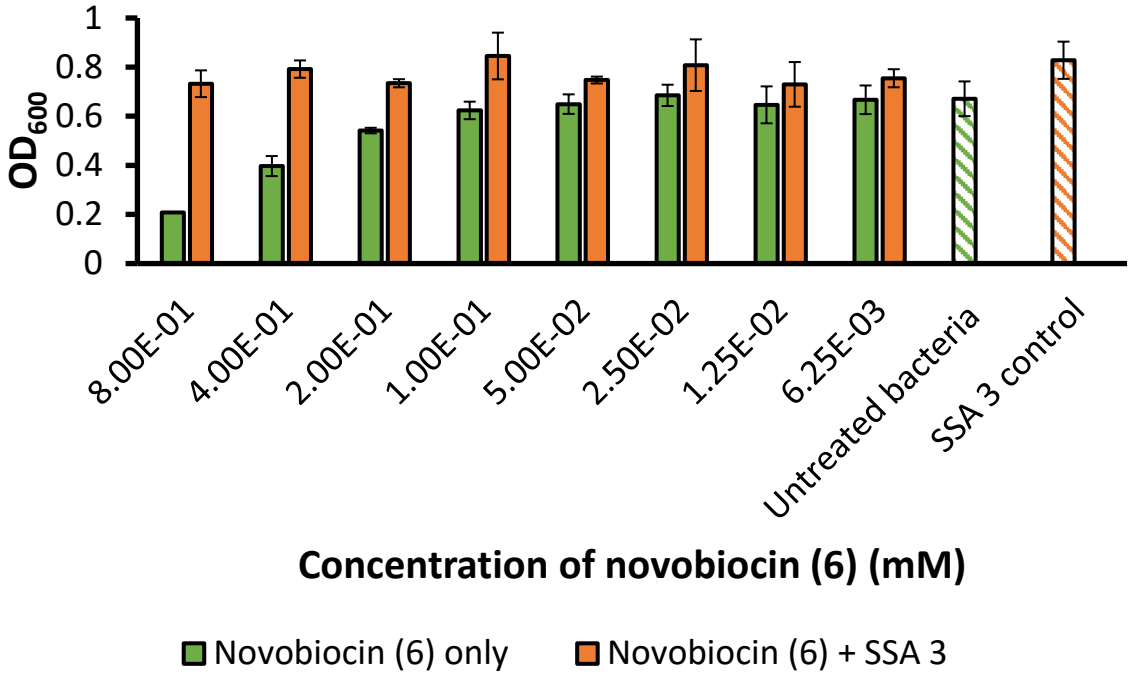


Figure S151 - SSA **3** (8 mM) was incubated with *E. coli* DH10β for ≈ 10 minutes before being added to a well containing novobiocin (**6**) at varying concentrations.

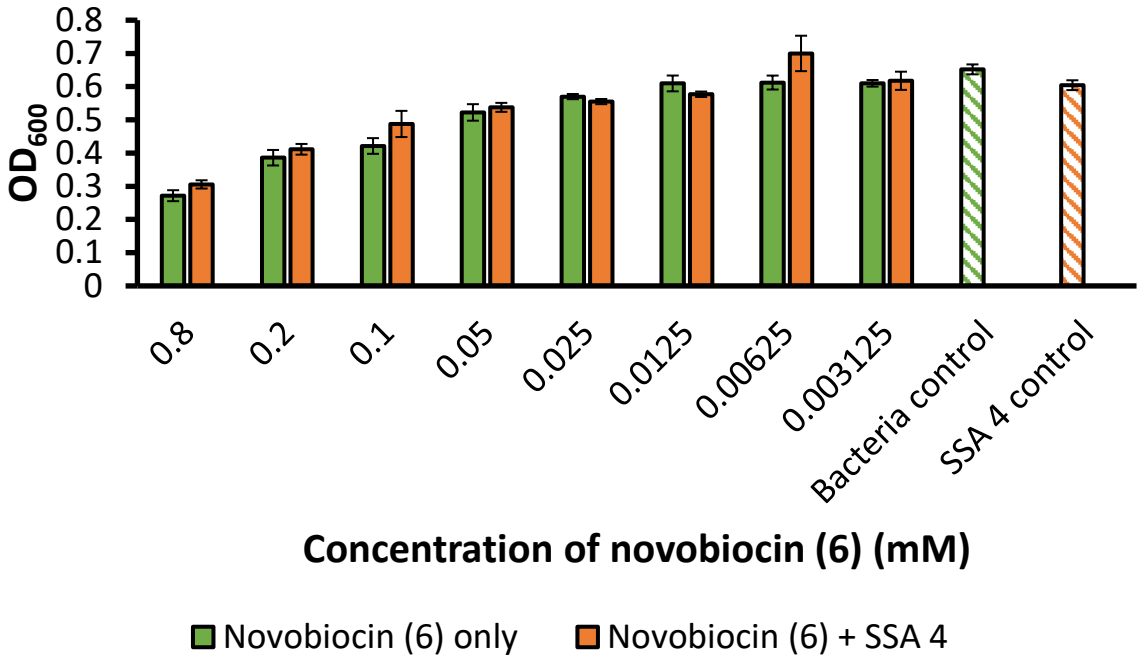


Figure S152 - SSA **4** (0.63 mM) was incubated with *E. coli* DH10β for ≈ 10 minutes before being added to a well containing novobiocin (**6**) at varying concentrations.

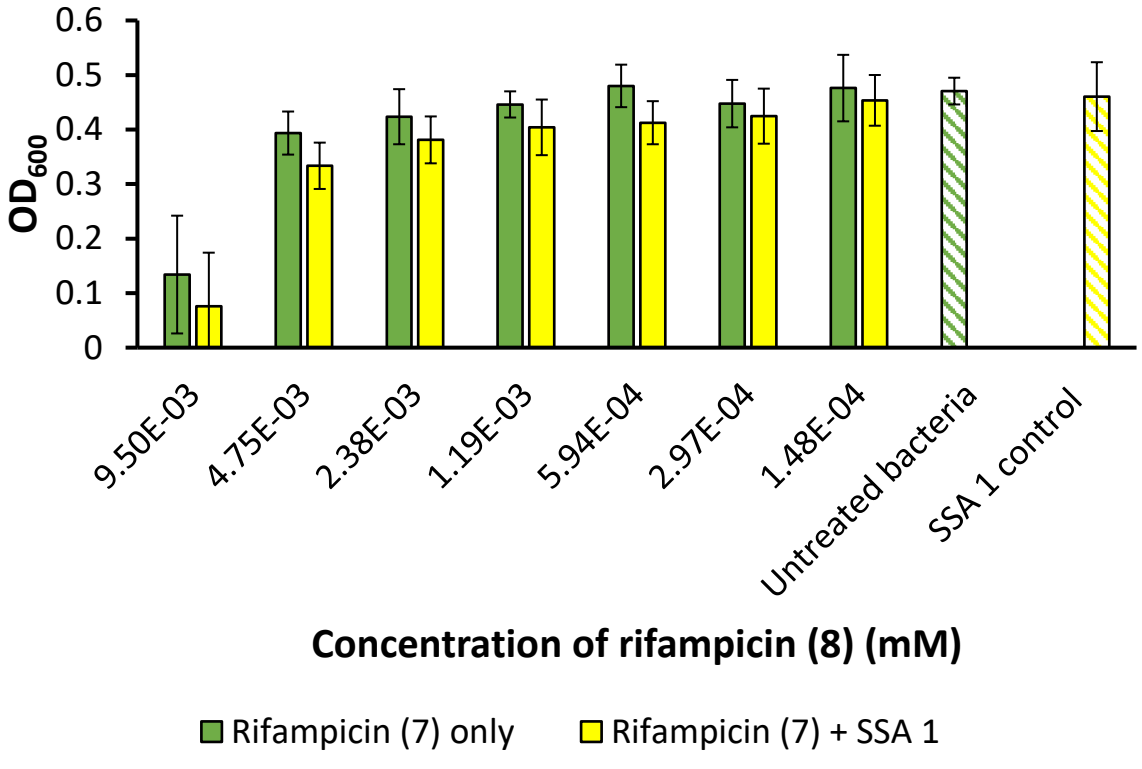


Figure S153 - SSA **1** (0.63 mM) was incubated with *E. coli* DH10β for ≈ 10 minutes before being added to a well containing rifampicin (**8**) at varying concentrations.

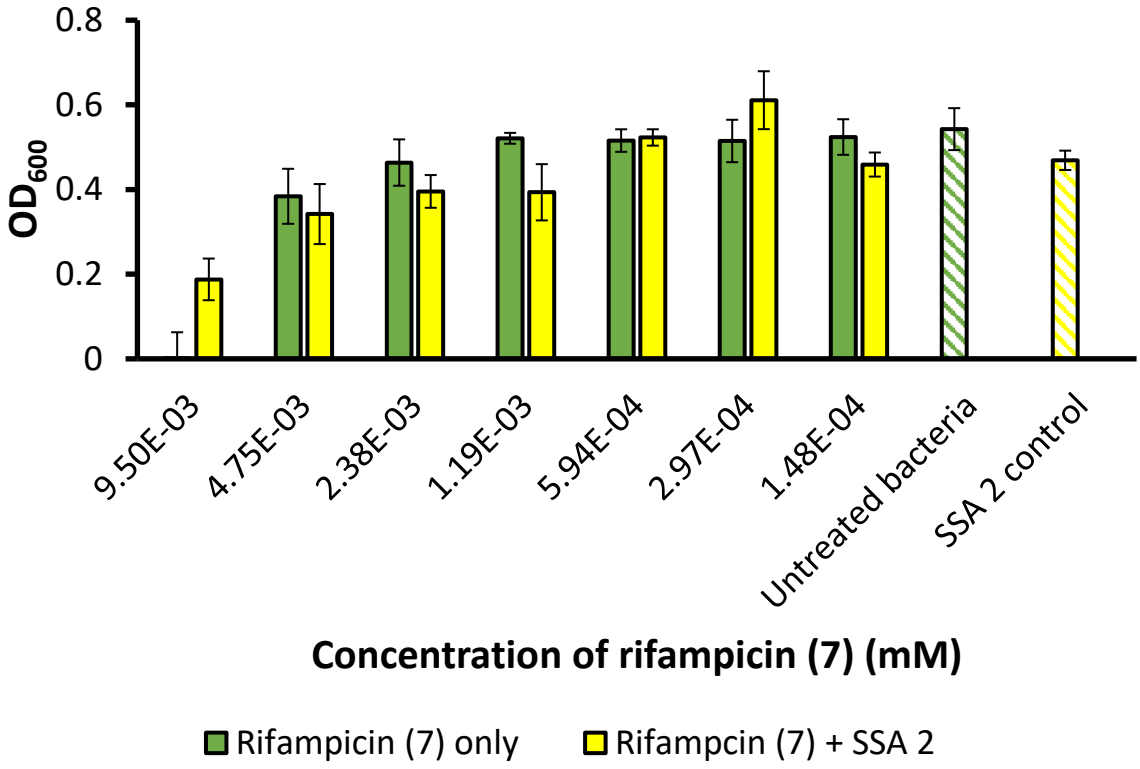


Figure S154 - SSA **2** (8 mM) was incubated with *E. coli* DH10β for ≈ 10 minutes before being added to a well containing rifampicin (**7**) at varying concentrations.

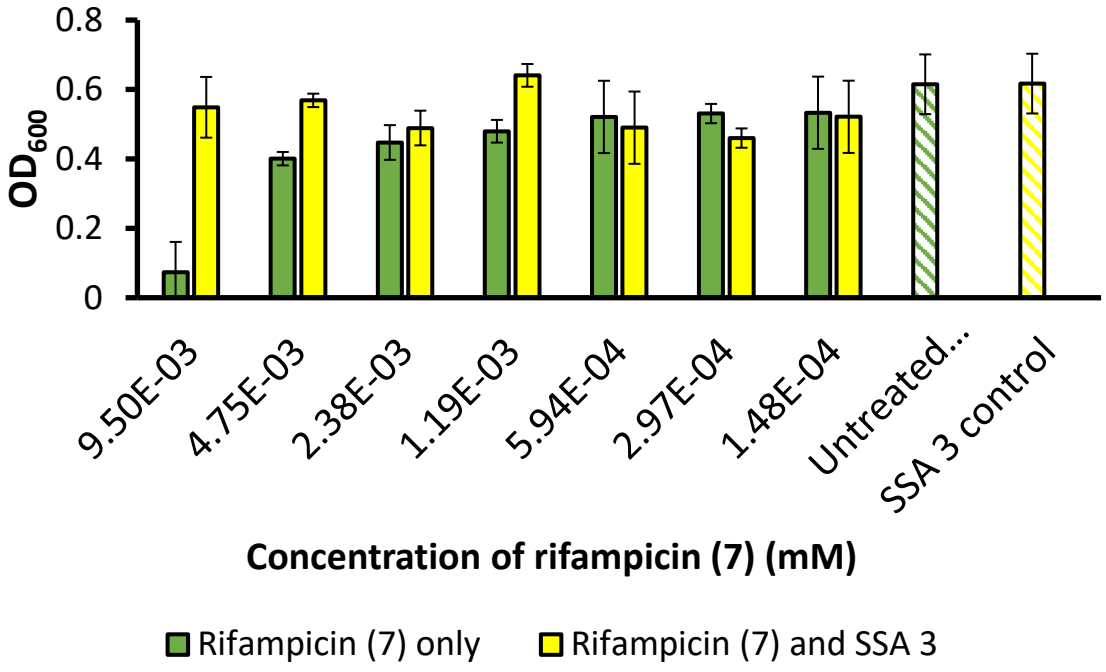


Figure S155 - SSA **3** (8 mM) was incubated with *E. coli* DH10β for ≈ 10 minutes before being added to a well containing rifampicin (**7**) at varying concentrations.

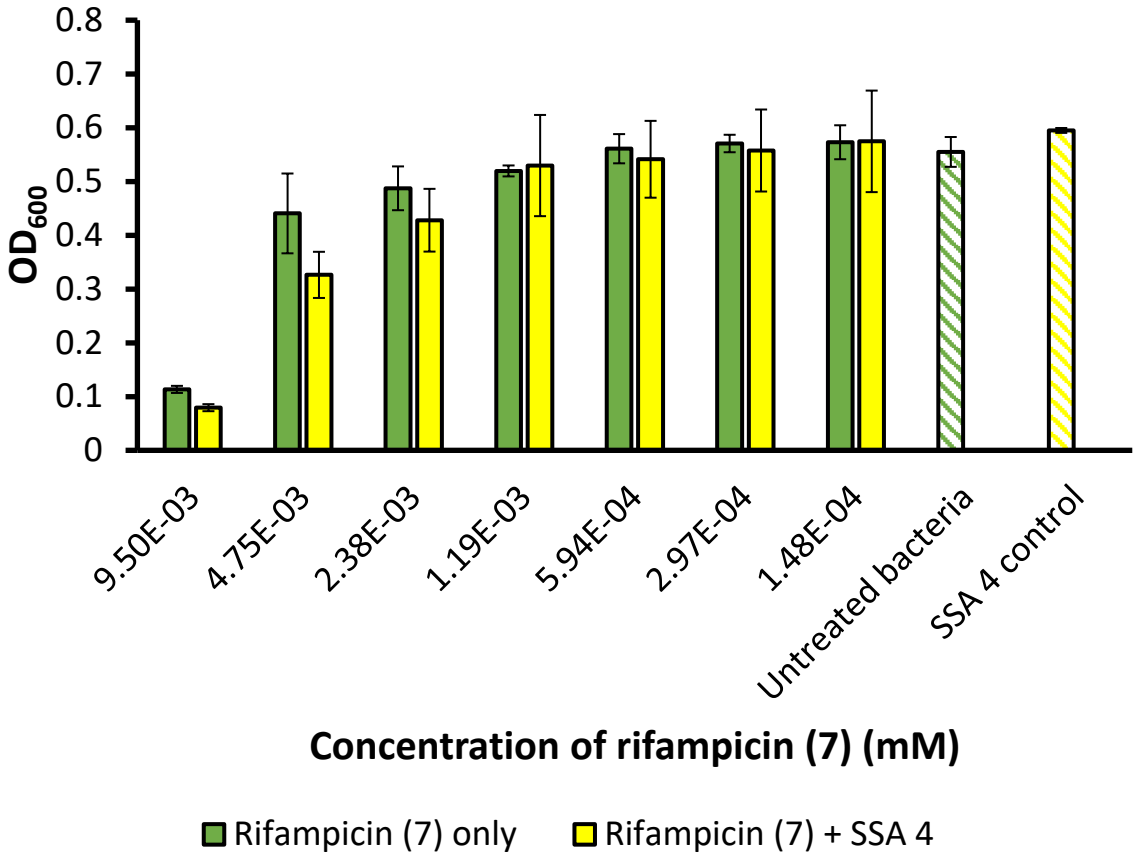


Figure S156 - SSA **4** (0.63 mM) was incubated with *E. coli* DH10β for ≈ 10 minutes before being added to a well containing rifampicin (**7**) at varying concentrations.

## Microscopy

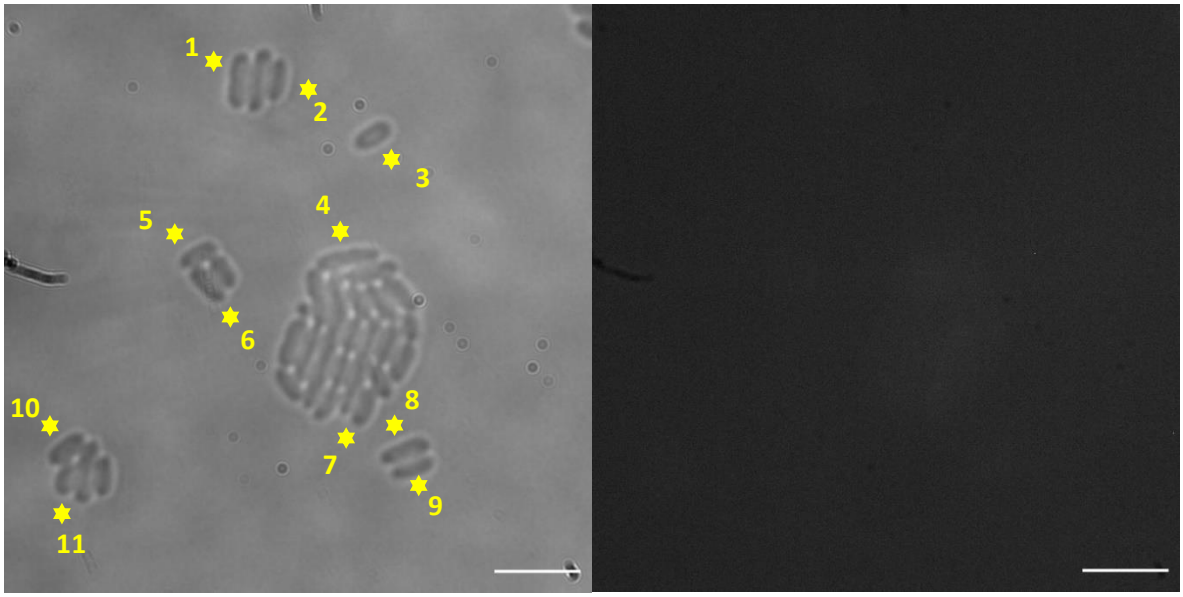


Figure S157 – *E. coli* transmitted image and fluorescence image at 450 used in fluorescence intensity calculations in the absence of both **2** and **8** at T = 4 hrs. Transmitted image used to locate cells on fluorescence image. Scale bar = 10µM.

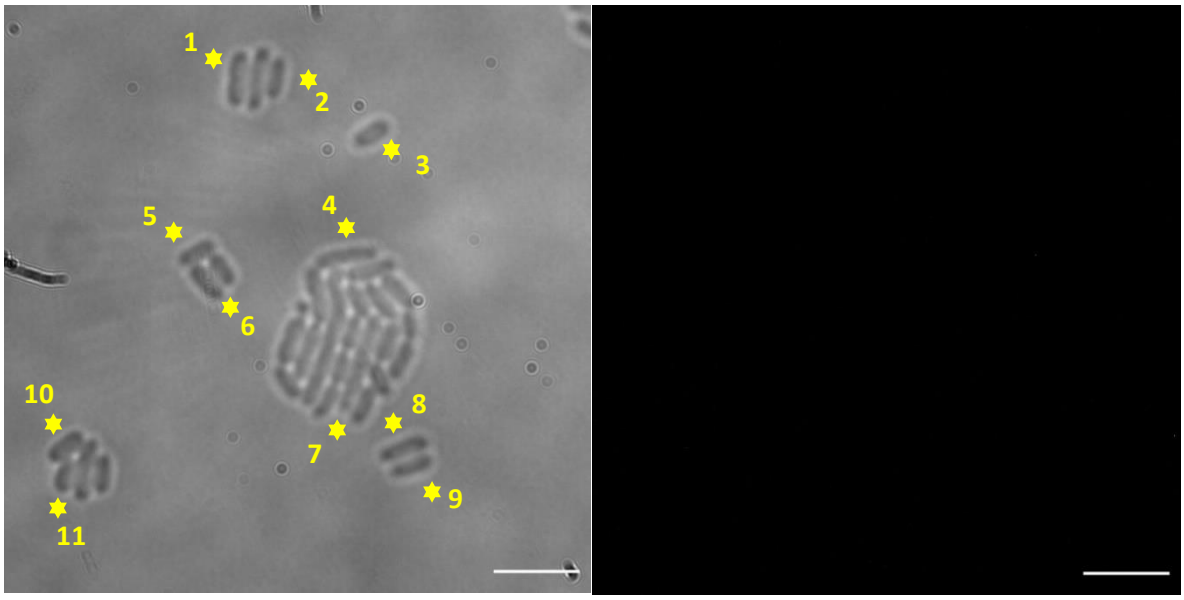


Figure S158 – *E. coli* transmitted image and fluorescence image at 605 nm used in fluorescence intensity calculations in the absence of both SSA **2** and **8** at T = 4 hrs. Transmitted image used to locate cells on fluorescence image. Scale bar = 10µM.

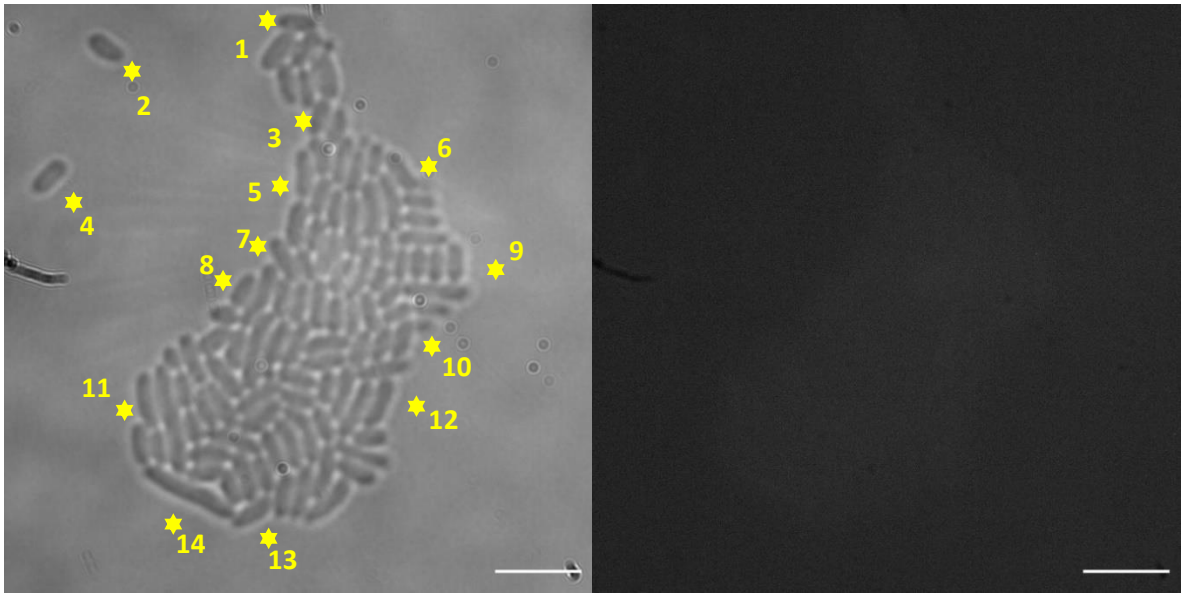


Figure S159 – *E. coli* transmitted image and Fluorescence image at 450 nm used in fluorescence intensity calculations in the absence of both **2** and **8** at T = 4 hrs. Transmitted image used to locate cells on fluorescence image. Scale bar = 10µM.

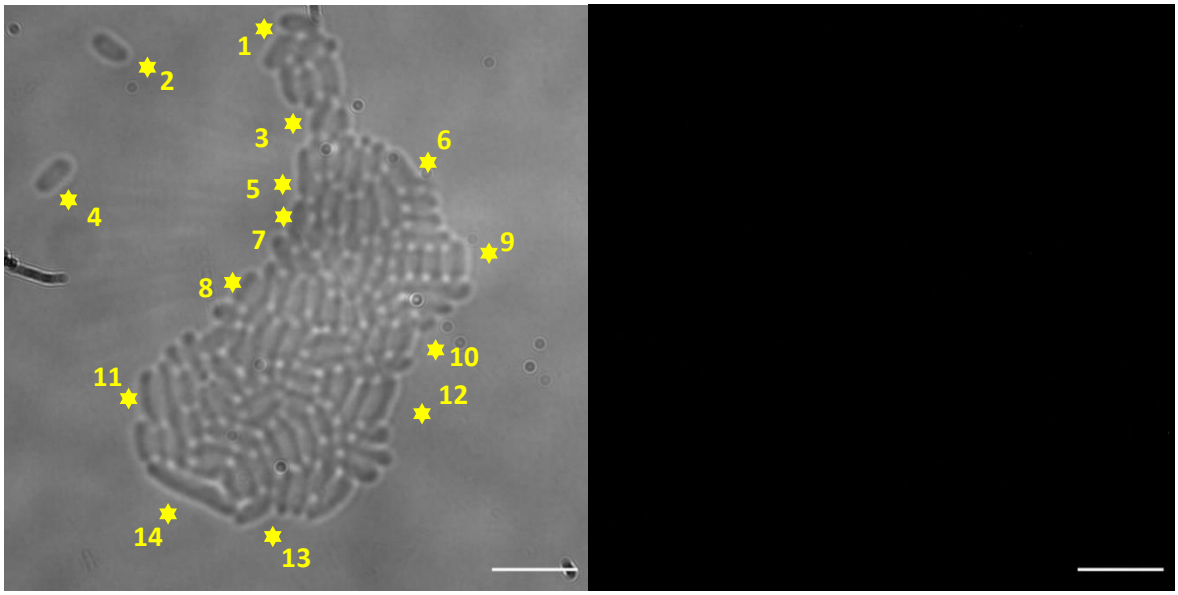


Figure S160 – *E. coli* transmitted image and fluorescence image at 605 nm used in fluorescence intensity calculations in the absence of both **2** and **8** at T = 4 hrs. Transmitted image used to locate cells on fluorescence image. Scale bar = 10µM.

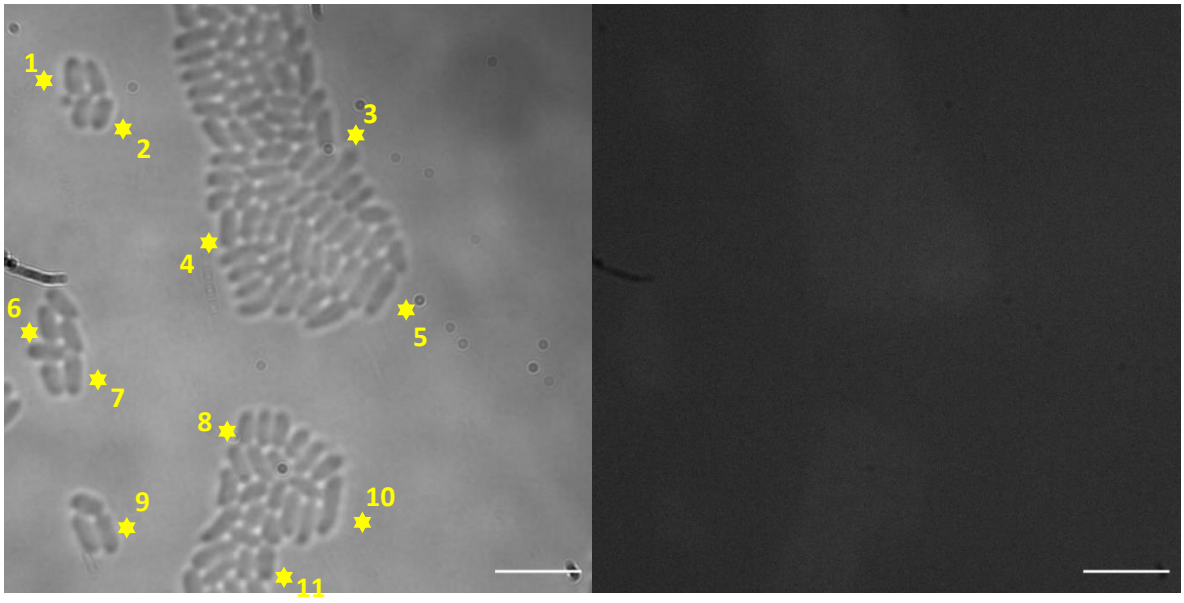


Figure S161 – *E. coli* transmitted image and fluorescence image at 450 nm used in fluorescence intensity calculations in the absence of both **2** and **8** at T = 4 hrs. Transmitted image used to locate cells on fluorescent image. Scale bar = 10µM.

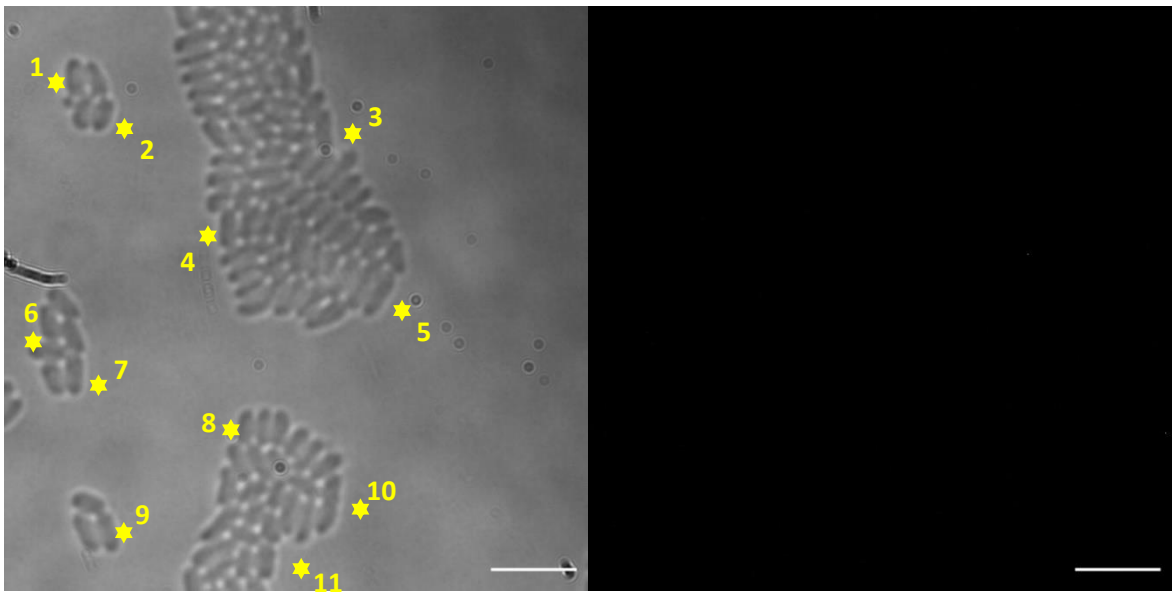


Figure S162 – *E. coli* transmitted image and fluorescence image at 605 nm used in fluorescence intensity calculations in the absence of both **2** and **8** at T = 4 hrs. Transmitted image used to locate cells on fluorescence image. Scale bar = 10µM.

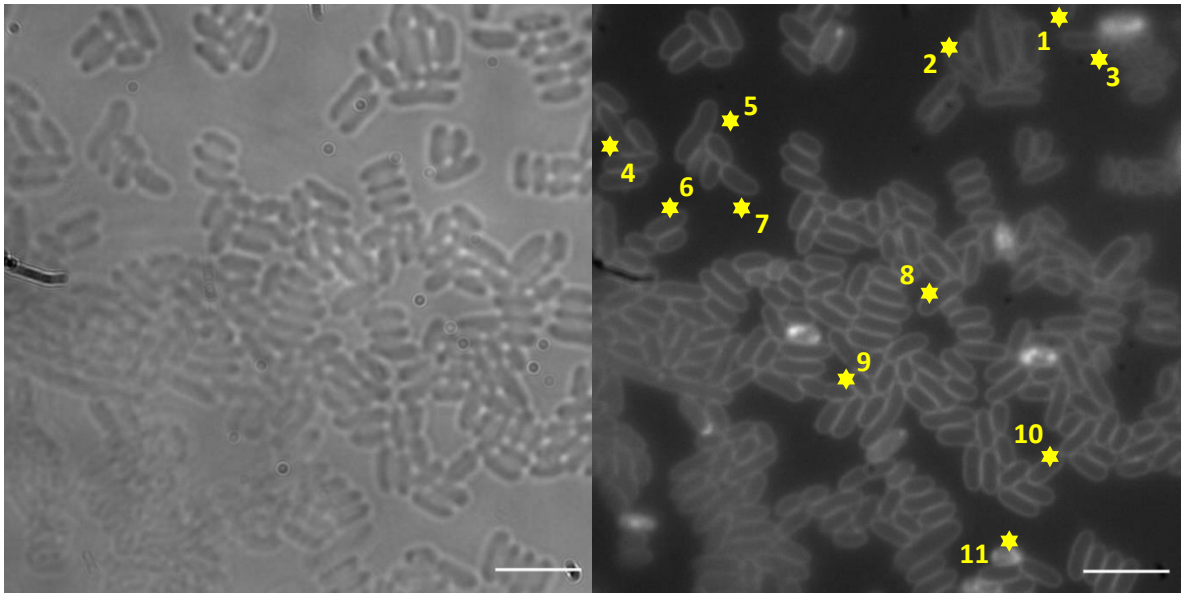


Figure S163 – *E. coli* transmitted image and fluorescence image at 450 nm used in fluorescence intensity calculations in the presence of **2** at T = 4 hours. Scale bar = 10µM.

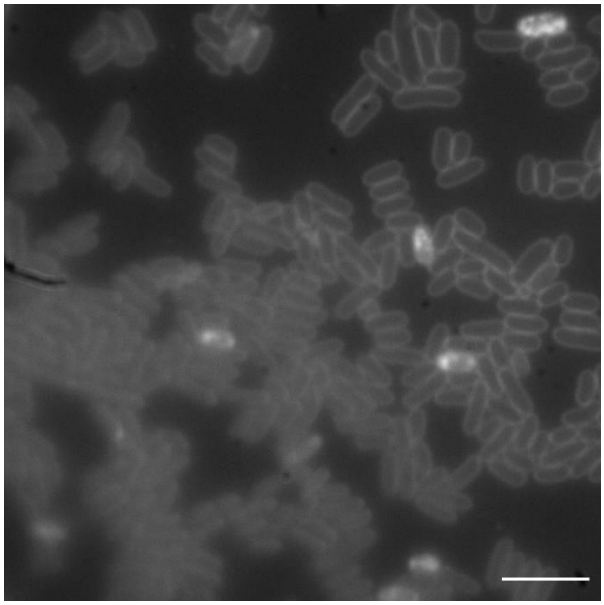

Figure S164 – Z-slice image used in combination with above figure to obtain more accurate fluorescence intensity calculations. Fluorescence image at 450 nm of *E. coli* in the presence of **2** at T = 4 hours. Scale bar = 10µM.

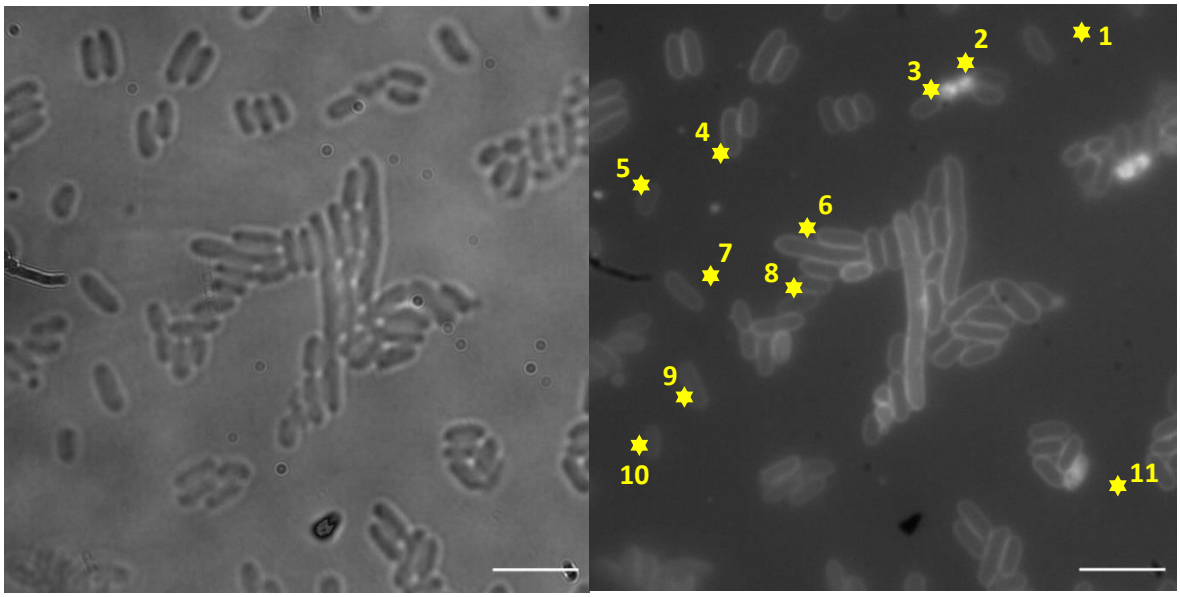


Figure S165 – *E. coli* transmitted image and fluorescence image at 450 nm used in fluorescence intensity calculations in the presence of **2** at T = 4 hours. Scale bar = 10µM.

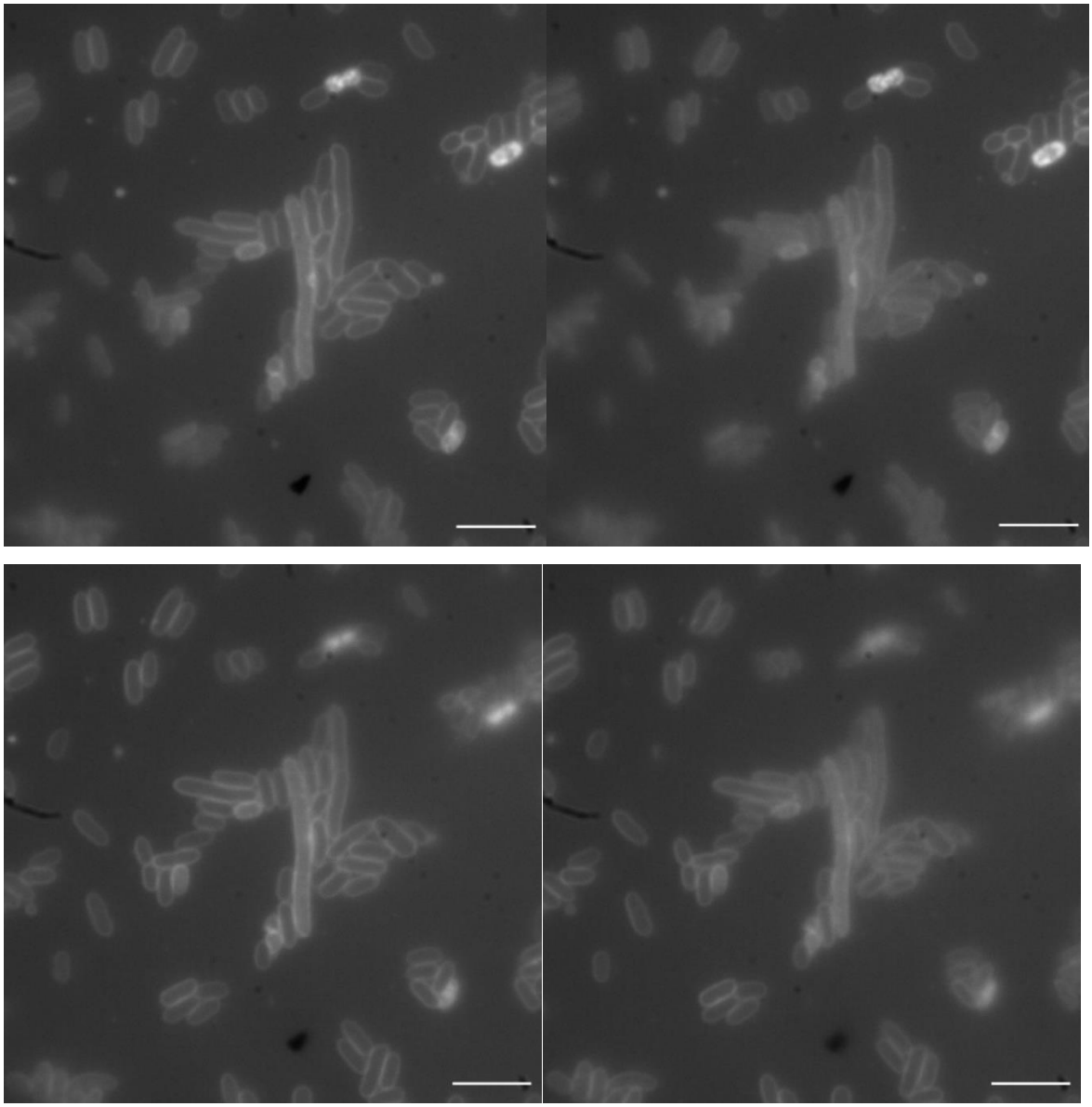

Figure S166 – Different z-slices used in combination with figure above to obtain more accurate fluorescence calculation*s.* Fluorescence images at 450 nm of *E. coli* in the presence of **2** at T = 4 hours. Scale bar = 10µM.

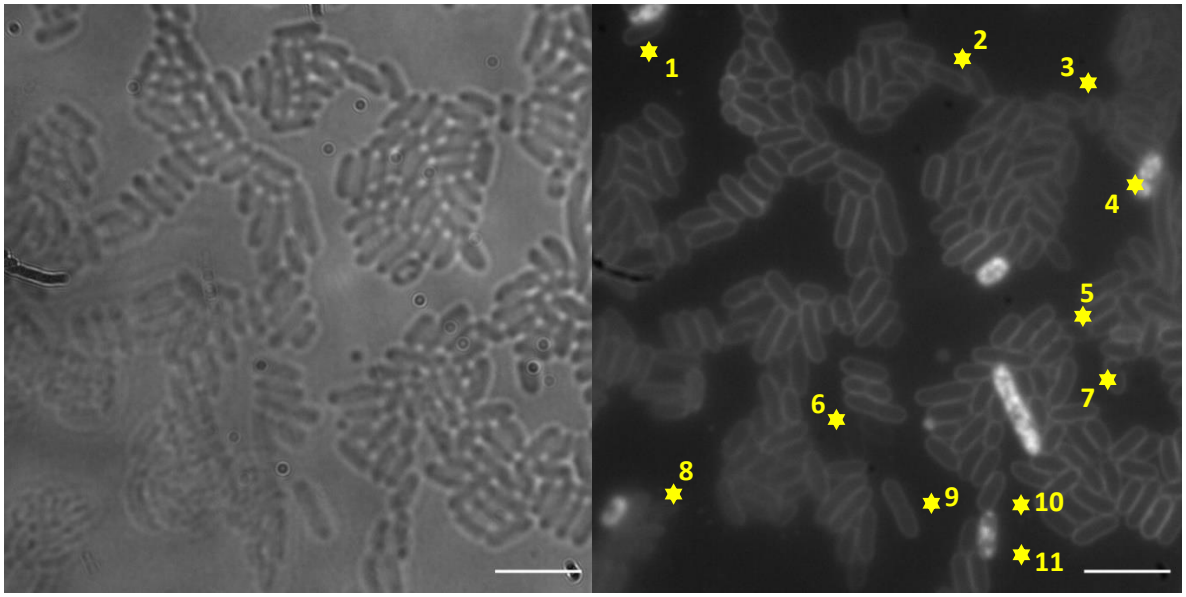


Figure S167 – *E. coli* transmitted image and fluorescence image at 450 nm used in fluorescence intensity calculations in the presence of **2** at T = 4 hours. Scale bar = 10µM.

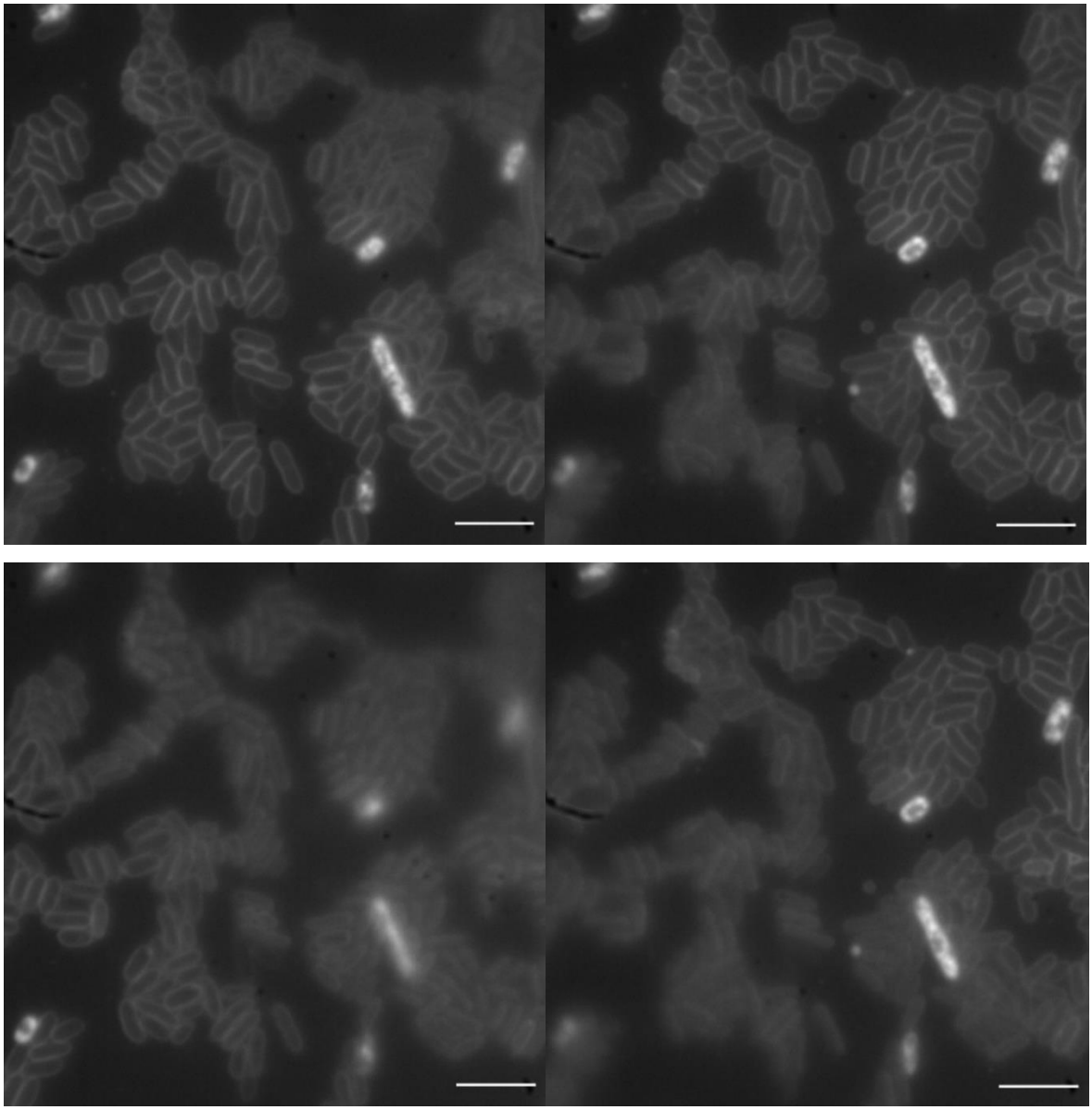

Figure S168 – Different z-slices used in combination to obtain more accurate fluorescence calculations. Fluorescence image at 450 nm of *E. coli* in the presence of **2** at T = 4 hours. Scale bar = 10µM.

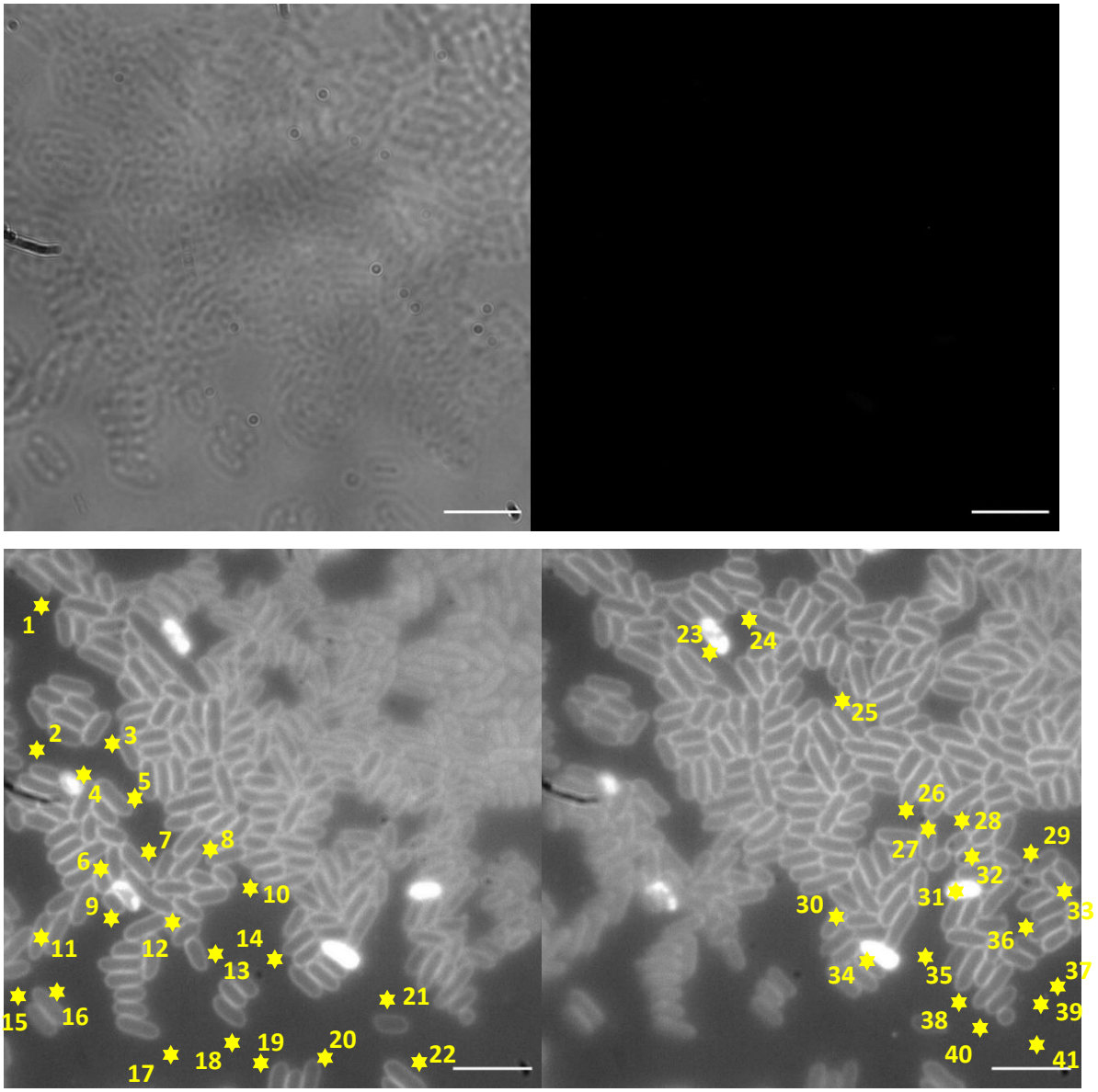


Figure S169 – (Above) *E. coli* transmitted image and fluorescence image at 605 nm used in fluorescence intensity calculations in the presence of **2** at T = 4 hours. (Below) fluorescent images at 450 used in combination with transmitted images to locate cells on fluorescence image at 605 nm. Scale bar = 10µM.

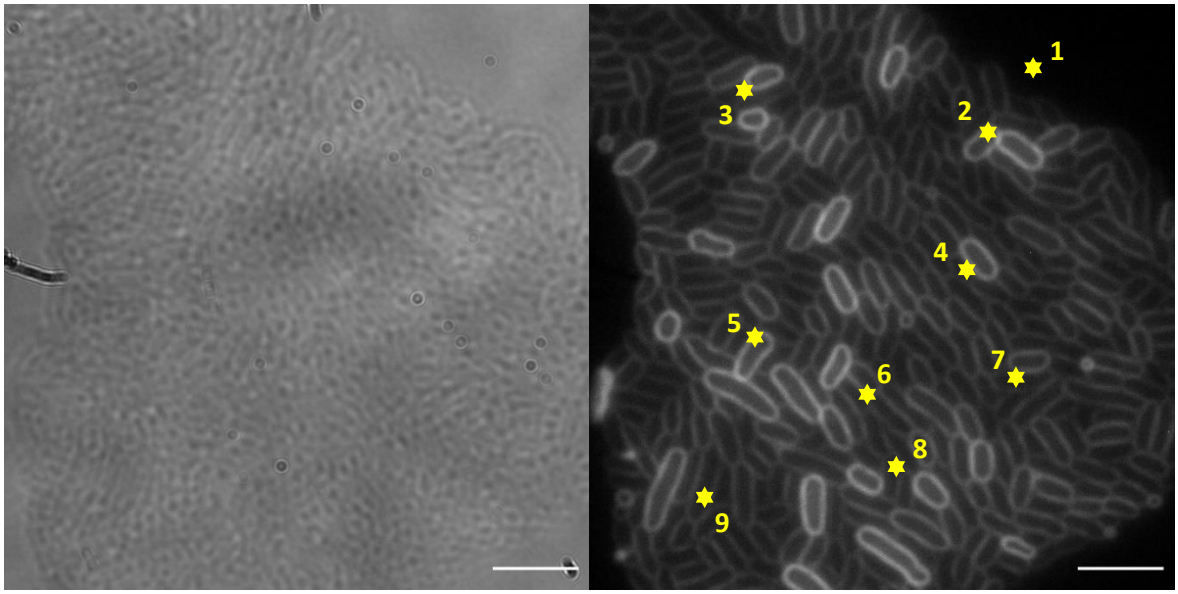


Figure S170 – *E. coli* transmitted image and fluorescence image at 605 nm used in fluorescence intensity calculations in the presence of **8** at T = 4 hours. Scale bar = 10µM.

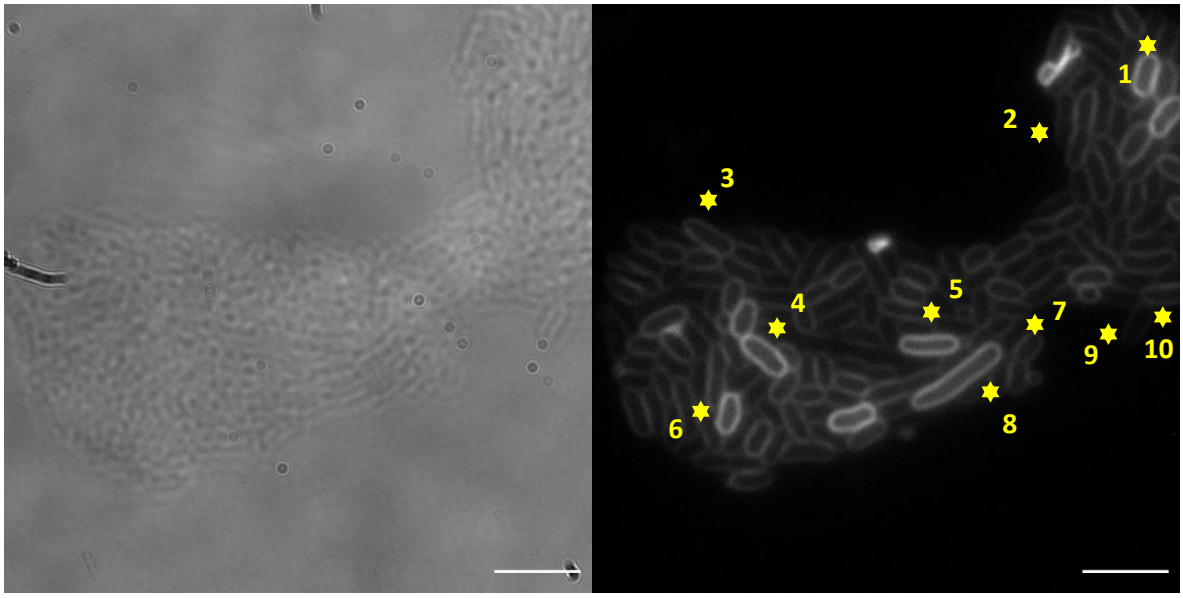


Figure S171 – *E. coli* transmitted image and fluorescence image at 605 nm used in fluorescence intensity calculations in the presence of **8** at T = 4 hours. Scale bar = 10µM.

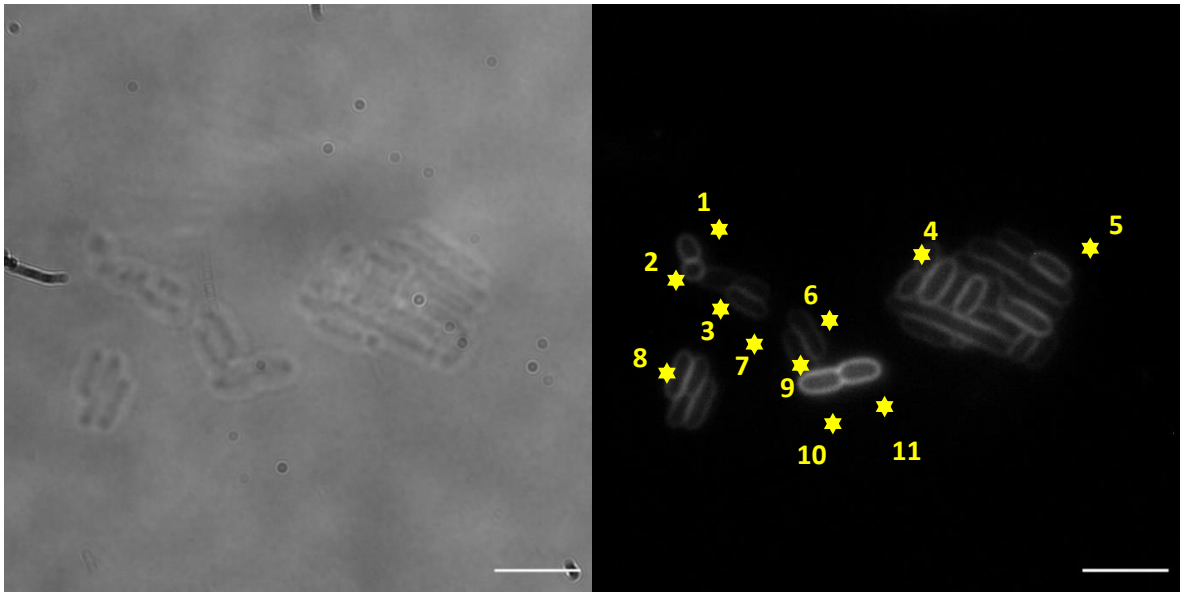


Figure S172 – *E. coli* transmitted image and fluorescence image at 605 nm used in fluorescence intensity calculations in the presence of **8** at T = 4 hours. Scale bar = 10µM.

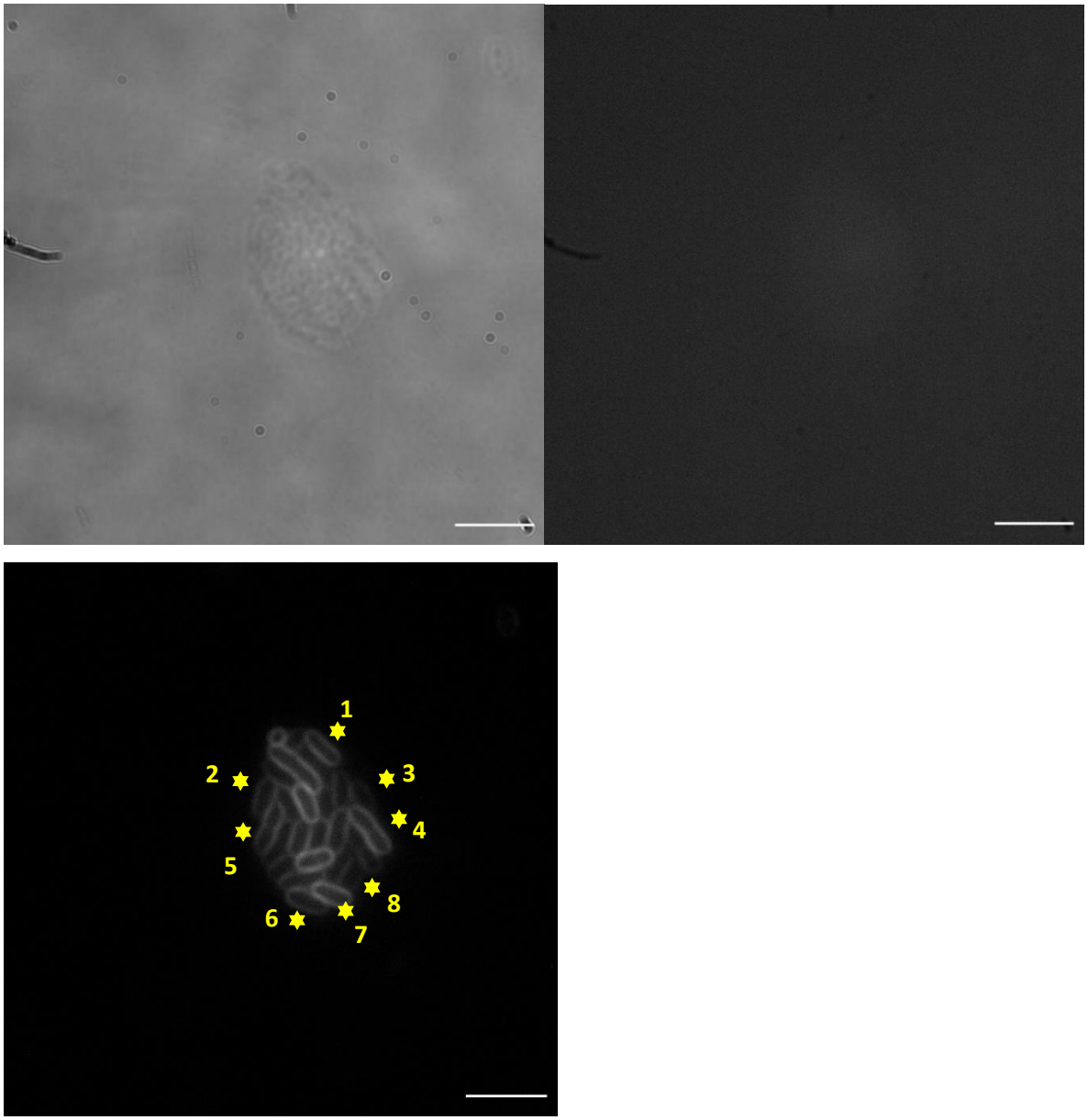


Figure S173 – (Above) *E. coli* transmitted image and fluorescence image at 450 nm used in fluorescence intensity calculations in the presence of **8** at T = 4 hours. (Below) Fluorescence image at 605 nm used to locate cells on fluorescence image at 450 nm. Scale bar = 10µM.

.

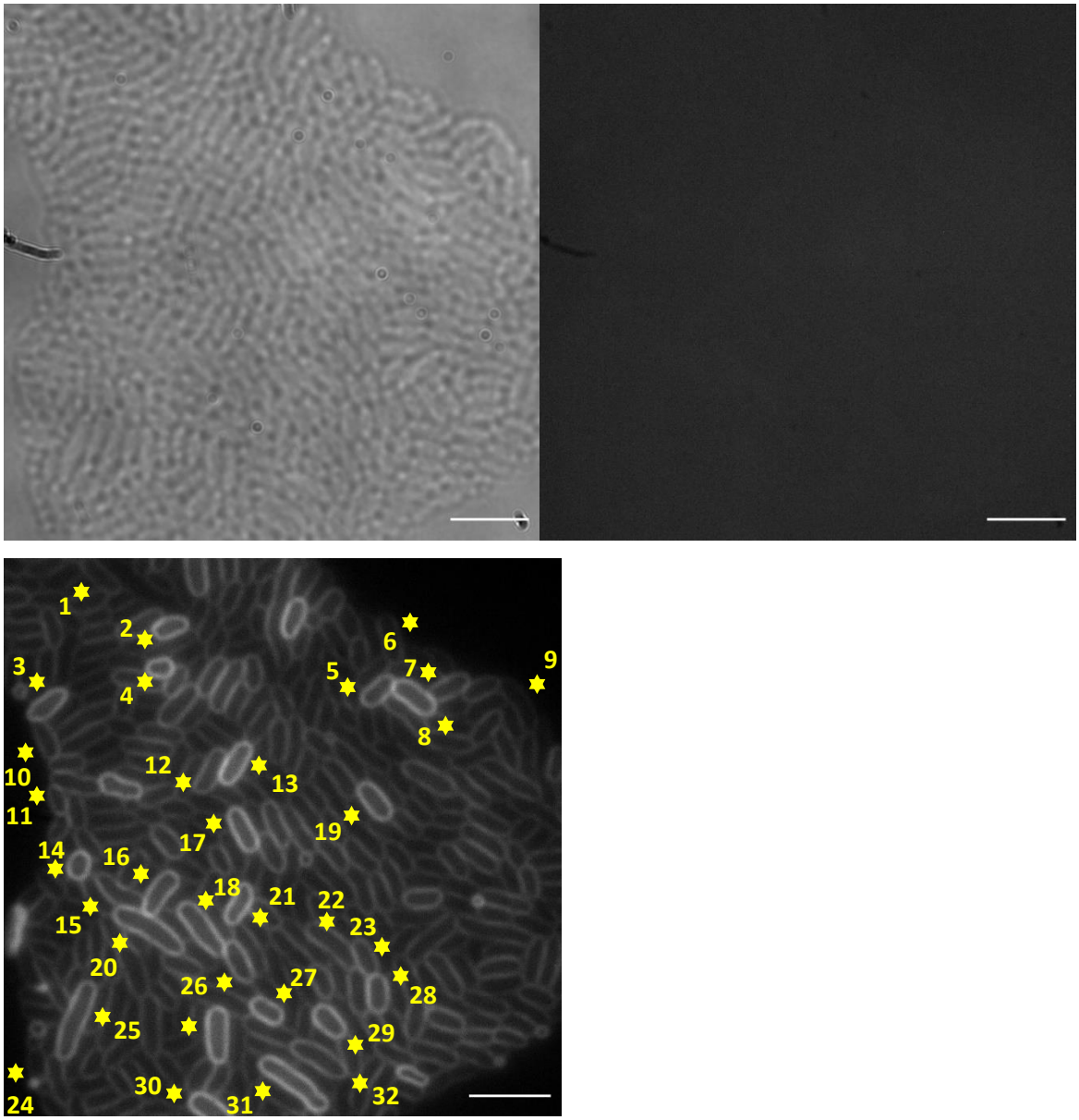


Figure S174 – (Above) *E. coli* transmitted image and fluorescence image at 450 nm used in fluorescence intensity calculations in the presence of **8** at T = 4 hours. (Below) Fluorescence image at 605 nm used to locate cells on fluorescence image at 450 nm. Scale bar = 10µM.

Table S3 - Fluorescence intensity of *E. coli* DH5B cells measured at 450 nm and 605 nm (DAPI or mCherry filters respectively) in the presence of; a solvent alone, **2, 8** and a combination of **2** and **8.** Results obtained at time c) T = 30 mins and d) T = 4 hrs.

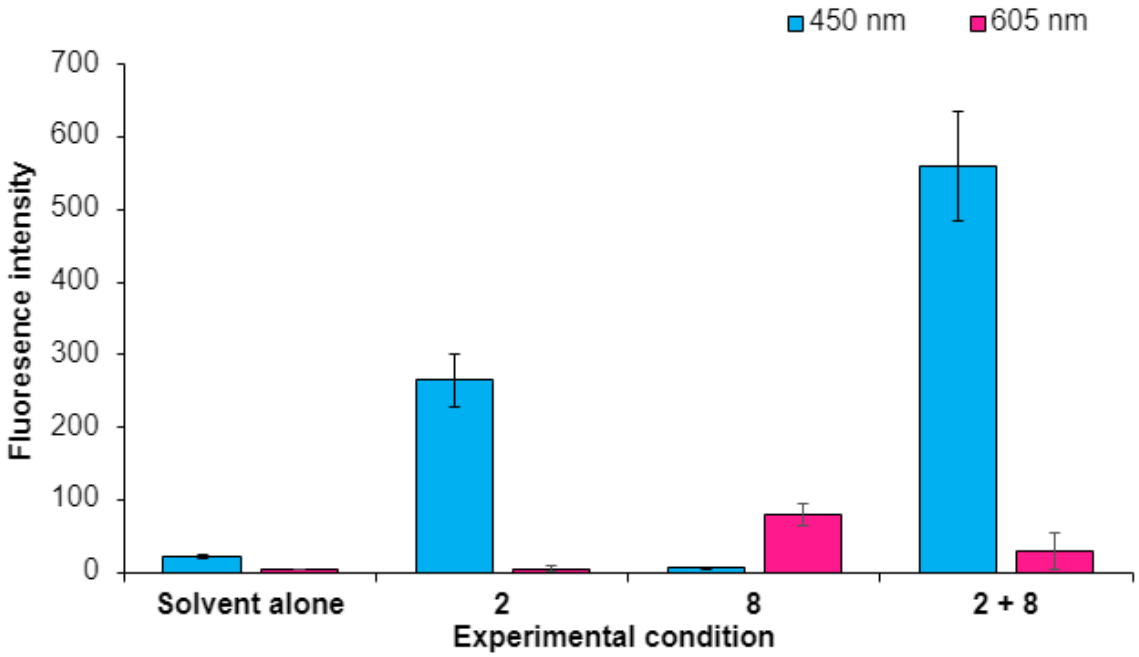

# References


1 G. M. Sheldrick, *Acta Crystallogr. Sect. C Struct. Chem.*, 2015, **71**, 3–8.

2 O. V. Dolomanov, L. J. Bourhis, R. J. Gildea, J. A. K. Howard and H. Puschmann, *J. Appl. Crystallogr.*, 2009, **42**, 339–341.

3 J. R. Hiscock, G. P. Bustone, B. Wilson, K. E. Belsey and L. R. Blackholly, *Soft Matter*, 2016, **12**, 4221–4228.

4 L. J. White, N. J. Wells, L. R. Blackholly, H. J. Shepherd, B. Wilson, G. P. Bustone, T. J. Runacres and J. R. Hiscock, *Chem. Sci.*, 2017, **8**, 7620–7630.

5 L. J. White, S. N. Tyuleva, B. Wilson, H. J. Shepherd, K. K. L. Ng, S. J. Holder, E. R. Clark and J. R. Hiscock, *Chem. - A Eur. J.*, 2018, **24**, 7761–7773.